ABSTRACTS

Oral and Poster

The Treatment of Claustrophobia During Cardiovascular Magnetic Resonance: Use and Effectiveness of Mild Sedation

J.M. Francis, D.J. Pennell. *The Royal Brompton and Harefield NHS Trust, London, UK*

Introduction: Claustrophobia: the morbid fear of being in a confined space is associated with cardiovascular magnetic resonance imaging (CMR) due to the nature of the imaging technique and the length of the examination time. Various methods have been described to alleviate patient's anxiety and panic. (1–6)

Method: We report the incidence and treatment of claustrophobia using intravenous (IV) and oral diazepam in the cardiovascular magnetic resonance unit from August 1997 to June 1999.

1754 adult patients referred for CMR for clinical and research purposes were included. Patients under 16yrs and adults with learning difficulties were excluded

Results: The initial refusal rate of clinical and research patients was 4.2% (54 clinical and 19 research). Ethical approval to administer anxiolysis to patients undergoing scans for research purposes had not been granted at the beginning of this study. Analysis of the results therefore excludes these nineteen patients.

Of the 54 clinical patients with claustrophobia, 31 were given IV diazepam with a successful examination being performed in 97% of cases. Eight patients refused sedation and scanning was not possible.

The examination was attempted without sedation by 5 patients in the claustrophobic group and was terminated early, however sufficient diagnostic information had been acquired in all cases. A further 4 patients had taken oral diazepam up to one hour prior to their appointment with 100% success rate in this group. Three patients refused to attend the department at all due to known severe claustrophobia (2) and concerns over gradient noise (1) and a further 3 had medical contra-indications to diazepam.

Therefore, following the option of administering diazepam to alleviate claustrophobia, the failure rate decreased to 20 patients, a reduction of 63%

The dose of IV diazepam ranged from 2.5mg to 20mg with a mean dose of 7.5mg. The function of diazepam was to achieve anxiolysis rather than deep sedation as patients may need to co-operate with breathold techniques which in themselves reduce examination time and provide a focus and control for the patient

Discussion: A protocol was drawn up for the administration of IV diazepam within the unit as follows:

- IV access established
- 2–20mg diazepam administered slowly until anxiolysis achieved
- Pulse oximetry to be used throughout
- ECG to be monitored
- Patient not to drive home and to be accompanied on public transport

Following the success of the use of this technique and the introduction of the protocol, ethical approval has been given for the administration of IV diazepam to patients giving informed, written consent for research studies.

This technique has a high level of patient acceptance. Six patients within the claustrophobic group have had one or more follow-up studies during and since the end of the study. A further patient who was initially sedated returned for a follow-up and completed CMR without sedation.

Conclusion: Intravenous diazepam is a safe, predictable and highly effective method of dealing with anxiety and claustrophobia in patients undergoing CMR.

References

1. Hricak H, Amparo EG. Body MRI: alleviation of claustrophobia by prone positioning. *Radiology* 1984; 152: 819.
2. Slifer KJ, Penn-Jones K, Cataldo MF, Conner RT, Zerhouni EA. Music enhances patients' comfort during MR imaging. *Am J Roentgenol*; 1991; 156: 403.
3. Communication device for patients undergoing nuclear magnetic resonance. *Radiology* 1983; 149: 855.
4. Prevention of claustrophobia induced by MR imaging: use of alprazolam[letter] *Am J Roentgenol* 1991; 156: 633.
5. Moss ML, Buongiorno PA, Clancy VA. Intranasal midazolam for claustrophobia in MRI. *J Comp Assist Tomogr* 1993; 17: 991–2.
6. Friday PJ, Kubal WS. Magnetic Resonance Imaging: improved tolerance utilizing medical hypnosis. *Am J Clin Hpn* 1990; 33: 80–4.

Cardiovascular Magnetic Resonance Assessment of Left Ventricular Function and Mass After Orthotopic Heart Transplantation: A Comparison with Echocardiography

N.G. Bellenger, N.J. Marcus, L. Grieve, M.H. Yacoub, N.R. Banner, D.J. Pennell. *CMR Unit and Thoracic Organ Transplant Centre, National Heart and Lung Institute, Royal Brompton and Harefield Hospital, London, UK*

Aim: Accurate measurement of left ventricular function and mass is important after heart transplantation to detect rejection and other cardiac complications. We compared fast breath hold cardiovascular magnetic resonance (CMR) and 2D directed M-mode echocardiography in the post transplant setting.

Method: 45 sets of echo and CMR data were prospectively acquired in 19 patients who had undergone orthotopic heart transplantation, at a time interval of between 1 month to 1 year. The intra-observer and inter-observer reproducibility of breath hold CMR in this group was examined. The left ventricular ejection fraction (EF) and mass determined by echo were compared with the CMR data.

Results: Average time between the CMR and echo was 1.3 ± 8 days (mean ± SD). CMR showed good reproducibility in this population with intra-observer percentage variability of 2.2 ± 2.4% for ejection fraction (EF) and 3.2 ± 2.7% for mass, and inter-observer percentage variability of 2.4 ± 1.9% for EF and 2.2 ± 1.9% for mass. The Bland-Altman limits of agreement between echo and CMR were wide for both EF (−9.8 to 14.8%) and mass (−53.6 to 166.2g). CMR detected a 6.5% difference in EF ($p < 0.0001$) and a 10.2% difference in mass ($p < 0.01$) between the baseline and later scan, while echo failed to detect any significant changes in either parameter.

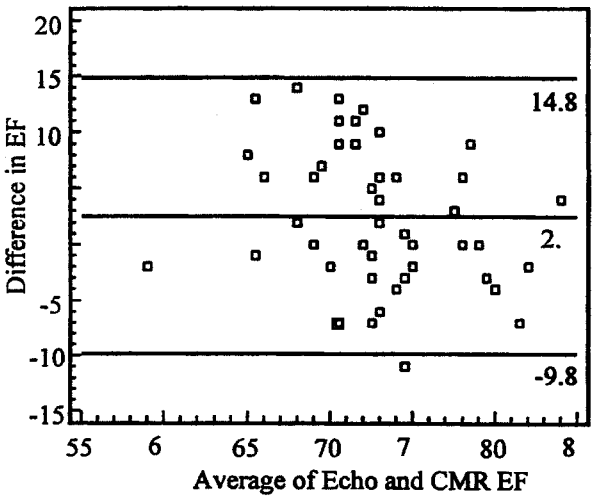

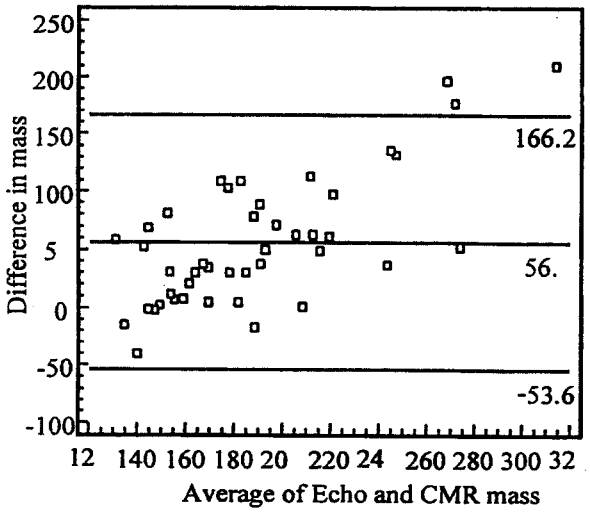

Conclusions: Fast acquisition CMR was highly reproducible in recipients of transplanted hearts and there was poor agreement with routinely used echo. CMR may be superior to echo for detecting changes in graft function due to acute on chronic rejection and left ventricular hypertrophy.

Left Ventricular Ejection Fraction in Heart Failure by Echocardiography, Radionuclide Ventriculography and Magnetic Resonance; Are they Interchangeable?

N.G. Bellenger,[1] M.I. Burgess,[2] S.G. Ray,[2] D.J. Pennell.[1] [1]*CMR Unit, National Heart and Lung Institute, Royal Brompton Hospital, London, UK;* [2]*Northwest Regional Cardiac Centre, Wythenshawe Hospital, Manchester, UK*

Background: The assessment of cardiac function has valuable diagnostic, prognostic and therapeutic implications for patients with ventricular dysfunction. Despite the increasing use of cardiovascular magnetic resonance (CMR) in clinical practice and therapeutic trials, studies have not assessed how rapid CMR functional analysis in heart failure compares with echocardiography and radionuclide ventriculography (RNV). It is important to know whether the results of each technique are interchangeable, and thereby how the results of large studies in heart failure utilising one technique can be applied to another.

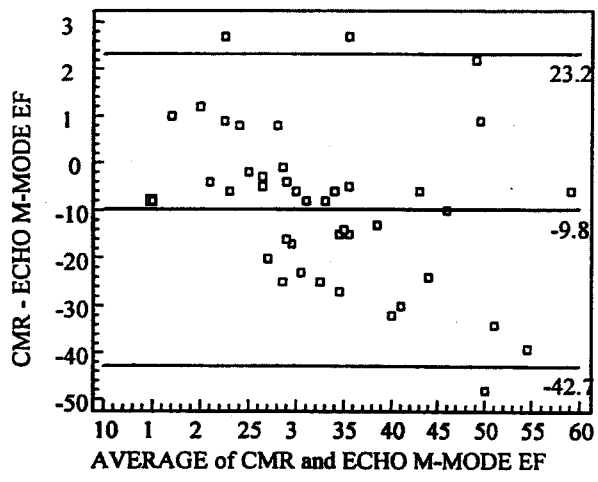

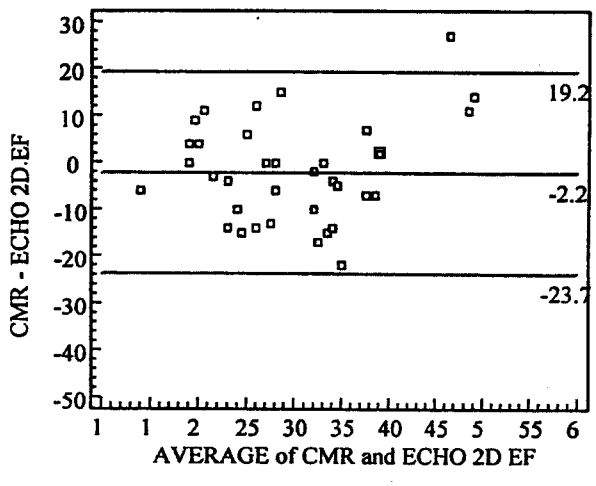

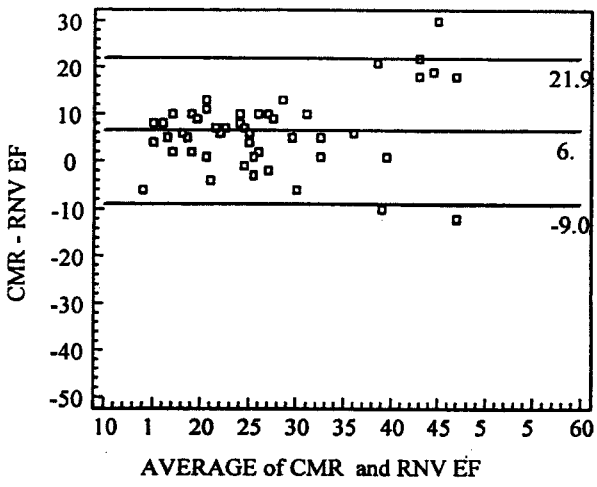

Methods: Fifty two patients with chronic stable heart failure (NYHA grade II-III) underwent M-mode echo, 2D echo, RNV and breath-hold FLASH CMR within 4 weeks. The scans were analysed independently in blinded fashion by a single investigator at three core laboratories.

Results: Of the echocardiograms, 86% had sufficient image quality to obtain left ventricular ejection fraction (EF) by M-mode cube method, but only 69% by Simpson's bi-plane analysis. All 52 patients tolerated the RNV and CMR, and all these scans were analysable. The mean LV EF by M-mode was 39 ± 16%, by the echo Simpson's bi-plane was 31 ± 10%, by RNV was 24 ± 9% and by CMR was 30 ± 11%. All the mean LV EFs by each technique were significantly different from all other techniques ($p < 0.001$), except for CMR EF and echo EF by Simpson's rule ($p = 0.23$). The Bland-Altman limits of agreement encompassing 4 standard deviations was widest for CMR vs cube echo at 66%, and was 58% for RNV vs cube echo, 44% for CMR vs Simpson's echo, 39% for RNV vs Simpson's echo, and smallest at 31% for CMR vs RNV.

Conclusion: These results suggest that EF measurements by various techniques are not interchangeable. In addition, there are very wide variances between techniques, which are most marked in comparisons using echocardiography. The conclusions and recommendations of research studies in heart failure should therefore be interpreted in the context of locally available techniques.

Prospective Respiratory Navigator Gating for Left Ventricular Quantification in Heart Failure: Comparison with Breath-Hold Acquisition

N.G. Bellenger, P.D. Gatehouse, K. Rajappan, J. Keegan, D.N. Firmin, D.J. Pennell. *CMR Unit, National Heart and Lung Institute, Royal Brompton Hospital, London, UK*

Background: Cardiovascular Magnetic Resonance (CMR) is the reference standard for the assessment of cardiac function. Faster sequences, such as breath hold (BH) FLASH, have made CMR more clinically acceptable and cost effective. A significantly large patient group, however, find it difficult to breath-hold resulting in poor quality images, through plane motion errors and misregistration. We compared prospective navigator echo respiratory gating (NE) which allows image acquisition during free breathing, and BH imaging in 15 patients with heart failure (NYHA III or IV) and 10 normal volunteers.

Methods: All patients were scanned on a 1.5T scanner using contiguous short axis breath-hold FLASH cines. The same short axis FLASH sequence was also used in conjunction with a navigator echo placed at the end of each cardiac cycle. Image data was only accepted when the diaphragm positions in both the preceding (A) and current cardiac cycle (B) lay within an end expiration acceptance window of 5mm.

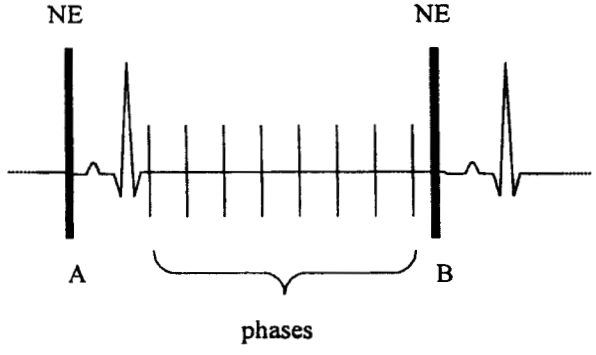

Results: There was good agreement between both NE and BH volumes, mass and ejection fraction. The image quality of both NE basal and apical slices was significantly better than the corresponding BH slices in both the heart failure ($p < 0.01$) and normal groups ($p < 0.05$). The NE image acquisition was more time efficient than BH in the heart failure group (8.7 vs 11.9min, $p < 0.01$), with no difference in the normal group (6.3 vs 5.6 min, $p = 0.2$).

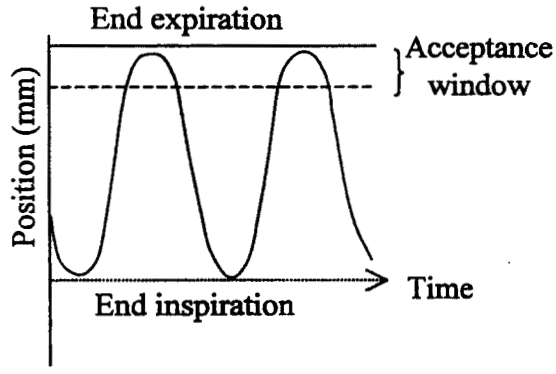

Conclusion: Prospective navigator echo gating, previously only described in coronary artery imaging, can be used in the assessment of cardiac function. It is particularly useful in patients who find it difficult to breath-hold, where NE provides good quality, time efficient images.

Sample Sizes Required by CMR to Show a Clinical Change in Volumes, Ejection Fraction and Mass in Patients with Heart Failure

N.G. Bellenger, L.C. Davies, J.M. Francis, D.J. Pennell. *CMR Unit, National Heart and Lung Institute, Royal Brompton Hospital, Imperial College, London, UK*

Background: Despite increased use, the reproducibility of fast Cardiovascular Magnetic Resonance (CMR) techniques for the assessment of cardiac volumes, function and mass has not been tested outside the normal population. This reproducibility determines the sample size required to show a clinical change.

Methods: Breath hold FLASH CMR was performed on 15 patients with heart failure and 15 normal subjects. Intra-observer, inter-observer and inter-study reproducibility of end diastolic and end systolic volumes, ejection fraction and mass were analysed. The total standard deviation of the difference (SD, where SD = $\sqrt{}$ [Intra-observer + inter-observer + inter-study SD]) was used to calculate the sample size.

Results: The percentage variability of the measured parameters in the HF group of intra-observer (2.0–7.4%), inter-observer (3.3–7.7%) and inter-study (2.5–4.8%) measurements was slightly larger than for the normal group (1.6–6.6%, 1.6–7.3% and 2.0–7.3% respectively), but remained comparable with previous studies using both conventional cine and breath-hold techniques in the normal population. The sample size required to show a. 20ml difference in EDV, a 10 ml difference in ESV, a 5% difference in EF and a 10g difference in mass were 2, 5, 7 and 5 patients respectively. This compares with 30, 53, 37 and 279 by 2D echocardiography using the same calculation for the total standard deviation of the difference. (1)

	Clinical Change	Echo[1]		CMR	
		SD	No	SD	No
EDV	20 ml	23.8	30	5.1	2
ESV	10 ml	15.8	53	4.7	5
EF	5%	6.6	37	2.7	7
Mass	10 g	36.4	279	4.5	5

No—number of patients required

Conclusion: Breath-hold CMR provides a reproducible assessment of failing as well as normal ventricles. The fast acquisition times availability on most current MR scanners, makes this an ideal technique for assessment and follow up of patients and for reducing the sample size required to show the results of an intervention in research studies.

Reference

1. Otterstad JE, Froeland G, St John Sutton M, Holme I. Accuracy and reproducibility of biplane two-dimensional echocardiographic measurements of left ventricular dimensions and function. Eur Heart J 1997; 18: 507–13

Increased Contractility with No Effect on Stroke Volume During Pharmacological Stress in Patients with a Chronic Pressure Overloaded Right Ventricle; Evidence for Impaired Filling

I.I. Tulevski, M. Groenink, E.E. vd Wall, P.L. Lee, J. Stoker, B.J.M. Mulder. *Academic Medical Center, Amsterdam, Leiden University Medical Center, The Netherlands*

Background: Little is known about the hemodynamic effects of contractility enhancement in patients with chronic right ventricular (RV) pressure overload. We studied the effects of low dose dobutamine stress on systolic function in patients with chronic RV pressure overload using magnetic resonance imaging (MRI).

Methods: MRI was used to determine end diastolic volume (EDV) and end systolic volume (ESV) in 8 patients (NYHA class I) with chronic RV pressure overload (PAP > 45 mm/Hg) (age 26 ± 2 years) and 6 matched controls. From EDV and ESV we determined LV and RV Ejection Fraction (EF) and stroke volume (SV). Valve regurgitation was ruled out by means of MR flow measurements. The MRI protocol was applied both in baseline conditions and during dobutamine infusion (start dose 5 µg/kg/min maximum dose 15 µg/kg/min). The stress values were calculated as % increase from the baseline values.

Results: At baseline, the 8 patients showed decreased EF and SV in both ventricles compared to the controls (RVEF:45% vs. 73%, p = 0.0006, RVSV:51ml vs. 100 ml, p = 0.0003, LVEF:63% vs. 77%, p = 0.04, LVSV:58ml vs. 101 ml, p = 0.003, respectively). During dobutamine infusion, heart rate increased significantly in both groups in a similar way. There was a significant increase in biventricular EF both in controls (RV: 16%, LV: 12%), and patients (RV:22%, LV: 11%), p < 0.04 for all values. Biventricular SV increased significantly in controls but not in patients. LVEDV increased significantly in controls (p = 0.02), but decreased in patients (p = 0.03). RVED showed a similar trend. Perceptual increase in SV and EDV are shown in the figures.

Conclusion: Both RV and LV contractility can be stimulated by low dose dobutamine and MRI is well suited to detect these effects. Our data suggest that the absence of increased SV during increased contractility in patients with RV pressure overload may be explained by a filling abnormality in both ventricles, caused by RV hypertrophy and biventricular interaction.

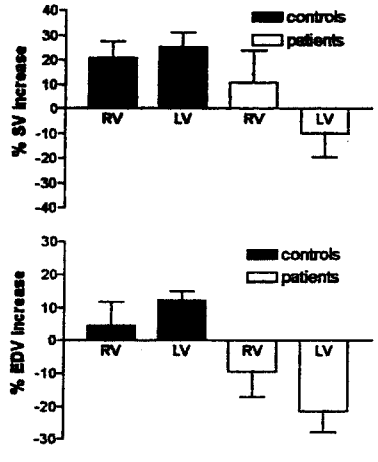

Evaluating Left Ventricular Function Using Real-Time TrueFISP: A Comparison with Conventional MR Techniques

W. Fang,[2] F.S. Pereles,[2] J. Bundy,[3] R. Kim,[1] E. Wu,[1] O. Simonetti,[3] P. Finn.[2] [1]*Northwestern University Departments of Medicine and* [2]*Radiology, and* [3]*Siemens Medical Systems, Chicago, IL*

Introduction: A rapid method for evaluation of cardiac function would be useful for assessing post-MI cardiac status and monitoring cardiac changes following intervention or throughout medical therapy. ECG-gated breath-hold cine techniques are commonly used in which a single slice-level is acquired in a breath-hold. The real-time TrueFISP technique (RT-Trufi) is capable of acquiring multiple short-axis slices of the heart within one single breath-hold (1,2). RT-Trufi is not dependent on cardiac gating or breath-holding and is therefore useful for scanning patients with poor ECGs or monitoring cardiac function during stress studies. Real-time imaging techniques, however, cannot achieve the spatial or temporal resolution of breath-hold cine imaging.

The purpose of this study is to determine if the RT-Trufi sequence is comparable to breath-held MR techniques for evaluation of LV function

Methods: Nineteen patients with a previous history of MI were scanned on a 1.5-T Siemens Magnetom Sonata. In all patients, 6 to 8 short axis slices of the heart were obtained. Nine patients were scanned using breath-hold FLASH (BH-Flash). The remaining 10 patients were scanned with breath-hold TrueFISP (BH-Trufi). In each patient group, the same slice positions were then acquired by RT-Trufi in a scan of 12–16 heartbeats (TR = 2.6, TE = 1.3, α = 50–70°). The acquisition was performed with breath-holding to ensure spatial registration of the slices. Using echosharing, a 63 × 128 matrix was reconstructed every 84 msec. The multi-slice RT-Trufi studies were ECG triggered to synchronize the cine series for each slice level with the beginning of systole. For each slice, one heartbeat was used for steady-state preparation and a second heartbeat was used for acquisition. Therefore, each study required a breath-hold length of 2n heartbeats, where n was the number of slices acquired. Myocardial mass, end-diastolic volume (EDV), end-systolic volume (ESV), ejection fraction (EF), and stroke volume (SV) were determined by epicardial and endocardial contouring using Siemens' Argus software.

Table 1. Comparison of Cardiac Mass and Volume Parameters Computed Using RT-Trufi, BH-FLASH, and BH-Trufi Techniques

Comparison of Average Values for LV Function Values are Normalized for Height and Weight			
Real-time TrueFISP vs Breath-hold TrueFISP (n = 9)			
	Real-time	Breath-hold Trufi	p-values
Mass (g)	76.8 ± 19.4	78.5 ± 21.3	0.11
EDV (mL)	40.6 ± 8.0	42.1 ± 7.1	0.27
ESV (mL)	17.7 ± 6.5	16.1 ± 7.7	0.072
EF (%)	57.2 ± 10.0	62.8 ± 14.5	0.019*
SV (mL)	23.0 ± 5.0	27.5 ± 6.0	0.046*
Real-time TrueFISP vs Breath-hold FLASH (n = 10)			
	Real-time	Breath-hold Flash	p-values
Mass (g)	89.9 ± 15.6	101.8 ± 17.0	0.0022*
EDV (mL)	57.9 ± 20.9	52.1 ± 18.1	0.0099*
ESV (mL)	33.6 ± 18.2	27.3 ± 15.5	0.0010*
EF (%)	44.7 ± 17.8	50.7 ± 17.3	0.00002*
SV (mL)	24.2 ± 11.5	24.9 ± 10.0	0.58

* denotes a significant difference between averages at p < 0.05

Results: Comparison of real-time data with breath-hold data shows significant differences (paired t-test, $p < 0.05$) for mass, ESV, EF, and SV. Close agreement is found between BH-Trufi and RT-Trufi for Mass, EDV and ESV while significant differences are found between BH-Flash and RT-Trufi for all LV properties except SV (Table 1). RT-Trufi images produce higher ESV and lower mass measurements compared with BH-Flash images in all cases ($n = 9$).

Conclusion: RT-Trufi compares very favorably with BH-Trufi for the evaluation of LV function. However, significant differences were found between RT-Trufi and BH-Flash techniques. Our results suggest that differences are attributable to the inherent properties of TrueFISP versus FLASH techniques, rather than to the reduced spatial and temporal resolution of real-time imaging. In TrueFISP, blood pool/myocardium contrast is largely dependent upon T2/T1 properties, whereas in FLASH, contrast is dependent upon blood flow. Stagnant or slow-flowing blood could be mistaken for myocardium when contouring from FLASH images. This would cause falsely elevated mass data and decreased blood volume measurements. Previous work (3) reported lower wall thickness measurements from Trufi images compared with Flash. Our findings suggest Trufi may be more suitable in ischemic heart disease cases where regional wall motion abnormalities cause reduced blood flow and saturation during cine imaging.

RT-Trufi shows promise as a quick method to evaluate LV function. Further work should be performed to compare the accuracy of TrueFISP and FLASH as measurement techniques for LV volume and mass.

References

1. A. Oppelt et al., *Electromedica* 54, 15 (1986)
2. O. Heid, 5th *ISMRM*, 1997
3. J. Bundy et al., 7th *ISMRM*, 1999

Determination of Infarct Size Post Myocardial Infarction by ^{23}Na NMR

Michael Horn, Claudia Weidensteiner, Mark de Groot, Helga Remkes, Martin Meininger, Markus von Kienlin, Stefan Neubauer. *Dept. of Medicine and Physics, University Würzburg, Germany*

Introduction: One major clinical question after myocardial infarction (MI) is the determination of infarct size. Due to ischemia, ATP levels in the infarcted area drop and the ion homeostasis becomes imbalanced. Recently, ^{23}Na images in acute MI were reported (1,2). In this study, the total sodium concentration ($[Na_{tot}]$) was determined during the time course of scar development. ^{23}Na NMR images of chronically infarcted hearts were measured in perfused hearts. If Na is increased in scar tissue, this may allow evaluation of myocardial viability.

Methods: Male Wistar rats were anesthetized and the LAD was ligated. For $[Na_{tot}]$ the animals were sacrificed after 1, 3, 7 days or 1, 2, 4 month Hearts were excised, cooled and the scar tissue was cut off. One specimen of the scar was bathed in iso-osmolar LiCl/$CaCl_2$ solution.

^{23}Na NMR spectra at 7 Tesla were acquired (1000 averages in 8 min 37 sec). FIDs were Gauss multiplied, Fourier transformed, phase corrected and integrated. $[Na_{tot}]$ were calculated from an internal standard (NaCl + Tris, [Na(TTHA)]). $[Na_{tot}]$ was also determined by ion chromatography as a gold standard.

For ^{23}NMR imaging, hearts were excised after 4 or 8 weeks and perfused with Krebs Henseleit buffer in Langendorff mode (RV collapsed) at 37 °C. A 3D gradient echo sequence was acquired in 13 min at 11.75 T. Contrast between perfusate and tissue was enhanced by a MTC pulse prior to excitation. Spatial resolution was 0.75*0.75* 22 mm, thus, voxel size was 1.125 µl.

Infarct size was determined from ^{23}Na NMR images and by histology.

Results: The $[Na_{tot}]$ determined by ^{23}Na NMR spectroscopy shows a 3.1-fold increase early after onset of ischemia. After day 1, the $[Na_{tot}]$ drop to values approx. 200 % of control. Values from ion chromatography (data not shown) showed no significant differences to the NMR spectroscopy data.

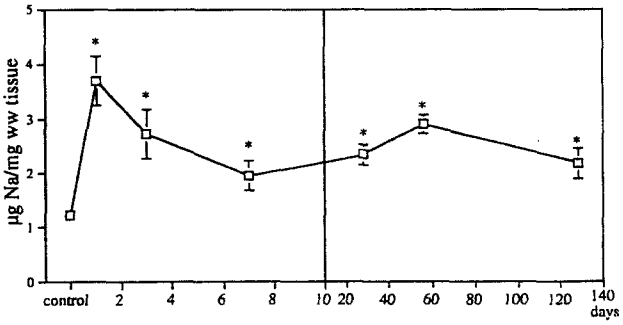

In ^{23}Na NMR images perfusate, left ventricular cavity and wall can be discriminated. Scar area appears brighter (arrow in figure) due to signal elevation and can be determined with an intensity increase larger than the double standard deviation of the noise level of the image.

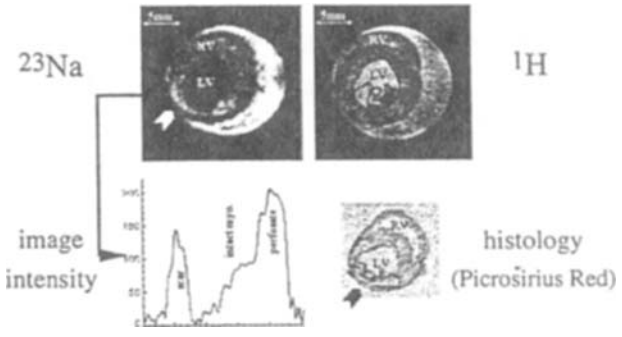

Results from NMR imaging and histology are well correlated ($r = 0.91$, $p < 0.0001$).

Summary: ^{23}Na NMR spectroscopy shows higher $[Na_{tot}]$ at all time points after MI. ^{23}Na NMR imaging can be used for non-invasive determination of size and location of scar tissue in the myocardium even month after the MI. This technique might be useful for determing myocardial viability in humans.

References

1. Kim et al, *Circ* 1997; 95: 1877–85.
2. Kim et al, *Circ* 1999; 100: 185–192

Dichloroacetate Does not Enhance Postischemic Na^+-K^+ ATPase Activity in Pyruvate-Reperfused Isolated Rat Hearts

J.G. van Emous, M.G.J. Nederhoff, T.J.C. Ruigrok, C.J.A. van Echteld. *Heart Lung Institute, University Medical Center, Utrecht and Interuniversity Cardiology Institute (ICIN), The Netherlands*

Introduction: Postischemic reperfusion with glucose in isolated rat hearts is accompanied by an immediate decrease of intracellular sodium (Na^+_i) via Na^+-K^+ ATPase activity. (1) In the absence of glycolytic-flux with pyruvate as substrate, however, the decline of Na^+_i is delayed. (2) Since the activity of the pyruvate-dehydrogenase (PDH)-complex is depressed during postischemic reperfusion, (3) we used the PDH-

activator dichloroacetate (DA) to assess whether reperfusion with both pyruvate and DA improves pyruvate oxidation and thereby increases Na^+-K^+ ATPase activity.

Materials & Methods: Hearts of male Wistar rats were perfused with a modified Krebs-Henseleit solution at 37°C and 76 mmHg while stimulated at 300 beats.min^{-1} (BPM). A left intraventricular latex balloon was used to monitor cardiac contractility (RPP (rate pressure product) = developed pressure × BPM). After initial preparations, perfusion with the ^{23}Na NMR shift reagent TmDOTP^{5-} (free [Ca^{2+}] 0.85 mM) was commenced. The contribution of extracardiac Na^+ to the NMR-signal was minimized using a Na^+-free flushing solution.

In all hearts, 5 min of glucose perfusion was followed by 20 min of substrate-free glucagon (500 ug/L) perfusion to deplete the endogenous glycolytic substrate glycogen. Subsequently, hearts were perfused for 1 min with pyruvate (or pyruvate + DA in DA treated hearts), followed by 20 min of global normothermic ischemia. Reperfusion (constant flow at 70% of preischemic flow rate) was performed with either glucose (G, 11 mM), pyruvate (P, 5 mM), or both pyruvate and DA (PDA, both 5 mM) for 30 min (n = 6, mean ± SEM).

^{23}Na NMR spectra (Fig 1) were acquired on a Bruker MSL 200 spectrometer and were quantified by a time-domain fitting routine. Between 15 min of ischemia and 10 min reperfusion 180 5-sec (24 scans) ^{23}Na spectra were accumulated. During the rest of the protocol 1-min spectra (260 scans) were obtained.

Results: During preischemic glucose perfusion RPP amounted to 20.4 ± 1.5, 23.7 ± 2.7, and 19.5 ± 1.8* 10^3 mmHg.min in G, P, and PDA groups (NS), resp., which values increased transiently during glucagon-perfusion (data not shown). Na^+_i increased throughout glucagon-perfusion, but during the subsequent 1 min of pyruvate perfusion a small decrease was apparent (Table 1). In all groups end-diastolic pressures (EDP) started to increase after ~2 min of ischemia and maximal contracture was achieved within 3.5 min. During ischemia Na^+_i increased significantly (Table 1) while EDP at 20 min of ischemia amounted to 66 ± 6, 53 ± 9, and 54 ± 5 in G, P and PDA hearts, resp.

During reperfusion Na^+_i decreased in all groups (Table 1, Fig 2). In G hearts, however, the initial decline (first 5 time points of reperfusion) of Na^+_i was faster than in P and PDA hearts, and amounted to −34.0 ± 6.0, −2.2 ± 9.9, and 3.1 ± 4.3% of the end-ischemic value.min^{-1}, resp. (G vs P and PDA, $p < 0.05$). Na^+_i had declined to nearly preischemic levels in all groups after 30 min of reperfusion (Table 1). Recovery of RPP was 66 ± 7, 78 ± 5, and 97 ± 11% of the preischemic value in G, P, and PDA hearts, resp. (PDA vs. G, $p < 0.05$) while EDP was lowest in PDA hearts (46 ± 8, 40 ± 11, and 33 ± 5 mmHg, resp.).

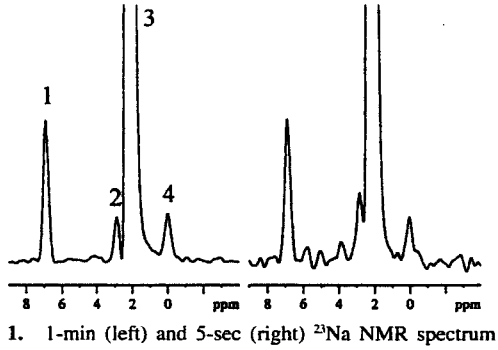

Figure 1. 1-min (left) and 5-sec (right) ^{23}Na NMR spectrum of an isolated perfused rat heart during preischemic perfusion. Numbered peaks: 1. reference signal, 2. residual extracardiac-, 3. extracellular-, and 4. intracellular Na^+, resp.

Table 1. Na^+_i (mmol/L) During Preischemia and At the End of Ischemia and Reperfusion

	G	P	PDA
5′ glucose	13.8 ± 1.0	13.7 ± 0.7	12.6 ± 1.0
20′ glucagon	16.5 ± 1.3	14.9 ± 1.2	14.2 ± 0.8
1′ pyruvate	16.2 ± 1.7	13.4 ± 1.1	13.9 ± 0.9
20′ ischemia	29.2 ± 2.2	27.6 ± 1.7	26.0 ± 1.6
30′ reperfusion	14.1 ± 1.8	13.2 ± 1.4	14.7 ± 1.2

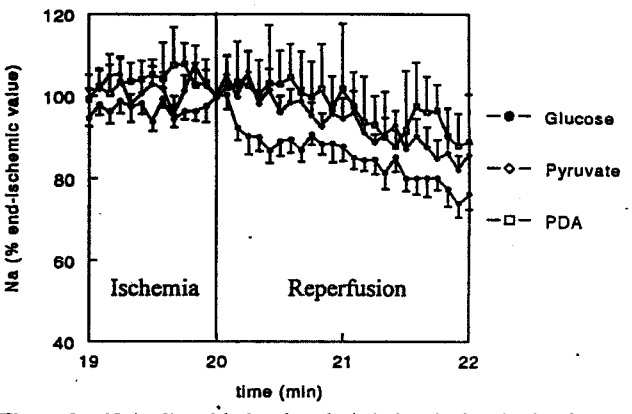

Figure 2. Na^+_i (% end-ischemic value) during the last 1 min of ischemia and the first 2 min of reperfusion.

Conclusions: Although glycolytic flux is not essential for the post-ischemic decline of Na^+_i and thus for Na^+-K^+ ATPase function,[1,2] initial activity is higher in hearts which may employ this pathway. The delay of Na^+-K^+ ATPase activity in P hearts is not overcome by DA, indicating that poor activity of the PDH-complex, e.g. by high levels of NADH during early reperfusion, is not a limiting factor in this regard. The improved functional recovery in PDA hearts has been observed before,[3] but cannot be explained by our present Na^+_i data.

References

1. Van Emous JG. et al. *J Mol Cell Cardiol* 1998; 30: 337–348.
2. Van Emous JG. et al. *MAGMA* 1998; 6: 177–178.
3. Lewandowski ED, White LT. *Circulation* 1995; 91: 2071–2079.

Fast Acquisition of Left Ventricular Volumes and Mass Using a Multiple-Slice Real-Time Method

S. Plein,[1] W. Smith,[1] J.P. Ridgeway,[2] A. Kassner,[3] D.J. Beacock,[1] T. Bloomer,[1] S. Williams,[1] U.M. Sivananthan.[1] [1]*Cardiac Magnetic Resonance Unit and* [2]*Department of Medical Physics, United Leeds Teaching Hospitals, Leeds, UK; and* [3]*Philips Medical Systems, Hammersmith, London, UK*

Background: Conventional imaging-sequences for the acquisition of short-axis slices through the left ventricle, as used for measurements of left ventricular mass and volumes, are either non-breathhold gradient echo or breathhold segmented k-space imaging. Both have a total acquisition-time of around 10 minutes. The recent development of high-performance gradient systems and the optimisation of fast image acquisition methods have enabled multi-phase images of the heart to be acquired in "real-time" (1,2,3,4). This technique can be used to provide a multiple-phase image data set of a single slice over the period of one cardiac cycle, substantially reducing the time for acquisition of images for mass and volume measurements. Following our initial experience

(5), we now present the results of the first 20 subjects imaged with this technique.

Methods: 10 healthy volunteers and 10 patients with cardiomyopathy (8 dilated cardiomyopathy, 2 hypertrophic cardiomyopathy) were studied. A "real-time" pulse sequence with a turbo gradient echo technique with an echoplanar readout (TFE-EPI) was implemented on a 1.5 Tesla Philips GYROSCAN ACS NT MR imaging system (Philips Medical Systems, Best, The Netherlands) with a gradient performance of amplitude 21mT/m and slew rate of 105mT/m/ms. All imaging was performed using a cardiac phased-array coil with the subjects holding their breath. 10 to 14 short axis slices were acquired from apex to base of the left ventricle at 1cm intervals.

In all 20 subjects three sets of images were acquired:

(a) A conventional, ECG-triggered, multiple heart-phase segmented k-space turbo-gradient echo (TFE) pulse sequence (TR 8.8 ms, TE 5.2 ms, $\alpha = 35°$, 256 × 119 matrix, 6mm slice-thickness, 12 heart phases, heart phase interval 74ms, acquisition time 13–18 seconds per slice, 1 slice per breathhold).

(b) A "real-time" multi-heart-phase segmented k-space TFE-EPI pulse sequence (TR 11ms, TE 3.4ms, $\alpha = 20°$, 7 EPI readouts, "halfscan" factor of 0.71, 128 × 95 matrix, 10mm slice thickness, heart phase interval 87ms, acquisition time 1.48 seconds per slice, 4–5 slices per breathhold. ECG-triggering was used to synchronise the start of each slice acquisition to end-diastole.

(c) A second, separate real-time sequence identical to the sequence described under (b) following new patient positioning and new scout-scans, for assessment of reproducibility of the real-time imaging sequence.

End-diastolic volume, end-systolic volume, ejection fraction and left ventricular mass were measured off-line. To assess intra- and inter-observer variability, one series of real-time images was measured twice by the same observer with at least two weeks delay as well as independently by a second observer. Agreement between data sets was assessed using Bland & Altman plots.

Results: Table 1 lists the mean percentage differences for all 20 subjects between conventional and real-time measurements, between the two real-time measurements by the first observer (intra-observer variability), between the two observers (inter-observer variability) and between the two sets of real-time data (reproducibility).

Table 1. Mean Percentage Difference (95% Confidence Intervals) for Conventional vs. Real-Time Sequence, Intraobserver Variability, Interobserver Variability and Reproducibility of the Real-Time Sequence. EDV = End-Diastolic Volume, ESV = End-Systolic Volume, EF = Ejection Fraction.

	EDV	ESV	EF	Mass
Convent. vs. Real-time	3.2	1.6	1.9	8.9
	(7.8)	(12.4)	(14.8)	(16.6)
Intraobs. variability	0.59	0.72	1.48	−2.99
	(5.4)	(11.6)	(13.1)	(8.7)
Interobs. variability	0.07	−3.13	2.49	1.37
	(14.26)	(22.4)	(14.9)	(14.4)
Reproducibility	0.99	1.24	0.68	−3.18
	(8.8)	(12.7)	(16.0)	(11.8)

Although image-quality was generally worse for the real-time images, there was good overall agreement between conventional and real-time imaging, good intra- and interobserver variability and good reproducibility. In separate sub-analyses for normal volunteers and patients, agreement was similar between both groups. Left ventricular mass-estimation was consistently lower with the real-time sequence compared with conventional imaging, both in volunteers and in patients.

The average acquisition-time for the conventional images was 10.5min compared with 1.45min for the real-time method.

Conclusion: This study indicates that fast acquisition of images for LV measurements using a "real-time" sequence can be reliably and reproducibly performed in normal and pathologically altered ventricles despite a loss of image-quality. The time required for image-acquisition is reduced substantially. A possible explanation for the under-estimation of left ventricular mass with the real-time sequence is the fat-water shift associated with the EPI-technique used for real-time imaging. Depending on the orientation of the phase-encoding direction, this can result in pericardial fat overlapping and covering myocardium, in particular at the left ventricular free wall. This problem could be overcome by careful setting of the phase-encoding direction or the use of fat-suppression techniques, although the latter could prolong acquisition times.

References

1. Stuber M et al. *Proc 5th ISMRM* 1999; 908
2. Kerr AB et al. *Magn Res in Med* 1997; 355–67
3. Ridgway JP et al. *Proc 6th ISMRM* 1998; 807
4. Fisher SE et al. *JCMR* 1999; 84
5. Ridgway JP et al. *Proc 7th ISMRM* 1999; 388

Fast Calculation of LV Mass and Volumes Using Guide Point Modeling

A.A. Young,[1] B.R. Cowan,[1] S.F. Thrupp,[1] W.J. Hedley,[1] L.J. Dell'Italia.[2] [1]*University of Auckland, Auckland, New Zealand;* [2]*University of Alabama at Birmingham*

Introduction: Although MRI is a useful tool for the noninvasive assessment of 3D heart wall motion, the clinical utility of cardiac MRI is currently limited by the prohibitively long time required for image analysis. We describe a method for accurate estimation of global cardiac function in less than 5 minutes, based on a 3D mathematical model of heart geometry and motion.

Methods: Guide Point Modeling A finite element model was used to represent the geometry of the LV. This model was similar to ones used previously to describe LV deformation (1). The model consisted of 16 elements, each with cubic interpolation in the circumferential and longitudinal directions. A polar coordinate system was used for the model parameters, as described in (1). Guide points were interactively placed on the images by the user and the 2D image coordinates converted to 3D coordinates using the slice position information encoded in the image header. The model shape was fitted to the 3D guide point positions by minimizing an error function consisting of the sum of a smoothing term and a data penalty term. As the user placed or modified guide points, the model fit was updated in real time. The user continued to interactively add or modify guide points until the model-image intersections provided a good representation of the boundaries of the LV (Figure 1).

Experimental Studies The method was applied to a group of healthy volunteers (n = 15, 10 male, average age 23) and a group of patients imaged at two weeks and three months after their first acute Q wave myocardial infarction (n = 13). Details of the patient group and imaging parameters can be found in Johnson et al. (2). Phase contrast images of the ascending aorta were also obtained for the normal volunteers, allowing independent calculation of stroke volume in these subjects.

Guide point models were created by two operators for each of the normal volunteers and MI patients, in order to provide an estimate of inter-observer error. Papillary muscles were excluded from the myocardium and included in the blood pool. If desired, image information

could be incorporated into the process by allowing the model to deform under image-based forces.

Manual Contouring and Slice Summation: To validate the model results, inner and outer boundaries of the LV were manually defined on each image. As above, papillary muscles were excluded from the myocardium and included in the blood pool. The manual contours were reviewed by a second observer and a consensus was achieved in cases where there was a difference in opinion. Volumes were calculated from the contours by slice summation, using a custom software package. To compare the results with manual contours, the intersections of the model with each image slice plane were used as "model contours" and input into the same volume and mass calculation software. Mass was calculated as the difference between volumes enclosed by the endocardial and epicardial contours, multiplied by 1.05 g/ml.

Results: Figure 1 shows the result of the fitting process on typical short and long axis images of a normal volunteer. About 3–6 guide points per slice were required to obtain good correspondence with the original images. LV mass and volumes could be estimated within 5 minutes.

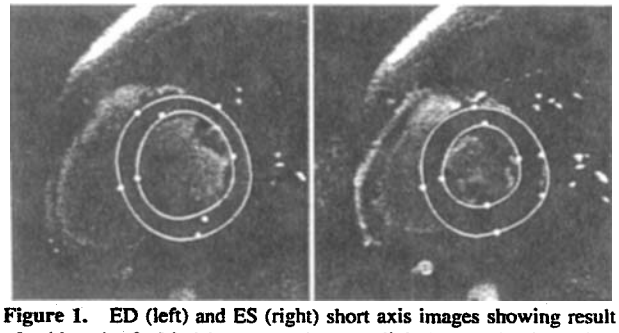

Figure 1. ED (left) and ES (right) short axis images showing result of guide point fit. Model contours shown as light lines and guide points shown as.

Table 1 shows the errors between modeling and manual methods, together with the inter-observer errors for the modeling method. All errors were within 5% of the measured values.

Table 1. Comparison Between Guide Point Modeling and Manual Contours

	Normal Volunteers (n = 15)				
	EDV	ESV	Mass	SV	EF
O1-MAN	4.8 ± 4.4*	4.6 ± 3.3*	1.3 ± 4.8	0.1 ± 5.9	−1.9 ± 2.6*
O2-MAN	0.7 ± 5.6	0.4 ± 4.3	1.3 ± 5.2	0.3 ± 4.4	−0.2 ± 2.4
O1-O2	4.1 ± 6.6*	4.2 ± 4.6*	0.1 ± 7.3	−0.1 ± 7.1	−1.7 ± 3.1
	MI Patients (n = 13)				
	EDV	ESV	Mass	SV	EF
O1-MAN	1.5 ± 3.5	2.7 ± 3.7*	2.5 ± 4.6	−1.1 ± 4.3	−1.5 ± 2.6
O2-MAN	1.6 ± 4.0	1.7 ± 2.6*	2.4 ± 5.3	−0.1 ± 4.7	−0.8 ± 2.1
O1-O2	−0.1 ± 4.6	1.0 ± 3.9	0.1 ± 6.3	−1.1 ± 4.9	−0.7 ± 2.8

EDV: End-diastolic volume (ml); ESV: end-systolic volume (ml); Mass: LV mass (g); SV: stroke volume (ml); EF: ejection fraction (%). O1 and O2 are the two operators of the modeling method, MAN refers to the manual contours. All values are mean difference ± standard deviation of the differences. *$p < 0.05$ for difference between estimates on paired t test.

The aortic flow calculated using the phase contrast (PC) images in the normal volunteers compared well with both the guide point modeling and manual contouring estimates of stroke volume (MAN vs. PC: 0.6 ± 5.4 ml; O1 vs. PC: 0.2 ± 9.0 ml; O2 vs. PC: 0.9 ± 7.7 ml).

Discussion: Although statistical differences exist in some of the functional indices between model and manual methods, and between observers for the modeling method, the magnitude of these differences are small in all cases and are unlikely to be clinically significant. These differences are likely due to small biases in contour placement by different users. The time saving obtained with the modeling method allows high resolution multiplanar MR studies of cardiac function to be efficiently utilized in routine clinical practice.

References

1. Young AA, Axel L. Three-dimensional motion and deformation of the heart wall: Estimation with spatial modulation of magnetization—a model-based approach. *Radiology* 1992; 185: 241–247.
2. Johnson DB, Foster RE, et al. Angiotensin-converting enzyme inhibitor therapy affects LV mass in patients with ejection fraction >40% after acute myocardial infarction. *Journal of the American College of Cardiology* 1997; 29: 49–54.

Errors in Defining End-Systole Cause Significant Errors in ESV Calculation in LV Cardiac MRI Analysis

B.R. Cowan,[1] A.A. Young,[2] C.J. Occleshaw,[3] S.F. Thrupp,[1] M. Bao,[1] L.J. Dell'Italia.[4] [1]*Department of Medicine,* [2]*Department of Anatomy with Radiology, University of Auckland, New Zealand;* [3]*Department of Radiology, Green Lane Hospital, Auckland, New Zealand;* [4]*Department of Medicine, University of Alabama*

Introduction: MRI is gaining increasing acceptance as an accurate method of determining end-diastolic volume (EDV), end-systolic volume (ESV), and left ventricular mass (LVM). In this study 8-9 parallel short axis scans were obtained through the left ventricle at between 11 and 25 phases in the cardiac cycle. The first phase following the R-wave trigger represented end-diastole, and typically the phase with the minimum volume is considered to represent end-systole. By segmenting the endocardial and epicardial boarders on these two phases, the EDV, ESV and LVM can be calculated.

Methods: A total of 50 patients were imaged at 7 days and 3 months after their first myocardial infarct with 8 or 9 short-axis non-breathhold slices (Phillips 1.5 Tesla, thickness = 8mm, NEX = 2, FOV = 350–475). A standard analysis was performed using the Mass program (version 1.0, University Hospital at Leiden). The data was then transferred to a separate site for detailed analysis where *all* of the approximately 18,000 images had an epicardial and endocardial contour drawn on them using the semi-automated software package Gnosis.[1] Every contour was then individually hand edited and stored. When complete, every slice was reviewed as an cine with the contours superimposed, and any additional errors identified were also hand corrected. This process was completed by two operators, and required a total of 18 months. The end-systolic phase was automatically determined for the detailed analysis by searching for the phase with the minimum total volume (sum of all slices). This end-systolic phase was then compared with that estimated in the standard analysis.

Results: Figure 1 shows that the correct phase was chosen in only 36% of cases and that a total of 33% were chosen too early. Figure 2 shows how the error in ESV rises as the selected phase deviates from its true value. Even at +/− 1 phase the error in ESV is 6% and this increases to 13% at +/− 2 phases.

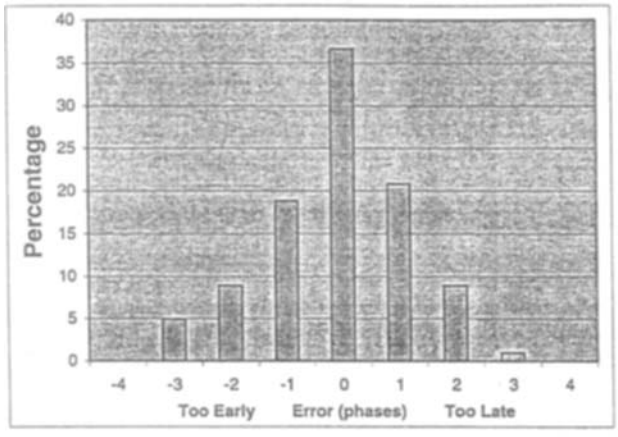

Figure 1. Histogram showing the frequency end-systole was identified correctly, too early (negative) or too late (positive) by the standard analysis.

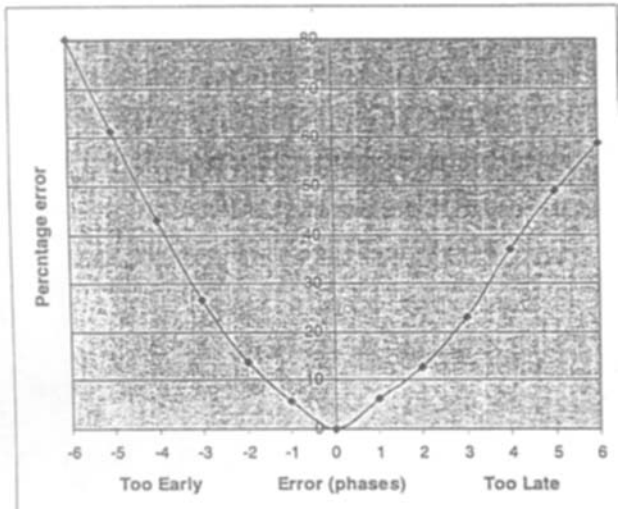

Figure 2. Average error in ESV for all studies as end-systolic phase deviates form its true value.

Discussion: Incorrectly choosing the end-systolic phase is due in part to the difficulty of estimating the exact time of end-systole from a cine loop, particularly when the left ventricular volume is changing relatively slowly. It is also tempting to use wall motion or wall thickening as the key indicator when it is blood volume that defines end-systole.

In a second study of 15 normal volunteers (10 male, aged 18–32 years) the phase containing the minimum area was determined for each of the 8–9 short-axis slices. Figure 3 indicates that the ESV for the mid-ventricular slices occurs 2 phases (80 msec) earlier than those at the base or apex.

In summary, significant error can be introduced into the determination of ESV by attempting to determine the end-systolic frame from a single cine loop. Ideally, more than one phase should be contoured and total volume calculated to confirm that the phase of minimum volume has been selected.

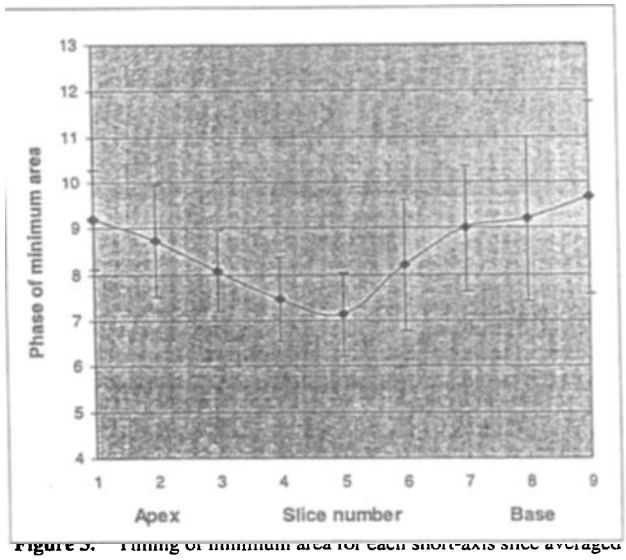

over 15 normal volunteers.

Reference

1. Singleton HR, Pohost GM. *MRM* 1997; 37: 418–24.

Correction of Through-Plane Motion Errors in Cardiac MR Volume Measurements

B.R. Cowan,[1] A.A. Young,[2] S.F. Thrupp,[1] T.L. Gentles,[3] R. Biosa,[3] C.J. Occleshaw.[4] [1]*Department of Medicine,* [2]*Department of Anatomy with Radiology, University of Auckland, New Zealand;* [3]*Department of Paediatric Cardiology,* [4]*Department of Radiology, Green Lane Hospital, Auckland, New Zealand*

Introduction: Tomographic imaging techniques have potential inaccuracies in LV volume measurement due to descent of the LV base through the fixed short-axis image planes during systole. Existing MR techniques either ignore this or simply discard the most basal short-axis slice during systole.

Methods: 15 healthy adults (mean age 23 years, range 18–32, 10 male) underwent both echocardiography and MRI within 24 hours. For the MR analysis, a plane was constructed in three-dimensional (3D) space to define the most basal extent of the LV at all phases of the cardiac cycle. The mitral valve plane (MVP) represents a natural landmark, and this was identified by the position of the hinge points of the mitral valve leaflets on three long-axis MR images.

The cavity and myocardial volumes were then calculated up to but not through this time-varying plane using standard mathematical techniques.

LV volumes were measured on echo using the area-length (AL) and Method-of-Discs (MoD) techniques, and were compared to those obtained from MR using no correction, a slice-omission technique (removing the most basal slice at end-systole) and the MVP corrected method.

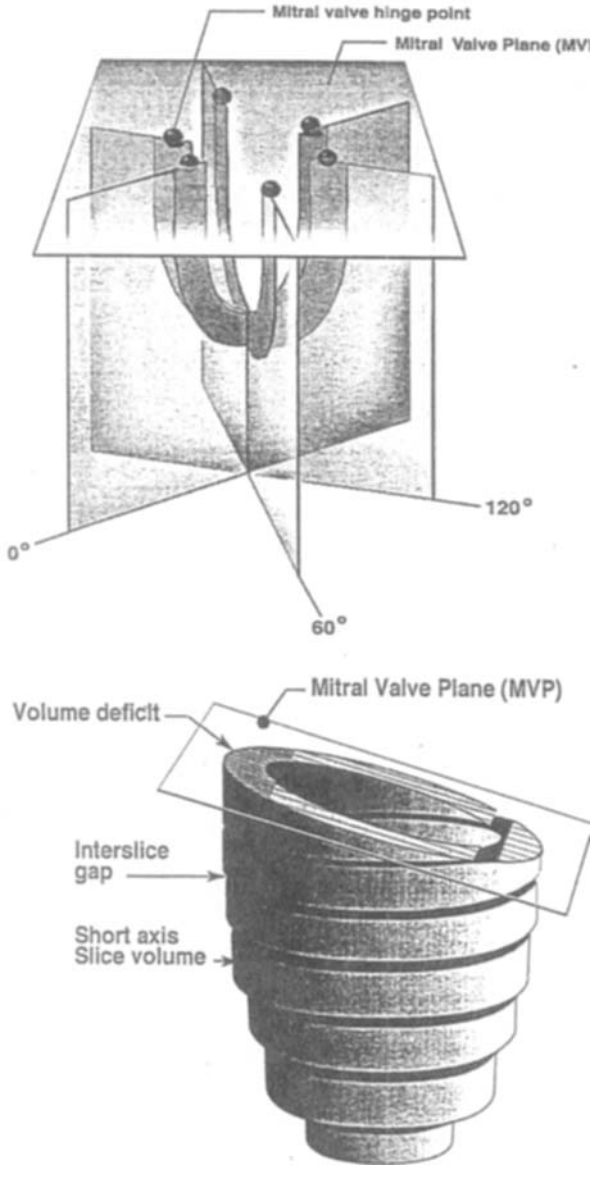

Results:

	EDV (ml)	ESV (ml)	EF %
MRI	140.0	51.4	63.3
MVP	(28.0)	(10.4)	(2.6)
MRI	142.8*	55.7*	61.0*
Slice-omission	(28.2)	(12.4)	(4.1)
MRI	142.8*	73.3*	48.8*
Uncorrected	(28.2)	(16.1)	(3.9)
ECHO	141.0	54.4	61.3*
AL	(31.6)	(12.2)	(3.4)
ECHO	118.3*	43.8*	63.0
MoD	(26.1)	(10.3)	(2.6)

Means and (std deviations). Results significantly different ($p < 0.05$) from the MVP method are indicated by*.

Without through-plane motion correction, the most significant error was the overestimation of the ESV (by 43%) and consequent underestimation of EF (from 63% to 48.8%). This is due to the descent of the base of the heart through the most basal imaging plane. The EDV was relatively unaffected by MVP correction because the most basal short-axis plane was planned to be aligned with the most basal extent of the ventricle on a long-axis scout acquired in diastole.

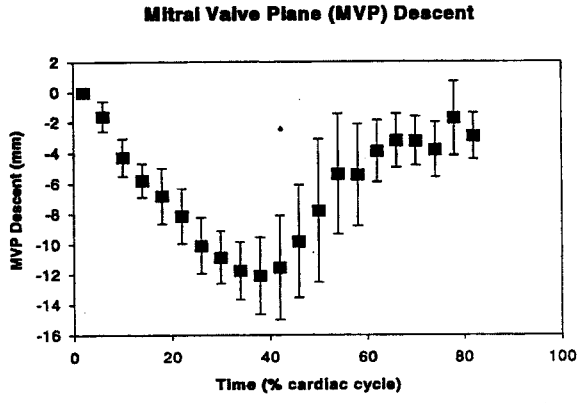

The average slice thickness (including the interslice gap) for the study was 11.5 mm (range 10–12.5mm) which was similar to the average maximum basal descent of 12.1mm and therefore the slice-omission technique produced a good estimate of ESV and EF. If the extent of basal descent were to change relative to the total slice thickness this agreement would be expected to deteriorate.

Increasing precision with this technique is potentially valuable in research studies requiring measurement of LV function, with a reduction in the number of subjects required, and resultant cost savings.

Reference

Rogers WJ, Shapiro EP et al. Circ 1991; 84: 721–31.

Enhanced Ventricular Function Following Repair of Coarctation of the Aorta is a Geometric Artifact Related to Concentric Hypertrophy

T.L. Gentles,[1] B.R. Cowan,[2] C.J. Occleshaw,[3] R. Biosa,[1] S.D. Colan,[4] A.A. Young.[5] [1]*Department of Paediatric Cardiology,* [3]*Department of Radiology, Green Lane Hospital, Auckland, New Zealand;* [2]*Department of Medicine,* [5]*Department of Anatomy with Radiology, University of Auckland, New Zealand;* [4]*Department of Cardiology, Children's Hospital, Boston, MA*

Introduction: Reports of enhanced LV contractility following repair of coarctation of the aorta (CoA) have used endocardial indices of LV shortening which overestimate myocardial fiber shortening in the presence of hypertrophy.

Methods: Echocardiography (Echo) and magnetic resonance imaging (MRI) were undertaken in 15 patients aged 19–26 years 17 to 23 years after repair of CoA, and in 15 age, body size, and gender matched controls. Echo M-mode LV dimension (D) and posterior wall thickness (h) were measured at end-diastole (ED) and end-systole (ES), and fractional shortening (FS) was calculated. Regional deformation was calculated by MRI using a 3-dimensional tissue-tagging finite element model that allows tracking of portions of myocardial volume through the cardiac cycle and therefore direct measurement of myocardial shortening.

Results: The Echo ED h/D ratio was elevated in CoA patients (0.18 ± 0.02 vs 0.15 ± 0.02, p = 0.002) indicating concentric hypertrophy. Importantly, the Echo FS was also elevated (37 ± 4.5% vs 33 ± 4.6%, p = 0.02) while MRI circumferential midwall shortening was not (21 ± 1.3% vs 21 ± 1.3%, p = NS). There was a positive relationship between ES h/D and Echo FS (r = 0.83, p < 0.001), but there was no relationship between h/D and MRI midwall shortening, indicating that FS increases in direct proportion to the degree of concentric hypertrophy.

Discussion: These data demonstrate that myocardial fiber shortening is normal after coarctation repair. The finding of elevated endocardial shortening is a geometric artifact, related to the thickness-dimension ratio and therefore exacerbated by concentric hypertrophy. Care should be taken when interpreting endocardial ventricular function indices in patients with concentric hypertrophy.

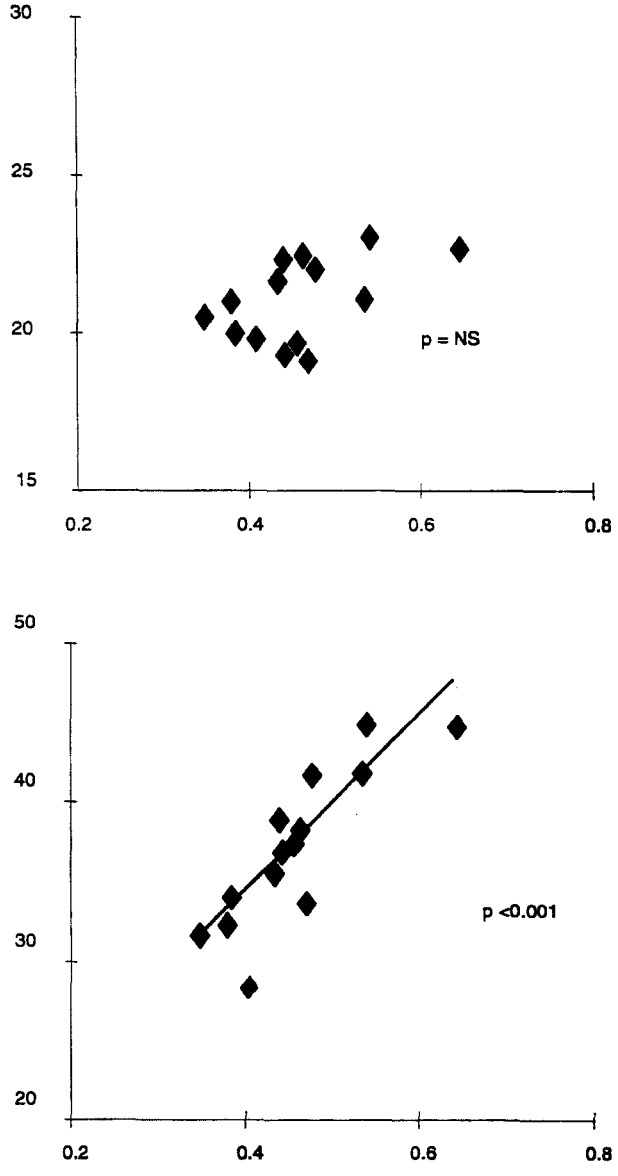

Four-Dimensional Magnetic Resonance Imaging of the Pulmonary Veins in Patients with Congenital Cardiovascular Disease

G. Wesley Vick, III, Raja Muthupillai. *Baylor College of Medicine, Houston, TX; Roxann Rokey, Marshfield Clinic, Marshfield, WI*

Assessment of pulmonary venous connections is an essential part of the evaluation of congenital cardiovascular disease. Three-dimensional virtual reality techniques have been employed to demonstrate the pulmonary veins. However, the phasic motions of the pulmonary veins and adjacent vascular and cardiac structures are not well defined by purely three-dimensional methods. New magnetic resonance imaging (MRI) techniques, which allow creation of a four-dimensional virtual reality representational model of the thorax and upper abdomen, can greatly facilitate delineation of the pulmonary veins.

Purpose: To assess four-dimensional computer MRI display methods in the evaluation of the pulmonary veins in patients with congenital heart disease.

Methods: Multiphasic bright blood segmented gradient echo acquisition sequences were employed. Relatively large anatomic blocks were imaged with multiple individually thin contiguous or overcontiguous sections acquired sequentially. Thin acquisition sections were utilized to maximize the flow signal from each slice. Echo times were varied to optimize the contrast effects of regions of turbulent blood flow. The number of shots per acquisition was minimized by the use of high-performance magnetic field gradient coils. After acquisition, slices were electronically rearranged into separate multislice slabs for each cardiac phase. The slabs were then individually projected or rendered in each of multiple orientations. Two primary processing methods were utilized:

1) A generalized ray-casting algorithm with depth cueing and variable voxel opacity was used to generate non real-time projections. Corresponding projections were automatically performed sequentially to simulate the phasic motion of the original cardiovascular structures. Sequences of projections from multiple adjacent viewing angles were saved as digital movies in standard computer formats and replayed as continuous loops.

2) Object space volume rendering was performed with specialized texture mapping computer graphics hardware. This approach facilitated real-time rendering and display of the slabs, optimization of voxel transfer function, and positioning of clipping planes. Over 200 studies were performed with these methods in patients with congenital cardiovascular disease. Malformations identified included partial anomalous connection of the right upper pulmonary vein to the superior vena cava (n = 5), partial anomalous connection of both right upper and right lower pulmonary veins to the right atrium (n = 4), partial anomalous connection of the left upper pulmonary vein to the innominate vein (n = 3), partial anomalous connection of the right upper and right lower pulmonary veins to the inferior vena cava (right-sided scimitar syndrome) (n = 3), partial anomalous connection of the left upper and left lower pulmonary veins to the inferior vena cava (left-sided scimitar syndrome) (n = 1).

Results: Four-dimensional displays were compared to standard MRI displays. In every instance, the four-dimensional displays provided additional information. Differentiation between pulmonary veins, pulmonary arteries, and systemic veins was facilitated by identification of disparities in their phasic motion. Four-dimensional displays further enhanced delineation of pulmonary veins by differentiating overlapping structures. Four-dimensional displays of excellent quality were produced automatically and with minimal human interaction. Additional patient imaging time was not required for generation of these displays. The ray-casting method achieved excellent results and had the advantage of being implementable with advanced personal computers. The object space volume rendering method had the advantage of providing real-time interactive parameter manipulation during

processing but had the disadvantage of requiring a specialized workstation.

Conclusion: Four-dimensional displays of multiphasic MRI datasets are an important enhancement of representational imaging of the pulmonary veins. Four-dimensional displays should be routinely employed to delineate pulmonary venous anatomy in patients with congenital cardiovascular disease.

MRI-Based 3D Regional Circumferential Wall Stress Changes from Partial Left Ventriculectomy

B. Sturm,[1] E.O. Carew,[2] K.A. Powell,[2] P.R. Schvartzman,[2] R.D. White.[2] [1]*The Ohio State University, Columbus, OH*; [2]*The Cleveland Clinic Foundation, Cleveland, OH*

Background: Janz's method for regional circumferential wall stress (CWS) evaluation (1) is based on a two-dimensional long-axis view of the left ventricle (LV). By taking advantage of the three-dimensional (3D) nature of magnetic resonance imaging (MRI), multiple long-axis sections of a LV can be generated through post-processing. These sections can then be grouped into regions based on anatomical landmarks (2). This approach was used to evaluate regional CWS in patients before and after partial left ventriculectomy (PLV) (3) for whom a reduction in global wall stress had been reported after PLV, but no regional analysis has been performed.

Methods: Data acquisition. Eight dilated cardiomyopathy (DCM) patients were imaged using dynamic cardiac MRI before (Pre) and three months (Post) after PLV. Nine healthy volunteers (Normal) were also imaged. The images were acquired on a commercially available 1.5 Tesla whole-body scanner with a phase-array chest coil. A segmented k-space and view-shared gradient-echo pulse sequence was used for the acquisition of cine image-loops. The data sets consisted of tomographic short-axis cine loops encompassing the whole LV and at least one long-axis view. The image matrix was 256 × 256 pixels with an in-plane resolution of 1.25 × 1.25 mm and a 10 mm slice thickness.

Pressure Measurements. The end-systolic LV intracavitary pressure was approximated as the mean peak-systolic blood pressure measurements obtained from a cuff measurement during imaging. The right ventricular pressure was obtained invasively during intervention in the Pre and Post cases, but was unavailable for the Normal cases.

Processing. The end-systole (ES) phase of each cine-loop was identified and the endocardial and epicardial borders of the LV were traced manually. The outlines were fitted with 3D spline surfaces. Ninety long-axis views were generated by identifying the intersections of the spline surfaces with a set of long-axis planes spanning the LV. Regional CWS was calculated as $\sigma = P_{ES}(A_c/A_w)$, where σ is the CWS, P_{ES} is the transmural ES pressure, A_c and A_w are the cavity and wall areas in the region of interest (1). The LV was divided into sixteen regions (2): three longitudinal (base, mid, and apex) sections which were further divided into six (base and mid) and four (apex) circumferential regions (see Table 1). Regional CWS values obtained for each plane were averaged over the sixteen regions. The CWS values observed in the Pre and Post cases were compared to each other and to those obtained in the Normal cases using a Student t-test (a value of $p \leq 0.05$ was considered statistically significant).

Results: The regional CWS results are reported in Table 1. Significant decreases in CWS were observed in the anterior region of the basal section, the anterior septum, the inferior septum, inferior, and anterior regions of the mid section, and all four regions of the apical section. The CWS values observed in the Pre and Post cases were significantly larger than in the Normal cases.

Table 1. Regional CWS ± S.D. in kdynes/cm²

Region	Pre	Post	Normal
BASE			
Anterior Septum	198 ± 49	223 ± 77	N/A
Posterior Septum	229 ± 66	201 ± 102	N/A
Posterior	355 ± 62	273 ± 86	150 ± 30 #†
Posterior Lateral‡	272 ± 101	255 ± 68	120 ± 19 #†
Anterolateral	269 ± 82	237 ± 77	112 ± 34#†
Anterior	324 ± 95	220 ± 52*	122 ± 29#†
MID			
Anterior Spetum	181 ± 40	137 ± 44*	N/A
Inferior Septum	222 ± 62	160 ± 59*	N/A
Inferior	466 ± 95	293 ± 47*	142 ± 29#†
Inferolateral‡	330 ± 40	335 ± 105	124 ± 23#†
Anterolateral	304 ± 106	291 ± 98	132 ± 43#†
Anterior	325 ± 77	216 ± 70*	141 ± 49#†
APEX			
Septum	265 ± 86	191 ± 86*	N/A
Inferior	450 ± 125	307 ± 126*	108 ± 46#†
Lateral	410 ± 153	270 ± 100*	94 ± 33#†
Anterior	536 ± 114	301 ± 118*	109 ± 26#†

‡ PLV site, * $p \leq 0.05$ Pre vs. Post, # $p \leq 0.05$ Pre vs. Normal, † $p \leq 0.05$ Post vs. Normal

Conclusions: The proposed method for 3D regional CWS calculations was successfully applied to the Pre, Post, and Normal populations. The results show that the reduction in CWS due to PLV is not global but concentrated in the apical section of the LV and the regions of the mid section of the LV in and around the septum. Furthermore, the Post CWS values remained larger than those observed in the Normal cases.

References

1. Janz RF. *Am J Physiol* 1982; 242: H875–81
2. Schiller NB, Shah PM, Crawford M, et al. *J Am S Echocardiography* 1989; 2: 358–67.
3. McCarthy PM, Starling RC, Wong J, et al. *J Thorac Cardiovasc Surg* 1997; 114: 755–63

Reproducibility of MRI Assessment of Left Ventricular Volume, Mass and Systolic Function in Overweight and Obese Subjects

C.J. Salton, M.L. Chuang, P.G. Danias, K.V. Kissinger, W.J. Manning. *Beth Israel Deaconess Medical Center and Harvard Medical School, Boston, MA*

Introduction: Obesity presents technical challenges to conventional cardiac imaging modalities and is often associated with suboptimal study quality. Obesity is also associated with excess cardiovascular disease and is widely prevalent in the general population, as approximately one-third of the population of the United States is obese (BMI > 30 kg/m²). Furthermore, a substantial fraction of the general population is overweight ($25 \leq$ BMI < 30 kg/m²). Cardiac magnetic resonance (MR) can provide high image quality datasets despite subject obesity and imaging plane orientation is not constrained by body habitus. We therefore hypothesized that MR can be of particular value for determination of ventricular size and function in obese (OB) and overweight (OW) individuals. This study was performed to compare observer reproducibility in OB and OW subject groups with reproducibility in lean (BMI < 25 kg/m²) subjects.

Methods: Subjects: Twenty-six clinically healthy adults (aged 46 ± 17 yrs) comprised three subject groups: LEAN (n = 8, 5M, 3F); over-

weight, OW (n = 9, 7M, 2F) and obese, OB (n = 9, all M). All subjects were in sinus rhythm, did not have contraindications to MRI and were scanned after obtaining written informed consent.

Imaging: was performed on a 1.5-T Gyroscan ACS/NT whole-body system (Philips Medical Systems, Best, The Netherlands) using a 5-element cardiac array coil. The left ventricle (LV) was covered by a stack of contiguous 10-mm thick slices in the cardiac short-axis orientation using a hybrid gradient echo-echo planar FFE-EPI cine sequence (TR = RR, TE = 9ms, 1.5 × 2.5-mm² in-plane resolution).

Data Analysis: Endocardial borders were manually segmented at end-diastole and end-systole by two experienced observers blind to subject BMI and each other's results. LV volumes were determined by summation of disks and ejection fraction (EF) was computed. Epicardial borders were also traced at end-diastole for LV mass calculation.

Statistical Analysis: Interobserver variation was assessed using a Bland-Altman limits of agreement analysis and by computation of coefficients of variation (mean squared differences between observations divided by mean observed values). Mean absolute differences between observers for each subject group were compared by 2-tailed Student's t-test with Bonferroni correction, a value of $p \leq 0.05$ was considered significant.

Results: Scanning was completed, yielding images independently deemed suitable for analysis by both observers, in all 26 subjects. BMI values by group were as follows (Mean ± SD): LEAN = 22.7 ± 1.6, OW = 27.7 ± 0.9, OB = 32.7 ± 2.2. Summary values by group for Observer#1 are presented in Table 1; there were no significant differences in LV volumes, EF or mass between subject groups. Bland-Altman results did not reveal systematic biases between observers (mean differences were small), and 95% confidence intervals indicated good agreement between observers (Table 2). Coefficients of variation are presented in Table 3. Figure 1 shows mean absolute differences between observers. There were no significant differences ($p > 0.22$ for all comparisons) between subject groups.

Table 1. Summary Values (Mean ± SD) for Subjects Grouped by BMI

	LEAN	OW	OB
EDV (ml)	131 ± 30	106 ± 28	137 ± 40
ESV (ml)	43 ± 17	39 ± 15	43 ± 13
EF (%)	68 ± 6	64 ± 6	69 ± 4
Mass (g)	148 ± 39	155 ± 32	160 ± 25

Table 2. Limits of Agreement (Mean Difference ± 2 SD) Between Two Independent Observers

	LEAN	OW	OB
EDV (ml)	1.3 ± 12.6	−3.6 ± 11.2	0.8 ± 13.7
ESV (ml)	−0.2 ± 6.5	−0.1 ± 5.9	1.5 ± 3.6
EF (%)	0.3 ± 3.8	−1.2 ± 4.7	−1.3 ± 4.5
Mass (g)	1.5 ± 10.8	2.1 ± 13.5	−1.9 ± 15.8

Table 3. Coefficient of Variation Between Observers for Each LV Parameter and Subject Group

	LEAN	OW	OB
EDV	7.6%	5.9%	4.8%
ESV	7.1%	7.2%	5.3%
EF	2.6%	3.9%	3.5%
Mass	3.6%	4.4%	4.8%

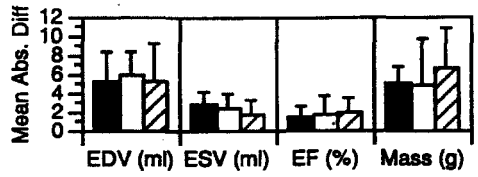

Figure 1. Mean absolute differences between observers for LEAN (black), OW (white) and OB (hatched) groups. The error bars represent 1 standard deviation.

Conclusions: Left ventricular volumes, EF and mass were determined with high interobserver reproducibility regardless of BMI among the 26 subjects in this study. MR assessment of LV size, mass and systolic function is not degraded in obese and overweight subjects. In contrast to other imaging modalities, MR therefore offers advantages across all types of body habitus.

Effect of Papillary Muscles and Trabeculae on Left Ventricular Parameters in Cine-Magnetic Resonance Images (MRI)

T. Ibrahim, C. Weniger, M. Schwaiger. *Department of Nuclear Medicine, Technical University Munich, Munich, Germany*

Background: MRI provides an excellent technique for evaluation of left ventricular (LV) function. Because of high resolution and good contrast between blood and myocardium it is sensitive to detect even small myocardial trabeculae. The purpose of this study was to investigate the effect of papillary muscle (PM) and trabeculae (TB) on LV parameters.

Methods: ECG-gated, short axis, breath hold gradient echo cine images (Philips ACS 1.5 T) were acquired in 52 healthy subjects (21 males, 39.5 ± 15.5 years) with 12 phases and a slice thickness of 8 mm covering the entire left ventricle. MR data were transferred to UNIX workstations. Endo- and epicardial contours were manually traced using MASS-software. All subjects were analyzed three times. Papillary muscles were both included as well as excluded from the bloodpool. Contours were also drawn excluding trabeculae. Based on these three contour sets, LV enddiastolic (ED) and endsystolic (ES) volumes, ejection fraction (EF) and LV-mass were calculated.

Results: We obtained very homogeneous LV parameters within the different analysed groups independent of gender and age of the subjects (Table 1).

Inclusion of PM to the bloodpool results in systematic higher ED as well as ES volumes and lower LV mass compared to exclusion of PM and TB ($p < 0.001$). Calculation of LV EF showed significant lower values, when PM were included into the bloodpool compared to exclusion ($p < 0.001$). Exclusion of TB from the bloodpool results in the highest EF values ($p < 0.001$) (Table 1). The coefficient of variation for EF ranged between 6–8% in all analyzed groups. LV volumes and mass yielded excellent results comparing the different analysis ($r > 0.95$).

Conclusion: Left ventricular papillary muscle and trabeculae significantly affect quantitative global LV parameters. Depending on the defined analysis, a comparison of these parameters should therefore be applied to corresponding normal databases.

Table 1. Effect of Papillary Muscles and Trabeculae on Left Ventricular Parameters.

	PM Included	PM Excluded	TB Excluded
ED Volume	130.8 ± 33.4	120.8 ± 31.7	101.1 ± 27.8
ES Volume	51.2 ± 15.5	42.4 ± 14.3	32.6 ± 11.1
EF Volume	60.9 ± 3.7	65.2 ± 4.4	68.2 ± 4.8
Mass	110.6 ± 23.1	118.7 ± 23.0	129.7 ± 25.1

Quantitation of Regional Myocardial Blood Flow: Comparison Between Magnetic Resonance Imaging (MRI) and Positron Emission Tomography (PET)

Tareq Ibrahim,[1] Stephan Nekolla,[1] Karin Schreiber,[1] Kenichi Odaka,[1] Stefan Volz,[2] Martin Güthlin,[2] Wolfram Delius,[2] Markus Schwaiger.[1]
[1]*Department of Nuclear Medicine, Technical University Munich, Germany;* [2]*Department of Cardiology, Bogenhausen Hospital Munich, Germany*

Background: Dynamic contrast enhanced MRI allows noninvasive estimation of myocardial blood flow (MBF). The purpose of this study was to determine regional MBF in patients with coronary artery disease (CAD) by both MRI and quantitative PET analysis.

Methods: A dynamic ECG-gated fast gradient echo sequence (3 short axis slices; 5 elements phased array cardiac coil; Philips ACS 1.5 T) with a Gd-DTPA bolus injection (0.05 mmol/kg) was performed at rest and under adenosine stress (140 µg/kg/min) of 6 min. duration in 25 patients (19 M; 63 ± 7 years) with angiographically proven CAD. All patients also underwent dynamic PET N-13 ammonia studies at rest and under adenosine stress. MRI time intensity-curves were fitted to measure maximal upslope. Upslope ratio (USR; stress vs. rest) was calculated as an index of coronary flow reserve (CFR). Polar maps were generated and regional USR was compared in 3 vessel regions to a normal database constructed of 20 healthy subjects, angiographic findings and CFR of dynamic PET analysis.

Results: Regional USR averaged 1.45 ± 0.33 in patients and 2.01 ± 0.46 in healthy subjects. MRI-USR was significantly lower than PET-CFR (2.21 ± 0.84) ($p < 0.05$). Both parameters correlated with the severity of stenoses (Table 1). Using a cutoff of 1.2θ, coronary artery stenoses ≥75% were detected with sensitivity and specificity of 78% and 89%, respectively.

Conclusion: With contrast enhanced MRI flow measurements detection as well as severity assessment of regional coronary artery disease is possible.

Table 1. MRI-USR and PET-CFR in Comparison to Angiography

Stenosis	0%	≤50%	50–74%	≥75%
MRI USR	1.59 ± 0.27	1.50 ± 0.26	1.35 ± 0.38	1.13 ± 0.17
PET CFR	2.26 ± 0.76	1.93 ± 0.42	1.87 ± 0.43	1.64 ± 0.45

Detection of Regional Myocardial Ischemia by Combined MR-Perfusion and Wall Motion Analysis

Tareq Ibrahim,[1] Stephan Nekolla,[1] Carmen Weniger,[1] Karin Schreiber,[1] Stefan Volz,[2] Martin Güthlin,[2] Wolfram Delius,[2] Markus Schwaiger.[1] [1]*Department of Nuclear Medicine, Technical University Munich, Germany;* [2]*Department of Cardiology, Bogenhausen Hospital Munich, Germany*

Background: MRI provides morphological and functional assessment of the left ventricle (LV). The purpose of this study was to investigate the feasibility of a combined MR-myocardial perfusion and wall motion analysis during the same adenosine stress and to determine the diagnostic value in comparison to coronary angiography.

Methods: We examined 16 patients with angiographically proven coronary artery disease (Philips ACS NT 1.5T). All patients underwent both a 3 short axis slice ECG-gated cine-gradient echo sequence (12 phases) as well as a corresponding dynamic contrast enhanced fast gradient echo sequence (Gd-DTPA bolus 0.05 mmol/kg). Both techniques were performed successively at rest and during the same adenosine induced stress (140 µ/kg/min) of 6 min. duration. Maximal upslope ratio (USR) was calculated from MRI-time intensity curves by dividing stress/rest. LV-ejection fraction (EF) and quantitative regional wall motion was calculated from cine-MRI. All parameters were analysed in 3 vascular territories and compared to a normal database constructed of 17 healthy subjects and to angiographic findings.

Results: EF did not significantly change under stress condition in healthy subjects as well as patients. Coronary artery stenoses ≥75% were detected with sensitivity and specificity of 64% and 82% by MRI wall motion analysis and with 77% and 94% by MRI perfusion analysis, respectively. A combination of wall motion and perfusion increased sensitivity to 93% while specificity decreased to 79%.

Conclusion: With MRI almost simultaneous assessment of regional myocardial perfusion and wall motion is feasible. A combination of different functional tests can increase the diagnostic accuracy in suspected coronary artery disease.

Quantitation of Three-dimensional Right Ventricular Systolic Deformation: Normal and Hypertrophic Hearts

I. Haber, V.A. Ferrari, D.N. Metaxas, L. Axel. *Philadelphia, PA*

Introduction: Right ventricular (RV) motion is difficult to study due to its complex geometry, normally thin wall (<5mm), and regional variation in contraction patterns. Tagged 2D MRI images have previously been used to study the deformation of the RV in normal (1,2,3,4) and hypertrophic (2) states. However, the tomographic images do not capture through-plane motion. For example, the base of the RV exhibits significant motion towards the apex (17–19mm) (5). Techniques which reconstruct 3D motion of the midwall surface of the RV free wall (6), or the volume of the biventricular unit (5), can provide a relatively dense set of 3D deformation information regardless of image plane locations. We here demonstrate the utility of 3D measurements of RV motion by applying the latter technique to data from multi-view planar tagged MR images of both normals and patients with right ventricular hypertrophy (RVH).

Methods: In previous work, we have developed a volumetric 3D motion reconstruction technique which accounts for through-plane motion and the geometric complexity of the RV (5). This method uses tag and contour data extracted from multiple images with a custom software package (7). The motion of model points, or nodes, is recovered by fitting a biventricular finite element mesh to this data. The method was previously validated by applying the technique to synthetic data generated from known deformation with resulting errors of approximately 0.5mm.

This technique was used to evaluate systolic RV and septal 3D deformation in 3 normals and and 3 patients who were diagnosed with RVH by echocardiography. Images were acquired with a 1.5 T clinical MR system (Signa, GE Medical Systems, Milwaukee, WI) using an ECG-gated fast gradient echo technique. The slice thickness was 6mm with a spacing of 2mm between short-axis (SA) image planes and 20 degrees between long-axis image planes. In order to quantify the deformation of the RV free wall and septum, we calculated homogeneous strains numerically in each finite element, given the deformation at the nodes. The strain tensor was used to derive: 1) E3: magnitude of the minimum principal strain, or greatest contraction; 2) α_{E3}: angle between the minimum principal directions and the SA image planes, (0° = strain direction aligned with short-axis image planes; 90° = longitudinal direction); 3) %S: $(100\% * (1 - \sqrt{2E3})$, 3D %shortening; and 4) % S_{SA}: component of principal %shortening in the SA image planes.

Results:

Table 1. Volume-Averaged E3, Angle Between E3 Direction and SA Images (α_{E3}), 3D %Shortening (%*S*), and SA %Shortening ($\%S_{SA}$)

Volume-Averaged Deformation Variables						
	Free Wall				Septum	
	Normal					
Case	E3	%*S*	$\%S_{SA}$	α_{E3}	E3	α_{E3}
N1	−0.237	27.6	20.8	37.3	−0.200	27.8
N2	−0.231	26.6	20.9	39.2	−0.209	16.8
N3	−0.250	29.2	23.9	33.9	−0.235	17.6
			RV Hypertrophy			
H1	−0.161	17.6	16.1	16.0	−0.199	23.7
H2	−0.174	19.2	15.0	38.5	−0.185	27.5
H3	−0.121	13.0	11.4	25.7	−0.134	23.9

The results for each normal and RVH patient are shown in Table 1.

A comparison of the results calculated in the normal free wall and septum reveals that the free wall exhibited greater contraction (more negative E3) and in a direction more oblique to the short-axis image planes (greater α_{E3}). The calculated $\%S_{SA}$ for the free wall were similar to those of previous MRI planar studies (1,2,4). However, this quantity was an average of %21 less than 3D %S.

All hearts with RVH exhibited a significant change in E3 ($p < .01$), and two patients exhibited a prominent decrease in α_{E3}. Similar changes in magnitude and direction of contraction was also seen by (6). The change in α_{E3} may be a result of the change in the fiber orientation seen during hypertrophy (8). The small number of cases precludes the use of a detailed statistical analysis.

Conclusion: A 3D motion reconstruction technique combined with tagged MR imaging provides potentially useful quantities. In this preliminary study, we found notable differences between normals and RVH patients. The fitting technique and motion quantitation can be easily adapted to 3D tagged MRI.

References

1. Nagel, E, et al, *Prov ISMRM* 1995.
2. Fayad, ZA, et al, *Mag Reson in Med* 1998, 39: 116–23.
3. Stuber, M, et al, *Proc ISMRM* 1995.
4. Klein, SS, et al, *Ann Bioeng* 1998, 26: 756–63.
5. Haber, I, et al, *Proc ISMRM* 1999.
6. Young, AA, et al, *Am J Physiol* 1996, 271: H2677–88.
7. Axel, L, et al, *Proc ISMRM* 1993.
8. Tezuka, F. *Tohoku J Exp Med* 1975, 117: 289–97.

MRI Evaluation of the Natural History of Heart Failure Subsequent to Reperfused Myocardial Infarction in a Mouse Model

W.D. Gilson, A.J. Ross, Z. Yang, S.S. Berr, B.A. French, J.N. Oshinski. *University of Virginia Health Sciences Center, Charlottesville, VA*

Background: Heart failure (HF) is an epidemic problem in the United States and is the single leading cause of hospital admissions. The burden that HF threatens to place on the US health care system makes it important to develop and test novel therapies directed against HF. Evaluation of novel therapies requires a realistic animal model of post-infarction HF and an accurate method to evaluate the effects of these therapies.

Purpose: In this study, we used cine MRI to evaluate the natural history of post-infarction HF in mice. Ejection fraction (EF) and left ventricular end-diastolic volume (LVEDV) were evaluated at several time points after experimental myocardial infarction (MI) in a series of mice.

Methods: Ten C57BL/6 mice were imaged at baseline (before MI). Six animals were subjected to a two-hour occlusion of the major left coronary artery followed by reperfusion. Mice were subsequently imaged at 1 day, and at 1, 2, and 4 weeks post-MI.

All imaging was performed on a Varian 200/400 VXR-S, 4.7T, 30 cm bore, MR system (Palo Alto, CA). A 2D FLASH sequence was used which collected 12 equally spaced phases per cardiac cycle. Resolution was 200 × 200 microns in-plane with a 1 mm slice thickness, TE was 3.9 ms and the flip angle was 20 degrees.

A custom-built 2.5 cm diameter Helmholtz receiver coil was used. ECG gating was achieved using 3 surface leads. No respiratory compensation was employed.

In each animal, single slice images were obtained in the vertical long axis and the horizontal long axis. Then, eight-to-ten slices were obtained in the short axis view and used for calculation of EF and LVEDV. EF and LVEDV were determined by manually tracing endocardial boundaries at end-systole and end-diastole using Image Pro Plus (Media Cybernetics, Silver Springs, MD), summing areas over all slices and multiplying by slice thickness.

Results: The mean baseline EF in the ten mice was 54 ± 2%. A precipitous drop in EF was noted one day after MI. The mean left ventricular EF was only 19 ± 1% at 4 weeks post-MI (Figure 1).

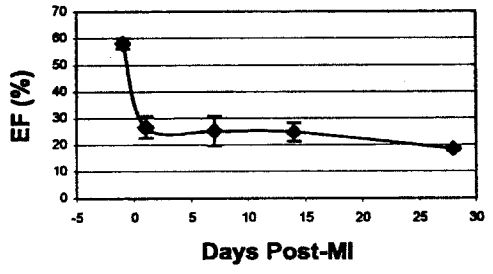

Concurrent with the drop in EF was an increase in LVEDV (Figure 2). The mean baseline LVEDV in the ten mice was 49 ± 3 μL. The LVEDV increased post-MI to 99 ± 15 μL at week 4. The majority of the early increase in LVEDV was completed by week 2.

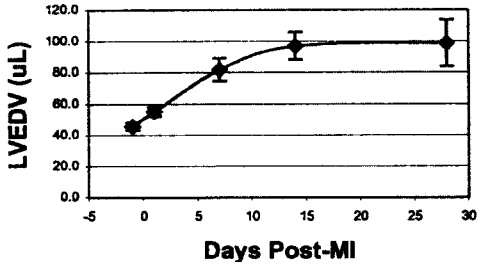

The dilatation of the LV and depression of LV function was accompanied by a loss of apical definition as shown in Figure 3. Figure 3a shows a horizontal long axis image before MI and Figure 3b shows a horizontal long axis image in the same mouse 4 weeks post-MI.

Conclusion: The ability of cardiac MRI to assess changes in EF and LVEDV make it an excellent choice for evaluating novel therapeutic approaches in small animal models of HF subsequent to MI.

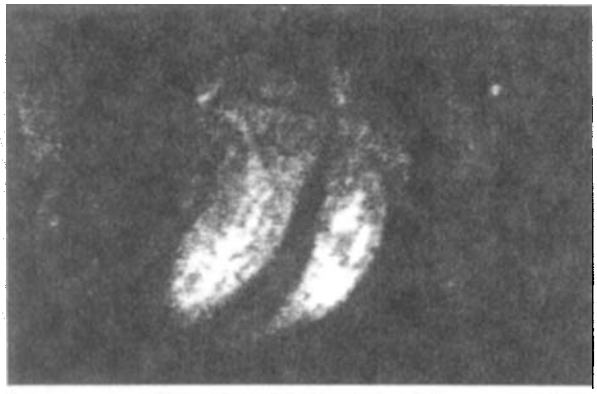

Figure 3a. Baseline before MI.

Figure 3b. Heart Failure, 4 weeks post-MI.

Complex Left Ventricular Angular Motion and Torsion Can Be Quantified Using High Frame Rate Tagged Cardiac Magnetic Resonance Imaging

C.H. Scott, B.S. Ivey, K.J. Duffy, V.A. Ferrari, D. Ivandjiiski, L. Axel, M.G. St. John Sutton. *University of Pennsylvania School of Medicine, Philadelphia, PA*

Introduction: Helical myocardial fiber orientation contributes to torsion of the left ventricle (LV) during systole. Limited assessments of torsion have been obtained using echocardiography, implanted markers and radially tagged MRI; however, temporal and spatial resolution have been low. We report the use of high frame rate 2D tagged MRI to evaluate the torsional motion of the normal LV.

Methods: Twelve normal subjects (mean age 32 ± 6, 9 male, 3 female) were screened by history, examination, and echocardiography before participation in the study. We used a fast segmented k-space MRI pulse sequence with tissue tagging (1) using the following parameters: cardiac frames = 30 − 40, field of view = 28cm, slice thickness = 6mm, acquisition matrix = 256 × 128, tag spacing = 6 mm, views per segment = 2, receiver bandwidth = 32KHz, TR = 6.7msec, TE = 1.8 msec. Five equally spaced short axis images were acquired using a clinical 1.5T scanner (Signa, General Electric Medical Systems). The ECG and respiratory bellows signals were combined using custom electronics and the result was used to suppress respiratory artifact during image acquisition (2). Angular displacement was defined as the change in angular position relative to the slice centroid of all tag intersections through the cardiac cycle. Torsion was defined as the difference in angular displacement between the most basal slice and each of the other slices. Differential torsion was defined as the difference in torsion between adjacent slices.

Results: During the first 80msec of systole, angular displacement was similar for all ventricular slices, implying an en block rotation of the ventricle (Figure 1). The more basal slice angular displacement began as positive but reversed direction early in systole, while the more apical slices continued to rotate in the same direction until end systole. In early systole, torsion was minimal. Torsion began to increase linearly only after the initial 80msec, and peaked at end systole. Maximum torsion was statistically different at each slice (Table 1). Differential torsion was similar from the base to the mid-apex, but apical differential torsion was increased.

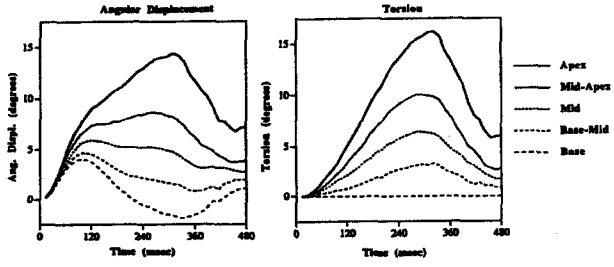

Figure 1. Mean angular displacement and torsion through the cardiac cycle. The base is used as the torsion reference.

Table 1. Mean ± SD of Maximum Torsion (MaxT) and Differential Torsion (DiffT) Values by Slice With the Base as Reference. All Values are in Degrees

	Base-mid	Mid	Mid-apex	Apex
MaxT	3.8 ± 1.5*	7.1 ± 2.0*	11.0 ± 2.7*	17.2 ± 5.3*
DiffT	4.1 ± 1.8	3.4 ± 1.0	3.7 ± 1.1	6.3 ± 2.9†

* $p < 0.001$ vs. all other slices. † $p < 0.04$ vs. all other slices.

Discussion: Helical fiber orientation is longitudinally oriented at the base and becomes more circumferentially oriented toward the apex (3). Torsion occurs as a result of the shortening of these helical fibers. In early systole, torsion is minimal due to bulk rotation of the LV and the base of the LV reverses direction during systole. Torsion increased from the base to the apex, and apical torsion is larger than expected if torsion were distributed linearly. This is consistent with the change in helical fiber orientation near the apex. High frame rate tagged MRI with cardiorespiratory gating allowing high temporal and spatial resolution evaluation of left ventricular torsion that may allow more accurate quantification of left ventricular systolic or diastolic function in many disease states.

References

1. Axel L, et al. *Radiology* 1989; 171: 841–5.
2. Yuan Q et al., *Proc Intern Soc for Mag Reson in Med*, 1998; Vol. 3: 2126.
3. Greenbaum RA. et al. *Br Heart J* 1981; 45: 248–63.

Magenetic Resonance Flow Measurements in Real Time: Comparison with a Standard Gradient Echo Technique

C. Klein,[1] E. Nagel,[1] B. Schnackenburg,[2] A. Bornstedt,[1] S. Schalla,[1] H. Lehmkuhl,[1] E. Fleck.[1] [1]*Internal Medicine/Cardiology, Charité, Campus Virchow, HU & German Heart Institute Berlin, Germany;* [2]*Philips Medical Systems, Hamburg, Germany*

Introduction: Magnetic resonance (MR) phase contrast velocity mapping offers a direct quantitative determination of flow dynamics which was shown in several in vivo and in vitro studies. With gradient echo techniques flow measurements covering the entire cardiac cycle (cine loop) can be acquired. However these techniques are very time consuming and require several minutes to acquire the data. In addition the results are averaged over several heart beats which prohibits the assess-

ment of short term changes of flow patterns which occur e.g. under pharmacological stress or during physiologic maneuvers. Furthermore, long acquisition times make these sequences sensitive to motion such as respiration which may significantly influence the results. To compensate for cardiac motion standard gradient echo flow measurements need to be ECG triggered causing a significant decay of image quality in patients with cardiac arrythmias such as atrial flutter or fibrillation or multiple ventricular premature beats because of large beat to beat variations. Faster gradients and new sequences allow an extremely fast data acquisition. The combination of turbo gradient echo and EPI allows to acquire high quality images of the heart in real time. The aim of the present study was to investigate the accuracy of a new real time sequence in measuring flow velocity (Vmax) and volume (VOL) in large and medium sized arteries and stenotic or insufficient cardiac valves.

Method: Vmax and VOL measured with the real time technique (RT) was compared with a standard gradient echo (FFE) sequence in the ascending and descending aorta, the common carotid and iliac artery and the mitral and aortic valve. The detail of the sequences are show in table 1.

Results: In all vessels and valves adequate flow images could be obtained (the images below show on top the anatomical images of the gradient echo (left) and of the real time technique (right) of the thoracic aorta and on the bottom the consecutive flow images).

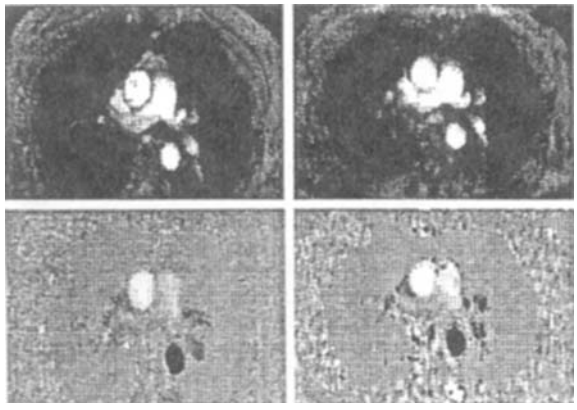

Table 1.

	FFE	RT
TR (ms)	14	15.5
TE (ms)	3.5	6.8
Flip angle	15	20
Field of view	300	300
Matrix[1]	115 × 128	64 × 128
Slice thickness (mm)	8	8
NSA	2	1
Temporal resolution (ms)	30	124
Spatial resolution (mm)	2.3 × 2.6	2.3 × 4.7
k-lines per shot	1	36
Encoded velocity (cm/sec)	200	200
EPI factor	—	9

Real time peak flow velocity measurements correlated well with the conventional cine phase-contrast data in large (n = 36) and medium sized (n = 33) vessels and cardiac valves (n = 12) with a correlation coefficient of 0.88, 0.81 and 0.88 respectively. For volume flow a correlation of 0.87 was found in large vessels. In contrast in medium sized vessels and cardiac valves only a weak correlation was found probably due to reduced spatial and temporal resolution.

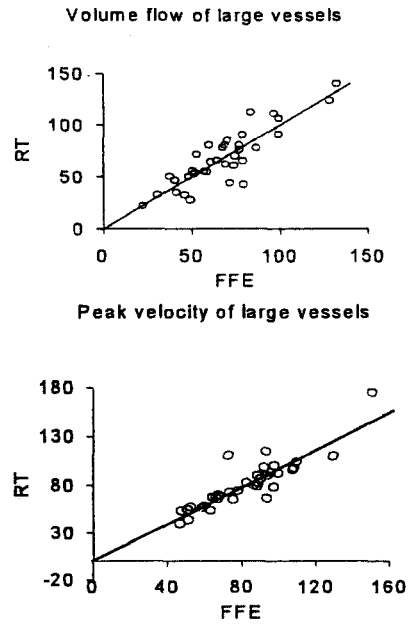

Conclusion: Real time flow measurements allow a reliable determination of peak flow velocity in large and medium sized vessels, as well as through cardiac valves and the determination of flow volume in large vessels. With the new technique scan time can be significantly reduced which is an important step towards the integrative examination of a patient. Further studies have to prove its accuracy in patients with arrhythmias.

First Experiences with the Blood Pool Contrast Agent Clariscan™ (NC100150 Injection) for Magnetic Resonance Coronary Imaging in Patients with Coronary Artery Disease.

C. Klein,[1] E. Nagel,[1] B. Schnackenburg,[2] A. Bornstedt,[1] V. Hoffmann,[3] A. Lehning,[3] S. Schalla,[1] E. Fleck.[1] [1]*Internal Medicine/ Cardiology, Charité, Campus Virchow, HU & German Heart Institute Berlin, Germany;* [2]*Philips Medical Systems, Hamburg, Germany;* [3]*Nycomed Amersham Imaging, Munich, Germany*

Introduction: 3D angiography of the proximal portion of the coronary arteries is possible with MR. However, certain limitations currently exist during noninvasive coronary artery imaging with MR which are partially due to a low signal and contrast to noise ratio. Without contrast agents, the contrast between blood and background tissue depends mainly on the inflow of unsaturated blood into the vessel and, thus, the signal in peripheral coronary arteries and distal to a severe stenoses is particularly low. Coronary artery imaging would, thus, benefit from a T1-shortening contrast agent. Currently, contrast agents, such as gadolinium diffuse rapidly into the interstitial space, and are, thus, not feasible for 3D coronary angiography which requires several minutes for data acquisition. An intravascular T1-shortening contrast agent would therefore be useful.

The aim of the present study was to test the safety and feasibility of Clariscan™ (NC100150 Injection) to visualise the coronary arteries in patients with suspected coronary artery disease and compare the results with images without contrast agent.

Method: Clariscan™ is a superparamagnetic iron oxide nanoparticle with an oxidized starch coating. Clariscan™ is a pure intravascular (blood pool) agent with both T1 and T2 shortening properties Twelve patients were examined with a 1.5 Tesla scanner (ACS NT, Philips,

The Netherlands,) in supine position using a 3D turbo gradient echo technique (TE 2.3 ms, TR 8 ms, flip angle 50, spatial resolution 0.7 × 0.9 × 1.5 mm, matrix 512 × 512, fat suppression). To suppress breathing motion artifacts a prospective navigator technique with real-time slice correction was used. Myocardial signal was suppressed with an inversion prepulse. Images were obtained at various doses of Clariscan™ (range from 1 to 5 Fe mg/kg body weight). To evaluate image quality signal to noise ratio between the coronaries (CSNR) and the aorta (ASNR), contrast to noise between coronaries and fat (CNR_{fat}) as well as coronaries and myocardium (CNR_{myo}) were calculated before and after administration of Clariscan™. Patients were monitored with a continuous 2 lead ECG and noninvasive blood pressure during the first two hours as well as ECG, vital signs, blood analysis and urinalysis 2, 24 and 72 hours after injection of the contrast agent.

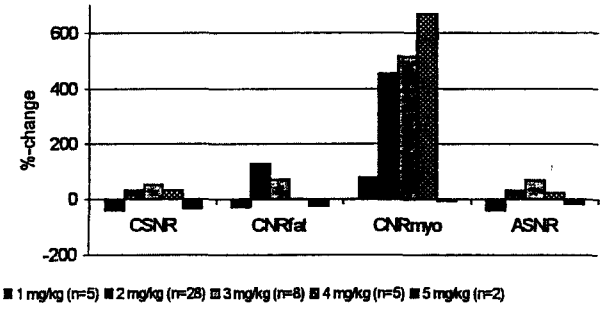

Figure 1. Percental change after different doses of Clariscan™.

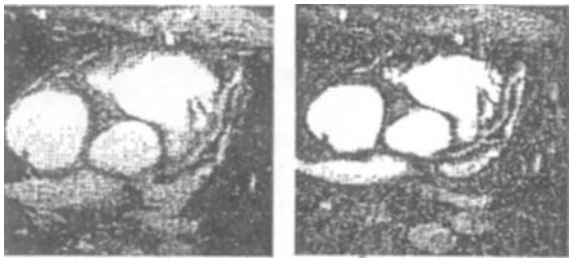

Results: Image quality was non diagnostic in one patient due to technical problems. Nineteen LAD, 7 RCA, 6 RCX and one ACVB were evaluated. In all patients, the use of Clariscan™ leads to an improvement of image quality (images above). CNR_{fat} improved up to a dose of 2 mg Fe/kg BW, SNR up to a dose of 3 mg Fe/kg BW and CNR_{myo} up to a dose of 4 mg Fe/kg BW ($p < 0.05$) (figure 1).

With higher doses a reduction of signal was observed probably due to the T2*-shortening effect and susceptibility artifacts were observed. Distal regions of the coronary arteries benefited particularly from the contrast agent (figure 2).

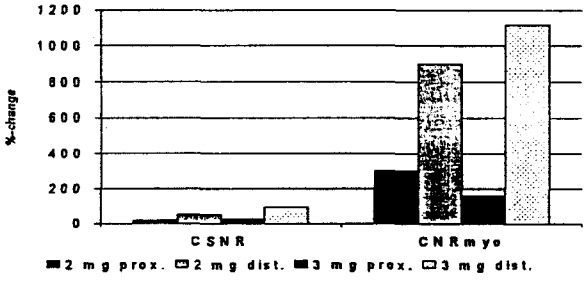

Figure 2. Differences in the Percental change after Clariscan™ In proximal and distal coronary arteries.

With Clariscan™ the visual length of the coronary arteries increased by 21.8 ± 23.1 mm. Clariscan™ was well tolerated by all patients. No drug related adverse event occurred.

Conclusion: In our experience Clariscan™ is safe, improves the signal and contrast to noise ratio of coronary arteries and makes the visualization of their more distal parts possible.

Myocardial Perfusion Reserve Early After Successful Revascularisation: Comparison of Stent and Balloon by Cardiac MR

N. Al-Saadi,[1] E. Nagel,[1] M. Gross,[1] C. Klein,[1] S. Schalla,[1] B. Schnackenburg,[2] E. Fleck.[1] [1]*Internal Medicine/Cardiology, Charité, Campus Virchow Clinic, Humboldt University, & German Heart Institute, Berlin;* [2]*Philips Medical Systems, Hamburg, Germany*

The initial morphological or functional degree of the success of a percutaneous transluminal angioplasty (PTCA) is not always optimal but can be improved by the use of intravascular stents (1). Several studies have shown a residual early impairment of myocardial perfusion reserve (MPR) in about 50% of the patients which has been mainly attributed to incomplete and inadequate dilatation of the stenotic coronary artery and to a lesser extent to alterations of vascular resistance and response (2). In general, evaluation of myocardial perfusion is promising in the follow up of these patients, since a reduction of myocardial perfusion is a sensitive sign of myocardial ischemia. The aim of this study was to evaluate the changes of MPR within 24 hours of a successful PTCA in patients with coronary artery disease.

Methods: Thirty five patients (27 male, 8 female, age 59 ± 10 years) with significant single or double vessel coronary artery disease (≥75% area stenosis) referred for elective PTCA were prospectively included. All patients underwent quantitative biplane, digital coronary angiography. PTCA was performed with or without stenting based on the decision of the physician performing the procedure.

Patients were studied with a 1.5 Tesla whole body MR tomograph (ACS NT, Philips, Best, The Netherlands), using a five-element phased array cardiac surface coil. After two surveys, a short axis view at the height of the origin of the papillary muscles was acquired using an ECG triggered T1-weighted inversion recovery single shot turbo-gradient echo sequence (inversion pulse, pre-pulse delay 360 ms, acquisition duration 360 ms, flip angle 15°, echo time 1.7 ms, repetition time 9 ms). Slice thickness was 8 mm with a spatial resolution of 1.7 × 1.9 mm. During an expiratory breath hold, a bolus of gadolinium-DTPA 0.025 mmol/kg body weight was injected via a central vein catheter. Dynamic images (one image per heart beat) were acquired during the first pass of the contrast agent before and after dipyridamole stress (0.56 mg/kg body weight for 4 minutes). The MR study was repeated within 24 hours after PTCA.

In all images the endo- and epicardial contours were traced. The myocardium was divided into 6 equiangular segments. Signal intensity was determined for all dynamics and segments. The upslope of the resulting signal intensity time curve was determined by the using a linear fit. The results were corrected for the input function by dividing the upslope of each myocardial segment by the upslope of the left ventricular signal intensity curve and perfusion reserve was calculated.

Using a previously defined ischemic threshold of 1.5 MPR (3) segments were classified as ischemic or non-ischemic.

Results: Fifty-two coronary artery stenoses were found by angiography. (LAD = 21, LCX = 15, RCA = 16). Two patients had triple vessel disease and were referred for surgical revascularization. In the remaining patients PTCA was successfully performed (residual stenosis of <75%) in all but two.

Before PTCA MPR was 1.13 ± 0.25 in segments supplied by a stenotic coronary artery and 2.18 ± 0.35 in control segments ($p < 0.001$). Sensitivity and specificity for the detection of significant stenosis were 89% and 83%.

After PTCA, MPR increased significantly in segments supplied by successfully treated vessels (1.07 ± 0.24 before and 1.89 ± 0.39 after PTCA, $p < 0.001$), however, it remained below the levels of the control segments ($p < 0.01$). Patients treated with stents (n = 18) showed a normalization of MPR (1.99 ± 0.36, vs. 2.18 ± 0.35, n.s.), whereas those treated with balloon PTCA only (n = 13) remained below the control group (1.72 ± 0.38, $p < 0.01$) and also below the patients treated with stents ($p < 0.05$). The increase of MPR was significantly higher in patients treated with stents (206 ± 67%,) when compared with those without (164 ± 49%, p = 0.02).

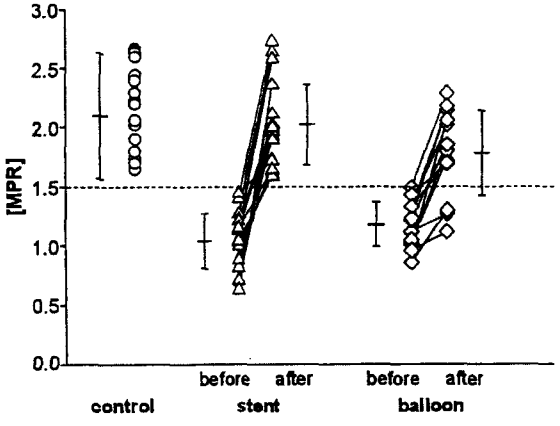

Conclusions: Cardiac MR perfusion measurements allow an accurate determination of MPR. Significant coronary artery stenoses can be detected with high diagnostic accuracy. After PTCA an improvement of MPR was found, which was more pronounced after stenting. This technique can be used for the follow up and control of revascularisation.

References

1. Serruys PW, di Mario C, Piek J, et al. *Circulation* 1997; 96: 3369–77.
2. van Liebergen RA, Piek JJ, Koch KT, et al. *Circulation* 1998; 98: 2133–10.
3. Al-Saadi N, Nagel E, Gross M, et al. *Circulation* 1999 (in press).

Comparison of Semiquantitative Perfusion Analysis with Cardiac Magnetic Resonance from Peripheral and Central Gadolinium-DTPA Injection Using a Linear Fit of the Upslope

N. Al-Saadi,[1] E. Nagel,[1] M. Gross,[1] B. Schnackenburg,[2] A. Bornstedt,[1] E. Fleck.[1] [1]*Internal Medicine/Cardiology, Charité, Campus Virchow Clinic, Humboldt University, & German Heart Institute, Berlin;* [2]*Philips Medical Systems, Hamburg, Germany*

Introduction: Most previous studies concerned with the analysis of myocardial perfusion from the signal intensity curves of the first pass of a gadolinium-DPTA (Gd) bolus with magnetic resonance imaging have used a gamma variate fit for (semi-) quantification (1). It was shown, that an adequate fit can only be performed if a very compact contrast agent bolus is administered, which requires central venous injection (2). We have recently shown, that a linear fit of the upslope of a contrast agent bolus administered into the superior vena cava yields reproducible and valid results in patients with suspected coronary artery disease (3). In this study we evaluate differences between central and peripheral injection of a contrast agent bolus, if a linear fit of the upslope is used for (semi-) quantification.

Methods: In 18 patients MR perfusion measurements were performed with a 1.5 T MR tomograph (Philips ACS NT) using fast gradient systems (23 mT/m amplitude, 105 T/m/sec slew rate) and a dedicated 5-element cardiac coil. Each heart beat 1 short axis view at the height of the origin of the papillary muscles was acquired during the first pass of 0.025 mmol/kg Gd using an ECG-triggered T1-weighted inversion recovery single shot turbo-gradient echo sequence (inversion pulse, pre-pulse delay 360 ms, acquisition duration 360 ms, flip angle 15°, echo time 1.7 ms, repetition time 9 ms). Slice thickness was 8 mm with a spatial resolution of 1.7 × 1.9 mm. During an expiratory breath hold, a bolus of Gd 0.025 mmol/kg body weight was injected. Dynamic images (one image per heart beat) were acquired during the first pass of the contrast agent.

The contrast agent bolus was injected into the superior vena cava via a central venous catheter. Twenty minutes later to allow clearance of the contrast agent, measurements were repeated with contrast agent injection into the right antecubital vein. In four patients perfusion reserve after vasodilation with dipyridamole (0.56mg/kg body weight for 4 minutes) was calculated for both, central and peripheral injection.

Using the MASS perfusion software (MEDIS) the endo- and epicardial contours were traced in all images. The myocardium was divided into 6 equiangular segments. Signal intensity was determined for all dynamics and segments. The upslope of the resulting signal intensity time curve was determined by the use of a linear fit. The results were corrected for the input function by dividing the upslope of each myocardial segment by the upslope of the left ventricular signal intensity curve (relative upslope) and perfusion reserve was calculated.

Intraobserver variability of the linear fit after central and after peripheral injection of Gd were determined in 100 segments each.

Linear regression and relative error were calculated for repeated injections and repeated measurements.

Results: intraobserver variability of the 100 segments for the determination of the linear upslope yielded excellent correlation for central ($r = 0.98$) and peripheral ($r = 0.96$) injection. Relative differences were 4.7 ± 5.4% and 11.3 ± 12.4% respectively (Fig. 1).

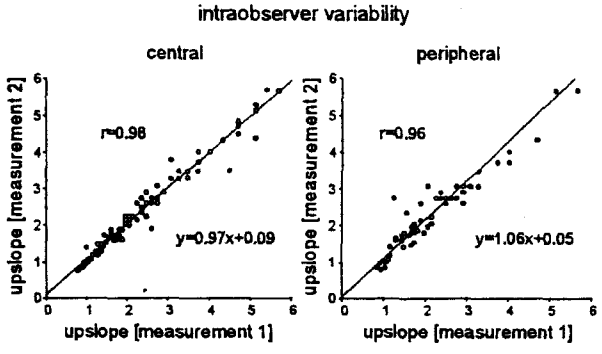

Central and peripheral Gd injection showed a close correlation for the relative upslope (n = 84 segments, $r = 0.91$, $p < 0.0001$) and for MPR (n = 24 segments; $r = 0.88$; $p < 0.05$) (Fig. 2). MPR in myocardial segments supplied by a stenotic coronary artery was significantly lower than in segments supplied by a nonstenotic coronary artery both in the central and peripheral group ($p < 0.001$).

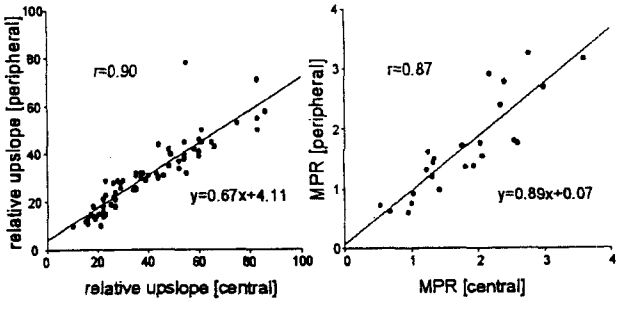

Conclusions: Peripheral injection yields reproducible results with minimal differences to central injection if the linear upslope of the signal intensity curves is used for (semi) quantification. This is in contrast to previous (semi-) quantification from a gamma-variate fit, which requires a central venous injection. This simple approach will facilitate perfusion measurements for clinical use.

References

1. Wilke N, Jerosch Herold M, Wang Y, et al. *Radiology* 1997; 204: 373–84. Wilke.
2. Keijer JT, van Rossum AC, Eenige MJ, et al. *Am Heart J* 1995; 130: 893–901.
3. N. Al-Saadi, E. Nagel, C. Klein et al. *Circulation* 1999 (in press).

Dobutamine Magnetic Resonance Myocardial Perfusion Reserve: A Step Towards the One-Stop-Shop

N. Al-Saadi,[1] E. Nagel,[1] M. Gross,[1] B. Schnackenburg,[2] A. Bornstedt,[1] E. Fleck.[1] [1]*Internal Medicine/Cardiology, Charité, Campus Virchow Clinic, Humboldt University, & German Heart Institute, Berlin;* [2]*Philips Medical Systems, Hamburg, Germany*

To circumvent the problems of absolute quantification of myocardial perfusion, myocardial perfusion reserve has been determined in several studies to assess myocardial flow (1). In these studies dipyridamole or adenosine for vasodilation were used, which have been shown to yield valid results. Vasodilators such as dipyridamole or adenosine are preferable for perfusion studies, as they induce maximal vasodilation with minimal influence on hemodynamics. In contrast dobutamine is superior for the induction of wall motion abnormalities (2). As dobutamine also increases myocardial perfusion by increasing coronary flow and cardiac work, it may also be used for the determination of perfusion reserve. This has been successfully demonstrated with PET and SPECT imaging and a good correlation to stenosis severity has been shown (3). The aim of the current study was to evaluate the value of dobutamine stress for the detection of significant coronary artery disease from the alterations of myocardial perfusion using magnetic resonance imaging.

Methods: To define normal values 24 myocardial segments in 5 patients without angiographic coronary artery disease (3male, 2 female, 53 ± 9 years) were studied. Then 23 patients (16 male, 7 female, 59 ± 8 years) with previously angiographically proven significant single (n = 14) or double (n = 9) vessel coronary artery disease were prospectively included. All patients underwent quantitative biplane, digital coronary angiography. Significant stenosis was determined as ≥75% area reduction.

Patients were studied with a 1.5 Tesla whole body MR tomograph (ACS NT, Philips, Best, The Netherlands), using a five-element phased array cardiac surface coil. After two rapid surveys, a short axis slice at the height of the origin of the papillary muscles was acquired using an ECG triggered T1-weighted inversion recovery single shot turbogradient echo sequence (inversion pulse, pre-pulse delay 360 ms, acquisition duration 360 ms, flip angle 15°, echo time 1.7 ms, repetition time 9 ms). Slice thickness was 8 mm with a spatial resolution of 1.7 × 1.9 mm. During an expiratory breath hold, a bolus of gadolinium-DTPA 0.025 mmol/kg body weight (Magnevist, Schering AG, Berlin) was injected via a central vein catheter. Dynamic images (one image per heart beat) were acquired during the first pass of the contrast agent before and after dobutamine stress (5, 10 and 20µg/min/kg body weight for 3 minutes each).

In all images the endo- and epicardial contours were traced. The myocardium was divided into 6 equiangular segments. Images acquired after premature ventricular beats or insufficient cardiac triggering were excluded from the analysis to guarantee steady-state conditions. Signal intensity was determined for all dynamics and segments. The signal intensity before contrast agent administration was subtracted and the upslope of the resulting signal intensity time curve was determined using a linear fit. The results were corrected for the input function by dividing the upslope of each myocardial segment by the upslope of the left ventricular signal intensity curve and perfusion reserve was calculated.

Results: Median area reduction was 88%, mean reference vessel diameter was 3.2 ± 7 mm.

In patients with single coronary artery disease (n = 14) myocardial perfusion reserve in ischemic segments was significantly lower than the contralateral segments (0.90 ± 0.18 versus 1.73 ± 0.32, $p < 0.0001$) or segments of the patients without coronary artery disease (2.0 ± 0.39, $p < 0.0001$). In all ischemic segments Myocardial perfusion reserve was 0.95 ± 0.22 ($p < 0.0001$ vs. controls) (Fig.).

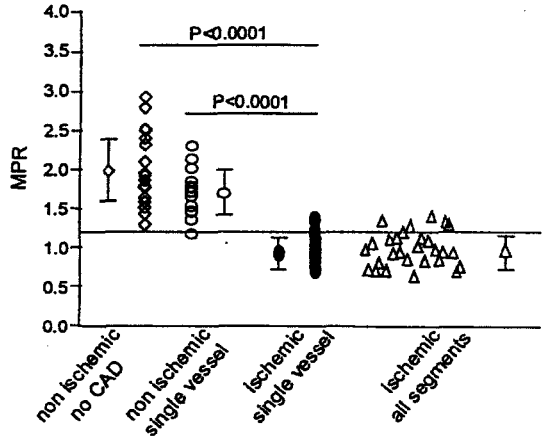

An ischemic threshold of 1.22 was defined from segments of patients without coronary artery disease (mean-2SD). The sensitivity, specificity, and diagnostic accuracy of this cut off value for the prospective detection of significant stenosis were 82%, 74% and 78% (Table).

	Stenosis ≥75%	Stenosis <75%
MPR ≤ 1.22	23	9
MPR > 1.22	5	26
	sensitivity = 82%	specificity = 74%

Conclusion: This study shows that the assessment of myocardial perfusion reserve with dobutamine using cardiac MR is feasible and yields a high diagnostic accuracy Dobutamine can be used for an integrative cardiac examination combining the detection of wall motion abnormalities and the assessment of myocardial perfusion.

References

1. Al-Saadi N, Nagel E, Gross M, et al. *Circulation* 1999 (in press).
2. Nagel E, Lehmkuhl H, Bocksch W, et al. *Circulation* 1999; 99: 763–70.
3. Pennell D, Underwood SR, Swanton RH, et al. *JACC* 1991; 18: 1471–9.

Magnetic Resonance Real-Time Imaging of Left Ventricular Function: Complete Examination Within 15 Seconds Using Multi Slice Dynamic Imaging

A. Bornstedt, E. Nagel, B. Schnackenburg, S. Schalla, C. Klein, E. Fleck. *Cardiology/Internal Medicine, Charité, Campus-Virchow Clinicum, Humboldt University & German Heart Institute, Berlin, Germany; Philips Medical Systems, Best, The Netherlands*

Introduction: Most cardiac examinations start with a functional study of the heart to determine left ventricular volumes, ejection fraction and/or left ventricular mass and to look at regional wall motion. To completely cover the heart 7–12 slices in a short axis view with approximately 15 cardiac phases each are required.

The reference method used today is a fast, ECG triggered gradient echo sequence with k-space segmentation (TFE) which lasts approximately 10–16 heartbeats per slice, depending on heart rate and temporal/spatial resolution. For each slice one breathhold measurement is needed.

One of the advantages of MR in comparison to other imaging techniques (Echocardiography, Angiography) is the acquisiton of complete volumes rather than multiple projections during an examination. However such a complete measurement lasts about 5 minutes. Due to the acquisition of the image during several heartbeats, image quality is best in patients with regular sinus rhythm, who can hold their breath for 10–16 heartbeats. Thus a fast (real-time) sequence which covers the heart completely and does not need cardiac triggering would be helpful to reduce patient setup and examination time. Current real-time methods have shown to be accurate, but do only allow the acquisition of single slice movies. To scan the entire left ventricle it would be necessary to perform multiple short (2–3 s) breathholds, which is time consuming, requires longer planning and introduces errors from different breathhold levels. Therefore a Multi Slice Dynamic Imaging sequence was developed.

Methods: The sequence was developed for a 1.5 Tesla whole body MR scanner (ACS NT, Philips, The Netherlands) equipped with a fast gradient system (23 mT m-1 amplitude, 105 T m-1 sec-1 slew rate). It is based on a segmented gradient echo/EPI hybrid sequence (1,2). Each gradient echo segment (shot) consists of n excitation (α–) pulses followed by an EPI-readout. To speed up the sequence for real-time imaging only one shot was acquired per image. The temporal resolution was 62 ms yielding 16 images per second (4 α-pulses with an EPI train of 9 readouts, T_r = 15.5 ms. The standard loop structure in the acquisition software does not allow to acquire n consecutive images of one slice immediately followed by n consecutive images of the next slice, it rather acquires n slices followed by the next image of the same n slices. Therefore an additional type of loop structure was introduced to the acquisition software to allow Multi Slice Dynamic Imaging and to get continuous slice movies in the dynamic (real-time) imaging mode. In addition the possibility to use an ECG trigger signal for the first dynamic acquisition of each slice was implemented. This allows the acquisition of volume data sets which are in phase.

The accuracy of the real time technique for the determination of ESV and EDV (endsystolic/diastolic volume) was validated in comparison to a standard TFE technique in 34 patients.

Results: The new technique proved to a be feasible and accurate for functional cardiac examinations. Excellent correlations were found for ESV (r = 0.96) and EDV (r = 0.95).

Conclusions: With this new Multi Slice Dynamic Imaging technique it is possible to perform a complete cardiac functional examination within 15–20 seconds and, thus within a single breathold, which is not necessary to preserve image quality, but eases evaluation. The examination does not have to be cardiac triggered and makes the examination of subjects with cardiac arrhythmias or atrial fibrillation possible without loss of image quality.

The first dynamic image of each slice can be cardiac triggered, even though this is not required for image quality and thus each slice movie starts in the same cardiac phase. This is important for volume data sets wich have to be in phase.

References

1. Mc Kinnon GC, *Magn Reson Med* 1993; 30: p. 629
2. Fischer SE, Wickline SA, Lorenz CH, *Proc of ISMRM* New York 1996 p. 682.

Magnetic Resonance Myocardial Perfusion Measurements Using Clariscan™ (NC100150 Injection): Experience in Pigs and Humans

E. Nagel,[1] Ch. Klein,[1] M. Valvelidis,[2] B. Schnackenburg,[3] A. Bornstedt,[1] V. Hoffmann,[4] A. Lehning,[4] N. Al-Saadi,[1] S. Schalla,[1] D. Modersohn,[2] E. Fleck.[1] [1]*Internal Medicine/Cardiology, German Heart Institute & Charité, Campus Virchow, Berlin;* [2]*Cardiovascular Surgery; Charité, Berlin;* [3]*Philips Medical Systems, Hamburg;* [4]*Nycomed Amersham Imaging, Munich, Germany*

Introduction: The assessment of myocardial perfusion with magnetic resonance from the first pass kinetics of a gadolinium DPTA (Gd) bolus has shown promising results. However, due to the rapid diffusion of Gd into the interstitial space measurements are severely influenced by the rate of diffusion. Clariscan™ (NC100150-injection; Nycomed Amersham, Oslo, Norway) consists of superparamagnetic iron oxide nanoparticles with an oxidized starch coating. It is a pure intravascular (blood pool) agent with both T_1 and T_2 shortening properties. The aim of the study was to assess the feasibility of Clariscan™ for the assessment of myocardial perfusion using the T_1 effect during the first pass of the bolus.

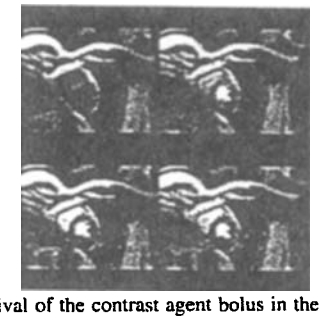

Figure 1. Arrival of the contrast agent bolus in the right and then in the left ventricle. The left ventricular myocardium is enhanced in the later images.

Methods: Seven explanted pig hearts perfused by a whole blood perfusate oxygenated via a dialysis membrane and eleven patients (age 61 ± 4.7 years, range 53–71 years) with suspected coronary artery disease (5 without and 6 with chronic myocardial infarction) were examined with a Philips ACS NT 1.5 T tomograph. Five short axis views covering the whole heart were acquired each heart beat for 70 heart beats during the first pass of a contrast agent bolus using a multi-slice turbo gradient echo/echo planar imaging hybrid sequence (TE 3.3 ms, TR 12.5 ms; EPI 11, flip angle 30°). Different doses (0.5/1.0/2.0 mg Fe per kg and 0.025 mmol Gd per kg) and different flow conditions simulating rest and stress in normal and ischemic myocardium were assessed in the pig hearts and Clariscan™ compared with Gd injections. In patients a single dose of 0.5 mg Fe/kg was injected as a bolus into a brachial vein. The myocardium was divided into 6 equiangular segments per slice and signal intensity curves were obtained. The time from the peak signal until it was reduced to 50% of the peak signal intensity (SI_{50}) and the percent remaining signal within the myocardium at steady state in comparison with the peak signal (SI%) were assessed.

Results: In the pig hearts the first pass of the Clariscan™ injection showed a rapid downslope and return to baseline in comparison with Gd injection at all flow conditions (results at rest: SI_{50} = 4.5 ± 0.05 vs 14 ± 8 sec for Gd; SI% = 2.2 ± 1.7% vs 38 ± 18% for Gd; both $p < 0.05$; figure 2). Similarly a rapid and clearly defined downslope of the myocardial signal intensity curves was found in the patients. In the patients T2* effects were only observed in the right and left ventricle but not in the myocardium after bolus injection. Segments with previous

myocardial infarction were clearly seen during the first pass of the bolus as areas with reduced enhancement (figure 3).

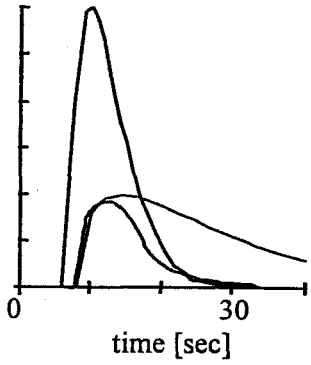

Figure 2. Time-intensity curves of the left ventricular cavity and the myocardium for Gd (grey) and Clariscan™ (black). Signal intensity in arbitrary units.

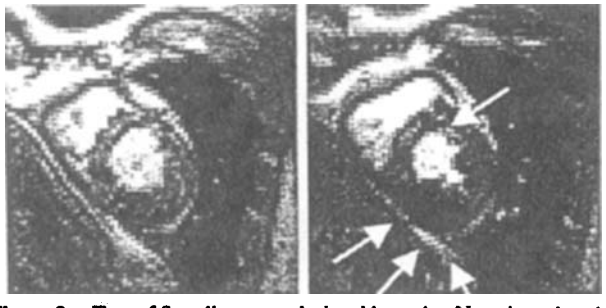

Figure 3. Two of five slices at peak signal intensity. Note the reduced enhancement of the inferior wall and the anterior septum with subendocardial accentuation (arrows).

Conclusions: T_1 perfusion measurements in patients are feasible with Clariscan™. In contrast to Gd the signal intensity curves of the blood pool agent have a more rapid and complete downslope which is independent of diffusion processes. Chronic myocardial infarction can be clearly detected in patients during the first pass of Clariscan™.

Magnetic Resonance Myocardial Perfusion Reserve for the Detection of Coronary Artery Disease: Experience in 139 Patients

Eike Nagel, Nidal Al-Saadi, Susan Foerster, Ingo Paetsch, Simon Schalla, Christoph Klein, Uta Schneider, Bernhard Schnackenburg, Axel Bornstedt, Hans B. Lehmkuhl, Eckart Fleck. *Internal Medicine/Cardiology, German Heart Institute & Charité, Campus Virchow, Berlin, Germany*

Introduction: With magnetic resonance imaging myocardial perfusion reserve can be determined from alterations of the signal intensity curves of the first pass of a gadolinium-DPTA (Gd) bolus before and after vasodilation (1,2). A linear fit of the upslope yields reproducible and valid results (3). In this study we assessed the value of this technique for the noninvasive detection of coronary artery disease in a larger series of unselected patients.

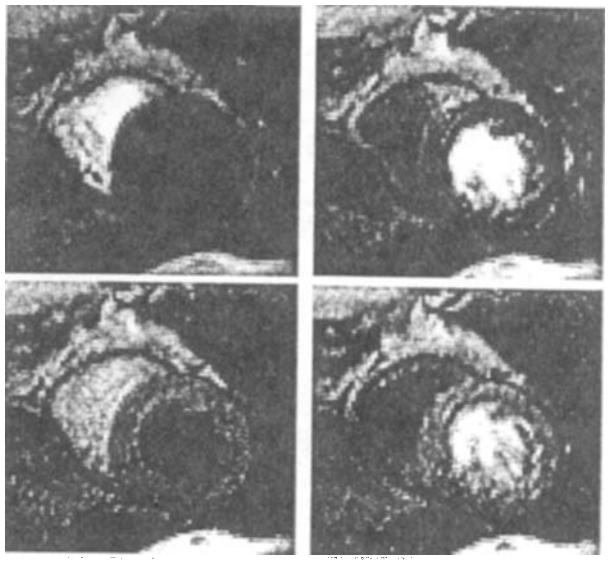

Figure 1. First pass kinetics of a gadolinium bolus. One of 5 slices. One image was acquired per heart beat, 4 of 70 dynamic images are shown. Myocardial signal without contrast agent was suppressed with a saturation prepulse.

Methods: 139 consecutive patients with suspected coronary artery disease, referred for a primary diagnostic coronary angiography were examined with a 1.5 T MR tomograph (Philips ACS NT) using fast gradient systems (23 mT/m amplitude, 105 T/m/sec slew rate) and a dedicated 5-element cardiac coil. Each heart beat 5 slices were acquired during the first pass of 0.025 mmol/kg Gd injected into the right cubital vein before and during adenosine (140 µg/kg body weight) vasodilation using a segmented k-space turbo-gradient-echo-EPI-hybrid sequence with a saturation prepulse.

Myocardial perfusion reserve was determined from the alteration of the upslope of the myocardial signal intensity curves for 6 equiangular segments per slice using the MASS perfusion software (MEDIS. Leiden).

A previously defined ischemic threshold was used to differentiate ischemic and nonischemic segments. Patients were defined as having significant coronary artery disease if any segment was below this threshold. A second analysis was performed using two segments as diagnostic criterion. Significant coronary artery disease was defined as an angiographic reduction of the luminal diameter of ≥75%.

Results: Prevalence of coronary artery disease was 53%. Diagnostic signal intensity curves were achieved in 83% patients. The results for one respectively two segments below the ischemic threshold to define significant coronary artery disease are shown in the table.

	1 Segment	2 Segments
Sensitivity	96%	94%
Specificity	67%	83%

Conclusions: Magnetic resonance perfusion measurements allow a noninvasive diagnosis of significant coronary artery disease in an unselected prospective patient population with high diagnostic accuracy similar or superior to results reported from szintigraphic techniques. Thus, MR perfusion measurements are a valid alternative for the examination of patients with known or suspected coronary artery disease.

References
1. N Wilke, M Jerosch-Herold, AE Stillman. *Magn Reson Quart* 1994.
2. SD Wolff, RA Day, L Santiago. *Proceedings of the ISMRM* 1999
3. N Al-Saadi, E Nagel, C Klein et al. *Circulation* 1999 (in press).

Magnetic Resonance ECG Basics: How to Obtain a Consistent ECG for MR Imaging

M.P. Watkins,[1] S.E. Fischer,[1,2] C.H. Lorenz[1]. [1]*Center for Cardiovascular MR, Barnes-Jewish Hospital at Washington University Medical Center, St. Louis, MO;* [2]*Philips Medical Systems, Best, The Netherlands*

Introduction: A consistent electrocardiogram is essential for high quality cardiovascular MR imaging. To obtain a reliable ECG several fundamental concepts should be considered, including ECG signal generation, patient evaluation and preparation, electrode and lead placement, how to recognize a stable ECG signal, and alternative lead placements.

There are some obstacles inherent within the MRI environment that corrupt the ECG signal, including the main magnetic field (B_o), gradient switching, and patient motion which can cause artifacts in the ECG such as the magnetohydrodynamic effect, low-amplitude, and low frequency changes of the baseline. Our objective here is to provide guidelines for cardiovascular MR staff for obtaining consistent, high quality ECG's in the MRI environment.

Materials and Methods: Based on our experience with over 800 patients and volunteers on a clinical 1.5T scanner (Philips Gyroscan ACS-NT, Best, The Netherlands), we have developed the following stepwise approach, shown in Figure 1, for obtaining a good ECG in MRI:

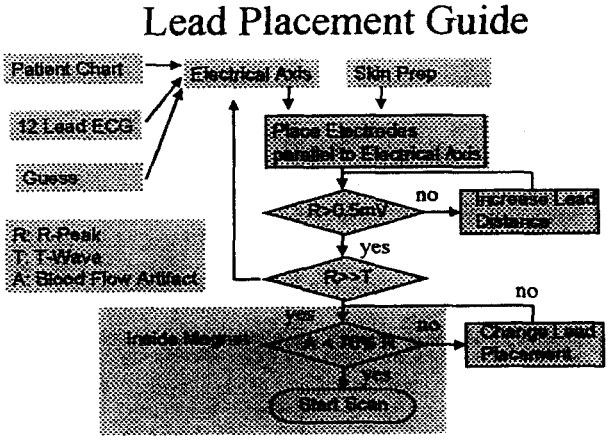

Step 1: Determination of electrical axis. The first step is to use the patient's medical records, if available, combined with a 12 lead ECG for an initial guess of the patient's electrical axis. If neither of these are available, one can make an initial guess based on the known history. The patient's body habitus, skin condition, and gender should also be noted to aid with lead placement.

The first lead placement attempted should be parallel to the electrical axis, which can be normal, deviated to the left or deviated to the right as shown in these suggested lead placement diagrams.

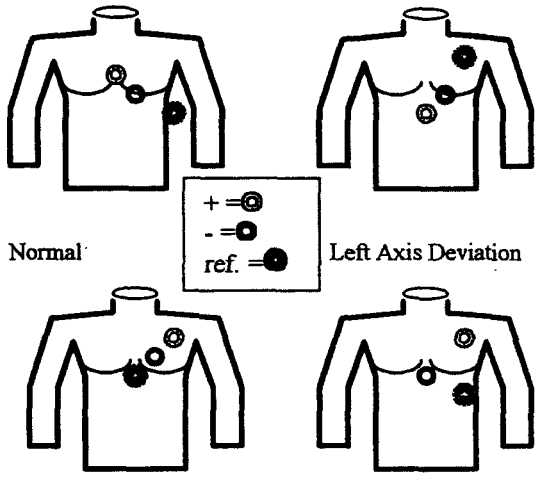

Step 2: Skin preparation and placement of electrodes. The chest shape and size are considerations for lead placement if the chest is concave or irregular. The skin condition should be checked to determine whether it is dry or oily, rough or smooth, and for chest hair. The skin should be prepared for electrode placement by cleaning and drying the site with an abrasive prep pad or gel. Then the site should be wiped dry. If there is excess amount of hair it should be shaved and removed. We have used ConMed 101–5731 adult electrode pads. It is important to use pads that are MR compatible, not expired and provide good skin adhesion. Breast or fatty tissue should be moved so the electrode can be placed on underlying solid tissue. Lift the tissue up or away so the electrodes can be placed on solid tissue. The electrodes should then be placed parallel to the electrical axis, as noted earlier. Electrode wires should be braided and not looped to minimize artifacts and avoid patient burns.

Step 3: Evaluation of ECG quality. The ECG should be checked both inside and outside the magnet, to assure that the magnitude of the R-wave is at least 30% higher than that of the magnetohydrodynamic artifact. If absolute voltages are available, the R-peak should be greater than 0.5 mV. The baseline amplitude of the ECG should not fluctuate with respiration. If the R-peak amplitude is not high enough, the electrodes can be placed further apart. In some cases, the electrode position should be altered. If respiration remains a problem, the electrodes can be moved higher on the chest or in a lateral position.

Discussion and Conclusions: Using the systematic guidelines presented here can improve the success rate in obtaining a good ECG for triggering within the MR environment, reduce patient setup time and improve image quality. Although exact lead placement recommended by the different MR manufacturers can vary, these general principles can still be applied.

Quantitative Assessment of Myocardial Perfusion by First-Pass Dynamic MRI Using a New Intravascular Contrast Agent: A Dose Finding Study in Pigs

W. Schreiber,[1] G. Horstick,[2] M. Schmitt,[1] S. Petersen,[2] T. Balzer,[3] K.-F. Kreitner,[1] T. Voigtländer,[2] J. Meyer,[2] M. Thelen[1]. [1]*Department of Radiology;* [2]*II. Medical Clinic, Johannes Gutenberg-University Mainz;* [3]*Schering AG, Berlin, Germany*

Introduction: Myocardial flood flow (MBF) can be measured using dynamic T1-weighted MR imaging and an intravascular contrast agent (1). Prerequisite for these measurements, however, is the existence of a linear signal-concentration relation, i.e. a low CM dose.

It was the aim of this study to determine the optimal dose of a new intravascular CM for quantitative MBF measurements.

Materials and Methods: Pulse Sequences: Measurements were performed at a 1.5 T Siemens Vision system (1.5 T) using a four-element phase-array receive coil. For the perfusion measurements a saturation recovery TurboFlash pulse sequence with (TR/TE/TI/Iα = 2.4ms/1.2ms/10ms/18° with an acquisition matrix of MA = 96 × 128 and 6/8 rectangular field-of-view were used. With a field-of-view of 300mm this resulted in an in-plane resolution of 2.34 × 2.34mm², the slice thickness was 12 mm.

In addition to the perfusion measurement a segmented cine pulse sequence (temporal resolution, 30 ms, TE = 4.8ms, FOV = 350ms, MA = 252 × 256) was performed for analysis of hemodynamic parameters. The cine measurement was performed 5 min after the perfusion measurement when the heart rate which increased during the perfusion measurement because of apnea had returned to the baseline value.

Measurements were performed in nine anesthetized and ventilated pigs (29.9 ± 3.3kg). Intravascular T1-CM SHU555C (Schering AG, Berlin, Germany) was applied at a dose of 1, 2, 5 or 10 mmol/kg. Manual injection of the CM followed by a saline flush of 20 mL was performed into the inferior Vena Cava.

Postprocessing: Normalized signal intensities (NSI) in the LV and in the myocardium were calculated by dividing the signal intensities by the precontrast signal. Hemodynamic parameters (stroke volume, cardiac output, ejection fraction) were evaluated using Siemens software Argus.

Results: A dose-dependent peak NSI in the LV was observed (Fig. 1) with the maximum signal increase obtained at a dose of 5 µmol/kg. However, interindividual variations were large (c.f. fig. 1). At a dose of 5 µmol/kg the NSI ranged from 2.4 to 4.9. Statistical analysis demonstrated correlation between the peak NSI and stroke volume with a correlation coefficient of $r^2 = 0.58$ (Fig. 2). No correlation was observed between peak NSI and ejection fraction or cardiac output ($r^2 = 0.28$). Due to the smaller blood volume in septal myocardium a smaller peak NSI of 1.19 ± 0.04, 1.6 ± 0.3, and 1.6 ± 0.4 for doses of 2 µmol/kg, 5 µmol/kg and 10 µmol/kg was obtained.

Discussion and Conclusion: The optimal dose for a quantitative analysis of first-pass perfusion measurements using SHU555C is 5 µmol/kg. However, large interindividual variations of the peak NSI were observed which appear to be a result of different hemodynamic states of the animals (c.f. Fig. 2). It appears that for an adjustment of the CM dose to the hemodynamic state of the animal an perfusion measurement the stroke volume should be measured before. A correlation was observed between the peak NSI and stroke volume probably because the stroke volume is related to the volume of blood in which the CM is diluted during the injection.

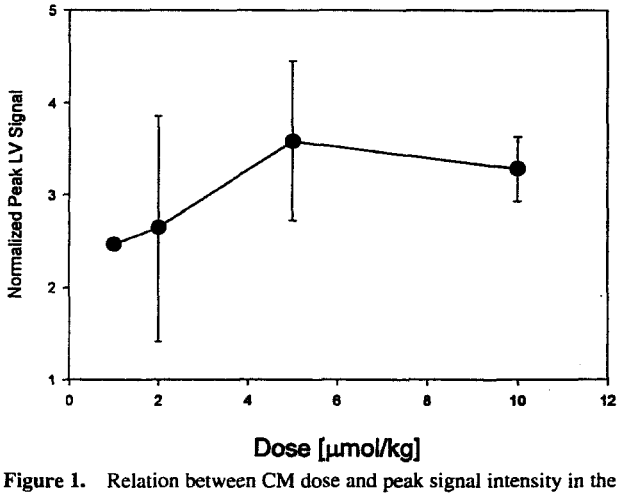

Figure 1. Relation between CM dose and peak signal intensity in the LV.

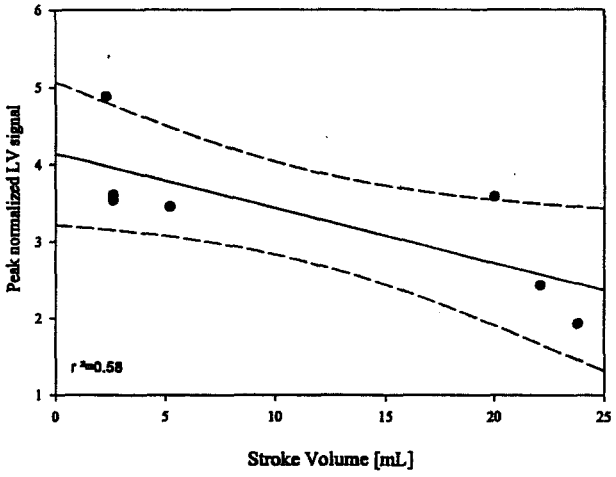

Figure 2. Relation between the stroke volume and the normalized peak signal intensity for a CM dose of 5 µmol/kg. Lines denote linear regression and 95% confidence intervalls.

Reference

1. N Wilke, K Kroll, H Merkle, et al., *JMRI* 1995; 5: 227–237.

'Delayed Enhancement' in Patients with Myocardial Infarction—First Insights

S.E. Petersen,[1] T. Voigtländer,[1] K.-F. Kreitner,[2] W. Schreiber,[2] T. Wittlinger,[1] J. Scharhag,[1] M. Schmitt,[2] L. Simonetti,[3] G. Laub,[3] M. Thelen,[2] J. Meyer.[1] [1]*2nd Medical Clinic,* [2]*Department of Radiology, University Hospital Mainz, Germany;* [3]*Siemens AG, Chicago, IL*

Background: In interventional cardiology as well as in cardiothoracic surgery the differentiation between viable and nonviable myocardial tissue is of paramount importance regarding therapeutical decisions. Investigations in animal models have already shown the potential of MRI to solve this problem. The aim of our investigation was to see, in a first step, whether the 'delayed enhancement' technique was able to depict the area of myocardial infarction in vivo and whether this area was indeed the area of the infarct related artery. If this can be shown to be the case investigations will be carried out focused on the potential to differentiate viable and nonviable myocardial tissue.

Materials and Methods: We have investigated 5 patients so far with myocardial infarction using a 1.5 T Scanner (Siemens Vision 1.5 T, TR: 2.3/1; TR: 5,0; TI: 200). As contrast medium we used gadolinium-DTPA in a concentration of 0.2 mmol/kg as a bolus via a venflon positioned in a cubital vein. After 5 minutes short and long axis views were acquired.

Results: In all cases, i.e. in the acute, subacute and chronic myocardial infarctions, a hyperintense area of myocardial tissue could be identified in the area of the infarct related artery.

The area of infarction showed border zones that could be easily delineated.

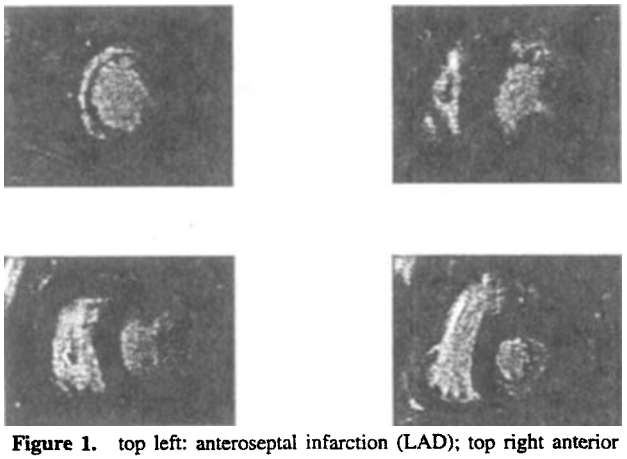

Figure 1. top left: anteroseptal infarction (LAD); top right anterior infarction (LAD); bottom left: lateral infarction (RCx); bottom right inferior infarction (RCA).

Conclusion: Using 'delayed enhancement' technique the area of myocardial infarction can reliably be depicted in vivo in a fairly simple manner. The border zones were easy to delineate due to an impressive contrast between the area of infarction and the healthy tissue. Comparing this method to gold standards (PET and myocardial scintigraphy) in detecting viable and nonviable myocardial tissue will be the next necessary step.

Flow Quantification of Shunt Volumes in Congenital Heart Diseases Using a Breath-Hold MR Phase Contrast Technique—Comparison with Oximetry

S.E. Petersen,[1] T. Voigtländer,[1] K.-F. Kreitner,[2] W. Schreiber,[2] P. Kalden,[2] T. Wittlinger,[1] J. Scharhag,[1] D. Becker,[1] G. Hommel,[3] M. Thelen,[2] J. Meyer[1]. [1] *2nd Medical Clinic,* [2]*Department of Radiology,* [3]*Institute for Medical Statistics, University Hospital Mainz, Germany*

Background: MRI has been shown to be a reliable method in evaluating shunt volumes in patients with atrial septal defects using a non-breathhold phase contrast technique (1). The determination of shunt volumes and Qp:Qs-ratios is of paramount importance for therapeutical decisions (corrective surgery for ratios ≥1.5). We compared a new breath-hold MR phase contrast technique in the estimation of cardiac shunt volumes with the invasive oximetric technique.

Materials and Methods: 17 patients with various cardiac shunts (10 ASD, 3 VSD, 1 PDA, 3 PFO) and 4 healthy volunteers were investigated with a 1.5 Tesla System. The mean flow velocity, the mean flow, the vascular area and the peak velocity in the ascending aorta, the left and right pulmonary artery were measured using MR phase contrast technique in breath-hold (through plane, FLASH 2D sequence, TR/TE 110/5 ms respectively, VENC 250 cm/s). The ratio of mean flow in the pulmonary (Qp: sum of mean flows in the left and right pulmonary arteries) and the systemic circulation (Qs: mean flow in the ascending aorta) was calculated and compared with invasively measured Qp:Qs ratios. Oximetry was performed within 24 hours of the MR investigation.

Results: The non-invasive shunt measurement in the 17 patients showed a mean Qp:Qs ratio of 2.00 ± 0.86. The mean shunt volumes were 42.30% ± 22.79%. Comparing the MR data with the invasively measured Qp:Qs showed a correlation coefficient of $r = 0.91$ ($p < 0.001$) (Fig. 1). In 16/17 (94.12%) patients both methods lead to the same therapeutical decision. The two methods were in excellent agreement according to the Bland & Altman plot (Fig. 2), especially so in the smaller shunts.

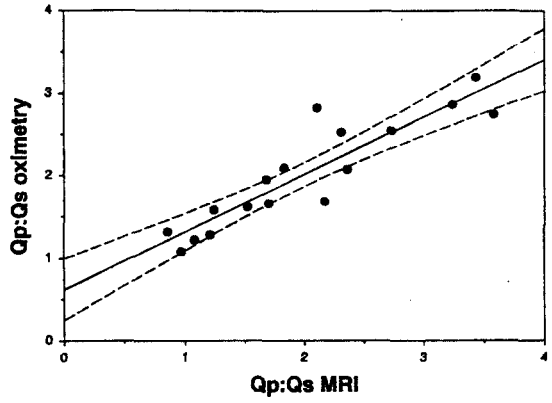

Figure 1. Pulmonary-to-systemic flow ratios (Qp:Qs) by MRI (horizontal axis) and by oximetry (vertical axis) for 17 patients with cardiac shunts. The regression line and the 95% confidence interval are shown ($y = 0.7*x + 0.62$; $r = 0.91$; $p < 0.001$; $SEE = 0.29$).

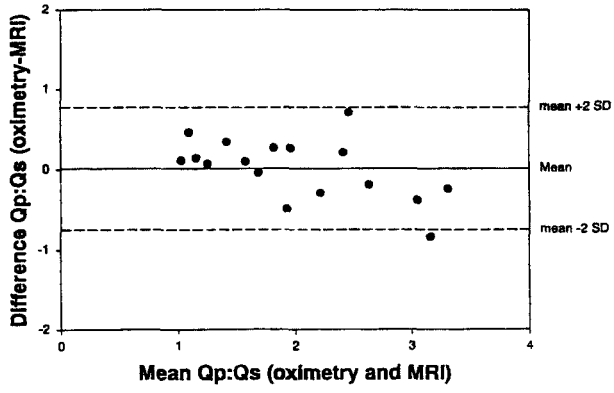

Figure 2. The mean pulmonary-to-systemic flow ratio (Qp:Qs) by MRI and by oximetry (horizontal axis) and the difference between oximetry and MRI measurements of Qp:Qs (vertical axis) for 17 patients with cardiac shunts. The mean difference (solid line) and ± 2SD from this difference (dashed lines) are shown. There is a good agreement between the two methods.

Conclusion: Cardiac shunt volumes can reliably be measured in a short acquisition time using a breath-hold MR phase contrast technique. The therapeutical decision can be made with this noninvasive investigation.

Reference

1. Hundley WG, Li HF, Lange RA, et al., *Circulation* 1995; 91: 2955–2960.

Vasodilator Reserve MR-Measurement in Coronary Grafts: Which Parameter Should Be Used—Mean Flow, Mean Velocity or Peak Velocity?

T. Voigtländer,[1] K.-F. Kreitner,[2] T. Wittlinger,[1] S. Petersen,[1] W. Schreiber,[1] G. Rippin,[3] M. Thelen,[2] J. Meyer.[1] [1]*2nd Medical Clinic,* [2]*Department for Radiology,* [3]*Department of Statistics University, Mainz, Germany*

Background: Vasodilator reserve measurement is widely accepted as golden standard in the assessment of the severity of coronary artery

disease. Conventionally these measurements were performed invasively by protruding a doppler wire in the coronary graft. Current MR phase change techniques allow a non-invasive measurement of vasodilator reserve in breath-holding. First results showed that normal and stenosed grafts can be discriminated by these measurements. Different parameters can be used to measure the vasodilator reserve. We tested the accuracy of the parameters mean flow, mean velocity and peak velocity in discriminating normal from diseased grafts.

Patients and Methods: MR measurements were performed on a 1,5 T system (Siemens, Vision, TR/TE 24/5 ms, temporal resolution 110 ms, VENC 75 cm/s, FOV 150 mm) using a body array coil in 34 patients with a total of 51 coronary grafts (14/51 IMA-LAD, 14/51 vein grafts LAD, 19 vein grafts RCA/RCX). During the cardiac cycle 5 image pairs were acquired. Mean flow and mean velocity were measured integrating the data over the cardiac cycle. Peak velocity was determined as the highest value of the 5 velocity sensitized data sets. After the first measurement a second was performed during adenosin infusion (140 µg/kg/min) and vasodilator reserves were calculated using the parameters mean flow, mean velocity and peak velocity. Conventional invasive angiography of the bypass grafts was performed within 24 hours. Measurement of grafts stenosis was performed quantitatively (AWOS, Siemens).

Table 1.

	Mean Flow (ml/min)	Mean Velocity (cm/s)	Peak Velocity (cm/s)
Normal grafts	3.33 ± 0.38	2.95 ± 0.31	1.77 ± 0.11
Diseased grafts (<50% stenosis)	1.26 ± 0.16	1.13 ± 0.15	1.24 ± 0.19
p-value	0.001	0.001	0.018

Table 2.

Vasodilator Reserve	Cut Point	Sensitivity	Specificity	Neg. Predictive Value	Pos. Predicting Value
Mean velocity	1.62	91.7%	75%	96.4%	55%
Mean flow	1.93	91.7%	69.4%	96.2%	50.0%
Peak velocity	1.90	91.7%	33.3%	92.3%	31.4%

Statistics: Descriptive data were expressed as mean and standard deviation. Comparisons of vasodilator reserves for normal and diseased grafts was performed using t-test analysis ($p > 0,05$ was assessed as significant). Sensitivity and specificity analysis (ROC test) was performed in order to find reliable cut points for the 3 parameters for the discrimination of normal and diseased grafts. McNemar's test compared the results of these parameters.

Results: Angiographically no atherosclerosis was present in 36 grafts and 11 grafts showed significant stenosis of >50% diameter stenosis (QCA: 83 ± 15.5%). For all 3 parameters the vasodilator reserves differed significantly between normal and significant diseased grafts (tab. 1).

ROC analysis showed the best results for mean velocity based vasodilator reserve measurement (Tab. 2). These results were significantly better compared to peak velocity ($p = 0.001$). The difference between mean velocity and mean flow was not significant.

Conclusion: MRI vasodilator reserve measurements discriminate normal and diseased coronary grafts using breath-hold technique. Mean velocity based measurement showed the most reliable results.

Evaluation of Coronary Artery Occlusions Using the 3D Navigator Magnetic Resonance Angiography

T. Wittlinger,[1] T. Voigtländer,[1] K.F. Kreitner,[2] J. Scharhag,[1] P. Kalden,[2] K. Grauvogel,[1] M. Thelen,[2] J. Meyer[1]. [1]2nd *Medical Clinic, and* [2]*Department for Radiology, University Hospital, Mainz, Germany*

The aim of the study was to evaluate the reliability of magnetic resonance imaging (MRI) in the assessment of coronary arteries.

Methods: On 30 patients with 15 stenosis and 24 occlusions x-ray angiography and magnetic resonance imaging (1,5 T, Vision, Siemens AG) were performed. 10 occlusions concerned the LAD, 7 occlusions the RCA and 7 the RCX. 8 stenosis were located in the LAD, 7 in the RCA. MRI was performed using a multislice, ECG-gated, breath-hold turbo spin echo sequence (Haste) and a 3-D-angiography sequence with navigator echo based respiratory gating (Navigator). The coronary arteries were divided into segments due to the american heart association guidelines.

Results: MRI was able to identify 92% of the segments in a good image quality. In the case of 18 vessels (8 LAD, 6 RCA 4 RCX) the occlusion could be definitely visualized with the Navigator-Sequence. The sensitivity for the detection of coronary artery occlusions was 75%, the sensitivity for the LAD and the RCA was 85%. In the proximal parts of the LAD and RCA all occlusions could be identified. The sensitivity for the detection of a coronary artery stenosis is only 50% due to the low spatial resolution.

Conclusion: MRI is able to visualize coronary artery occlusions with a sensitivity of 75% and 85% for the LAD and RCA. The best results are available for the proximal parts of the LAD and RCA, where all segments could be detected correctly.

An evaluation of the cardiac risk is possible in patients to avoid a conventionell coronary x-rax angiography due to multiple risk faktors. The method is limitated in the diagnosis of coronary artery stenosis due to spatial resolution and motion artefacts.

References

1. Manning WJ, Li W, Edelmann RR. *NEJM* 1993, 328: 828–823.
2. Post JC et al. Current limitations of two-dimensional breath-hold MR angiography in coronary artery disease. In: Proceedings of the 13th annual scientific meeting of the Society of Magnetic Resonance in Medicine. San Francisko: Society of Magnetic Resonance in Medicine, 1994:508.

Assessment of Diameters of Coronary Artery Bypass Grafts. Comparing Magnetic Resonance Imaging to Quantitative Coronary Angiography

T. Wittlinger,[1] T. Voigtländer,[1] S. Petersen,[1] K.F. Kreitner,[2] J. Scharhag,[1] P. Kalden,[2] K. Grauvogel,[1] M. Thelen,[2] J. Meyer.[1] [1]2nd *Medical Clinic and* [2]*Department for Radiology, University Hospital, Mainz, Germany*

Quantitative coronary angiography (QCA) is considered to be the gold standard in the assessment of coronary artery diameters. The aim of the study was to evaluate the reliability of magnetic resonance imaging (MRI) and QCA in the assessment of coronary artery bypass diameters.

Methods: In 50 patients with 102 bypass grafts, QCA and MRI (1.5T, Vision Siemens AG) were performed. MRI was performed using a ECG-gated, breath-hold turbo spin echo sequence (Haste). QCA was performed using the AWOS Work Station 4.01 (Siemens AG).

Results: In total 258 assessments were done in 102 bypass vessels. The medium diameter of all bypass vessels was 3.3 mm for QCA in comparison to 3.6 mm for MRI with a significant correlation ($p < 0,005$). In the proximal and middle parts a good correlation between the two methods was found. In the distal parts, MRI assessments were too high. The best correlation can be found in the proximal area of venous bypass grafts to the RCA and LAD. There is no correlation of both methods assessing IMA bypasses, for MRI the assessment was 40% too high.

Table 1. Diameter Assessment

	QCA	MRI
LAD	3.3 mm	3.9 mm
CX	3.6 mm	3.8 mm
RCA	3.3 mm	3.5 mm
D 1/PLA	3.2 mm	3.4 mm

Conclusions: MR assessment of bypass diameters is possible with a good correlation to QCA. An overassessment of the distal diameters is due to the low spatial resolution of the MRI for narrow-calibrated vessels. The exact determination of vessel diameters can facilitate the diagnosis of bypass stenoses that cannot be sufficiently diagnosed at present.

References
1. Pennel DJ, Bogren HG, Keegan J, Firmin DN, Underwood SR. *Heart* 1996, 75: 127–133.
2. Dodge JT, Brown BG, Bolson EL, Dodge HAT. *Circulation* 1992, 86: 232–246.

A Comparison of MRI Pulse Sequences for the Visualization of Myocardial Injury

Orlando Simonetti,[1] Raymond J. Kim,[2] David S. Fieno,[2] Hanns Hillenbrand,[2] Edwin Wu,[2] Jeffrey M. Bundy,[1] J. Paul Finn,[2] Robert M. Judd.[2] [1]*Siemens Medical Systems and* [2]*Northwestern University Medical School, Chicago, IL*

Purpose: The ability to detect and delineate myocardial injury by MRI is directly influenced by the imaging pulse sequence employed. The goal of this study was to compare a variety of MRI techniques that have been proposed for direct visualization of myocardial injury, and to demonstrate the clinical performance of the technique chosen based on the comparison.

Methods: Two categories of techniques were investigated: T2-weighted imaging without contrast agent injection, and T1-weighted imaging following contrast agent injection. Within these two basic categories, ten specific pulse sequences and acquisition strategies were explored on a Siemens Magnetom Sonata MRI System (Siemens AG, Erlangen, Germany).

Table 1. Ten Pulse Sequences Evaluated for Visualization of Myocardial Injury

Pulse Sequence Acronym	Sequence Description
T2 TSE	T2-weighted Black-Blood Turbo Spin Echo
T2 STIR	T2-weighted Black-Blood TurboSTIR
T1 SE	T1-weighted Spin Echo
T1 TSE	T1-weighted Turbo Spin Echo
T1 IR-TSE	T1-weighted Inversion Recovery Turbo Spin Echo
MD-FLASH	Magnetization Driven FLASH
True FISP	True FISP
IR TF1 (Pre)	Inversion Recovery Single-Shot TurboFLASH Pre-contrast nulling of myocardium
IR TF1 (Post)	Inversion Recovery Single-Shot TurboFLASH Post-contrast nulling of normal myocardium
Seg IR TF1 (Post)	Inversion Recovery Segmented TurboFLASH Post-contrast nulling of normal myocardium

All sequences were ECG triggered and all except the T1-SE were acquired during breath-hold. All sequences were run with equivalent spatial resolution (1.25 mm × 1.25 mm × 5 mm) to avoid differences in partial volume effects on image contrast. Timings were selected similar to commonly used settings.

The ten sequences were used to image in vivo canine hearts (n = 6) previously subjected to myocardial infarction. The T2-weighted sequences were used before and the T1-weighted sequences after I.V. administration of 0.2 mmol/kg Prohance (Bracco Diagnostics, Princeton, NJ). The resulting images were randomized and analyzed by two blinded independent observers. The best technique based on this comparison (Segmented IR TurboFLASH) was then used to image 18 patients with documented previous myocardial infarction. From each of the 18 patient studies a single short-axis image showing the largest hyperenhanced region as well as normal regions of myocardium was analyzed. Image intensity ratios were calculated as mean image intensity of the hyperenhanced region divided by mean image intensity in the remote region.

Results: Canine results are summarized in Table 2. The greatest differences in image intensities were observed using T1-weighted techniques post-contrast. Using inversion-recovery segmented turboFLASH with the T1 set to null post-contrast normal myocardium, the image intensity in infarcted myocardium was 1080% ± 524% higher than remote. This was nearly twice that of the next best sequence tested. Similarly, the contrast-to-noise ratio using SEG IR TFL was higher than the other sequences.

Table 2. Summary of Results Obtained From the Ten Pulse Sequences Tested in Canine Model of Myocardial Infarction

	Δ% INF/REM		Contrast-to-NR	
Sequence	Mean	SEM	Mean	SEM
T2 TSE	94.2	46.7	4.19	3.79
T2 STIR	120.1	88	3.16	2.75
T1 SE	67.2	36.7	2.95	2.3
T1 TSE	64.7	22.1	5.97	2.21
T1 IR-TSE	497.3	211.5	5.89	1.7
MD-FLASH	140.1	61	8.3	3.61
True FISP	148.1	45.1	14.44	5.98
IR TF1 (Pre)	111.6	42.7	8.21	2.44
IR TF1 (Post)	510.4	256.6	10.14	3.59
Seg IR TF1 (Post)	1080.4	524.1	18.93	7.31

In the 18 patients, the intensity in infarcted myocardium was 485% higher than remote. One example is shown in Figure 1.

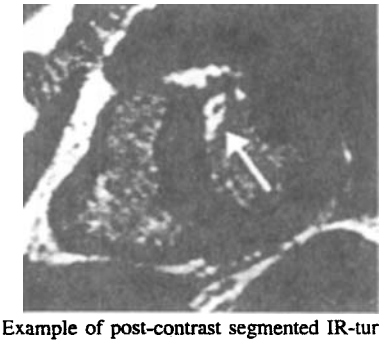

Figure 1. Example of post-contrast segmented IR-turboFLASH image of antero-septal MI in a patient.

Conclusions: The inversion-recovery segmented breath hold turboFLASh sequence allowed the best visualization of myocardial infarction in dogs and man.

The Transmural Extent of Viable Myocardium Predicts Wall Motion Recovery After Acute Infarction

H.B. Hillenbrand, D.S. Fieno, R.J. Kim, F.J. Klocke, R.M. Judd.
Feinberg Cardiovascular Research Institute, Northwestern University Medical School, Chicago, IL

Introduction: We hypothesized that the transmural extent of viable myocardium defined by contrast enhanced MRI (ceMRI) determines the longterm recovery of wall motion after myocardial infarction (MI).

Methods: Six dogs were submitted to coronary occlusion for 45min, 90 min or permanently. CeMRI and cineMRI were performed at 3 days, 10 days and 28 days. Viable myocardium (no delayed hyperen-hancement) was quantified on day 3 using a 60 segment model and the amount was expressed as a percentage of each segment. Wall motion by cine-MRI was read in corresponding segments by two readers, blinded to the results of ceMRI. Wall motion was graded as normal, mildly hypokinetic, severely hypokinetic, akinetic or dyskinetic.

Results: On day 3, 173 of 312 segments (55%) were dysfunctional. The transmural extent of viable myocardium on day 3 was a stronger predictor for wall motion recovery than the wall motion abnormality at 3 days ($p < 0.0001$ vs $p = 0.028$ at 10 days and $p < 0.001$ vs. $p = 0.27$ at 28 days). The table below summarizes the likelihood of wall motion recovery (WMR) as a function of the transmural extent of viable myocardium (VM). For segments in which 100% of the myocardium was viable, 95% improved. Conversely, 0% of segments with less than 25% viable myocardium improved.

Segments	129	11	18	10	5
VM (%)	100	75–99	50–74	25–49	0–25
WMR (%)	95	91	89	70	0

Conclusions: We conclude that the transmural extent of viable myocardium defined by ceMRI predicts wall motion recovery.

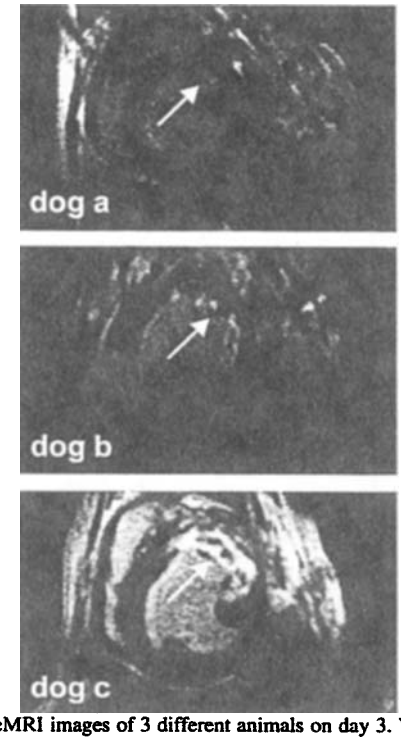

Figure CeMRI images of 3 different animals on day 3. Wall motion was abnormal in all three cases in the areas shown by the white arrow. By 10 days, wall motion improved for dogs a and b, but not dog c.

Detection of Chronic Myocardial Infarction by Contrast-Enhanced Magnetic Resonance Imaging

E. Wu,[1] R.M. Judd,[1] A. Rafael,[1] E.L. Chen,[1] K. Dhillon,[1] M.A. Parker,[1] O. Simonetti,[2] R.O. Bonow,[1] F.J. Klocke,[1] R.J. Kim[1].
[1]*Northwestern University Medical School,* [2]*Siemens Medical Systems, Chicago, IL*

Introduction: It is controversial whether delayed hyperenhancement by contrast-enhanced MRI (ceMRI) occurs in patients with chronic myocardial infarction (MI).

Methods: We studied nineteen patients (13 male, 6 female) with chronic MI (mean 283 days post MI, range 50-1579 days; 8 with non Q-wave MI) documented by serum enzymes (peak CK 219 to 5912; peak MB 11.5 to 791.5). Seven additional patients with non-ischemic cardiomyopathy (NICM) documented by coronary angiography were also included as controls. Cine MR images were acquired at six short and two long axis locations. Contrast enhanced images were acquired at the same locations using an inversion recovery sequence fifteen minutes after IV contrast (0.2 mmol/kg Gd-DTPA or Gd-DO3A).

Two blinded observers scored a fourteen segment model for wall motion and contrast enhancement by MRI and for the territory of the infarct related artery (IRA) by coronary angiography. MR images from patients with chronic MI and patients with NICM were grouped together and randomized prior to scoring to remove potential observational biases. Segments were scored for the presence or absence of hyperenhancement (image intensity greater than two standard deviations over remote) as well as for the transmural extent of hyperenhancement. Remote region image intensity was determined by the intensity of the segment opposite the left ventricular cavity from the IRA territory.

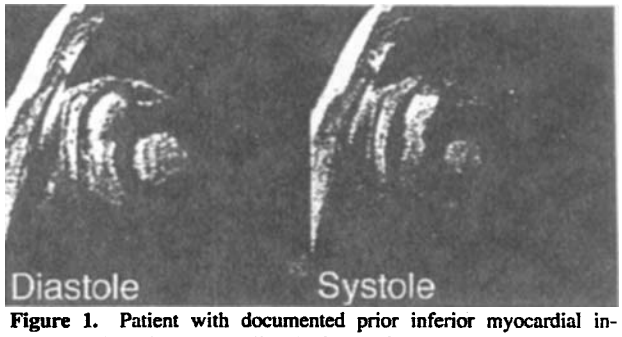

Figure 1. Patient with documented prior inferior myocardial infarction. Diastolic and systolic still frames from the cine MRI demonstrate normal wall thickening globally.

Results: For patients with chronic MI, 18 of the 19 patients exhibited hyperenhancement. In one patient, the cardiac enzyme levels were borderline abnormal (peak CK 283; peak MB 12.4), and the MRI performed three months later did not exhibit hyperenhancement. Hyperenhancement was in the correct territory for all seventeen patients in whom the IRA was determined by coronary angiography. Image intensity of the hyperenhanced region was 516 ± 121% (±SD) of remote regions. Hyperenhancement was non-transmural in 6/11 patients with Q-wave MI and in 7/8 patients with non Q-wave MI. Additionally, of all segments that hyperenhanced, 25% (26/105) had normal wall motion.

Figures 1 and 2 show typical images in one representative patient. This patient had a documented prior MI (peak CK 1586; MB 138) caused by a total occlusion of his right coronary artery confirmed on coronary angiography. MRI performed eight months later demonstrated normal wall motion globally (Fig. 1). The contrast enhanced images, however, showed hyperenhancement of the subendocardial half of the inferior wall (Fig. 2).

Conclusion: Contrast-enhanced MRI is sensitive for the detection of chronic myocardial infarction throughout a range of infarct sizes and infarct ages.

Figure 2. Contrast enhanced MRI of the same patient demonstrates subendocardial hyperenhancement of the inferior wall (arrow).

Infarct Resorption During the First Four Weeks After Myocardial Infarction

D.S. Fieno, H.B. Hillenbrand, R.J. Kim, F.J. Klocke, R.M. Judd. *Feinberg Cardiovascular Research Institute, Northwestern University Medical School, Chicago, IL*

Introduction: Although infarct resorption and compensatory hypertrophy characterize postinfarct ventricular remodeling, these processes are difficult to examine independently. Recent data, however, suggest that contrast-enhanced MRI is capable of differentiating between infarcted and noninfarcted tissue throughout the process of infarct healing. We therefore designed the present study to measure serial changes in infarct size and left ventricular mass during the first four weeks after myocardial infarction.

Methods: Twenty-three dogs with myocardial infarction were studied using delayed contrast-enhanced MRI. Under sterile technique, a thoracotomy was performed and a coronary artery was occluded either for 90 minutes or permanently. The dogs were allowed to recover and divided into two groups. In Group I, animals (n = 12) were imaged following 0.3 mmol/kg intravenous Gd-DTPA and sacrificed at three days (n = 4), ten days (n = 4), and four weeks (n = 4). In vivo images acquired every five millimeters from base to apex were compared to histologic slices every two millimeters from base to apex at each time point for both reperfused and non-reperfused pathophysiologies. In Group II, dogs (n = 11) were studied longitudinally after infarction and were imaged in the same manner at three days, ten days, and four weeks. Infarcted and non-infarcted masses at each time point were calculated and expressed as percent of the left ventricle.

Results: The results of Group I indicated that hyperenhancement was identical to infarct size at all time points (see Table 1). We therefore defined hyperenhanced tissue as the infarcted region and non-hyperenhanced tissue as the non-infarcted territory for the second group of animals. In Group II, with the area of hyperenhancement at three days defined as 100%, infarct size fell to 65 ± 14% by ten days and to 32 ± 8% by four weeks ($P < 0.01$, see Figure 1). Similarly, the mass of non-infarcted tissue grew to 109 ± 4% at ten days and 118 ± 2% at four weeks when compared to three days ($P < 0.01$). These changes were accompanied by no significant changes in the total mass of the left ventricle during this time period (values for ventricular mass at ten days and four weeks were 97 ± 4% and 97 ± 6% of values at three days, respectively, P = NS).

Conclusions: We conclude that myocardial infarcts shrink approximately three-fold during the first four weeks.

Table 1. Hyperenhancement Matched Infarct Size (% LV) Defined Histologically in 12 Dogs

(a)			
REPERFUSED	3 Days	10 Days	4 Weeks
#Slices	44	47	50
Bias ± SD	−1.7 ± 2.9	0.02 ± 0.4	0.1 ± 1.0
R Value	0.99	0.99	0.95
(b)			
NON-REPERFUSED	3 Days	10 Days	4 Weeks
#Slices	50	38	33
Bias ± SD	0.2 ± 1.2	1.0 ± 1.2	0.2 ± 1.4
R Value	0.99	0.99	0.99

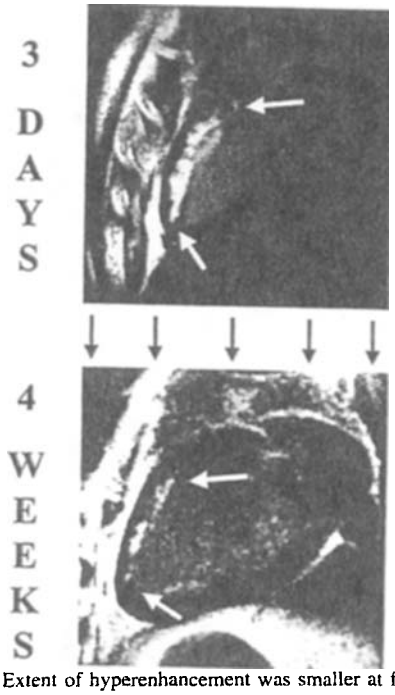

Figure 1. Extent of hyperenhancement was smaller at four weeks (bottom image) than at three days (top image) in 11 additional dogs.

Relationship of Regional Gd-DTPA Concentrations to Myocardial Electrolytes Following Reversible and Irreversible Ischemic Injury

W.G. Rehwald, D.S. Fieno, E. Chen, R.J. Kim, R.M. Judd. *Feinberg Cardiovascular Research Institute, Northwestern University Medical School, Chicago, IL*

Introduction: MRI hyperenhancement is observed in acute and chronic myocardial infarcts following administration of Gd-DTPA. The mechanism responsible for hyperenhancement of infarcted regions is unknown. In addition, whether or not hyperenhancement occurs in regions subjected to severe but reversible ischemic injury is controversial. To investigate these issues, we examined regional concentrations of Gd and myocardial electrolytes by Electron Probe X-Ray Microanalysis (EPXMA) in infarcted regions at 1 hour, 1 day and 2 weeks, in reversibly injured regions secondary to 10 min of ischemia, and in reversibly injured regions surrounding infarction.

Methods: Gd-DTPA was administered to four groups of rabbits (33 animals). Group 2W (14 animals) was occluded permanently and Gd-DTPA was given 2 weeks post occlusion. Group 1H and 1D were occluded for 25 min and reperfused for 1 hour (1H, 6 animals) and 1 day (1D, 8 animals), respectively, prior to Gd-DTPA infusion. Another group was subjected to 10 min severe but reversible ischemic injury (SBR, 5 animals) due to coronary artery occlusion followed by 1 hour reperfusion. Infarcted regions were identified by TTC and/or the absence of staining by anti-myoglobin antibodies in acute animals (1D, 1H, and SBR) and trichrome staining in chronic animals (2W). Regions at risk of infarction were defined using fluorescent microparticles.

In all animals, Gd-DTPA was allowed to circulate for 25 min, the hearts were excised, rapidly frozen, sectioned as wholemounts, freeze-dried, and examined by EPXMA (102 spectra in 2W, 111 in 1D, 58 in 1H, 50 in SBR). In each tissue section, spectra were acquired in three regions (if present in the sample): infarcted (I), at risk but not infarcted (RNI), and remote normal myocardium (R).

Results: The results are shown in the figure below as percent concentrations of remote. These data demonstrate that Gd-DTPA accumulates in acutely and chronically infarcted regions, but not in regions subjected to severe but reversible ischemic injury. The presence of Gd is closely correlated to an elevation of tissue Na, and a decrease of tissue K. In the acute setting, this may indicate impaired Na/K pump function and possibly cell membrane rupture. In scar, this might relate to an increased distribution volume for Gd-DTPA and extracellular electrolytes outside the collagen matrix.

Conclusions: Elevated concentrations of Gd-DTPA are associated with abnormal concentrations of myocardial electrolytes. The mechanism of Gd-DTPA hyperenhancement in irreversibly injured myocardium appears to relate to an absence of viable myocytes to exclude Gd-DTPA from the MRI voxel.

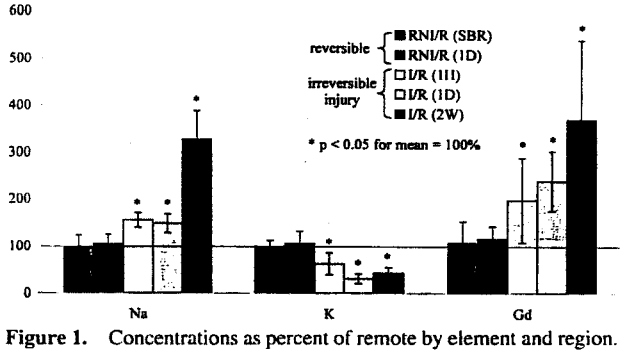

Figure 1. Concentrations as percent of remote by element and region.

A Method for Obtaining Myocardial Gd-DTPA Compartmental Model Parameters from MRI Data Without Blood Input Calibration

Edward V.R. Di Bella, Lars Luckner, Hyo-Chun Yoon. *Department of Radiology, University of Utah, Salt Lake City, UT*

Introduction: The ability to provide high resolution in-vivo quantitative measurements of myocardial perfusion with a standard MRI scanner would be of great clinical value. Recently, this has been shown to be possible for a single slice using a Gd-DTPA bolus injection (1–2). One step of the process involves converting the Signal Intensity (SI) measured with the MRI scanner to Gd-DTPA concentrations ([Gd]). Typically this conversion of signal intensity to [Gd] is determined using a combination of pulse sequences and experimental data, as well as requiring [Gd] to be below the level where significant signal decay from T2 effects occurs. At most Gd concentrations found in viable tissue, signal decay from T2 decay is not important. However, accurate measurement of the peak of the blood input function is critical for unbiased kinetic parameter estimation. With large bolus injections of Gd-DTPA, T2 effects could become important. If only the tissue peak concentration, rather than the blood peak, had to be accurately converted into [Gd], more contrast could be injected resulting in a higher signal to noise ratio.

It may be possible to estimate kinetic parameters without use of the input function by exploiting the common assumption that a single input function drives all of the tissue regions. That is, under certain conditions, the parameters of different regions can be estimated blindly (3).

Methods: To test the potential of the method, a computer simulation was performed. Values for the blood input function were taken from (1). Four regions were simulated using the values in rows one and three of Table 1. True tissue signal intensity curves were created and are shown in Figure 1. Gaussian noise (200 realizations) was added to the tissue curves and the four curves were input to the blind estimation algorithm. The algorithm was implemented as described in (3). No information about the blood input was provided.

Also, a scan was performed on a normal volunteer using a very fast spoiled gradient echo sequence recently developed by Picker to follow the kinetics of the Gd-DTPA injection. Four slices per heartbeat were acquired sequentially. Kinetic parameters were computed from the blood input and two manually chosen tissue regions, after conversion from signal intensity to [Gd]. These values were compared to those obtained with the blind estimation method. A scale factor calculated from blood [Gd] values at late time points was used since the method only matches within a scale factor.

Results: Data from one noise realization are shown in Figure 1(a). After estimating the kinetic parameters, it is possible to deconvolve them from the measured tissue curves to obtain an estimate of the blood input—Figure 1(b). Table 1 summarizes the results of the simulations. Washin (k_1) estimates were scaled so that the maximum estimate equaled 1.37 ml/min/g.

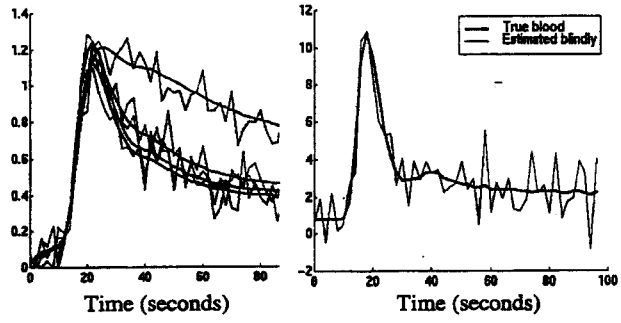

Figure 1. Curves from contrast simulation, one noise realization. (a) Tissue curves (noisy and noise-free). (b) Deconvolved blood.

Table 1. Simulation Kinetic Parameters

Region#	1	2	3	4
True k_1	1.1	1.2	1.37	0.9
Est. k_1	1.12 ± 10	1.2 ± 12	1.36 ± 03	0.94 ± 08
True k_2	6.11	8.0	8.56	3.0
Est. k_2	6.16 ± 0.7	7.92 ± 1.0	8.43 ± 95	3.11 ± 20

The washin parameter representing flow for the normal volunteer was 0.55 and 1.37 ml/min/g for two regions using the blood input from the images, and 0.34 and 0.86 ml/min/g without using the blood input.

Discussion: The simulation demonstrated the potential of the method to estimate kinetic parameters blindly. This may enable more accurate compartmental modeling when using bolus inputs which may otherwise not be accurately converted into [Gd]. However, the method is sensitive to the number of regions used, the characteristics of the blood input and the tissue regions, and to noise. Relative flows matched those in two regions in a volunteer, but were lower in value (implying a higher peak blood input). It is not known if the current scheme scales the values correctly. Further development and testing of the method is warranted.

References

1. Vallee J-P, Sostman HD, MacFall JR, et al. *MRM* 1997; 38: 981–989.
2. Vallee J-P, Lazeyras F, Kasuboski L, et al. *JMRI* 1999; 9: 197–203.
3. DiBella EVR, Clackdoyle R, Gullberg GT. *Phys Med Biol* 1999; 44: 765–780.

Real-Time Coronary MRA

Krishna S. Nayak, John M. Pauly, Adam B. Kerr, Bob S. Hu, Dwight G. Nishimura. *Department of Electrical Engineering, Stanford University, Stanford, CA*

Introduction: 2D and 3D MR coronary angiography methods have produced images with high spatial and temporal resolution, while relying on interbeat consistency (gating) and some form of compensation for respiration (navigators or breathholds). The use of a real-time system eliminates both of these problems, while introducing issues of SNR and resolution achievable in a small imaging time (1,2).

We have investigated the feasibility of doing high-resolution real-time imaging of the coronary arteries. With improved gradient hardware and novel k-space strategies, we have produced real-time 2D coronary images with 0.8 mm × 1.6 mm spatial resolution acquired in less than 150 ms. As this is an interleaved real-time sequence, sliding window reconstruction can provide image rates of up to 30 images/s.

Method: Studies were done on a GE Signa 1.5T system with gradients supporting $|G| < 40$ mT/m and $|dG/dt| < 150$ T/m/s. This was augmented with a Sun work-station that provided a real-time interface and real-time reconstruction (2). The pulse sequence consisted of a water-selective excitation followed by interleaved spiral or CEPI readouts. In this work, we also examined a variation of partial k-space CEPI (pkCEPI) in which trajectories are stretched in the readout direction to provide an elliptical k-space footprint, and therefore, asymmetric resolution. In the context of a real-time system, the direction of higher resolution can be specified interactively for optimal viewing of the vessel. Figure 1 shows example k-space trajectories for spirals, pkCEPI, and 2:1 asymmetric pkCEPI, where 2:1 is the ratio of the high and low resolutions.

Figure 2 shows the resolution advantages of using 2:1 asymmetric pkCEPI compared to spirals and conventional pkCEPI. In this comparison, the FOV is 20 cm, readouts are 16.384 ms, and for partial k-space trajectories 55–60% coverage is assumed.

Results: Several normal volunteers have been scanned using this system. Figure 3 contains three views of the right coronary artery (RCA) acquired using 2:1 pkCEPI at a resolution of 0.8 mm × 1.6 mm and an image time of 150 ms. In these images the horizontal direction is the higher resolution direction. Notice that the RCA is well defined during frames in systole and diastole.

Conclusions: In summary, we have demonstrated that real-time MR can achieve high resolutions for imaging coronary arteries. Future work will focus on reducing the acquisition time and improving SNR. In addition we hope to explore the use of contrast agents and k-space coverages with greater asymmetry.

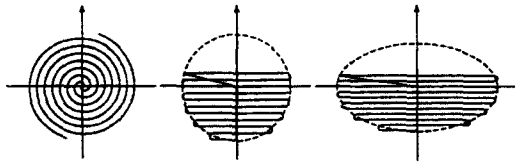

Figure 1. k-space trajectories. spiral, pkCEPI, and 2:1 asymmetric pkCEPI.

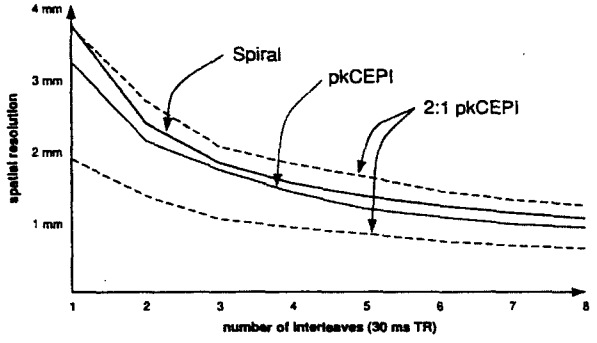

Figure 2. Temporal and spatial resolution tradeoffs.

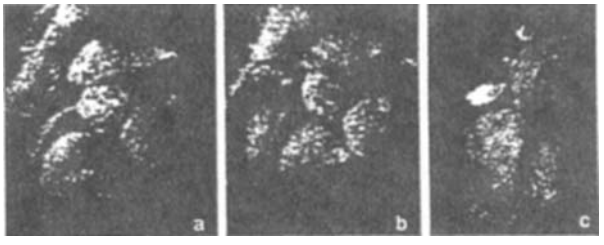

Figure 3. Real-time coronary images. (a) RCA in systole, (b) RCA in diastole, and (c) aortic root.

References

1. Hardy, CJ, et al., *Proc. 7th ISMRM*, 1999; p231.
2. Kerr, AB, et al., *MRM*, 1997; 38, p355.

A Comparison of Image Quality in SMASH and SENSE Cardiac MR Images

C.A. McKenzie, D.K. Sodickson. *Department of Medicine, Cardiovascular Division, Beth-Israel Deaconess Medical Center and Harvard Medical School, Boston, MA*

Introduction: Imaging speed and efficiency are crucial considerations for MRI of the cardiovascular system. A number of techniques for using arrays of RF coils to accelerate MR imaging have been proposed (1–3). Recently two of these techniques, SMASH (4) and SENSE (5), have been applied to cardiac imaging. However, to date no comparisons have been made of the effectiveness of these two approaches. The purpose of this work is to begin to elucidate the relative strengths and weaknesses of these methods by determining two metrics of image quality—signal to noise ratio (SNR) and artefact power—for images reconstructed with each technique.

Methods: For this study, the image quality of both phantom and in vivo images was compared. For the phantom study, a six-element surface coil array custom designed for rapid cardiac imaging (6) was used to acquire images of a standard resolution phantom. To allow accurate determination of image SNR, twenty-four repetitive image sets were acquired for each image plane. In the in vivo experiments, a single set of images of a double oblique volume containing the right coronary

artery (RCA) were obtained in a healthy adult subject using the same array.

The fully encoded phantom and RCA data sets were decimated (every second k-space data line was removed) to produce partially encoded data used in the SMASH and SENSE reconstructions. SMASH reconstruction was performed using the procedure outlined in (1) while SENSE reconstruction was performed as described in (3,7). Fast low-resolution images of the target phantom or in vivo image planes were used as coil sensitivity references. For SENSE sensitivity calibration, an additional phantom or in vivo reference image set was acquired using the body coil (7).

Phantom SNR was determined on a pixel-by-pixel basis by dividing the mean and the standard deviation of pixel intensity across the set of image replicas, as described in (8). A single SNR figure was then obtained by averaging the pixel-by-pixel SNR over a region of interest (ROI) inside the phantom.

SNR in the in vivo data was determined in by drawing a large ROI over the heart in the reconstructed images, calculating its mean signal intensity and dividing that mean by the standard deviation of pixel intensity in a region of noise outside the volunteer's body.

Artefact power is a measure of the absolute difference between the "true" distribution of image intensity and the intensity distribution in a reconstructed image. A reference image formed from the fully gradient encoded data prior to decimation was used as a measure of the "true" image intensity. Artefact power was then determined from the following equation:

$$artefact\ power = \frac{\sum_j \left| I_{reference}(j) - I_{reconstructed}(j) \right|^2}{\sum_j I_{reference}(j)^2}$$

where j is a pixel index, $I_{reference}$ is the reference image and $I_{reconstructed}$ is the SMASH or SENSE image reconstructed from the decimated reference data.

Results: The results of artefact power and SNR calculations, averaged over the various image planes studied, are summarised in Table 1. Figure 1 shows examples of SMASH and SENSE reconstructions of in vivo images containing segments of the RCA.

Discussion: Artefact power in the SMASH and SENSE reconstructed images was similar, despite the fact that residual aliasing artefacts were more clearly visible in some of the SMASH images. SENSE artefacts, though equally pronounced, were less visually apparent in some cases because the pixel-by-pixel nature of the SENSE reconstruction results in more localized reconstruction errors.

SNR was also similar in the two techniques. Since SNR in SMASH and SENSE is known to vary with coil array and image plane geometry, further investigations will be required to explore SNR performance in different imaging situations, and with different imaging hardware.

While SMASH and SENSE both fall in the general category of parallel imaging techniques, they take radically different approaches to image reconstruction, which result in a number of additional practical differences. For example, image reconstruction time is significantly longer for SENSE reconstructions than for SMASH reconstructions, largely due to the computationally intensive method used to calibrate sensitivities in SENSE (7). Despite these differences, for the coil array and image plane geometries investigated, the SMASH and SENSE techniques showed comparable image quality. This suggests that there may be profit in developing hybrid approaches that exploit the practical advantages of both techniques.

References

1. Sodickson DK, et al., *MRM* 1997; 38: 591–603.
2. Ra JB, et al., *MRM* 1993; 30: 142–145.
3. Pruessmann KP, et al., *Proc. ISMRM* 1998; 579.
4. Sodickson DK, et al., *Proc. ISMRM* 1999; 387.
5. Weiger M, et al., *Proc. ISMRM* 1999; 385.
6. Creemers M, et al., *Proc. SCMR* 1999; 009.
7. Pruessmann KP, et al., *Proc. ISMRM* 1998; 2087.
8. Sodickson DK, et al., *MRM* 1999; 41: 1009–1022.

Table 1. Summary of Calculated SNR/Artefact Power

	Phantom	In vivo
SMASH	25.5/0.0044	22.6/0.016
SENSE	25.1/0.0057	24.6/0.019

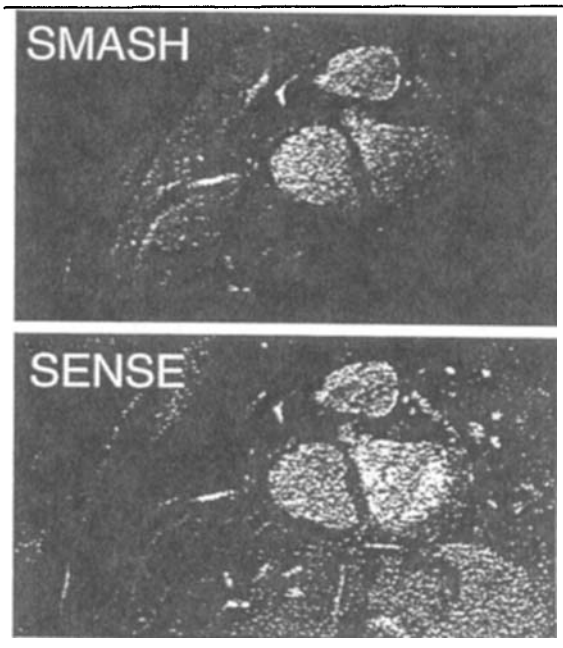

Figure 1. Examples of SMASH and SENSE reconstructions of identical data sets.

Free-Breathing Coronary Vessel Wall Imaging

R.M. Botnar,[1,2] M. Stuber,[1,2] K.V. Kissinger,[1] W.J. Manning[1]. [1]*Beth Israel Deaconess Medical Center and Harvard Medical School, Boston, MA;* [2]*Philips Medical Systems, Best, The Netherlands*

Background: Conventional x-ray coronary angiography and bright blood magnetic resonance angiography (MRA) (1) only allow for assessment of the lumen of the coronary arteries, and do not provide any information on coronary vessel wall thickness or the presence of atherosclerotic plaque. Recently MR images of the coronary vessel wall were reported (2–4). We sought to extend these techniques to a navigator gated and real-time corrected free breathing approach, which might be preferable in patients. We hypothesize that this technique should allow imaging of the coronary vessel wall and coronary plaque in-vivo.

Purpose: The purpose of this study was to demonstrate the feasibility of navigator gated and corrected free-breathing coronary vessel wall imaging in humans using a black blood fast spin echo technique.

Methods: Subjects without history of coronary artery disease were examined in supine position with a Philips Gyroscan ACS-NT MR scanner (Philips Medical Systems, Best, NL) using a commercial 5-element cardiac synergy coil and an advanced cardiac software package (CPR6). All scans including the localizers were performed during uncoached free breathing. Cross-sectional slices perpendicular to the right coronary artery (RCA) were planned using a fast 3D TFE/EPI navigator gated high-resolution localizer scan (Figure 1a) (5). Multiple adjacent

cross-sectional slices (Figure 1b,c) were acquired perpendicular to the proximal RCA using a 2D free-breathing T2 weighted fat suppressed dual inversion recovery fast spin echo sequence (TI = 550ms, TR = 2 heartbeats, TE = 60ms, echo train length = 20, echo spacing = 5.7ms, acquisition window = 120ms, slice thickness = 5mm, FOV = 260 * 260mm, matrix = 256 * 512, NSA = 4). A right hemi-diaphragmatic navigator was used for gating and real-time correction (6).

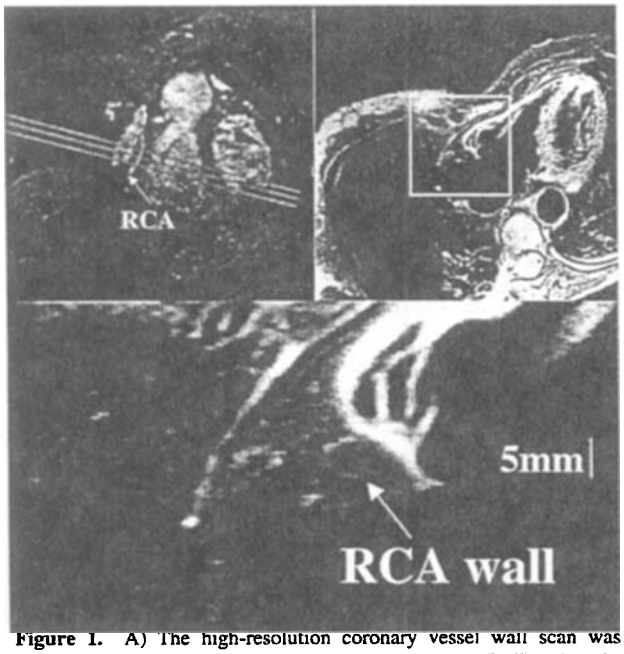

Figure 1. A) The high-resolution coronary vessel wall scan was planed using a free-breathing 3D TFE/EPI scout scan. B) Free-breathing coronary vessel wall imaging using a navigator gated dual inversion fast spin echo (TSE) sequence. C) Magnified cross-sectional view of the right coronary artery wall (RCA-wall).

Results: In all subjects the right coronary vessel wall could be visualized without signs of respiratory motion artifacts (Figure 1b). The coronary vessel wall could be delineated from surrounding epicardial fat and myocardium (Figure 1c). Average scan time per 2D slice was approximately 1 minute.

Conclusions: Free-breathing coronary vessel wall imaging has been successfully implemented in humans. Current limitations are spatial resolution and signal-to-noise, which might be improved using a 3D approach. The presented technique might have potential applications in patients with known or suspected atherosclerotic coronary artery disease.

References

1. Manning WJ, Li W, Boyle NG and Edelman RR. *Circulation* 1993; 87: 94–104.
2. McConnell MV, Goldfarb JW, Manning WJ and Edelman RR. In: *ISMRM, 5th Annual Meeting.* Vancouver: International Society for Magnetic Resonance in Medicine, Berkeley, California, USA; 1997. p 797.
3. Meyer CH, Bob BS, Macovski A and Nishimura DG. In: *ISMRM, 6th Annual Meeting.* Sydney: International Society for Magnetic Resonance in Medicine, Berkeley, California, USA; 1998, p 15.
4. Fuster V, Fayad ZA and Badimon JJ. *Lancet* 1999; 353 Suppl 2: SII5–9.
5. Botnar RM, Stuber M, Danias PG, Kissinger KV and Manning WJ. *JMRI* 1999 (in press).
6. Stuber M, Botnar RM, Danias PG, Kissinger KV and Manning WJ. *Radiology* 1999; 212: 579–587.

In-Vivo Imaging of Atherosclerotic Plaque and Thrombus After Plaque Rupture Using MRI

R.M. Botnar,[1,2] A.S. Perez,[1] W.J. Manning,[1] M.T. Johnstone[1]. [1]*Beth Israel Deaconess Medical Center and Harvard Medical School, Boston, MA;* [2]*Philips Medical Systems, Best, The Netherlands*

Background: Plaque rupture and subsequent thrombus formation is the common pathophysiologic cascade leading to acute coronary syndromes. With the availability of an atherosclerotic animal model in which plaque rupture can be stimulated (1) plaque vulnerability using MRI can be examined under in-vivo conditions. As first reported by Toussaint (2) and subsequently by others (3) T2 weighted (T2w) black blood imaging is a promising tool to look at vessel wall and atherosclerotic plaque.

Purpose: The purpose of this study was to validate MR imaging of atherosclerotic plaque and thrombus formation following plaque rupture in a rabbit model of atherosclerosis.

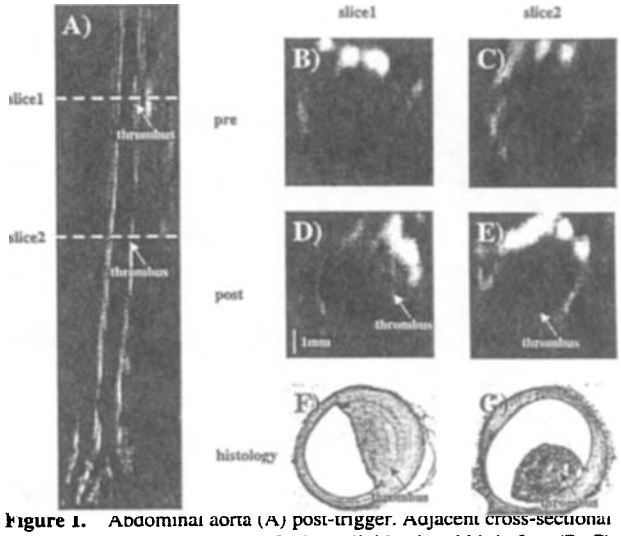

Figure 1. Abdominal aorta (A) post-trigger. Adjacent cross-sectional slices of the abdominal aorta of a hyperlipidemic rabbit before (B, C) and after (D, E) plaque rupture induction. Intra-aortic thrombus is indicated. Corresponding histological specimens (F, G).

Methods: Nine white male (3.5–4.5kg) New Zealand rabbits were studied. According to the previously described model (1), aortic atherosclerosis was induced by balloon endothelial injury of the thoracic and abdominal aorta and a high cholesterol diet for 8 weeks. Each animal underwent baseline MR imaging at the end of this 8 week period. Subsequently, plaque rupture was induced by injection of Russel's viper venom and repeated MR imaging was performed 48 hours later. All scans were performed on a 1.5 Tesla Philips Gyroscan ACS-NT MR scanner (Philips Medical Systems, Best, NL) using a 5 element cardiac phased array coil for signal reception and an advanced cardiac software patch (CPR6) with the anesthetized animal in prone position. Twenty-four cross-sectional contiguous T2w Turbo Spin Echo (TSE) images of the abdominal aorta below the renal arteries were obtained. Imaging parameters were TR = 6 heartbeats, TE = 60ms, echo train length = 12, slice thickness = 5mm, FOV = 120 * 120mm, matrix = 512 * 256, and 8 averages. Average imaging time per slice was 1 minute.

Results: In all animals, thickening of the aortic wall and plaque formation were present on the baseline 8-week scan (Figure 1b, c). Forty-eight hours following Russel's viper venom injection, intraluminal thrombus was visualized (Figure 1d, e) in 6 (67%) of 9 rabbits and was histologically confirmed in all 6 cases (Figure 1f,g). The thrombi were predominantly crescent shaped with an lateral extension of 5mm to 20mm and cross-sectional narrowing from 10% to 50%. In all 3 ani-

mals that MRI failed to identify intra-aortic thrombus, there was also no evidence of thrombosis in the histological specimens.

Conclusions: In this study of experimental atherosclerosis, MRI was able to reliably visualize atherosclerotic plaque and thrombus formation after plaque rupture in-vivo. This technique may have potential application for imaging of human atherosclerotic plaque in acute coronary syndromes.

References

1. Abela GS, Picon PD, Friedl SE, et al. Triggering of plaque disruption and arterial thrombosis in an atherosclerotic rabbit model. *Circulation* 1995; 91: 776–784.
2. Toussaint JF, LaMuraglia GM, Southern JF, Fuster V and Kantor HL. Magnetic resonance images lipid, fibrous, calcified, hemorrhagic, and thrombotic components of human atherosclerosis in vivo. *Circulation* 1996; 94: 932–938.
3. Fayad ZA, Fallon JT, Shinnar M. et al. Noninvasive in vivo high-resolution magnetic resonance imaging of atherosclerotic lesions in genetically engineered mice. *Circulation* 1998; 98: 1541–1547.

Magnetic Resonance Assessment of Aortic Elasticity in Obesity

P.G. Danias, Tritos N.A., Kissinger K.V., Manning W.J. *Beth Israel Deaconess Medical Center and Harvard Medical School, Boston, MA*

Introduction: Obesity is highly prevalent in the United States and is associated with hypertension and increased cardiovascular risk. However, it is unknown whether obesity is associated with abnormalities of vascular elasticity, a possible marker of cardiovascular disease. We investigated the aortic elastic properties of obese (but otherwise healthy young men), and compared these data with a cohort of lean male controls.

Methods: Thirty-eight healthy adult men (age 20–40 years), including 18 obese (BMI > 30 kg/m^2) and 20 lean controls (BMI 19–25 kg/m^2) were studied. All imaging was performed with a 1.5 T whole body system (Gyroscan ACS/NT, Philips Medical Systems, Best The Netherlands) equipped with standard gradient hardware (Powertrack 6000) and advanced cardiac software (CPR 6.0). A 5-element cardiac synergy coil was used for signal reception. Imaging was performed in the supine position for all subjects and data were analyzed by an experienced observer off-line, using a dedicated analysis workstation (Easy Vision, Philips Medical Systems). After initial scout images, we obtained transverse cine images perpendicular to the aorta at the level of the sinotubular ridge (STR) and the abdominal aorta (ABD) immediately proximal to the renal arteries. The imaging protocol included a hybrid gradient echo-echoplanar sequence with the following characteristics: Field-of-view: 330 mm^2, matrix: 256 × 128, slice thickness: 8 mm, TR = RR interval, EPI factor = 7. Effective spatial resolution of 1.3 × 2.6 mm^2, effective temporal resolution = 30–35 msec. During imaging, blood pressure was noninvasively measured using an automated sphygmomanometer.

Images were individually segmented and the maximal and minimal aortic cross-sectional areas were measured. Aortic compliance (AC), stiffness index and pressure-strain elastic modulus (Ep) were computed for the aortic STR and ABD levels (ref).

Results: Data are summarized in the table. As expected, obese subjects had an increased BMI. There was no difference in age or height. Abdominal aortic compliance was significantly decreased (~30%) In obese subjects.

Stiffness index, which is blood pressure independent, and pressure-strain elastic modulus were both significantly increased in the obese cohort. There were no significant differences of aortic elasticity indices at the STR level.

Table (Values ± SD)

	Obese	Lean	*p* value
Age (yr)	29.2 ± 7	29.2 ± 5	0.99
Height (m)	1.78 ± 0.07	1.76 ± 0.07	0.3
BMI (kg/m2)	34.6 ± 3.0	22.9 ± 1.5	<0.001
SBP (mmHg)	140 ± 19	117 ± 17	<0.001
Aorta STR			
AC (mm^2/kPa/mm)	0.27 ± 0.08	0.29 ± 0.16	0.6
Stiffness Index	8.9 ± 2.6	9.2 ± 4.5	0.8
Ep (kPa)	106 ± 40	96 ± 46	0.5
Aorta ABD			
AC (mm^2/kPa/mm)	0.15 ± 0.06	0.22 ± 0.1	0.015
Stiffness Index	8.7 ± 2.9	6.7 ± 1.6	0.013
Ep (kPa)	104 ± 42	71 ± 19	0.004

Conclusions: Cardiovascular MR imaging is uniquely suited for assessment of aortic elasticity in a broad spectrum of patients. In otherwise healthy young men, obesity is associated with decreased elasticity of the abdominal aorta.

Bibliography:
Salomaa V, et al. *Circulation* 1995; 91: 1432–1443.

3D Real-Time Navigator Corrected Black-Blood Coronary MRA

M. Stuber,[1,2] R.M. Botnar,[1,2] K.V. Kissinger,[1] W.J. Manning[1]. [1]*Beth Israel Deaconess Medical Center, Boston, MA;* [2]*Philips Medical Systems, Best, The Netherlands*

Introduction: Conventional sub-millimeter bright-blood coronary magnetic resonance angiography (MRA) without exogenous contrast enhancement may not sufficiently suppress the signal coming from the coronary vessel walls (1). As a consequence, quantitative coronary MRA diameter data may appear biased with respect to x-ray angiography which primarily displays the coronary lumen. We therefore have developed a free-breathing sub-millimeter prospective navigator gated and real-time 3D motion corrected coronary MRA technique which combines a dual-inversion pre-pulse (2) and a turbo spin-echo sequence for black-blood coronary MRA (1).

Materials and Methods: Four volunteers and two patients with x-ray confirmed coronary artery disease (CAD) were investigated on a 1.5T Philips Gyroscan ACS-NT system equipped with a commercial 5-element cardiac synergy coil. For the definition of the double oblique high-resolution imaging planes in parallel to the native coronary arteries, an ultrafast 3D TFE-EPI scout scan was applied in conjunction with a 3-point plan-scan tool (3). For black-blood coronary MRA, a dual inversion pre-pulse was applied immediately after the detection of the R-wave of the ECG. The first non-selective inversion pre-pulse (INV-NS, Fig. 1) was followed by a second, slice selective inversion pre-pulse (INV-SS, Fig. 1) at the level of interest. Another slice selective inversion pulse was applied at the dome of the right hemidiaphragm (RESTORE, Fig. 1) to restore inverted magnetization for subsequent diaphragmatic navigator interface detection. The navigator (Fig. 1) precedes the imaging part of the sequence and is applied for gating (5mm gating window) and prospective 3D real-time correction (m, p and s direction). Seven overlapping slices (3mm thickness; −1.5mm overlap) were imaged (TI = 590ms) using a 2D turbo spin-echo imaging sequence with a linear k-space acquisition, an interecho spacing of 6.6ms, a TE of 40ms, an echo train length of 23 and a TR of 2 cardiac cycles (360mm FOV; 512 × 384matrix).

Results: In all measured individuals, extensive portions including higher-order branches (Fig. 1, dashed arrow) of the left and right coro-

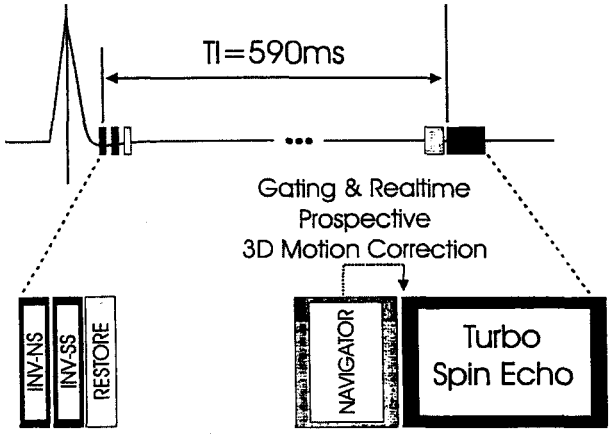

Figure 1. Dual-inversion free-breathing 3D navigator coronary MRA sequence.

nary system could be consistently visualized with a high contrast between blood and the surrounding tissue. In the patient with angiographically confirmed CAD, the moderate narrowing of the LM was verified on the black-blood coronary MRA (Fig. 2, solid arrow). Average imaging duration for each 2D slice was <60sec.

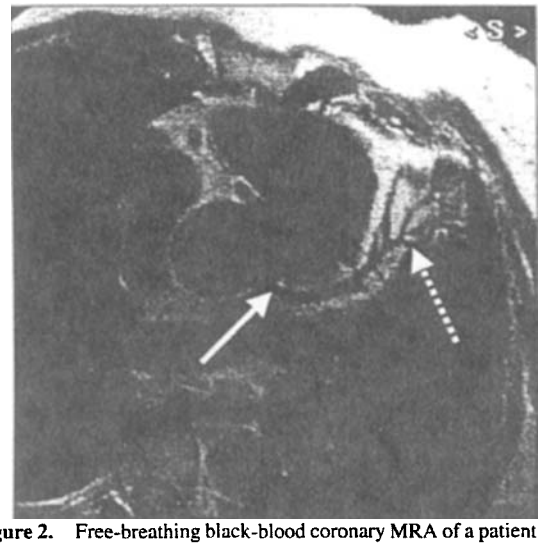

Figure 2. Free-breathing black-blood coronary MRA of a patient with an x-ray angiographically confirmed LM narrowing (solid arrow). Image resolution: 0.7 × 1.0mm.

Discussion: Free-breathing high-resolution black-blood coronary MRA has been successfully implemented and applied in patients and volunteers. It potentially enables for coronary lumen imaging which may be more analogous to x-ray angiography. Imaging duration is substantially shortened with respect to earlier proposed high-resolution free-breathing coronary MRA techniques (3). Using a turbo-spin-echo sequence, signal is maximized. Extended with a 3D imaging sequence, the method may have a potential for a further enhancement towards x-ray angiographic image resolution.

References

1. McConnell MV. et al.: *Proc ISMRM* 1997; 2: 797 (abstract).
2. Sinha S. et al.: *J Magn Reson Imaging* 1996; 6: 484–94.
3. Stuber M. et al.: *J Am Coll Cardiol* 1999; 34: 524–531.

Comparison of Breath-Hold and Free Breathing Acquisitions For Left Ventricular Volume and Mass

K.V. Kissinger,[1] M. Stuber,[1,2] R.M. Botnar,[1,2] C.J. Salton,[1] W.J. Manning[1]. [1]*Beth Israel Deaconess Medical Center, Boston, MA;* [2]*Philips Medical Systems, Best, The Netherlands*

Background: Breath-hold cine gradient echo MRI is widely used in the evaluation of ventricular function. This imaging technique has been shown to be both accurate and effective in most patients for acquiring ventricular volume and mass data (1,2). While this method yields excellent image quality in most patients, some cardiac patients are unable to adequately hold their breath for these acquisitions. Alternative methods are available to overcome these difficulties including hyperventilation or supplemental oxygen to increase the patient's ability to maintain a breath-hold (3) as well as faster imaging sequences such as real time MRI.

When considering instruction and recovery time, breath-hold cine MR acquisitions are inherently 25% efficient. We therefore hypothesized that non breath-hold approaches with multiple signal averages might serve as a viable alternative for those unable to cooperate with breath-hold and without prolonging overall scan time.

Purpose: The purpose of this study was to evaluate the effectiveness and accuracy of a free-breathing cine imaging technique for the quantification of left ventricular volumes and mass.

Materials and Methods: Eight healthy subjects (5M/3F age = 36 ± 11) were imaged with a 1.5T Philips Gyroscan ACS-NT MR Scanner (Philips Medical Systems, Best, NL) using a commercial 5 element cardiac synergy coil and an advanced cardiac software package (CPR6). Transverse scouts were performed during free breathing. A breath-hold two chamber (vertical long axis) cine was acquired for the selection of the short axis imaging plane. Contiguous short axis cine slices were acquired using two strategies: 1) Conventional FFE-EPI breath-hold sequence (TR = 1 R-R interval, TE = 9ms, EPI factor = 9, FOV = 320 × 224, matrix = 118 × 256, slice thickness = 10mm, NSA = 1) and 2) Non breath-hold TFE-EPI sequence (TR = 11ms, TE = 3.9ms, EPI factor = 5, shots = 13, FOV = 320 × 224, matrix = 185 × 256, slice thickness = 10mm, NSA = 4). All images were evaluated on a Philips Easy Vision 4.0 workstation with commercially available cardiac analysis software. LV endocardial contours at end diastole and end systole as well as LV epicardial contours at end diastole were prescribed manually. Calculations for EDV, ESV, EF and ED mass were made automatically by the software for each of the scans.

Results: There was excellent correlation ($r^2 = 0.96$) of end diastolic LV mass between the breath-hold and non breath-hold imaging methods. For both techniques, no significant differences were found for end systolic volume (Figure 1) or left ventricular ejection fraction. There was good correlation (Figure 2, $r^2 = 0.86$), but end-diastolic volume was significantly underestimated by TFE-EPI ($p = 0.02$). The TFE-EPI required less time to acquire than the breath-hold FFE-EPI (7.3 min/ 9.6min), ($p = 0.0004$).

Discussion and Conclusions: For patients who are unable to perform breath-hold cine MR for the evaluation of LV function, a free breathing TFE-EPI sequence utilizing multiple signal averages may be a viable alternative for measurement of LV volumes and mass. Issues of breath-hold compliance are eliminated with the TFE-EPI sequence. The difference found in end diastolic volume may be related to the relative time delay to the acquisition of the first phase in the TFE-EPI data set (24ms vs. 8ms). Continued studies are required to compare the accuracy of this non breath-hold technique to the accepted breath-hold methods.

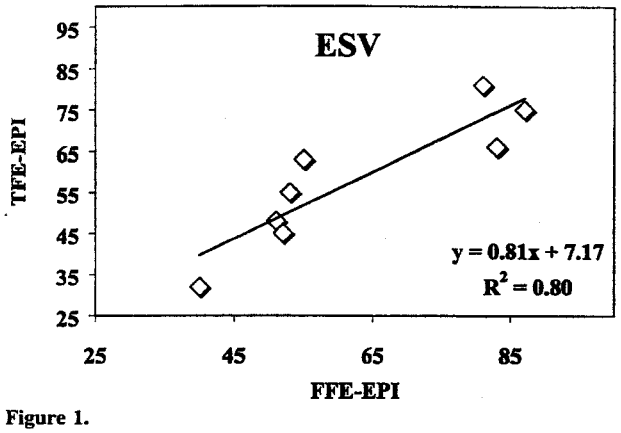

Figure 1.

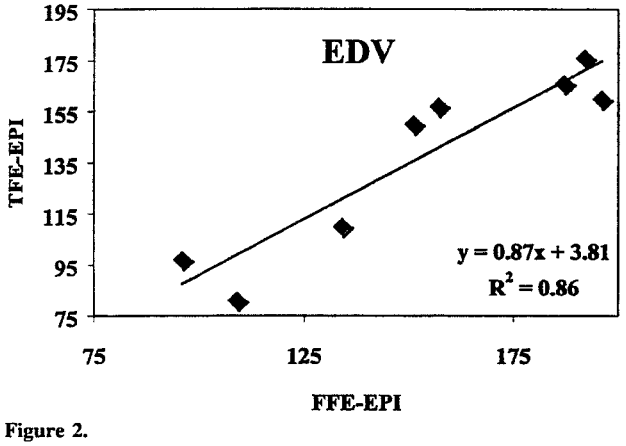

Figure 2.

References
1. Lorenz, CH et. al. *JCMR* 1999 1(1): 7–21
2. Chuang, ML et. al. *JMRI* 1997 Sep-Oct; 7(5): 811–4
3. Danias, PG et. al. *AJR* 1998 Aug; 171(2): 395–7

Superiority of Prone Position in Free-Breathing 3D Coronary MRA in Patients with Coronary Disease

M. Stuber,[1,2] P.G. Danias,[1] R.M. Botnar,[1,2] K.V. Kissinger,[1] W.J. Manning[1]. [1]*Beth Israel Deaconess Medical Center, Boston, MA;* [2]*Philips Medical Systems, Best, The Netherlands*

Introduction: Navigator gated and corrected 3D coronary MR angiography (MRA) enables sub-millimeter image acquisition during free breathing. However, diaphragmatic excursion superior to the gating window and possibly relative phase shifts of chest wall motion are limiting factors for image quality and scanning duration (1,2). We hypothesized that image acquisition in the prone position would minimize artifacts related to chest wall motion and suppress superior diaphragmatic excursion.

Materials and Methods: Twelve patients with x-ray confirmed coronary artery disease and 6 healthy adult volunteers were studied in both the prone and the supine position on a 1.5T Philips Gyroscan ACS-NT system equipped with a 5-element commercial cardiac synergy coil (Philips Medical Systems, Best, NL). Double oblique 3D coronary MRA along the major axes of the left and right coronary system (3) (512 matrix, 360mm. FOV, TE = 2.6ms, TR = 8.8ms, 3mm slice thickness, 70ms acquisition window) were acquired during free breathing using diaphragmatic navigator gating (5mm window) and motion correction. A T2Prep pre-pulse (TE = 50ms) was applied for contrast enhancement between myocardial muscle and blood (4). Objectively assessed image quality (CNR, SNR, vessel definition (4)) and the relative diaphragmatic positions (1) during free breathing were compared.

Results: Superior or cranial (relative to the gating window) end-expiratory diaphragmatic excursion occurred less frequently in the prone position (Fig. 1, 'Superior Excursion') (23 ± 17% vs. 40 ± 26% supine, $p < 0.05$) and navigator efficiency was higher (Fig. 1, 'In Window'). In the prone position, we found a 36% improvement in SNR (15.5 ± 2.7 vs. 11.4 ± 2.6, $p < 0.01$) and a 34% improvement in CNR, (12.5 ± 3.3 vs. 9.3 ± 2.5, $p < 0.01$). The prone position also resulted in a 17% improvement in coronary vessel definition ($p < 0.01$).

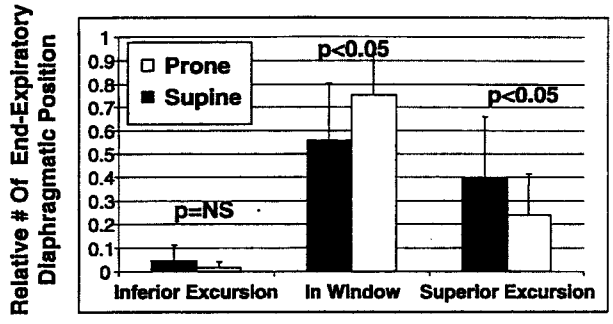

Figure 1. Relative End-Expiratory Diaphragmatic Excursion.

Discussion: Prone coronary MRA results in improved SNR and CNR with enhanced coronary vessel definition (Fig. 2). Superior end-expiratory diaphragmatic excursion was also reduced and navigator efficiency was enhanced. In the prone position, the expansion of the rib cage is mechanically constrained, and as a consequence, patients with a tendency for chest-wall breathing appear to be 'forced' into a diaphragmatic breathing pattern. When feasible, prone imaging is recommended for free-breathing coronary MRA.

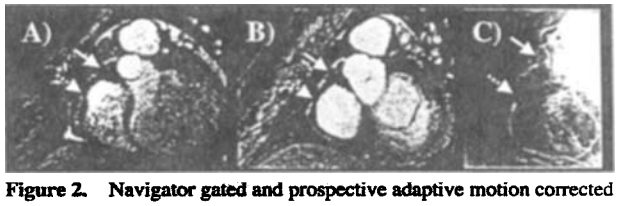

Figure 2. Navigator gated and prospective adaptive motion corrected 3D T2Prep coronary MRA acquired in the supine (A) and in the prone (B) position of a patient with X-ray angiographically confirmed coronary disease (C).

References
1. Taylor AM, et al. *JMRI* 1997; 7: 629–636.
2. Taylor AM, et al. *Proc ISMRM* 1998; 1: 21 (abstract).
3. Stuber M, et al. *J Am Coll Cardiol* 1999; 34: 524–531.
4. Botnar RM, et al. Circulation 1999; 99: 3139–3148.

Diastolic Forward Flow in the Ascending Aorta: Quantification by Magnetic Resonance Imaging

M.J. Ross,[1] R.M. Botnar,[1,2] K.V. Kissinger,[1] M.F. Riley,[1] W.J. Manning.[1] [1]*Beth Israel Deaconess Medical Center and Harvard Medical School, Boston, MA;* [2]*Philips Medical Systems, Best, The Netherlands*

Background: It has been suggested that aortic compliance correlates inversely with atherosclerotic load, as defined by the number of cardiovascular risk factors and events present (1). Magnetic resonance phase velocity mapping (PVM) is a validated technique for determining accu-

rate velocity and flow measurements through a cross sectional slice (2). We describe here the use of PVM to characterize diastolic forward flow in a population of young healthy adults.

Methods: Eleven healthy adults (28 ± 3 years) free of aortic insufficiency by Doppler echocardiography were examined in a 1.5 Tesla Philips Gyroscan scanner (Philips Medical Systems, Best, NL). Phase velocity data were obtained of the ascending aorta at the level of the sinotubular ridge (STR) and at the transverse pulmonary artery (trPA), using retrospective ECG gating. 34 phases were obtained throughout the cardiac cycle. All measurements were flow compensated in readout and preparation direction. In-plane resolution was 1.2 mm, slice thickness was 8 mm, and the echo time was 2.8 msec. Partial echo sampling was used, with velocity encoding of 200 cm/sec.

Aortic areas were manually circumscribed and velocity measurements were recorded at both the STR and trPA throughout all phases of the cardiac cycle. Flow through the aorta at each phase was calculated as Flow = Velocity × Area, and plotted as a function of time during the cardiac cycle. The area under this curve was integrated to determine the volume of forward blood flow.

Results: For each subject, aortic blood flow and cross-sectional area were plotted as a function of time throughout the cardiac cycle (Example, Figure). Planimetry and PVM measurements were as follows (Table).

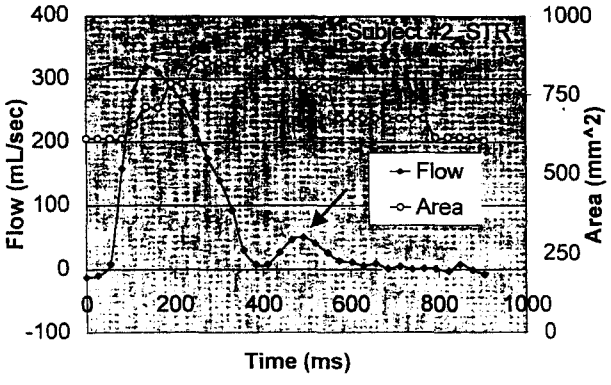

Aortic area was recorded at end-diastole and at peak dilation. Peak dilation occurred at mean times of 323 and 290 msec (p = NS), and mean increases in aortic area of 28.6% and 23.4% (p = NS) were noted in the STR and trPA planes, respectively.

A peak in forward flow velocity during ventricular systole occurred in the STR and trPA slices at mean times of 125 and 129 ms, respectively (p = NS). A secondary peak in forward flow during ventricular diastole (Figure, arrow) was noted in 11 of 11 subjects, and occurred at mean times of 482 and 491 ms (p = NS). The mean ratio of the forward diastolic component to the forward systolic component was 10.3% and 9.6% in the STR and trPA planes (p = NS).

Mean forward blood volume during ventricular systole in the STR and trPA planes was found to be 76.7 and 76.6 mL (p = NS). Mean forward blood volume during ventricular diastole in the STR and trPA planes was 5.2 and 5.5 mL (p = NS). This represented 6.8 and 7.2% of the total forward blood volume at each cross-sectional plane (p = NS).

Conclusions: Forward diastolic blood flow in the ascending aorta is common in young healthy adults and is likely related to aortic compliance. This contribution of aortic compliance to total forward cardiac output is relatively small. Magnetic resonance PVM provides a simple non-invasive method for quantifying the diastolic component of forward flow, and its physiologic contribution to cardiac output. Further investigation is warranted to demonstrate the effects of aging and medical disease processes on this phenomenon.

References

1. Lehmann ED et.al. *Hypertension* 1998; 32: 565–9.
2. Firmin DN et.al. *J Comput Assist Tomogr* 1987; 11: 751–6.

	STR	trPA
Aortic Area		
End-diastolic (mm^2)	586.0 ± 138.5	605.9 ± 130.1
Maximum (mm^2)	753.7 ± 171.8	747.5 ± 137.9
Increase (mm^2)	167.7 ± 54.8	141.6 ± 42.9
% increase	28.6 ± 9.8	23.4 ± 9.1
Flow		
Peak systolic (mL/sec)	401.6 ± 90.9	409.6 ± 81.1
Peak diastolic (mL/sec)	41.5 ± 16.2	39.3 ± 13.0
Ratio (%)	10.3 ± 5.0	9.6 ± 4.7
Forward Volume		
Ventricular systole (mL)	76.7 ± 19.4	76.6 ± 14.0
Ventricular diastole (mL)	5.2 ± 2.3	5.5 ± 2.9
Ratio (%)	6.8 ± 3.0	7.2 ± 4.2

Evaluation of Aortic Insufficiency by Breath-hold Magnetic Resonance Imaging: Impact of Echo Time on Visually Apparent Signal Void Areas

M.J. Ross,[1] R.M. Botnar,[1,2] K.V. Kissinger,[1] M.F. Riley,[1] W.J. Manning.[1] [1]*Beth Israel Deaconess Medical Center and Harvard Medical School, Boston, MA;* [2]*Philips Medical Systems, Best, The Netherlands*

Background: Evaluation of aortic insufficiency (AI) by conventional gradient echo cineangiographic magnetic resonance (MR) imaging has been well described and validated (1,2). Turbulence/dephasing due to diastolic regurgitant flow is recognized as a signal void in the left ventricular outflow tract (LVOT). It has been demonstrated that variation in imaging parameters, including echo times (TE) and flip angles, can cause variation in measured areas of the signal void (3).

In more recent years, the use of segmented k-space gradient echo has allowed the entire cardiac cycle to be imaged in a single breath-hold (4). This more rapid imaging approach has now become the standard technique at many cardiac MR centers. These breath-hold sequences utilize shorter TE than non-breath-hold techniques. The effect of this parameter on the visual evaluation of AI has not been previously reported.

Methods: Thirty subjects (mean age 48 years), including 22 with varying grades of AI (defined by Doppler echocardiography) and 8 healthy adults free of AI by Doppler echocardiography were examined in a 1.5 Tesla Philips Gyroscan scanner (Philips Medical Systems, Best, NL). No subjects had more than mild echocardiographic mitral regurgitation. Fast field echo (FFE) cine MR imaging of the LVOT was performed in all subjects (TE 13 msec, flip angle 30°, slice thickness 8 mm, FOV 32 cm, image matrix 128 × 256). Turbo field echo (TFE) segmented k-space imaging of the LVOT was performed in a single breath-hold in each subject (flip angle 30°, slice thickness 8 mm, FOV 32 cm, image matrix 114 × 256), first with a TE = 3.2 msec, then with a TE = 6.2 msec. In both TFE and FFE sequences, data acquisition was ECG triggered, and cardiac phases were imaged at approximately 70 msec intervals.

Visually apparent diastolic aortic regurgitant signal voids were measured on the cine MR images by manually circumscribing areas of low intensity signal originating at the orifice of the aortic valve and extending into the left ventricle (LV) during diastole. For each imaging sequence, the LV area was circumscribed in the cardiac phase with maximal regurgitant signal void. The ratio of the area of the signal

void (ASV) to the total LV area in that section was calculated as a measurement of the degree of AI.

Results: Mean ASV/LV area are plotted for each imaging sequence, and for each echocardiographic grade of AI (Figure).

In patients with no echocardiographic AI, mean signal void ratios were 0.00 for all imaging sequences (p = NS). In patients with mild AI by Doppler echo, mean signal void ratios were 0.06, 0.10 and 0.00 at echo times of 13, 6 and 3 msec, respectively (p = 0.018). In patients with moderate AI, signal void ratios were 0.31, 0.13 and 0.00 at echo times of 13, 6 and 3 msec (p < 0.001). In patients with greater than moderate AI by Doppler echo, signal void ratios were 0.46, 0.20 and 0.00 at echo times of 13, 6 and 3 msec (p < 0.001).

Conclusions: Visual assessment of AI severity is heavily dependent on the choice of TE. The use of shorter echo times in breath-hold TFE cineangiographic MR imaging significantly decreases the size of the visually apparent signal void seen in the presence of moderate or greater AI. Consideration of imaging parameters is required for the evaluation of regurgitant valvular lesions using breath-hold techniques. Alternative MR methods such as flow velocity mapping may be better suited to the evaluation of aortic insufficiency.

References
1. Plugfelder et.al. *AJR* 1989; 152: 729–35.
2. Higgins et.al. *Circulation* 1991; 84(Suppl): 1198–1207.
3. Suzuki et.al. *AJR* 1990; 155: 723–727.
4. Atkinson et.al. *Radiology* 1991; 178: 356–360.

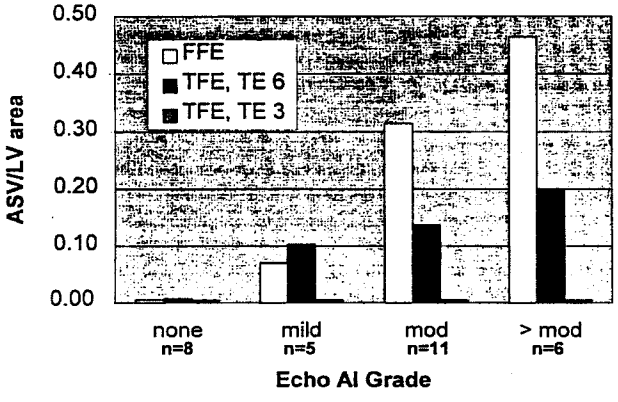

Improved ECG Triggering with the T-wave Terminator[1]

D.C. Bloomgarden,[1,4] G.R. Morris,[2] J. Valentine,[2] A.J. Powell,[3] T. Chung.[4] [1]*Department of Radiology, Beth Israel Deaconess Medical Center, Boston, MA;* [2]*Magnetic Resonance Equipment Corp., Bay Shore, NY;* [3]*Department of Cardiology, and* [4]*Department of Radiology, Children's Hospital, Boston, MA*

Introduction: MR imaging of the heart and thoracic vessels requires ECG gating to compensate for cardiac motion. Triggering is accomplished by synchronizing the image acquisition pulse sequence to the R-wave of the ECG. However, the magnetic fields within the bore of the scanner can cause artifacts in the ECG waveform which result in gating and triggering errors. In addition, small variations in electrode position can result in an unusable ECG signal (2).

Despite recent technical advances that have improved ECG signal quality, including fiber-optic cables and radiofrequency filtering, establishing reliable gating in the clinical realm is often problematic (3). In particular, patients with congenital heart disease, ischemic or hypertrophic cardiomyopathy, or who have undergone thoracic surgery often manifest alterations in the directions and relative magnitudes of the R and T waves that yield high voltage T-waves once placed inside the bore of the magnet.

In order to improve ECG gating reliability, we designed and constructed hardware to selectively suppress the T-wave in the ECG waveform and evaluated it in human subjects. We call it the T-wave Terminator (TwT).

Methods: The TwT was designed by modeling the effect of varying filtering circuits on the ECG waveform using simulated data and simulated noise from blood flow artifacts. Based on the results of software simulation, a standard ECG bandpass filter (0.67Hz to 40Hz) was combined with an additional single pole high pass filter which preferentially suppresses frequencies below 10 Hz (3dB down). This combined filter was inserted into a fiber optic transducer FOX™ module (Magnetic Resonance Equipment Corp, Bay Shore, NY). The output signal was then fed back into the MR system signal processor.

We prospectively recorded ECG strips on 12 consecutive patients (ages 4–51 years) while on the gurney under 4 conditions: inside and outside the magnet bore, with and without the TwT. All patients were undergoing cardiac MRI at our institution for clinical evaluation of congenital heart disease. The patients were imaged with 2 phased array coils on a 1.5T Horizon LX (GEMS). In addition, 3 normal adult volunteers underwent cardiac MRI with ECG leads placed high on the left chest to simulate elevated T-waves. The volunteers were scanned with ECG gating with the FOX™ module with and without the TwT, with a spin echo pulse sequence with respiratory compensation. Gating accuracy was assessed by counting the number of false positive (triggering on the T-wave) and false negative (missed beat) events. The additional time (beyond calculated time) required to complete the scan was recorded. Similar data was acquired from 3 normal volunteers with the same gating circuits with the patients inside and outside of a 4 Tesla scanner (GEMS).

Results: While in the magnet bore, the R-wave to the T-wave ratio was significantly greater with the T-wave terminator (4.0 versus 2.3, p = 0.01). In fact, in all patients the TwT reduced this ratio. Using the TwT, gating was successful and diagnostic quality images were obtained in all patients. In 4 of 12 patients the T wave was greater than 70% of the R wave versus in none of the patients using the TwT. No adjustments of electrode positions were required after switching to the TwT.

The TwT performed better than the standard filter in the volunteers with altered lead placement to simulate tall T waves, when scanned using 1.5T and 4T systems. In the 3 volunteers in the 1.5T scanner, the TwT reduced the false positive rate from 46.3 to 5 beats per series.

Discussion: Use of the TwT resulted in a significant increase in the R/T ratio and was necessary for successful gating in at least 2 patients. Moreover, its use in volunteers with simulated increased t waves clearly resulted in superior gating.

Frequently 10 to 20 minutes of technician and physician time are required at the beginning of a cardiac MR study to optimize the ECG signal and ensure that the gating is adequate. This process often involves changing the electrode positions, moving the patient in and out of the scanner, further delaying the start of the exam. Consequently, use of the TwT may significantly reduce the total exam time as well as the associated frustration of the staff. Moreover, the improved ECG signal from the TwT should reduce the number of triggering errors, leading to shorter scan time and improved image quality by eliminating artifacts from unsynchronized heartbeats.

Conclusion: A new bandpass filter was added to a fiber optic ECG gating circuit significantly improving the ECG waveform and subsequent gating during cardiac imaging.

References
1. Bloomgarden DC, et al., *Proc ISMRM* 1999; 7: 1995.
2. Dimick RN, Hedlund LW, et al., *Inv Rad* 1987; 22: 17–22.
3. Felbinger J, et al., *Magn Res Med* 1994; 32: 523–9.

Cine Magnetic Resonance Imaging Shows Improved Regional Thickening in Remote and Chronic Ischemic Myocardium After Transmyocardial Laser Revascularization

Olaf M. Muehling,[1] Norbert M. Wilke,[1] Yimei Huang,[1] Sam Wann,[1] Ying Wang,[1] Michael Jerosch-Herold,[2] Mary M. Cayton,[2] Mahmood, M. Mirhoseini.[2] [1]*Center of Magnetic Resonance Research, Department of Radiology, University of Minnesota;* [2]*Heart and Lung Institute Wisconsin and St. Luke's Hospital, Milwaukee, WI*

Background: It is not proven, whether there is a hemodynamic benefit along with relief of angina, after treatment with transmyocardial laser revascularization (TMLR). Recently, it has been shown that there is improved regional function in the ischemic zone after TMLR (1). So far, there are no data available of regional function of the adjacent non-ischemic myocardium after laser treatment. Using cine magnetic resonance imaging (CMR) as a non-invasive, quantitative, diagnostic tool, we hypothesized that there is improvement of remote and ischemic myocardial function after TMLR and preservation of left ventricular (LV) function.

Methods: In 14 pigs (20–25 kg) ischemia was induced by catheter-guided hollow bead embolization of the LCx. One week after induction of ischemia the animals were randomized either to a treatment (TMLRs) or control group (controls). TMLR was performed in 7 of 14 animals. With a high powered (850 W) CO_2-laser 30 ± 5 channels were created over the postero-lateral segment of the heart. Follow-up CMR was performed before (n = 14), and 8 weeks (n = 13) after TMLR. Global LV function was assessed by the cardiac output index (CO-Index, ml/min/kg). Global and regional wall motion was analyzed using the modified Centerline method using MASS software (2,3). Regional wall thickening (RWT in mm) was determined in a midventricular slice. The myocardium of the left ventricle was divided into three regions according to the three main vessels (4) a total of 50 adjacent cords in the septal, anterior, and lateral region were assigned to the region perfused by the left anterior descending artery (LAD, remote area). 25 cords adjacent to the lateral LAD region were assigned to the area supplied by the LCx (ischemic area). Microsphere studies were obtained to document changes in regional myocardial blood flow (MBF, ml/min/g). TTC-tissue staining was made to determine infarct size.

Results: RWT in the target region was significantly impaired vs. the remote region at 1 week (0.8 ± 0.9 vs. 4.8 ± 1.3 $p < 0.01$). After 8 weeks RWT in the ischemic area improved in TMLRs (0.4 ± 0.4 vs. 2.8 ± 1.5, $p < 0.02$) and resulted in a significantly greater wall thickening of TMRLs vs. controls (2.8 ± 1.5 vs. 1.2 ± 0.7, $p < 0.04$). RWT in the remote area was increased in TMLRs vs. controls (5.4 ± 1.2 vs. 3.9 ± 0.8, $p < 0.04$). CO-Index was decreased vs. baseline in controls (172 ± 34 vs. 79 ± 18, $p < 0.01$) and significantly decreased vs. TMLRs after 8 weeks (79 ± 18 vs. 117 ± 10, $p < 0.01$). MBF was improved in the target and remote zone of controls vs. TMLRs (0.2 ± 0.04 vs. 0.6 ± 0.2, $p < 0.04$; 0.8 ± 0.12 vs. 1.2 ± 0.03, $p < 0.02$) and TTC-stains revealed significant decrease in infarct size (6.6% ± 1.6 controls vs. 3.6% ± 1.5 T, $p < 0.01$).

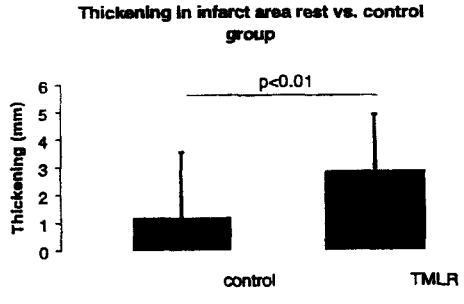

Conclusion: As demonstrated for the first time with CMR, TMLR improves regional myocardial function not only in the ischemic region but also in the remote myocardium. Furthermore, there is preservation of global left ventricular function, most probably due to improved myocardial blood flow in the target and remote zone and a reduced infarct size after TMLR.

References

1. Horvath KA, Greene R, Belkind N et al. *Ann Thorac Surg* 1998; 66: 721–725.
2. Buller VG, van der Geest RJ, Kool M.D. et al. *Invest Radiol* 1997; 32: 529–539.
3. Holman ER, Buller VG, de Roos A et al. *Circulation* 1997; 95: 924–931.
4. Weaver ME, Pantely GA, Bristow JD et al. *Cardiovasc Res* 1986; 20: 907–917.

Cine Magnetic Resonance Imaging Shows Preserved Global and Diastolic Function in Chronic Ischemia After Transmyocardial Laser Revascularization (TMLR)

Olaf M. Muehling,[1] Norbert M. Wilke,[1] Yimei Huang,[1] Sam Wann,[1] Ying Wang,[1] Michael Jerosch-Herold,[1] Mary M. Cayton,[2] Mahmood M. Mirhoseini.[2] [1]*MR Core Laboratory, Center of Magnetic Resonance Research, Department of Radiology, University of Minnesota Medical School;* [2]*Heart and Lung Institute of Wisconsin and St. Luke's Hospital, Milwaukee, WI*

Introduction: TMLR improves symptoms and myocardial perfusion in patients with refractory angina and end-stage coronary artery disease (1,2). However, it is controversial if the relief of angina correlates with functional improvement. Breath-hold cine-magnetic resonance imaging (MRI) is a comprehensive diagnostic tool capable of quantitative left ventricular assessment (3,4). We hypothesize that MRI with its non-invasive nature as well as its high spatial and temporal resolution provides valid information necessary to accurately monitor the effects of TMLR.

Methods: Ischemia was induced in 12 pigs (20–25 kg) by catheter-guided hollow bead embolization of the LCx. The animals were randomized to treatment (TMLR) or control group (controls) one week after induction of ischemia. With a high-powered (850 W) CO_2-laser 30 ± 5 channels were made over the postero-lateral segment of the heart in 6 of the 12 animals. Follow-up cine magnetic resonance imaging (CMR) was performed before (n = 12), at 3 weeks (n = 8), and 8 weeks (n = 12) after treatment. Left ventricular function was determined by weight corrected stroke volume (SV, ml/kg) and cardiac output (CO, ml/min/kg). Diastolic function was assessed by normalized early peak filling rate (NPFR, 1/s). Microsphere studies were obtained to measure changes in regional myocardial blood flow (MBF, ml/min/g). TTC-staining was performed to determine infarct size.

Results: At 3 weeks after surgery, CO and SV decreased in TMLR (119 ± 23 vs. 84 ± 9 ml/min/kg, $p < 0.05$; 1.4 ± 0.3 vs. 1.0 ± 0.1 ml/kg, $p < 0.02$), then returned to near normal values after 8 weeks (117 ± 10 ml/min/kg, 1.3 ± 0.2 ml). In controls, these parameters decreased throughout the experiment (172 ± 34 vs. 79 ± 18 ml/min/kg (at 8 weeks); $p < 0.01$; 1.4 ± 0.3 vs. 1.0 ± 0.2 ml/kg (at 8 weeks), $p < 0.02$). There was a significant difference in CO and SV between controls and TMLR at 8 weeks (CO: 79 ± 18 vs. 117 ± 10, $p < 0.01$; SV: 1.0 ± 0.1 vs. 1.3 ± 0.2, $p < 0.02$). NPFR decreased slightly in TMLR and was not different from baseline at 8 weeks; whereas it decreased significantly in controls (9.3 ± 2.3 vs. 6.2 ± 0.8, $p < 0.01$). MBF was increased in the ischemic zone of TMLR vs. controls (0.6 ± 0.2 vs. 0.2 ± 0.1, $p < 0.04$). TTC-staining revealed a significant decrease in infarct size in TMLR group (3.6% ± 1.5 vs. 6.6% ± 1.6 $p < 0.01$).

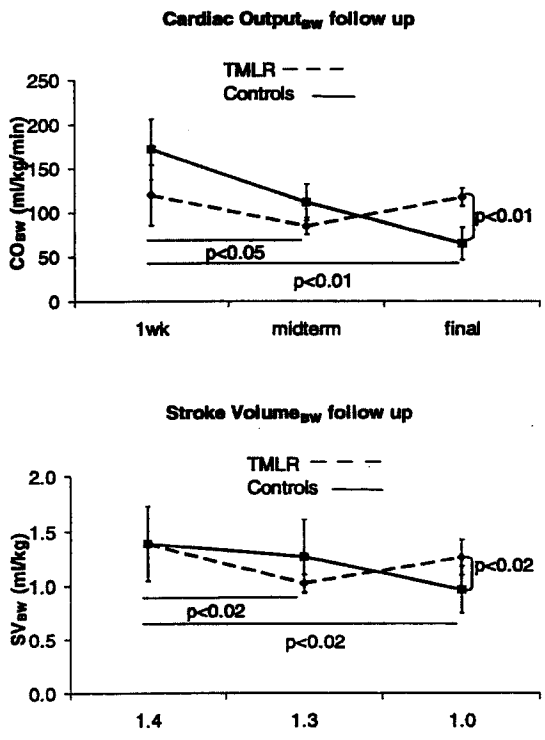

Conclusion: In the present porcine study we used magnetic resonance imaging as an emerging quantitative diagnostic tool to assess morphology and function of the chronic ischemic left ventricle after treatment with TMLR. TMLR prevents a decline in diastolic and overall left ventricular function secondary to a decreased infarct size and improved perfusion. Recently published multicenter trials (5,6) attribute a beneficial effect of TMLR in patients with coronary artery disease, but did not support conclusively the hypothesis of an improved cardiac function after TMLR. Quantitative non-invasive CMR shows for the first time a global functional benefit after TMLR.

References

1. Frazier OH, March RJ, Horvath KA. *N Engl J Med* 1999; 341: 1021–1028
2. Allen KB, Dowling RD, Fudge TL et al. *N Engl J Med* 1999; 341: 1029–1036
3. Rehr RB, Malloy CR, Filipchuk NG et al. *Radiology.* 1985; 156: 717–9
4. Longmore DB, Klipstein RH, Underwood SR et al. *Lancet* 1985; 1: 1360–1362
5. Horvath KA, Cohn LH, Cooley DA et al. *J Thoras Cardiovasc Surg* 1997
6. Schoffield PM, Sharples LD, Caine N et al. *Lancet* 1999; 353: 519–524

Quantitative MR First-Pass Perfusion Imaging: Sensitivity and Specificity vs. SPECT vs. PET vs. Coronary Angiography in Detecting Coronary Artery Disease in Individual Vessels

A. Zenovich,[1] O.M. Muehling,[1] M.E. Dickson,[2] Huang,[1] M. Jerosch-Herold,[1] B.V. Wilson,[2] F. Zhao,[1] H. Huang,[1] R.F. Wilson,[2] J.H. Traverse,[2] T. Henry,[3] I.S. Anand,[4] and N.W. Wilke.[1] [1]*Cardiovascular MRI Core Laboratory, Center for MR Research;* [2]*Division of Cardiology, Department of Medicine, University of Minnesota Medical School;* [3]*Hennepin County Medical Center,* [4]*VA Medical Center, Minneapolis, MN*

Background: At present, 201-Thallium scans, PET, SPECT, MRI, coronary angiography and echocardiography with and without pharmacological stress are used clinically for detecting existence and severity of CAD. The technique with the highest sensitivity and specificity may be able to accurately predict the risk of major mortal cardiovascular events. In this regard, we compared the sensitivity and the specificity of Magnetic Resonance First-Pass Perfusion imaging (MRFPP) with PET, SPECT and coronary angiography in detecting coronary artery disease in individual vessels.

Methods: Sixty patients with angiographically confirmed 2 or 3-vessel CAD were selected to undergo rest-stress ^{99}mTc-MIBI-SPECT (n = 40) and $^{13}NH_3$-^{18}FDG PET (n = 20). Rest-stress double-oblique, short axis MRFPP was performed in all patients at 1.5 T whole-body MR system (Siemens Vision SP) with a crisp bolus of Gd-DTPA (0.03 mmol/kg) followed by 15 ml of 0.9% saline solution using MedRad Injector as described in details elsewhere (2). The pharmacological stress was imposed by inducing vasodilation with IV Adenosine (140μg/kg/min, titrated over 4 minutes). Region of interest (ROI) analysis was performed on MRFPP images by two experienced observers to obtain regional transmural signal intensity/time curves with ARGUS analysis software (NUMARIS/3, Siemens Medical Systems, Iseline, NJ). A Fermi-function model of constrained deconvolution was applied to calculate the maximum impulse response (Rf(t)) of the contrast bolus. Myocardial blood flow (MBF, ml/min/g) was calculated in each ROI at rest and during hyperemia and then combined according to the distribution of the perfusion beds of the major coronary arteries in the myocardium. Myocardial perfusion reserve was determined as a ratio of hyperemic/resting MBFfor each ROI and for each coronary artery territory. Angiograms were interpreted by an experienced cardiologist. Using a semiquantitative, categorical determination of the extent of collaterals with RENTROP scale, collateral vessels and flow were graded according to tomographic location and position relative to the perfusion beds of major coronary arteries. For comparison, PET, SPECT and MRFPP images were matched tomographically based on anatomical landmarks. Also, based on the angiographic findings and RENTROP score, segments with demonstrated retrograde collateral filling of a subtotally occluded artery were compared to myocardial segments supplied by coronary arteries with non-critical (< 70%) stenosis and no collaterals visible on angiographic films.

Results: When calculated for the individual vessels, the sensitivity of quantitative MRFPP versus coronary angiography (the current "gold" standard for detecting CAD in individual vessels), SPECT and PET was 90%, 85% and 83% and the specificity was 90%, 87% and 80% respectively. The results of this study compare well with the data from Wilke et al (4), where quantitative MRFPP exhibited a higher sensitivity than qualitative Tc-MIBI SPECT (90% versus 82%) and also a better specificity (81% versus 77%) when compared for detection of CAD in individual vessels.

The *overall* sensitivity and specificity of MRFPP versus angiography, SPECT and PET are 92%, 90%, 85% and 93%, 96%, 87% respectively.

Myocardial segments supplied by coronary arteries without collateral vessels visible on angiographic films showed mild perfusion defects and the segments with critical stenoses displayed severe perfusion defects as quantified by MRFPP. However, in collateral-dependent myocardial segments that appear as "fixed" defects on SPECT and PET images, MRFPP showed preserved perfusion, which matched the angiographic findings of retrograde collateral filling in proximal occluded arteries.

Conclusion: MRFPP is a reliable diagnostic tool for assessment of myocardial perfusion in individual vessels in patients with multivessel CAD. MRFPP detects collateral-dependent perfusion defects whereas SPECT or PET cannot discern collateral-dependent myocardial segments. The overall sensitivity and specificity of SPECT and PET for detecting CAD appear higher than when calculated for the individual coronary vessels, therefore, if this was considered for SPECT and PET, their sensitivity and specificity might be improved.

References
1. Wilke et al. *Radiology* 1997; 204: 373–384
2. Wilke et al. *JMRI* 1999 (in press)
3. Wilke et al. *Cardiology Clinics* 1998; 16(2): 227–46

Intra- and Interobserver Agreement of Quantitative Magnetic Resonance First-Pass Perfusion Imaging

Olaf M. Muehling,[1] Matthew E. Dickson,[1] Andrey Zenovich,[1] Yimei Huang,[1] Michael Jerosch-Herold,[1] Betsy V. Wilson,[2] Robert F. Wilson,[2] Inderjit S. Anand,[3] Norbert M. Wilke.[1] [1]*MR-core Laboratory, Department of Radiology;* [2]*Division of Cardiology, Department of Medicine, University of Minnesota Medical School;* [3]*VA Medical Center, Minneapolis, MN*

Due to recent technical progress it is now possible to quantify myocardial perfusion with magnetic resonance first-pass imaging (MRI). The feasibility of myocardial blood flow quantification has already been validated. (1) Longitudinal clinical trials employing first-pass MRI as a diagnostic- and treatment-monitoring tool are being conducted. Therefore it is necessary to assess inter- and intraobserver correlation, which has not yet been shown.

Methods: 17 midventricular, short-axis images (including 3 stress studies) of 14 patients were obtained by multislice, first-pass imaging in patients with multivessel coronary artery disease or microvascular dysfunction. Two experienced observers blinded to the disease of the patient analyzed the pictures. For intraobserver reproducibility 10 studies were analyzed twice one week apart by one of the observers. Regional transmural time activity tissue curves were obtained with the Argus Cardiac Image Evaluation Software (Siemens Medical Systems, Iseline, NJ). The image quality was graded as excellent, good or poor. A Fermi-function model of constrained deconvolution calculated the maximum impulse response (Rf(t)) and maximum signal intensity (SI_{max}) of the contrast bolus.[2] Intra- and interobserver agreements were determined with the intraclass correlation coefficient (R) by using repeated measurement ANOVA. (3,4) R is expressed as a number between 0 and 1. A value of 0.75 is required for a good agreement between observations. Precision of measurements was further defined by the 99% confidence intervall (CI 99%). R was determined for the entire ring and for the separate myocardial regions before and after exclusion of images with poor quality and stress images.

Results: For inter- and intraobserver agreement n = 141 and n = 80 regions were analyzed. The image quality was graded as poor in three studies (one stress study) (18%, n = 25), good in 8 studies (47%, n = 70) and excellent in 6 studies (35%, n = 48). Two regions (1.4%) had to be excluded due to image artefacts. Intraobserver agreement for Rf(t) and SI_{max} were excellent (R = 0.90 (CI 99% = 0.11) and R = 0.94 (CI 99% = 0.07), n = 80). Interobserver agreement of Rf(t) was fair (R = 0.55 (CI 99% = 0.13), n = 141) but improved remarkably when images with poor quality and stress images were excluded (correct.) (R = 0.89, CI 99% = 0.15, n = 99). SI_{max} showed a good interobserver agreement (R = 0.73 (CI 99% = 0.08, n = 141) and improved when corrected for image quality (R = 0.81 (CI 99% = 0.10), n = 99). R values for the individual myocardial regions are shown in the tables below.

Rf(t)	Total (n = 35, * 39)		Correct. (n = 24, *27)	
R-Values	R	CI 99%	R	CI 99%
Anterior*	0.81	0.23	0.94	0.30
Lateral	0.69	0.26	0.95	0.32
Posterior	0.65	0.25	0.90	0.20
Septal	0.82	0.24	0.85	0.22
Mean	0.74		0.91	

SI_{max}	Total (n = 35, *39)		Correct. (n = 24, *27)	
R-Values	R	CI 99%	R	CI 99%
Anterior*	0.77	0.15	0.74	0.19
Lateral	0.91	0.15	0.90	0.20
Posterior	0.81	0.14	0.88	0.18
Septal	0.81	0.12	0.84	0.14
Mean	0.83		0.84	

Discussion: Perfusion analysis with quantitative, first-pass magnetic resonance imaging provides a method with excellent intraobserver (R = 0.90 and 0.94) agreement. The correlation of interobserver studies for the Rf(t) is highly dependent on image quality. The R-value increased remarkably when studies with poor quality were excluded (R = 0.55 to 0.89). When myocardial regions were analyzed individually the interobserver agreement was good and increased further when corrected for image quality. The subanalysis of the myocardial regions elucidated, that the reproducibility of the posterior and to a lesser degree of the lateral region were impaired by image quality. One explanation for this observation is the reduced signal-to-noise ratio in this region and it might be overcome by increased acquisition frequency and improved pulse sequences in the near future. The SI_{max} is less sensitive to image quality and seems to be especially useful in this case. The intra- and interobserver agreement of magnetic resonance first pass imaging is in good agreement with methods that are already widely employed for myocardial perfusion imaging. The R scores of planar Thallium-201 scintigraphy (5) ranged from 0.72 to 0.91 for all regions and from 0.54 to 0.92 for individual segments. Interestingly, their individual observer scores were low (0.32–0.51) compared to our intraobserver agreement (0.90–0.94). Positron emission tomography (6) showed higher r-values (0.96), whereas a different statistics methods had been used (correlation coefficient instead of intraclass correlation coefficient) and half of the subjects in their study were normal controls. The superiority of repeated measurement ANOVA has been shown. (5) Our results are encouraging to further employ this method in longitudinal clinical trials. A next step will be the assessment of interstudy reproducibility of magnetic resonance first-pass perfusion imaging.

References
1. Wilke N, Jerosch-Herold M, Wang Y et al. *Radiology* 1997; 204: 373–384
2. Jerosch-Herold M, Wilke N. *Int J Card Imag* 1997; 13: 205–218
3. Streiner DL, Norman GR. New York: Oxford University Press; 1991: 79–95
4. Wiener BJ. New York: McGraw Hill; 1971: 283–285
5. Brambilla M, Inglese E, Cannizzaro G et al. *J Nucl Med* 1994; 35: 601–608
6. Sawada S, Muzik O, Beanlands RS et al. *J Nucl Cardiol* 1995; 2: 413–422

Isometric Handgrip Exercise Testing of Cardiac Metabolism at 4.1 Tesla using Fast, Low-Angle Phosphorus NMR Spectroscopic Imaging (31P-MRSI)

S.D. Buchthal, J.A. den Hollander, W.T. Evanochko, G.M. Pohost. *University of Alabama at Birmingham, Birmingham, AL*

Isometric handgrip exercise has been previously used to study cardiac metabolism in patients with cardiovascular disease at 1.5 Tesla (T).(1) Those subjects with severe LAD stenosis showed an abnormally large decrease in myocardial phosphocreatine/ATP (PCr/ATP) ratios during stress compared to either age matched healthy controls or non-cardiac patients using phosphorus-31 nuclear magnetic resonance spectroscopy (31P-NMRS). This test has also been used in cardiac transplants (2) and women with chest pain but no angiographic coronary stenoses. (3) The mechanism of this response in these populations is thought to be microvascular disease. By taking advantage of the greater sensitivity and spectral resolution at 4.1 T, information on myocardial pH, not usually available at 1.5 T, may be obtained. It is possible to obtain 3D 31P MRSI data sets in 8 minutes at 4.1 T, which allows us to perform an isometric handgrip stress test for multiple volumes of the human heart in a reasonable time frame.

Methods: The 31P NMRS examinations were conducted on a 1 m bore, 4.1 Tesla research magnet, equipped with a Bruker Avance spectrometer. Proton scout images were obtained through a 20 cm surface coil tuned to 174.86 MHz, placed on the chest of the supine subject. After locating the heart, the 20 cm coil was replaced with a 10cm surface coil tuned to 70.785 MHz for 31P data acquisition. A similarly tuned birdcage body coil was driven in the linear mode for rf excitation.

The 3D 31P MRSI data sets were acquired with TR = 75 ms; flip angle of 10–15°, matrix size = 10 × 10 × 36, greatest resolution in the AP direction, FOV equal to 36^3. Rewinder gradients and a crusher gradient were used with rf phase spoiling. A total of 6400 transients were collected in 8 minutes with a gaussian weighting in k-space with FWHM of 24 in the AP direction and 6 in the other directions. The maximum number of acquisitions was 7 for the k = 0 profile. The 4D data set was processed without windowing in k-space, but with lorentz-gauss windowing in the time domain. The data set was divided into 10 slices for display purposes. Quantitation was by fitting in the time-domain, after fourier transformation in k-space only.

Consecutive data sets were acquired before, during and after isometric handgrip stress exercise at 30% maximum voluntary contraction. Stress level was monitored by computer. Heart rate and blood pressure were monitored throughout data acquisition

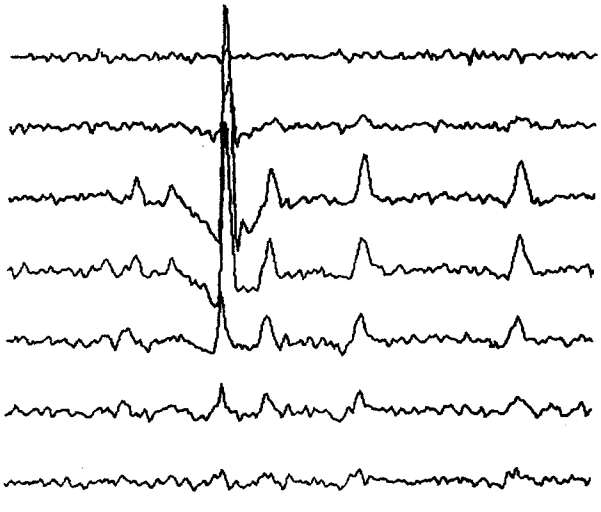

Results: Four volunteers were examined following the MRSI and exercise protocol described above. The figure shows a typical result obtained on a male volunteer, age 42, during rest and show successively deeper voxels through the chest wall and into the myocardium. There was no significant change in PCr/ATP ratios during stress compared with non-stress (ΔPCr/ATP = 2% ± 6).

These results demonstrate that the rapid 31P MRSI method allows one to obtain excellent spectral and spatial resolution on the hearts of normal voluteers at 4.1T. The preliminary results of the stress test indicate it will be useful in studying subjects who may have ischemic heart disease.

References

1. Weiss RJ, Bottomley PA, Hardy CJ, Gerstenblith G. *New England Journal of Medicine*, 1990. 323: p. 1593–1600.
2. Evanochko WT, et al. 1st Annual Meeting Soc. *Cardivasc. Magnetic Resonance.* 1998. p 94.
3. Buchthal SD, den Hollander JA. Rogers WJ. Pohost GM. *Proc Intl Soc Magn Reson Med* 1999. 7. p 1489

Clinical Performance of Vectorcardiographic Triggering MR Imaging

J.M. Chia,[1] S.E. Fischer,[1,2] S.A. Wickline,[1] C.H. Lorenz[1]. [1]*Center for Cardiovascular MR, Cardiovascular Division, Washington University Medical Center, St. Louis, MO;* [2]*Philips Medical Systems, Best, The Netherlands*

Introduction: In a substantial number of patients undergoing cardiac MRI examinations, image quality or scan efficiency is reduced due to poor QRS detection to trigger the scan. To improve QRS detection, ideal ECG lead positions has to be found by trial and error, which considerably prolongs patient setup time. This leads to an unacceptable reduction of clinical effectiveness in cardiac MRI. Commonly, for MR triggered scans standard QRS detection algorithms are applied, which achieve a performance index (PI) of up to 99% (3) outside the MR environment. However in the MR environment, these algorithms have difficulties in dealing with the magnetohydrodynamic artifact, RF related and gradient switching noise. Previously, we have shown that the use of spatial information from the vectorcardiogram (VCG) (1) from multiple ECG channels dramatically improves the QRS detection accuracy (2). Here the clinical application and performance of an MR compatible VCG system for triggering during a cardiac MRI examination is tested.

Methods: Two pairs of electrodes are placed on the patient in the positions shown in Figure 1 on the surface of the chest in a cross orientation to achieve ECG projections close to x and y orthogonal leads of the VCG.

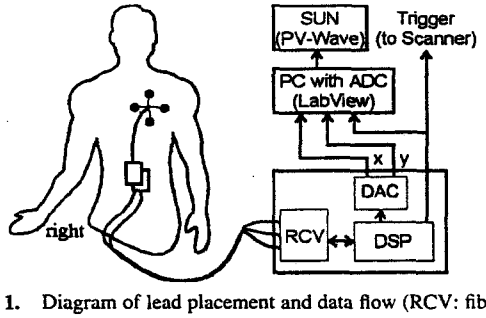

Figure 1. Diagram of lead placement and data flow (RCV: fiberoptic receiver interface. DSP: digital signal processor. DAC: digital analog converter).

The electrodes are connected to a battery powered. MR compatible sensor module with fiber optic output (FOX module) (Magnetic Reso-

nance Equipment Corporation. Bay Shore, NY). The two channels are demodulated by a receiver interface, which is connected to a digital signal processing board (DSP) (2). After 1–40 Hz digital bandpass filtering, the onset of the R-wave is detected by a target distance algorithm based on the VCG (2) and transmitted to the MR scanner (Gyroscan ACS-NT, Philips Medical Systems).

ECG waveforms and trigger signal were acquired in 8 volunteers at 50 Hz during a standard cardiac MR functional study of about an hour. A standard functional study is comprised of scout and diagnostic cine scans using different scan methods, such as gradient echo, turbo gradient echo, and echo planar imaging at full gradient performance (23 mT/m strength and 105 T/m/s). After the MR scan the QRS complexes were identified semi-automatically, compared to the trigger signal, and the performance of the triggering algorithm was evaluated using equation 3.

$$PI = \frac{N - (FP + FN)}{N} \times 100 \qquad (3)$$

In this equation, N is the number of QRS complexes detected. FP and FN are number of false positives and false negatives. To determine the propagation delay (time from detection of the QRS complex to the arrival of R-wave), data were acquired at a sampling rate of 1kHz in 20 second windows.

Results and Discussion: Figure 2 shows sample output signals from the VCG system.

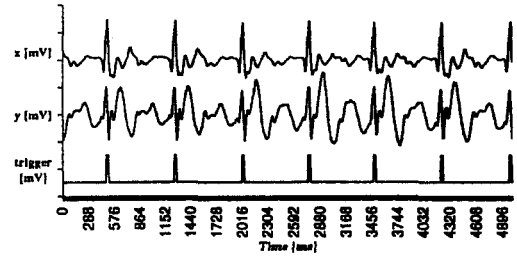

Figure 2. Output signals from the VCG triggering system.

Table 1 shows the summary of results for the 8 volunteers. The propagation delay of the trigger to the R-peak of the ECG was a consistent −10 ms for all the different scans. For the full study, a total of 30275 R-waves were evaluated with 19 FP and 6 FN. Thus, the sensitivity was calculated to be 99.98%, and the specificity was found to be 99.94%. The performance index (PI) was 99.92%.

Table 1 Summary of Results

ID#	Sex	Healthy	# of QRS	FP	FN	PI (%)
1	M	No	4374	2	1	99.93
2	M	Yes	4384	3	0	99.93
3	M	Yes	5089	2	1	99.94
4	F	No	4615	8	2	99.78
5	M	Yes	3744	0	0	100.00
6	F	Yes	3239	2	1	99.91
7	M	Yes	2544	2	1	99.88
8	M	Yes	2286	0	0	100.00
Total			30275	19	6	99.92

Conclusions: The feasibility of VCG-gated MR acquisitions has been demonstrated. The increased QRS detection accuracy and short propagation delay should increase the image quality as well as scan efficiency. The standard lead placements avoid trial and error iterations to find a suitable ECG waveform: thus, reducing the patient setup time.

References
1. Frank E. *Circulation* 13, 737 (1956).
2. Fischer SE et al. *MRM* 42, 361–370 (1999).
3. Friesen GM et al. *IEEE Trans. Biomed Eng* 37, 85 (1990).

Quantification of Image Quality Due to Poor Triggering

J.M. Chia,[1] S.E. Fischer,[1,2] S.A. Wickline,[1] C.H. Lorenz[1]. [1]*Center for Cardiovascular MR, Cardiovascular Division, Washington University Medical Center, St. Louis, MO;* [2]*Philips Medical Systems, Best, The Netherlands*

Introduction: Magnetic resonance image quality can be affected by a number of factors such as triggering accuracy, respiratory motion, and blood flow pulsatility. In order to image cardiovascular system, acquisition of the information for the data must be synchronized with the heart motion by the use of the QRS complex of the ECG as a landmark to trigger the scan. However, in the MR environment the ECG waveform is altered, making consistent QRS detection more difficult, resulting in lower scan efficiency as well as poor image quality. In cardiac MR poor image quality can affect volume determination, wall motion analysis, and coronary diameter measurement. The link between improved triggering performance and resulting image quality improvement is not straightforward. Therefore, we designed a series of experiments using simulations in k-space to determine how inaccurate triggering impacts image quality to identify the triggering-related impact independent of other factors such as respiratory motion or blood flow.

Methods: A simulation program developed in our lab was designed to approximate a short axis image of the heart with coronary arteries also in the field of view as shown in Figure 1.

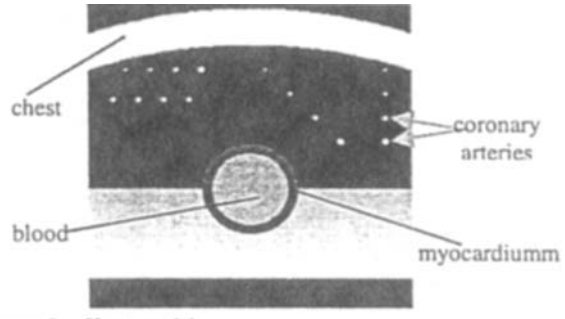

Figure 1. Heart model.

In this model the wall thickens as a function of the heart cycle according to a standard beating heart model with an ejection fraction of 60%. In addition, the coronary artery motion is based on data measured in vivo (1). The resolution is 256 × 256 1 mm pixels. From this original model, the user could control the number and timing of false triggers over the entire 256 line k-space acquisition for different scan types such as gradient echo, echo planar imaging, and retrospectively gated gradient echo imaging.

Results and Discussion: Figure 2 shows the simulated results for a standard gradient echo sequence with prospective triggering and 5%, 15%, 25%, and 35% triggers generated at the onset of the blood flow artifact instead of the QRS complex, distributed randomly throughout k-space. Here ghosting is clearly seen to increase as the percentage of mistriggers increases. In addition, blurring increases with increased percentage of mistriggers in the coronary arteries as well as in the myocardium due to the motion of these objects. Also, images with a higher percentage of mistriggers appear to be darker due to the lower signal to noise ratio.

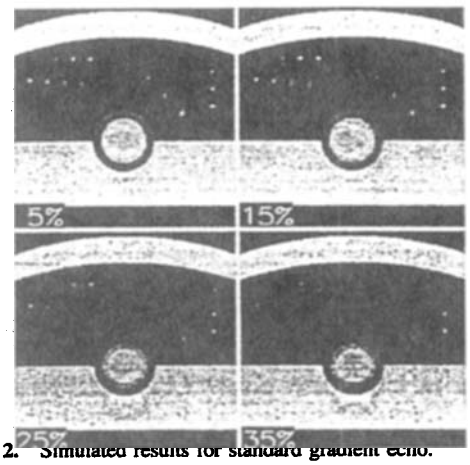

Figure 2. Simulated results for standard gradient echo.

Figure 3 shows the signal to noise (SNR) for the blood. The displayed time points of the heart cycle were 0 ms, 150 ms, 350 ms, 450 ms, and 750 ms which corresponded to end-diastole, onset of systole, end-systole, onset of rapid filling, and late diastolic phases of the heart, respectively (2). Here, it can be seen that with increased mistriggers, the SNR decreases, especially during heart phases with rapid motion such as during systole.

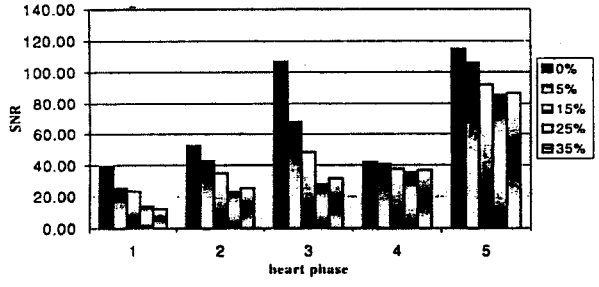

Figure 3. SNR of blood. Here heart phase 1 is time point 0 ms, 2 is 150 ms, 3 is 350 ms, 4 is 450 ms, and 5 is 750 ms.

Conclusions: The triggering simulation program presented here allows flexible, quantitative evaluation of the impact of mistriggering on cardiac MR image quality. Applications include evaluation of resistance to artifacts of certain types of sequences, or evaluation of error in volume/wall motion determination due to mistriggering. Future additions of irregular respiratory motion and bulk patient motion will allow quantitative evaluation of different types of motion on cardiac MR image quality.

References

1. Hofman, MBM et al., *JMRI* 8, 568–576 (1998).
2. Lentner, C. *Geigy Scientific Tables: Volume 5 Heart and Circulation.* 8th ed. (1990).

Diagnostic Value of the Electrocardiogram During MRI

S.E. Fischer,[1,2] P. Vugts,[2] J.M. Chia,[1] S.A. Wickline,[1] D. Feldman,[3] C.H. Lorenz[1]. [1]*Center for Cardiovascular MR, Cardiovascular Division, Washington University Medical Center, St. Louis, MO;* [2]*Philips Medical Systems, Best, The Netherlands;* [3]*Berlex Laboratories Diagnostic Imaging Division, Montville, NJ*

Introduction: In addition to gating an MR scan, a second purpose for the ECG during MRI is for monitoring (i.e. of critical ill or sedated patients,for cardiac stress tests, or during clinical trials of new drugs or MR contrast agents.) However, the diagnostic information of ECG waveforms obtained during a MR examination is hampered by two factors. First, the ECG waveform is disturbed by artifacts from the MR environment due to the main magnetic field, RF pulses and fast switching gradient fields (1). Second, for patient safety reasons the MR environment requires special, MR compatible monitoring equipment, which may not satisfy the standards for diagnostic ECG equipment. Also the term "MR compatible" defined by the FDA (2) only regulates image disturbances by devices but not disturbances of physiologic parameters by the MR environment. To describe the effect of the MR environment on the diagnostic value of monitoring parameters three operational levels have to be differentiated:

- Level 1: MR compatible monitoring equipment used with the patient outside the 5 Gauss line.
- Level 2: Monitoring in the B_0-field without MR scanning.
- Level 3: Monitoring during an MR scan.

The purpose of this study was to determine the diagnostic value of the ECG at the different levels.

Methods: In 12 healthy male volunteers vectorcardiograms (VCG) were digitized at 1kHz using a standard Frank lead system (Hewlett Packard, 1507-11A) inside a whole-body 1.5 T MR scanner (Philips Gyroscan ACS-NT). Before the evaluation of the different ECG features, individual PP intervals were normalized to 1 second using a heart timing model and averaged over 12 s. In 5 patients (4 with normal ECG, 1 with known ST segment elevation under stress) a single ECG lead parallel to the electrical axis of the heart was recorded during a dobutamine stress test with doses from 5 to 40 μg/kg/min.

Results and Discussion: The ECG sensors in MR compatible monitoring systems include additional filtering to deal with MR related artifacts. Further, non standard lead placements are recommended. Thus, at operational level 1 these monitoring systems do not conform to the set standards for monitoring (3). Levels 2 and 3 have in common the effect of the static magnetic field. We evaluated the effect of the B0 field for various diagnostic parameters of the ECG.

P-wave: In patients exposed to a magnetic field of 1 T or more, the P-wave amplitude, axis and time intervals related to the P wave cannot be measured (2) with diagnostic accuracy.

QRS-complex: The QRS complex can be identified even at 2 T. This and other studies have shown that the R-peak amplitude is preserved in the ECG obtained inside a magnet. Despite the fact that the electrical axis is preserved (9 ± 7° angle difference) the beginning and termination of the QRS loop are disturbed as shown in Fig. 1. The correlation of the ECG waveforms from inside and outside the B_0 field showed that the correlation factor from a 10 ms sliding window dropped below 0.75 outside an interval of −31 ms to +35 ms from the R-peak. This confidence interval was found to be only 73 ± 17% of the QRS duration.

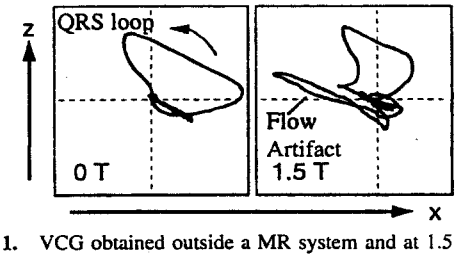

Figure 1. VCG obtained outside a MR system and at 1.5 T.

- ST-Segment and J-point: The majority of aortic blood flow occurs during the ST segment. All the large vessels, such as aorta and pulmonary arteries and also the ventricles themselves contribute to the magnetohydrodynamic artifact. The complexity of the flow patterns (i.e. heli-

cal flow in the aorta, swirling in the ventricles) makes it impossible to predict the artifact waveform. The spectrum of the blood flow artifact overlaps with that of the ST-segment. Fig. 2 demonstrates that the waveform of blood flow artifact is highly dependent on the heart rate,or more precisely on the blood flow velocity and stroke volume. Thus, the ST segment and J-point acquired during MRI is not diagnostic.

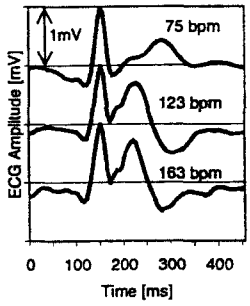

Figure 2. Heart rate dependency of the magnetohydrodynamic artifact at 1.5 T during the ST-segment of a healthy volunteer during a dobutamine stress test.

T-wave: The T-wave of the ECG obtained inside an MR scanner is buried below the magnetohydrodynamic artifact. The onset of the peak amplitude of the first or second major wave after the QRS complex cannot be correlated with the T-wave obtained outside the magnet. The mean maximum amplitude, normalized to the R-peak was 0.87 ± 0.75.

Conclusions: Heart rate and electrical axis can be derived from the ECG acquired in the MR environment, although heart rate should be analyzed manually in the presence of magnetohydrodynamic artifacts of amplitude 50% or more of the R-peak, and also during scanning. ECG landmarks and waveforms including related time intervals, such as the P-wave, ST-segment and T-wave cannot be identified with diagnostic accuracy. Only arrhythmias based on altered timing or axis of the QRS complex, such as tachycardia or ventricular extra systoles can be identified with diagnostic precision.

References

1. FDA Primer on medical device interaction with MRI systems, 2/7/97.
2. Weikl A et al., *Z. f. Kardiologie* 78(9), 578–586 (1989).
3. American National Standard: diagnostic electrocardiographic devices. *ANSI AAMI ECII* (1991).

Evaluation of 3D Magnetic Resonance Coronary Angiography with Clariscan™ in Humans: Correlation with X-Ray Angiography

R.M. Setser, L.O.M. Johansson, S.A. Wickline, C.H. Lorenz. *Center for Cardiovascular Magnetic Resonance, Barnes-Jewish Hospital, St. Louis. MO*

Introduction: The advantages of intravascular contrast agents for MR coronary angiography (MRCA) have been demonstrated previously (1). We have shown in pigs that MRCA with one such agent. NC100150 Injection (Clariscan™, Nycomed Amersham Imaging, Wayne, PA), correlates well with x-ray angiography (2). The purpose of this study was to evaluate NC100150 Injection in patients and to compare MRCA with x-ray angiography for detection of coronary stenoses.

Materials and Methods: Eight patients with known or suspected coronary artery disease underwent MRCA and x-ray angiography (6M/2F, 68 ± 12 yrs). MRCA was performed on a clinical 1.5T scanner (Gyroscan NT, Philips Medical Systems, Best, NL) and consisted of scout scans to locate the origins of the LM and RCA, followed by contrast agent administration. Three patients received a dose of 5 mg Fe/kg NC100150 Injection and five received a 2 mg Fe/kg dose. Initial results at 5 mg/kg showed significant T2* related signal loss and thus, subsequent patients were imaged at 2 mg/kg. Next, the right and left coronary systems were imaged separately with ECG triggered, 3D turbo gradient echo acquisitions with fat saturation, consisting of 30–40 1 mm thick slices (interpolated). Other scan parameters included TR 6–7 ms, TE 2.2–2.5 ms, 256 mm² FOV, and 256 × 212 matrix, yielding an in-plane resolution of 1.0 × 1.2 mm². An inversion pre-pulse (TI = 450 ms) nulled the myocardial signal. A flip angle sweep maintained constant signal over the acquisition window, which was 90–95 ms per R-R interval in the first three patients, but reduced to 70–75 ms for the remaining five.

The SNR of blood and CNR between blood and myocardium were measured in the source images. The lengths of visible segments of the RCA, LM, LCX and LAD were measured from curved reformats on an Easy Vision workstation (Philips Medical Systems). In all patients, the presence and severity of lesions was graded on both x-ray angiography and MRCA by two independent observers, each blinded to the results of the other.

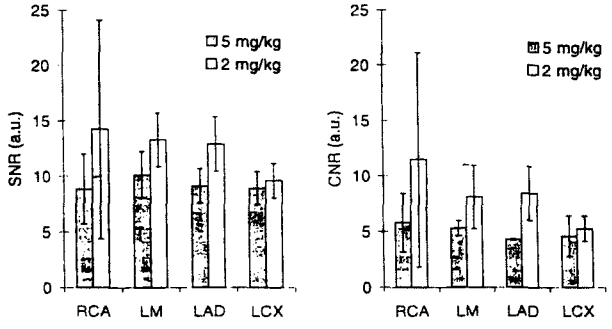

Figure 1. SNR and CNR measured in the MRCA images.

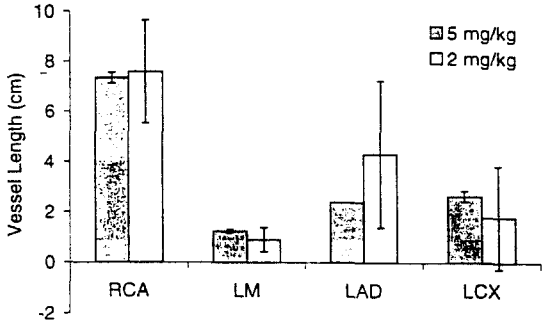

Figure 2. Vessel lengths measured in each coronary artery by MRCA at each of two doses of NC100150 Injection. No significant differences were found between doses.

Of 31 possible analyzable arteries, 26 were diagnostically evaluable by MR (84%;). and all 31 were evaluable by x-ray (100%). The table below contains preliminary results of the comparison between MRCA (pooled results from both doses) and x-ray. A true positive result (++) indicates a >50% lesion as graded by MRCA and x-ray; true negative (−−), lesions <50% (or absent) by both; false negative (−+), a negative result on MRCA seen as a >50% lesion on cath; and false positive (+−), a >50% lesion on MRCA not seen with x-ray. If each artery is considered separately, the RCA, 8 cm of of which was visualized by MRCA, had 5/6 stenoses correctly identified. Lengths of the LAD and LCX were significantly shorter in MRCA than x-ray due

to poor motion compensation, and only 1/6 (LAD) and 1/2 (LCX) lesions were correctly located. In the short LM, 0/1 stenosis was correctly identified.

		x-ray +	x-ray -
MRCA	+	7	4
	-	3	12

Discussion and Conclusions: MRCA with NC100150 Injection was performed at two doses: 2 mg/kg and 5 mg/kg. No significant differences were found between SNR, CNR or vessel length imaged at either dose. Most missed lesions on MRCA could be attributed to blurring of the artery due to respiratory and/or heart motion. Furthermore, grading of lesions on MRCA was difficult due to limited spatial resolution in these small arteries (2–4 mm diameter) and the limited length of LAD and LCX evaluable by MRCA. In conclusion, further improvements in image resolution, vessel coverage and motion compensation need to be made to take full advantage of NC100150 Injection for MRCA.

References
1. Johansson LO. et al., *JMRI*, 9, 552–556, 1999.
2. Johansson LO. et al., *JCMR*, 1(2), 139–143, 1999.

Intravascular Contrast Agent Clariscan™ Improves Image Quality in Long Axis Images of the Left Ventricle

R.M. Setser, L.O.M. Johansson, C.H. Lorenz. *Center for Cardiovascular Magnetic Resonance, Barnes-Jewish Hospital, St. Louis, MO*

Introduction: The advantages of intravascular contrast agents for coronary artery imaging have been demonstrated previously (1,2). We have also shown in pigs that NC100150 Injection, Clariscan™ (Nycomed Amersham Imaging. Wayne PA), can significantly enhance blood-myocardial contrast in long-axis images of the left ventricle (LV) (3). Because slow flow in patients with impaired LV function can result in signal saturation and loss of contrast, especially in long-axis images where the majority of flow is inplane, we sought to determine if image quality could be improved in patients using NC100150 Injection.

Materials and Methods: Five patients with known coronary artery disease underwent a limited MR functional examination consisting of long-axis (two chamber) and short-axis cine images, at baseline (no contrast) and two doses of NC100150 Injection, 1.0 mg/kg and 2.0 mg/kg. Imaging was performed on a 1.5T scanner (Philips Medical Systems, Best, NL) with an ECG triggered, partial echo, turbo gradient echo pulse sequence. One 8 mm thick slice was acquired in each orientation, as follows: FOV 350 mm, RFOV 70%, 2 NSA, α 30°, TR 4.4 ms, TE 2.1 ms, for a resolution of 1.4 × 2.3 mm^2 and 25 frames/cardiac cycle. The body coil was used in one patient and a cardiac synergy coil in the remaining four. The same sequence, optimized for pre-contrast imaging, was used both pre- and post-contrast.

Signal to noise and contrast to noise ratios (SNR, CNR) were measured at end systole and end diastole (ES, ED) at both the apex and base in long axis images, and in the center of the blood pool in short axis images. One way ANOVA was used to test the significance of differences between doses. Segmental wall motion was assessed in all images by a blinded observer using the following grading scheme: 0—segment not evaluable; 1—evaluable.

Results:

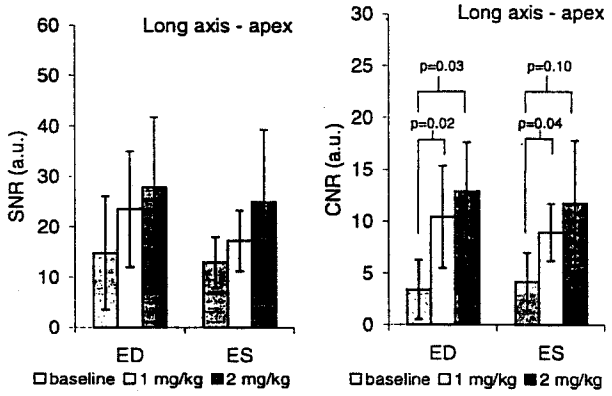

Figure 1. SNR and CNR measured at the LV apex in long axis images as a function of contrast agent concentration. From these preliminary results, statistical differences between groups at or below the 0.1 level are shown.

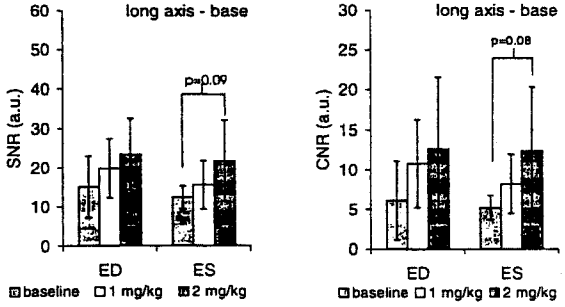

Figure 2. SNR and CNR at the LV base in long axis images.

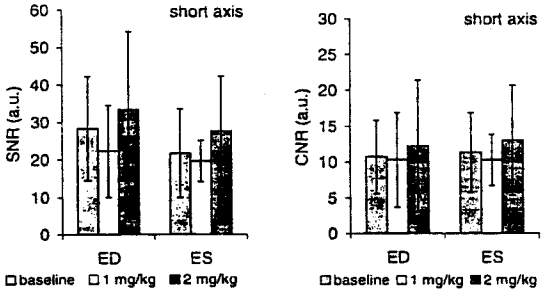

Figure 3. SNR and CNR measured in short axis images.

Table 1. Segmental Wall Motion Analysis—Evaluable Segments

	Baseline	1 mg/kg	2 mg/kg
Long-axis			
Total	14/30	30/30	30/30
Apical	1/10	10/10	10/10
Mid	5/10	10/10	10/10
Base	8/10	10/10	10/10
Short-axis			
Total	22/25	25/25	18/20

Discussion and Conclusions: These preliminary results demonstrate the potential utility of NC100150 Injection in cardiac MR functional imaging. It can be used to enhance blood-myocardial contrast in LV long axis images, which commonly suffer from signal saturation and poor contrast due to slow in-plane flow, and can provide a more uniform blood signal than non-contrast imaging. The magnitude of improvement, however, will be pulse sequence dependent, mainly due to T2* and TE effects. Improvements in CNR and blood signal uniformity were related to improved visual assessment of wall motion, especially at the apex. Use of NC100150 injection may also improve the performance of automated edge detection algorithms that often fail in regions of blood signal inhomogeneity.

References

1. Johansson LO, et al., *JMRI*, 1999; 9: 552–556
2. Johansson LO, et al., *JCMR*, 1999; 1(2): 139–143
3. Wagenseil JE, et al., *JMRI*, in press. 1999.

Targeted Magnetic Resonance Contrast Agent for Detection of Thrombus

S.J. Flacke, S.E. Fischer, C.S. Hall, M.J. Scott, J.N. Marsh, P.J. Gaffney, C.H. Lorenz, S.A. Wickline, G.M. Lanza. *NIBSC, Potters Bar, UK; Cardiovascular Devision, Washington University, St. Louis, MO*

Introduction: Atherosclerotic plaque rupture and its clinical sequelae, stroke and myocardial infarction, are commonly preceded by the formation of fibrin-filled, microfissures. These vulnerable plaques cannot be detected by routine imaging methods. However, unstable plaques may be sensitively and specifically identified by molecular imaging with a novel, fibrin-targeted, lipid encapsulated, perfluorocarbon emulsion (200 ± 30 nm) modified with thousands of gadolinium-DTPA complexes on the outer surface. In the present study, we determined the concentration of surface Gd-DTPA required to maximize the sensitivity of fibrin deposit detection with T1-weighted MRI imaging.

Materials and Methods: Lipid-conjugated Gd-DTPA was incorporated into the surfactant layer of biotinylated perfluorocarbon emulsions at concentrations a 0, 1.25, 2.5, 5, 10 and 20 mole%. Biotinylated anti-fibrin monoclonal antibodies (NIB 5F3) and avidin were used to couple the emulsion nanoparticles to fibrin clots.

Magnetic resonance imaging of the targeted clots suspended in blood was performed on a clinical 1.5T scanner (Gyroscan NT, Philips Medical Systems, Best, NL). In a second imaging experiment pure and diluted emulsions of the contrast agent at various Gd-DTPA concentrations were imaged. Imaging consisted of conventional 3D T1 weighted gradient echo recalled imaging: TE/TR/α 6.3/30/20 FOV 160mm, matrix 256 × 256, 2mm overcontiguous slices, to visualize the binding of targeted contrast agent to the clot surface and a Look-Locker sequence to measure the longitudinal relaxation time of the different emulsions. Imaging parameters for the Look-Locker sequence were as follows: TE/TR/α: 3.53/3000/10°, acquisition matrix 128 × 128 interpolated to 256 × 256, FOV 340 mm, image spacing 30 ms.

Images of the different emulsions were analyzed using the MASS software (Medis, Leiden, Netherlands), and signal-intensity time curves for each phantom were generated. The curves were fitted to the predicted longitudinal magnetization curves for this imaging sequence as previously described (1) to determine T1.

Results: Increasing concentrations of Gd-DTPA improved T1 shortening of targeted clots monotonically. T1 relaxation was decreased maximally ($p < 0.05$) at the 20 mole% level (602 ms) vs. control (1218 ms). Figure 1 shows the binding of the contrast agent to clot surface. Figure 2 shows the linear increase of relativity with increasing concentration (1) for each single preparation along the dilution steps and (2) linear to the primary load of Gd-DTPA (mol%) in the perfluorocarbon emulsions. The relaxivity of the bound Gd-DTPA was 12 ± 1 mmol/l/s without significant differences between the different preparations.

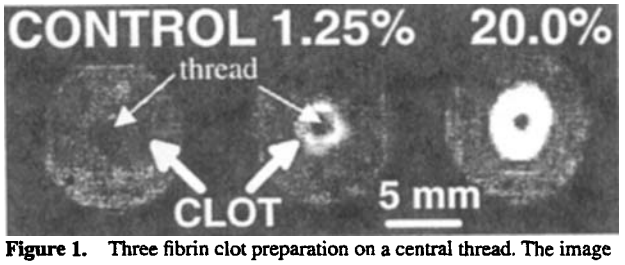

Figure 1. Three fibrin clot preparation on a central thread. The image signal of the clot surface increases with increasing concentration of the Gd-DTPA mole% in the lipid encapsulated, perfluorocarbon emulsion.

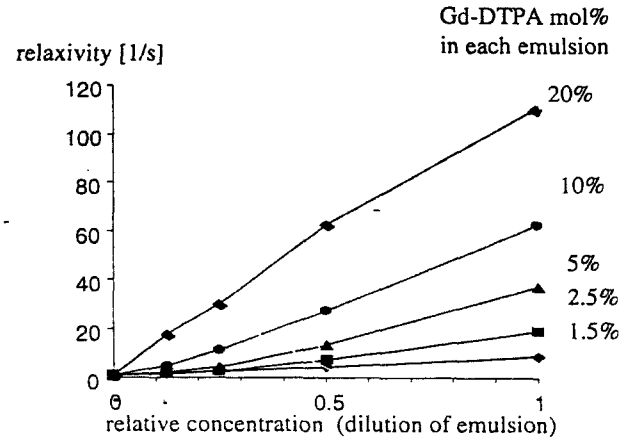

Figure 2. Relativity versus relative concentration of five different preparations of the fibrin-targeted contrast agent, each with a different initial GD-DTPA mole-percentage.

Discussion and Conclusions: Detection of fibrin deposits, particularly microthrombi on the surface of vulnerable atherosclerotic plaques requires high concentrations of gadolinium to provide adequate sensitivity. Fibrin-targeted perfluorocarbon emulsion nanoparticles can provide a stable platform ideally suited to deliver tens of thousands of gadolinium atoms into microscopic fissures in unstable plaques. This novel targeted MRI agent may allow sensitive, early detection of unrecognized vascular pathology in high-risk patients and allow implementation of preventative therapies to reduce associated morbidity and mortality.

References

1. Look DR, Locker DL *Rev Sci Instum* 1970; 41: 250
2. Lanza GM et al *Acad Radiol* 1998; 5:Suppl. 173–176

Evaluation of the Gd-DTPA Partition Coefficient in Humans

S.J. Flacke, S.E. Fischer, C.H. Lorenz. *Center for Cardiovascular Magnetic Resonance, Cardiovascular Division, Barnes-Jewish Hospital, St. Louis, MO*

Introduction: Several investigators are evaluating the use of the 'equilibrium' distribution of Gd-DTPA for the purpose of determination of

myocardial viability (1–3). The tissue-blood partition coefficient for Gd-DTPA, λ, is a key parameter for this type of evaluation, but to date, has only been measured in animals, or indirectly from signal intensity changes in humans (1–3). The objectives of this study were (1) to establish a method for measuring the partition coefficient of Gd-DTPA in vivo in humans, and (2) to evaluate the spatial and intersubject variation in the partition coefficient of normal myocardium as a basis for comparison with acute and chronic infarction.

Materials and Methods: Ten subjects with no prior history of cardiovascular disease were imaged on a clinical 1.5T scanner (Gyroscan NT, Philips Medical Systems, Best, NL). Imaging consisted of scout scans to determine the 4-chamber view, and a Look-Locker sequence at four short axis levels using a phased-array cardiac coil to measure myocardial and blood longitudinal relaxation time. Each subject was imaged prior to contrast agent administration and again following contrast administration. The contrast protocol consisted of a 5 cc/sec bolus injection (Spectris injector, Medrad, Maastricht, NL) of Magnevist™ (Berlex, Wayne, New Jersey) at 0.2 mmol/kg followed by a constant infusion for 30 minutes (0.004 mmol/kg/min) to establish equilibrium (4). Imaging parameters for the Look-Locker sequence were as follows: TE/TR/FL: 3.53/3000/10°, acquisition matrix 128 × 128 interpolated to 256 × 256, FOV 340 mm, image spacing 50 ms pre contrast and 30 ms post contrast.

Images were analyzed using the MASS software (Medis, Leiden, Netherlands), and signal-intensity time curves for eight circumferential sectors of myocardium and the LV cavity blood pool were generated. The curves were fit to the predicted longitudinal magnetization curves for this imaging sequence as previously described (5) to determine T1 for each circumferential myocardial sector and the blood. The partition coefficient for Gd-DTPA is defined as the ratio of the equilibrium concentration of Gd-DTPA in tissue to the concentration in blood. Assuming that the concentration is related to the ΔR1 the partition coefficient was calculated using the pre- and post-contrast blood and myocardial T1 values according to the following equation (2):

$$\lambda = \Delta R1_{myo}/\Delta R1_{blood}$$

where ΔR1 is defined as 1/Tlpost—1/T1 pre for either blood or myocardium.

Results were averaged per sector and per slice over all subjects to determine spatial variation in the partition coefficient estimation. In addition a pooled average of the partition coefficient was determined, over all subjects, slices and sectors. Differences were compared using a one-way ANOVA and Scheffe's post hoc test with $p < 0.05$ defined as significant.

Results: Figure 1 shows sample images from the Look-Locker sequence (left: early after the 180° inversion pulse, middle: near the time of the blood zero crossing, and right: near the time of the myocardial zero crossing).

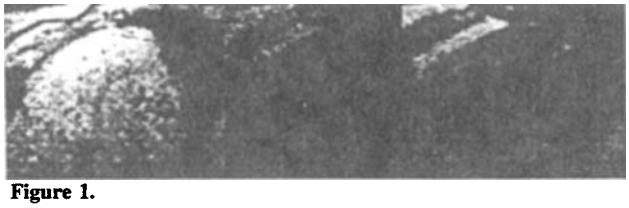

Figure 1.

The overall mean value of the partition coefficient was 0.56 ± 0.06 ml/g. The regional variation can be seen in the table below. In this table, slice 1 is the most apical slice, and slice 4 is the most basal slice. The eight circumferential sectors describe the septum (sep), anterior (ant), lateral (lat) and inferior (inf) walls.

λ (ml/g)	Slice 1	Slice 2	Slice 3	Slice 4
Inf-sep	0.77 ± 0.10*	0.73 ± 0.11	0.67 ± 0.10	0.63 ± 0.05*
Sep	0.66 ± 0.12	0.57 ± 0.13	0.50 ± 0.12	0.46 ± 0.09
Sep-ant	0.58 ± 0.11	0.58 ± 0.15	0.53 ± 0.07	0.51 ± 0.05
Ant	0.52 ± 0.08	0.57 ± 0.13	0.53 ± 0.12	0.44 ± 0.05
Ant-lat	0.56 ± 0.08	0.54 ± 0.12	0.51 ± 0.14	0.41 ± 0.10
Lat	0.61 ± 0.12	0.57 ± 0.13	0.57 ± 0.14	0.45 ± 0.13
Lat-inf	0.62 ± 0.13	0.57 ± 0.13	0.57 ± 0.09	0.50 ± 0.12
Inf	0.65 ± 0.09	0.61 ± 0.07	0.56 ± 0.08	0.51± 0.06

* significant difference within slice, $p<0.05$

The magnitude of the estimated partition coefficient was uniform over the entire myocardium, with elevated values in the septum which just reached statistical significance in slice 1 and 4. This elevation is likely due to partial volume effects of mixed blood-myocardium voxels at the RV-LV junction. No significant differences between sectors were reached if data were pooled over all slices.

Discussion and Conclusions: The absolute magnitude of the partition coefficient is somewhat higher than that reported for animals previously (1,2), but the standard deviation is small over the entire myocardium. Therefore, it should be useful for reliable differentiation between normal and non-viable myocardium in human studies, where the partition coefficient is expected to rise well above 1 ml/g.

References

1. Arheden H et al. *Radiology* 1999; 211: 698–708
2. Harris PA et al. *MRM* 1997; 38: 541–545
3. Inoue S et al. *JMRI* 1999; 9: 215–9
4. Pereira RS et al., *MRM*, 1999, 42, 60–68
5. Look DR Locker DL *Rev Sci Instum* 1970; 41: 250

Representation of Complex Flow Using Rapid Imaging Sequences

M. Doyle, M.E. Kortright, A. Anayiotos, A. Fuisz, R.W.W. Biederman, G.M. Pohost. *University of Alabama at Birmingham, Birmingham, AL*

Introduction: Previously we described the application of the rapid BRISK (block regional interpolation scheme for k-space) approach to image pulsatile flow in a straight tube. BRISK is a sparse sampling approach, employing temporal interpolation to derive unsampled data. BRISK can markedly reduce scan time (in this case by a factor of 3) and is expected to perform well in situations where a large number of adjacent pixels are highly correlated over time. A limitation of our straight tube study was that the flow field was highly correlated over the whole cross-sectional view. Representation with BRISK of more complex flow fields, as might exist in the human vasculature, has previously not been investigated.

Methods: In a phantom, helical flow was generated by pumping water in a pulsatile manner through a 'U' shaped tube (inside diameter 19mm). The pulsatile flow waveform was similar in nature to aortic flow (60 BPM, stroke volume 70cc) and the tube was similar in appearance to the human aortic arch. The imaging plane was selected to be at the apex of the arch, and oriented such that a circular cross-section was imaged. Through plane and in-plane flow were encoded using sensitivities of ±150 cm/s and ±30 cm/s, respectively. For the two in-

plane velocities, lower velocity sensitivities are desirable, but result in unacceptable artifacts. Imaging parameters were based on clinical acquisitions: in-plane resolution 1 × 1 mm, slice thickness 8 mm, TE 11 ms. The phantom was imaged with conventional, BRISK and turbo-BRISK scans with turbo factors ranging from 2–5 (turbo-5 BRISK resulted in a time reduction of factor of 15 compared to the conventional scan).

Results: For the through-plane flow the maximum velocity recorded was 76 cm/s, and for the horizontal and vertical in-plane components the maximum velocities recorded were 11 cm/s and 3 cm/s, respectively. By visual inspection the turbo-factor 2 BRISK scan appeared virtually indistinguishable from the conventional data, while higher order turbo BRISK scans gradually lost fidelity only in minor circulatory features associated with the helical flow pattern. The regression 'r' values for the time evolution for a representative pixel in each of the three velocity directions is given in the Table. The stroke volume was measured to be 74.3 cc by the conventional scan while the BRISK through turbo-5 BRISK values were 70.9, 71.5, 72.9, 72.2, and 71.4, respectively.

Time plot 'r' values

	BRISK	BRISK Turbo 2	BRISK Turbo 3	BRISK Turbo 4	BRISK Turbo 5
Through	0.99	0.99	0.98	0.97	0.97
Horizontal	0.93	0.96	0.94	0.82	0.89
Vertical	0.65	0.63	0.66	0.59	0.52

Discussion: BRISK and turbo BRISK depict the main features of the dynamic velocity components of complex flow fields with good accuracy, even for high turbo factors. The lower velocity horizontal in-plane component (14% of the through-plane velocity) was well represented up to turbo factor 3, while the very low velocity data (3% of through-plane velocity) for the vertical in-plane flow was poorly represented. However, neither of the in-plane velocity components contribute to stroke volume, which is derived entirely from through plane velocities; these are well represented by turbo-BRISK and measured stroke volumes were all within 6% of the expected (which is within established limits).

Conclusions: The accuracy with which BRISK and turbo BRISK represent complex flow fields is sensitive to the dynamic range of velocity encoding. When the dynamic range used is high (e.g. 50% of max) velocity data is well represented, even up to high turbo factors. Even for fairly low velocities (>10% of dynamic range) the flow data is well represented by lower turbo factors. The stroke volumes measured by turbo BRISK are in excellent agreement with the conventional data. The time savings inherent in turbo BRISK may allow greater applicability of three-dimensional flow imaging to clinical studies.

Determinants of Coronary Flow Reserve

M. Doyle, A. Fuisz, R.W.W. Biederman, M.E. Kortright, E.G. Walsh, V. Bittner, W.J. Rogers, G.M. Pohost. *University of Alabama at Birmingham, Birmingham, AL*

Introduction: In the NIH sponsored Women's Ischerdia Syndrome Evaluation (WISE) study, 108 women with chest pain were evaluated by coronary angiography and first pass magnetic resonance (MR) perfusion imaging. The MR study was performed under resting and vasodilatation conditions (0.56 mg/kg dipyridamole). Considerable variation has been described in the coronary flow reserve (CFR) response to dipyridamole, with a lower response being associated with lower accuracy in diagnosing epicardial coronary artery disease. While the coronary flow reserve can be measured using MRI, it is currently unknown what patient characteristics are associated with a high (H_{CFR}) or low CFR (L_{CFR}). Knowledge of these characteristics may suggest modifications to future vasodilatation procedures/agents and allow the prediction of patients likely to have a poor response to the standard agents.

Methods: The resting and vasodilatation first pass gadolinium slope parameters were normalized by division by the left ventricular blood pool slopes. An MR perfusion CFR index was obtained from the ratio of resting to vasodilatation time-intensity slopes. H_{CFR} patients were defined as those having slope ratio ≥ 1.5 for ≥ 2 out of 12 myocardial segments. Patient characteristics were compared using a t-test with a p value <0.05 considered to be significant.

Results: The Table shows that resting hemodynamic parameters (HR, SBP, PP, and RPP) as opposed to those at post dipyridamole more clearly differentiate H_{CFR} and L_{CFR} patient groups. Further, the average number of risk factors (smoking, diabetes, hypertension, family history of CAD, dislipidemia) for the H_{CFR} group is less than for the L_{CFR} group (2.4 ± 0.9 vs 3.0 ± 1.1, $p < 0.01$). No difference in medication between groups was detected, including long lasting nitrates, calcium antagonists and beta-blockers. Further, no difference was found between groups in the absolute change of heart rate or systolic blood pressure from rest to vasodilatation.

Discussion: We show that neither medication nor absolute changes in hemodynamics reflect the CFR. The higher resting rate pressure product noted for the L_{CFR} group compared to the H_{CFR} group is consistent with a higher resting coronary flow level. Thus, if the resting coronary flow is elevated, there is diminished capacity for the flow to increase in response to a vasodilatation agent. The effectiveness of a vasodilatation agent might well be expected to be blunted in the patient group with higher baseline flow conditions.

Conclusions: While resting and vasodilatation parameters distinguish groups of patients with H_{CFR} and L_{CFR}, a H_{CFR} is more strongly associated with low resting HR, SBP, and RPP. The H_{CFR} and L_{CFR} groups are not distinguished by changes in the heart rate, systolic blood pressure, or by the heart rate reached at post vasodilatation. This suggests that conditions most strongly influencing the CFR are established at rest and may be intrinsic to the patient, diminishing the possibility

Hemodynamics of H_{CFR} and L_{CFR}

	REST					VASODILATION			
	SBP	HR	PP	RPP	PCM	SBP	HR	PP	RPP
H_{CFR}	136 ± 23	67 ± 11	61 ± 16	9144 ± 2419	1.00 ± 34	134 ± 24	85 ± 11	61 ± 18	11333 ± 2449
L_{CFR}	151 ± 21	72 ± 16	74 ± 18	11041 ± 2986	0.83 ± 0.32	145 ± 24	89 ± 15	70 ± 19	12836 ± 3044
P	0.001	0.05	0.001	0.001	0.01	0.05	NS	0.05	0.01

SBP is the systolic blood pressure, HR is the heart rate, PP is pulse pressure, RPP is the rate pressure product, and PCM is the peripheral vascular compliance. Numbers are mean ± standard deviation, and P indicates significance between H_{CFR} and L_{CFR} groups.

of raising the CFR by administration of a vasodilatation agent. Furthermore, this observation may allow prediction of the accuracy of a perfusion test based on the patient's baseline characteristics. Further work is indicated to determine the effectiveness of alternate vasodilators, such as adenosine, in light of these results.

Does LV Volume Reduction Surgery Also Correct Regional Geometry?

R.W.W. Biederman,[1] M.E. Kortright,[1] M. Doyle,[1] A.R. Fuisz,[1] A.W.H. Stanley,[2] C. L. Athanasuleas,[2] G.D. Buckberg,[3] D.C. McGiffin,[1] J.K. Kirklin,[1] G.M. Pohost.[1] [1]*University of Alabama at Birmingham, Birmingham, AL;* [2]*Carraway Methodist Medical Center, Birmingham, AL;* [3]*University of California at Los Angeles, Los Angeles, CA*

Introduction: LV volume reduction surgery in pts with dilated cardiomyopathy (CM) seeks to reduce Laplacian stress and thereby improve LV function. However, the role of changing LV geometry has not been explored. We assessed an MRI-derived geometric index in pts who underwent the Dor procedure (LV endoventricular patch plasty with apical reconstruction). This technique seeks to reduce LV volume while simultaneously redirecting proper myocardial fiber orientation by fashioning an apex with a prolate ellipse geometry.

Methods: Fourteen subjects participated in the study. Six pts (5 ischemic, 54 ± 7 yr) with end stage dilated CM (EDD = 66 ± 8mm, EDV = 282 ± 40 ml, EF = 20 ± 4%, NYHA 3.3) underwent MRI analysis pre/post surgery. Eight normals underwent similar MRI evaluations. A global prolate ellipse was fit to each LV in the RAO and 4 chamber views using the major and minor axes at the base. Secondly, an apical prolate ellipse was fit to a section positioned at 2/3 of the major axis to more appropriately define the newly reconstructed apical geometry. Finally, the ratio of the apical/global minor axis ellipses in each projection characterizing the agreement (or the amount of heterogeneity) between the two prolate ellipses was examined. Consequently, as the ratio approaches unity, the apical ellipse approximates the global ellipse, implying that the apical shape precisely tracks the global geometry.

Results: The figure shows the mean ± SD apical/global geometric indices for the patients pre-operation(Pre) and post-operation (Post) relative to normals (Nls). The insert diagrammatically illustrates the derived global and apical ellipses. Notably, Nls vs pre-surgery were significantly different as expected ($p < 0.05$). However, post-surgery, the measured apical/global heterogeneity index moved leftward and down, approaching that of the normals and revealing a very strong trend towards LV geometric normalization.

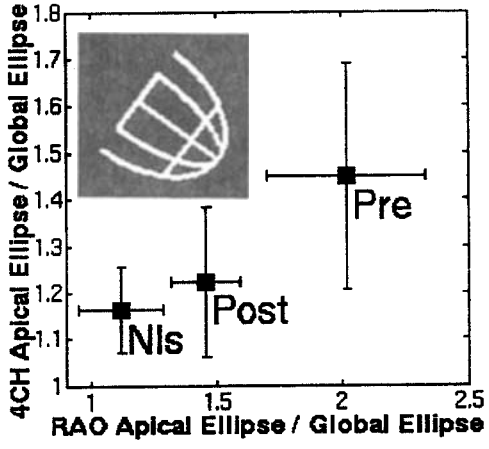

Conclusion: We show that normals have high agreement between the idealized global ellipse and the apical ellipse, in contrast to patients with dilated CM, who are grossly mismatched. However, after the Dor LV volume reduction surgery, patients acquire a geometric index much closer to normal. This MRI analysis indicates that, in addition to the simple volume reduction, geometric remodeling is a significant component of the Dor LV reconstruction.

High Diagnostic Accuracy of MR Perfusion Imaging for the Detection of Coronary Artery Disease: A Comparison with Positron Emission Tomography and x-Ray Coronary Angiography

J. Schwitter, K. Bertschinger, D. Nanz, S. Kneifel, M. Buechi, T.F. Luescher, B. Marincek, G.K. von Schulthess. *University Hospital Zurich, Switzerland*

Background: Assessment of ischemia in patients with coronary artery disease (CAD) is crucial for guidance of revascularization and risk stratification. Echoplanar-based MR perfusion imaging (1) may provide full myocardial coverage during first pass of contrast medium (CM), but rapid pulsing may compromise T1 relaxation and hence, may limit signal response in the myocardium.

Purpose: To evaluate the performance of two hybrid echoplanar MR perfusion sequences in comparison with positron emission tomography (PET) and conventional x-ray coronary angiography in patients with CAD.

Material and methods: The MR perfusion measurement was based on a echoplanar hybrid sequence (1.5T, LX-system, GE, WI) as described earlier (2). First, various sets of parameters were tested in phantoms over a wide range of GdDTPA concentrations (in saline). From these measurements two sequences were derived providing either enhanced CM sensitivity (sequence A) or extended cardiac coverage (sequence B).

Eight volunteers were studied twice with sequence A and B. In 18 patients with suspected CAD, an MR perfusion study (sequence A), a PET study, and a conventional X-ray coronary angio-graphy were performed. In the first 12 patients both MR sequences (A and B) were applied in two separate examinations.

a) MR Imaging and Data Analysis: For both sequences A and B in volunteers and patients, the imaging parameters were as follows: TR/TE: 5.9/1.5ms, echo-train length: 4; field of view: 36–40 × 36–40cm2, matrix: 128 × 96. Band width: ±125kHz. To achieve optimal CM sensitivity (sequence A), or expanded cardiac coverage (sequence B): preparation flip angle was 90° and 50°, saturation recovery time was 120 and 10 ms, and flip angle of read out: 50° and 10°, respectively, allowing the acquisition of 4–6 and 6–8 slices/2RR intervals, respectively. In all subjects extravascular GdDTPA (0.1 mmol/kg IV) was administered during hyperemia (dipyridamole 0.56 mg/kg IV) and parametric maps of CM wash-in were generated by pixelwise linear fits after correction for gross cardiac motion, baseline signal intensity, and input (parametric slope map divided by slope of signal intensity increase in the left ventricular cavity). On these parametric maps 8 sectors/slice were analyzed resulting in a total number of sectors/heart of 32 and 48 for sequence A and B, respectively. These regions were assigned to the territories of corresponding coronary arteries. Disease of a coronary artery was defined as a slope of <mean-2SD of controls.

b) PET Imaging and Data Analysis: Dynamic ^{13}N-ammonia PET measurements (Advance, GE Medical Systems, WI) were performed at rest as well as during hyperemia (dipyridamole 0,56 mg/kg IV). In the short axis view, 8 regions of interest (ROI's) were placed as described for the MR data set resulting in 48 ROI's/heart. In these ROI's a two-compartment model was applied to calculate resting and hyperemic myocardial blood flow (in mL/min/g) as well as coronary flow reserve (CFR). Sectors were assigned to corresponding vascular territories as

for the MR data. Disease of a coronary artery was defined as a CFR of <mean-2SD of controls.

c) Conventional X-ray coronary angiography: Coronary angiography was performed in all patients within 2 weeks of MR and PET studies. By means of quantitative coronary angiography (QCA), 11 segments of the coronary tree were analyzed and assigned to corresponding myocardial sectors (diseased vessel: ≥ 50% stenosis).

Results: For GdDTPA, phantoms revealed a linear CM concentration-signal intensity relationship up to 0.5 and 0.2 mmol/l of CM with sequence A and B, respectively. In the myocardium of controls signal-to-noise ratio increased by 198 ± 39% and 77 ± 23% with sequence A and B, respectively ($p < 0.005$, paired t test). For sequence A the sensitivity/specificity for the identification of individually diseased coronary arteries was 81%/71% vs PET and 78%/71% vs QCA (ROC analysis); for sequence B: 73%/53% and 68%/48%, respectively. For sequence A (18 patients and 8 controls), sensitivity/specificity for detection of CAD was 89%/80% vs QCA, and 94%/86% vs PET, respectively.

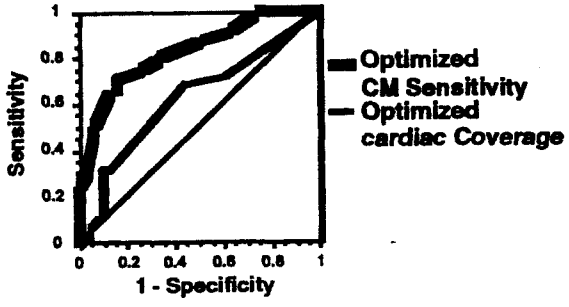

Figure 1. MR sequence A and B vs QCA (≥50% Stenosis).

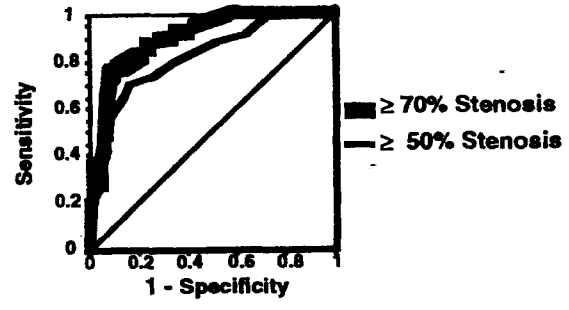

Figure 2. MR sequence A vs QCA (≥50%/≥70% stenosis).

Conclusions: MR-derived parametric perfusion maps avoid subjective assessment of perfusion defects and are highly reliable in CAD detection.

References

1. Schwitter J, Debatin JF, von Schulthess GK, et al. *MRM* 1997; 37: 140–7.
2. Ding S, Wolff SD, Epstein F. *MRM* 1999; 39: 514–9.

3D Coronary Artery Imaging with Multiple Breath-Holds and Real-Time Adaptive Position Correction

S.M. Shea,[1] R. Kroeker,[2] J. Zheng,[3] J.P. Finn,[1] D. Li[1]. [1]*Dept. of Radiology, Northwestern University,* [2]*Siemens Medical Systems, and* [3]*Bracco Diagnostics, Chicago, IL*

Introduction: Breath-holding has been shown to be an effective method for removing respiratory image artifacts in coronary MRI. However, it also places strict limitations on scan time, since an entire scan must be collected in one 15–20 second breath-hold. Collecting data in several breath-hold periods would alleviate this limitation. However, inconsistencies in breath-hold positioning will cause motion blur in images. A real-time slice following method has been used for respiratory gated free-breathing coronary artery imaging (1–3). In this work, we collected 3D k-space data in two breath-holds to improve image resolution of volume targeted (VCATS) (4) coronary artery imaging and used real-time slice following to correct for position shift between breath-holds. Extracellular contrast agent was used to improve the signal-to-noise ratio of coronary arteries.

Methods: Each breath-hold acquired half of the 3D k-space. At the beginning of each breath-hold scan, a navigator echo was first collected, followed by a segmented 3D FLASH sequence to acquire image data (Fig. 1). The diaphragm position detected from the navigator echo of the first breath-hold was used as a reference; no position correction was performed for the first breath-hold. The diaphragm position detected from the second breath-hold was compared to that of the first and a position shift was calculated in real time. This diaphragm position shift was converted to coronary artery position shift using a scale factor of 0.6 (2) and the slab position was adjusted accordingly before initiating the 3D segmented FLASH data acquisition. In this way, the position of coronary arteries should be the same for the two breath-hold scans.

The 3D FLASH sequence had a TE of 1.9 ms, TR of 3.8 ms, FOV of 300 × 225 mm², matrix of 512 × 176, 8–16 partitions, 3 mm slice thickness, 25–39 lines/cardiac cycle. Data was collected over 2 breath-holds, with each breath-hold lasting for 24 heartbeats. A double-dose of extracellular contrast agent, Prohance (Bracco), was infused over 20 sec before data acquisition. An inversion recovery preparation scheme was used to suppress the myocardial tissue.

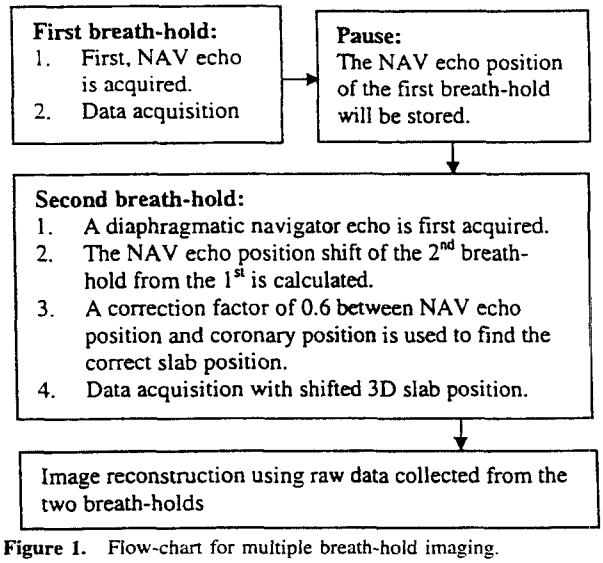

Figure 1. Flow-chart for multiple breath-hold imaging.

Results: Good delineation of coronary arteries was demonstrated in healthy volunteer studies. With data acquisition over two breath-hold periods, the resolution and coverage of the imaging slab all increased over single-breath-hold 3D coronary artery imaging. Image artifacts caused by position shift between breath-holds were significantly reduced by real-time slice following.

Conclusion: 3D coronary artery imaging over multiple breath-hold periods alleviate the constraint on imaging time by a single breath-hold while eliminating respiratory motion, allowing for improved resolution and coverage. Further studies are required to evaluate the consistency of the method in volunteers and the potential application in patient studies.

References:
1. Oshinski JN, et al. *Int J Card Imaging* 1998; 14: 191–9.
2. Botnar RM, et al. *Circulation* 1999; 99: 3139–3148.
3. Taylor AM, et al. *J Cardiovasc Magn Reson* 1999; 1: 131–138.
4. Wielopolski PA, et al. *Radiology* 1998; 209: 209–19.

Coronary Artery Imaging Using IR Prepared Contrast-Enhanced 3D Segmented EPI

V.S. Deshpande,[1] P. Wielopolski,[2] S.M. Shea,[1] J. Carr,[1] J. Zheng,[3] D. Li,[1]. [1]*Northwestern University, Chicago, IL;* [2]*Dr. Daniel den Hoed Kliniek, Rotterdam, Netherlands;* [3]*Bracco, Chicago, IL*

Introduction: A volume targeted 3D segmented FLASH technique (VCATS) has been used previously in coronary imaging (1). However, with the constraint of imaging time within a single breathold, it is limited by low resolution and small coverage. Segmented EPI provides a much faster method of imaging resulting in higher resolution and a higher imaging efficiency (2,3). In this study, we intend to investigate the effectiveness of extravascular contrast agents for improving SNR in coronary imaging using 3D segmented EPI.

Methods: A 3D segmented EPI sequence was implemented on a Siemens 1.5T Sonata system (maximum gradient strength: 40 mT/m, slew rate: 200 mT/m/ms). The sequence adopted an interleaved segmentation scheme. Six echoes per rf pulse were collected with an interval of 1.07 ms between echoes and the lines were sequentially ordered in the phase encoding direction. Eleven rf pulses were applied in every cardiac cycle. The flip angle was varied linearly over the partitions. All data were collected during the entire trapezoidal readout pulse. These data were sinc interpolated in the partition direction with a factor of 2.

Studies were performed on healthy volunteers (n = 4). All images were acquired within a single breathold. The FOV was 260 × 150 mm², the matrix size 108 × 256, and the resolution 0.9 × 1.4 mm². Half Fourier imaging was used to reduce the imaging time. The slice thickness was 1.6 mm and the sequence was run with TE = 2.4 ms and TR = 7.93 ms. 32 partitions were acquired and data interpolated to reconstruct 64 partitions.

For post-contrast studies, a 25 ml bolus of the extravascular contrast agent Prohance (Bracco) was injected at 0.9 ml/s in the anticubital vein of the right arm. Inversion recovery with TI = 300 ms was incorporated in the sequence to suppress the myocardial signal. Based on previous experience, the sequence was run approximately 25s after the initiation of the contrast agent to obtain maximum contrast.

Results: Fig. 1 and fig. 2. show examples of contrast-enhanced coronary artery images. Note the excellent delineation of the LAD and RCA. The distal portion of the arteries, not identified in the pre-contrast images is clearly visible post-contrast. The increase in SNR measured here is 26 ± 10%. There is a 123 ± 21% increase in the CNR in the post-contrast images as measured in the coronaries and the adjacent myocardium.

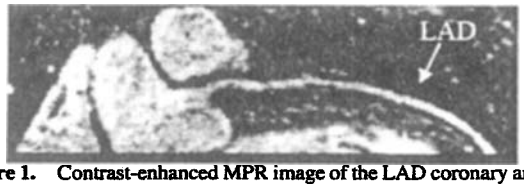

Figure 1. Contrast-enhanced MPR image of the LAD coronary artery. The original images were obtained using an IR-prepared, 3D segmented EPI sequence.

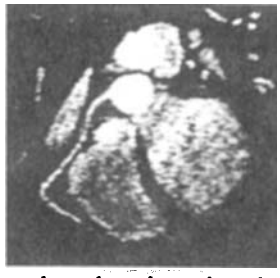

Figure 2. Contrast enhanced maximum intensity projection of the RCA.

Conclusion: Segmented EPI provides a fast means of imaging with a relatively high resolution and large coverage when compared with a conventional FLASH sequence. Contrast agents can significantly improve coronary SNR and the coronary/myocardium CNR. Contrast-enhanced 3D segmented EPI is thus a promising technique for coronary artery imaging.

References
1. Wielopolski PA, et al. *Radiology* 1998; 209: 209–19.
2. Wielopolski PA, et al. *J Magn Reson Imag* 1995; 5: 403–410.
3. Botnar RM et al. *SCMR, Second Annual Meeting* 1999; Abstract #17.

MR Angiography of Coronary Arteries Using Magnetization-Prepared Contrast-Enhanced Breath-Hold Volume-Targeted Imaging (MPCE-VCATS)

D. Li, J. Carr, S. Shea, J. Zheng, R. Kroeker, P. Wielopolski, R. Kim, E. Wu, G. Laub, J. P. Finn. *Northwestern University, Chicago, IL*

Introduction: Breath-hold volume targeted imaging (VCATS) (1) is a promising technique for coronary artery imaging. However, because of the constraint of imaging time, the spatial resolution, the SNR of coronary arteries and CNR between coronary arteries and myocardium tend to be limited. The goal of the current work was to improve the SNR and CNR of coronary arteries in VCATS imaging using conventional extracellular contrast agent (2,3).

Methods: Nine healthy volunteers were imaged. For each subject, a 3D segmented EPI scan was first obtained within a single breath-hold to cover the entire heart. Multiple planar reconstruction (MPR) was performed to find the orientations of the proximal portions of both left (LM + LAD) and right (RCA) coronary arteries. Two 20-ml Prohance (Bracco) injections were given to each volunteer, each injection was followed by a first-pass, breath-hold VCATS scan, to cover left and right coronary arteries, respectively, along the orientations determined from MPR images. Imaging parameters included: TR/TE = 3.8/1.9 ms, flip angle = 20–25°, 25–39 lines/heartbeat, in-plane resolution = 1.4 × 1.0 mm², slice thickness = 3 mm, number of partitions per 3D slab = 8 (16 with sinc-interpolation). An inversion recovery magnetization preparation was applied before data acquisition in each cardiac cycle with a TI of 300 ms to suppress myocardial signal. The imaging time per scan was 16–24 heartbeats, and the total imaging time for each subject was less than 30 min. All studies were performed on a 1.5T Siemens Symphony imaging system with a high performance gradient sub-system (gradient strength 40 mT/m and slew rate 200 mT/m/ms).

Results: SNR and CNR increases of post-contrast vs pre-contrast images are 22 ± 16% and 352 ± 142% ($p < 0.01$), respectively. As a result, the delineation of coronary arteries was markedly improved. The lengths of continuous visualization of RCA and LM + LAD are 10.9 ± 3.0 cm and 7.9 ± 1.2 cm, respectively. Fig. 1 compares pre-

and post-contrast images for left coronary artery delineation. The visualization of distal LAD (arrow) is substantially improved because of the enhancement of blood signal and suppression of myocardial signal (Fig. 1a). A local maximum intensity projection (MIP) image clearly shows LM, LAD, a diagonal branch, and proximal RCA (Fig. 1b).

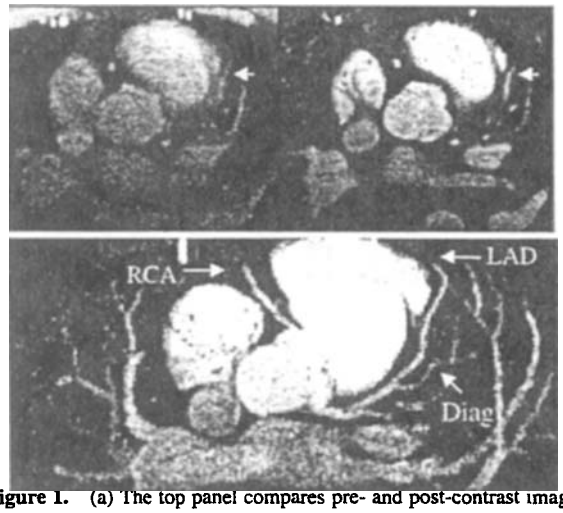

Figure 1. (a) The top panel compares pre- and post-contrast images. (b) The bottom panel is a MIP image from post-contrast 3D data.

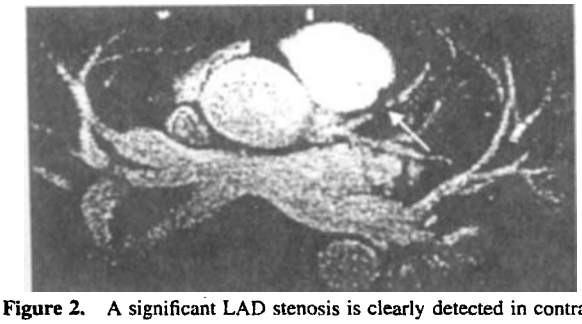

Figure 2. A significant LAD stenosis is clearly detected in contrast-enhanced MRA (arrow).

Conclusion: Breath-hold, magnetization prepared, contrast-enhanced volume targeted imaging (MPCE-VCATS) is a promising technique for MR coronary artery imaging. Intravascular contrast agents will offer even greater SNR/CNR improvements and longer window of data acquisition to allow for higher resolution and larger volume coverage.

References

1. Wielopolski PA. *Radiology* 1998; 209: 209–19
2. Goldfarb JW. *Radiology* 1998; 206: 830–834
3. Zheng J. *JCMR* 1999; 1: 33–41

Visualization of Human Mitral Valve Leaflet Motion by MRI

K.O. Agyeman, K.E. Bove-Bettis, A.E. Arai. *Laboratory of Cardiac Energetics, National Heart, Lung, and Blood Institute, National Institutes of Health, Bethesda, MD*

Introduction: Cardiac MRI provides morphological and functional information that can be valuable in the assessment of valvular heart disease. However, direct visualization of moving human heart valves has been difficult. The normal valve is thin <2mm, rapidly moving and the contrast between the valves and the surrounding blood is poor. In particular, diastolic motions have been difficult to image.

Purpose: To objectively determine how often we could visualize mitral valve leaflets and leaflet motion using segmented fast gradient echo MRI.

Methods: MRI of the heart was performed on 112 patients with a wide range of cardiac diagnosis (HCM n = 48, CAD n = 28, valvular disease n = 4, normal n = 17, other n = 15). All studies were performed at 1.5 Tesla using a GE MR scanner with enhanced gradient subsystems utilizing a dedicated four-channel, cardiac phased array coil. The complete cardiac cycle was imaged with a prospectively segmented, retrospectively sorted ECG-gated cine GRE sequence (1). Typical imaging parameters were: flip angle 15, TR 10–12 ms, TE 4–6 ms. Images had 1.9 × 1.9 mm spatial resolution, 72 ms temporal resolution, and 20 images were reconstructed per cardiac cycle.

These studies were then reviewed for subjective and objective evidence of adequate visualization of the mitral valve leaflets in the MRI equivalent of the echocardiographic three chamber view. Evaluation was based on cine loops and frame-by-frame review on a workstation. Subjectively the valve leaflet was considered identifiable only if distinct motions of early diastolic opening, partial closure during diastalsis, and opening after atrial contraction could be detected. Quantitative analysis included frame-by-frame measurements of the anterior and posterior mitral valve leaflet length during diastole on the three-chamber long axis view. In a subset of subjects in which the full mitral valve motion was not detected we constructed phase contrast flow-volume loops to characterize diastole by an independent method.

Results: The mitral valve was seen in 112/112 studies. Mitral leaflets were seen well enough to be measured in 107/112 studies and confirmed the echocardiographic finding that the anterior mitral leaflet is longer than the posterior mitral leaflet (26 +/− 5mm vs12 +/−4mm, $p < 0.001$).

In 90/112 studies (80%), mitral valve leaflet motion depicting both early diastolic opening and distinct motion after the atrial contraction was detected. Incomplete visualization of mitral leaflet motion after the atrial contraction was explained by limited image quality in only 7/112 studies (6%). Mitral valve leaflet motion was never missed in normal volunteers but occurred most commonly in diagnoses associated with diastolic filling abnormalities (HCM 12/48 (25%), CAD 6/28 (21%). In 15 of 112 studies, diastolic filling abnormalities were confirmed by transmitral filling velocity measured on phase contrast MRI eliminated the ability to evaluate partial closure of the mitral valve in diastasis. Failure to visualize mitral motion after the atrial contraction was associated with higher heart rates (75+/−12 vs 61 +/−8, $p < 0.001$) but not height, weight, sex or blood pressure.

Conclusions: Fast cine gradient echo routinely visualizes the mitral valve leaflets well enough to measure them. Our measurements are consistent with the literature for other techniques including ex-vivo leaflet assessment. This MRI methodology captures the entire cardiac cycle, as evidenced by the ability to see distinct mitral leaflet motion after atrial contraction. Only a small fraction of mitral valves could not be seen related to image quality.

References

1. Feinstein JA, Epstein FH, Arai AE, Foo TKF, Balaban RS, Wolff SD. *JMRI* 1997; 7(5): 794–8.
2. Weissman NJ, Pini R, Roman MJ et al *Am J Cardiol* 1994: 73 1080–88.

Quantitative Assessment of Cardiac Function by MRI During Exercise-Induced Stress

J.F. London, F.H. Epstein, R. Wassmuth, C.R. Weiss, M.A. Guttmann, A.E. Arai. *Laboratory of Cardiac Energetics, NHLBI, National Institutes of Health, Bethesda, MD*

Purpose: The aims of this study were to determine if adequate exercise can be achieved using an MRI compatible supine ergometer and if car-

diac MRI could be used to quantitatively measure global and regional cardiac function during exercise-induced stress.

Methods: Ten consecutive healthy volunteers (7 male, age 35 +/− 8) were studied using an 1.5 T MRI scanner (GE Signa CV, Milwaukee, WI). Exercise was achieved using an MRI compatible ergometer (Lode, Groningen, Netherlands). MR cine imaging was done using FGRE-ET, (1) with 2.3 × 3.4 mm in-plane resolution, 10 mm slice thickness, 28 ms temporal resolution, and ECG gating. The scan duration for each slice was 5 heartbeats.

Five short axis images were acquired with and without myocardial tagging at rest. Subjects then exercised. The workload was increased by 25 watts every 2 minutes until subjects reached fatigue. Immediately following exercise a series of five cine slices were acquired. Exercise and imaging were repeated in the same fashion to acquire tagged images. When necessary, additional exercise was performed.

Stress and rest ejection fraction were calculated from the non-tagged cine images. The rate of myocardial circumferential shortening (Ecc/Δt) for 4 sectors of the mid-ventricular slice was calculated. All results are reported as means +/− SD.

Results: Subjects exercised for 6.4 +/− 1.3 minutes achieving 91 +/− 27 watts. The average heart rate increased from 68 +/− 9 bpm to 152 +/− 6 bpm with exercise ($p < 0.0001$). Systolic blood pressure increased from 131 +/− 16 mmHg to 174 +/− 19 mmHg ($p < 0.0001$). Rate pressure product increased from 89 +/− 16 to 263 +/− 28 ($p < 0.0001$).

All five imaging planes were acquired within 54 +/− 12 seconds of completing exercise. Non-tagged images were analyzable in all subjects. Tagged images were quantifiable in 8 of 10 subjects. Non-tagged images detected an increase in LVEF from 73 +/− 7 to 87 +/− 5% ($p < 0.0001$). The mean systolic ejection rate increased from 258 +/− 78 at rest to 464 +/− 100 ml/s at stress ($p < 0.001$). The rate of regional circumferential shortening on the tagged images increased from 0.72 +/− 0.2 at rest to 0.96 +/− 0.46 s^{-1} at stress ($p < 0.01$).

Conclusions: A high level of exercise was achieved with the ergometer. Global and regional LV systolic function were quantified for exercise-induced stress and showed significant increases compared to resting values. Exercise MRI is a promising technique for stress testing made possible by fast cardiac imaging.

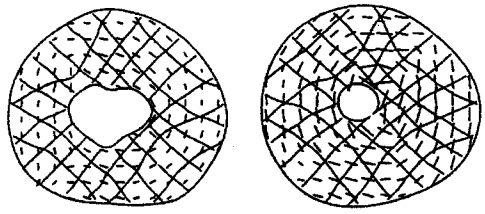

Figure 1. Example rest (left) and stress (right) systolic strain rate diagrams.

Reference

1. Epstein FH, Wolff SD, Arai AE. Segmented k-space Fast Cardiac Imaging Using an Echo-Train Readout. *MRM* 1999; 41: 609–613.

Physiological Consequences of Spiral and Non-spiral Forms of Hypertrophic Cardiomyopathy

R.Y. Kwong, H. Taheri, L. Fananapazir, D.A. Begley, A.E. Arai. *Laboratory of Cardiac Energetics, NHLBI, National Institutes of Health, Bethesda, MD*

Introduction: Normal global left ventricular (LV) systolic function is dependent on a helical pattern of myofibrils and slippage between muscle sheaths within the left ventricular wall. Many patients with hypertrophic cardiomyopathy (HCM) have localized areas of hypertrophy. On three-dimensional analysis of magnetic resonance images, we noted the area of hypertrophy follows a spiral pattern from base to apex in some subjects. We hypothesized that HCM in a non-spiral pattern might represent an underlying abnormality in muscle fiber orientation in addition to localized hypertrophy. The purpose of this study was to determine the pathophysiological consequences of spiral versus non-spiral forms of HCM.

Methods: We performed cine fast gradient echo cardiac MRI on 108 patients with HCM. Ventricular hypertrophy was classified as asymmetric if the ratio of maximal to minimal LV end-diastolic wall thickness (LVWT) was at or above 1.5. The angle of maximal LVWT was measured on multiple short axis slices relative to the right ventricular insertion into the anterior LV. The asymmetric cases were further classified as spiral if the maximal LVWT rotated by ≥ 90° around the short axis.

LV ejection fraction (LVEF) at rest and exercise were measured by radionuclide ventriculography. The increase in LVEF was obtained by subtracting LVEF at rest from LVEF with exercise.

LV end diastolic pressure (LVEDP) and LV outflow (LVOT) gradient were measured at rest during cardiac catheterization. The provokable LVOT gradient was measured during the catherization as the maximal LVOT gradient during isoproterenol infusion.

All results are presented as mean ± standard deviation.

Results: Among the 108 HCM subjects, 86 (80%) were asymmetric and 22 (20%) were concentric. A spiral pattern of HCM was found in 32 of the 86 (37%) asymmetric HCMs and 54 (63%) were non-spiral.

At rest, the LVEF and LVOT gradient were not statistically different between the spiral and the non-spiral groups (75 ± 10 vs 71 ± 16%; 28 ± 37 vs 15 ± 41mmHg).

With exercise, the LVEF increased in patients with spiral HCM +5 ± 8% but did not in patients with non-spiral HCM −1 ± 8% ($p < 0.02$). This resulted in significantly higher exercise EF in spiral HCM (80 ± 10%) than in non-spiral HCM (71 ± 17%, $p < 0.03$).

The provokable LVOT gradient was higher in spiral HCM (59 ± 57 mmHg) than in non-spiral HCM (25 ± 25%, $p < 0.003$). LVEDP was not different between the spiral and the non-spiral groups.

Conclusion: Spiral ventricular thickening represents a new subtype of hypertrophic cardiomyopathy commonly associated with LVOT obstruction. This pattern of hypertrophy appears to allow a more complete systolic ejection during exercise. This is associated with a higher degree of outflow tract obstruction with isoproterenol stress, compared to the non-spirals. The non-spiral HCM has reduced global systolic reserve in response to exercise and isoproterenol stress. These findings are consistent with the hypothesis that a non-spiral pattern of hypertrophy may result in compromised left ventricular systolic function related to an abnormal myofibril fiber orientation.

References

1. Young AA, Kramer CM, Ferrari VA, et al: Three-dimensional Left Ventricular deformation in hypertrophic cardiomyopathy. *Circulation* 1994; 90: 854–867.
2. Maron BJ, Bonow RO, Cannon RO, et al: hypertrophic cardiomyopathy. *N Engl J Med* 1987; 316: 780–789.
3. Ingels NB, Jr. Myocardial fiber architecture and left ventricular function. *Technol Health Care* 1997; 5: 45–52.

Noninvasive Detection of Unstable Atherosclerotic Plaques by High Resolution MR Imaging of the Carotid Arteries: Identifying Thin and Ruptured Fibrous Caps

L.M. Mitsumori, C Yuan, T.S. Hatsukami, M.S. Ferguson. *Univ. of Washington, Seattle, WA*

Introduction: Similar to the coronary circulation, acute cerebrovascular symptoms are believed to result from carotid plaque rupture followed by superimposed luminal thrombosis and intraplaque hemorrhage (1).

To better understand the pathophysiology of plaque rupture, comparative histological studies of advanced plaques from symptomatic and asymptomatic endarterectomy patients were performed. The results have shown that thinning, disruption, or cellular infiltration of the fibrous cap are associated with the development of ischemic symptoms, thereby, suggesting that these features represent markers of plaque instability (2,3,4).

Based on these findings, having the ability to assess the state of the fibrous cap in vivo would provide a means of identifying vulnerable plaques and allow the design of prospective studies to identify factors responsible for disease progression or evaluate the efficacy of interventions (5).

Presently, duplex sonography and angiography are unable to reliably demonstrate the fibrous cap (3,4). Although intravascular ultrasound visualizes the arterial wall in vivo (5), the invasive nature of the modality limits its use in large serial studies and on low risk patients. A promising alternative is high resolution MRI, which is capable of characterizing plaque morphology noninvasively and reproducibly in serial studies (6,7,8). While early ex vivo MR experiments showed the fibrous cap as a juxtaluminal band of low signal intensity on T2w Spin Echo (SE) images (9); recent unpublished work, performed at this institution, suggests that the use of a 3D time-of-flight (TOF) sequence enhances visualization of the fibrous cap of in vivo carotid plaques.

Thus, the purpose of this study was to determine the ability of multispectral MRI to noninvasively depict the fibrous cap of advanced carotid plaques and identify the features (thinning, rupture, cellular infiltration) associated with unstable lesions.

Methods: After informed consent was obtained, the carotid arteries of 18 endarterectomy patients were preoperative imaged using specially-designed phased array surface coils in a 1.5T GE Signa Scanner. T1w, Shared Echo-Fast SE (proton density and T2w), and 3D TOF axial images were obtained of both carotid arteries of each patient (2 cm proximal and 2 cm distal to the bifurcation).

Histological/image Analyses: The operative specimens were histologically processed (3). MR images were reviewed for evidence of indistinctness, thinning (<0.7 mm (9)), interruptions in, or absence of the hypointense juxtaluminal band, believed to represent the fibrous cap. Identification of any one or a combination of these findings was considered as an indication of an unstable cap in the image. The MR results were then compared with the histological specimens that were matched to each image based on their location relative to the carotid bifurcation.

Results: The 18 exams provided 91 images that were compared with histology. Blinded review of the images demonstrated 33 unstable caps, 27 of which were confirmed histologically (sensitivity 81.8%, specificity 90%). Difficulties in image interpretation were caused by flow artifacts, juxtaluminal calcifications, intraluminal thrombus, and small (<0.03 mm^2) ulcers.

Conclusions: The results of this initial study suggest that MR imaging is capable of noninvasively assessing the state of the fibrous cap of advanced carotid plaques. Continued improvements in scanning techniques and the use of intravascular contrast could further improve the accuracy of the modality. In addition, future technical advances may allow application of these methods in the coronary circulation.

References

1. Fisher M, et al. *Arch Neurol*, 1987;44: 1086–89.
2. Bassiouny HS, et al. *J Vasc Surg*, 1997; 26: 585–94.
3. Hatsukami TS, et al. *Stroke*, 1997; 28(1): 95–100.
4. Carr S, et al. *J Vasc Surg*, 1996; 23(5): 755–764.
5. Ge J, et al. *Heart*, 1999; 81: 621–27.
6. Ingersleben G, et al. *Radiographics*, 1997; 17: 1417–1423.
7. Skinner MP, et al. *Nature Med*, 1995; 1: 69–73.
8. Toussaint JF, et al. *Circulation*, 1996; 94(5): 932–938.
9. Rhim EY, et al. *J Vasc Investigation*, 1997; 3(1): 42–51.

An Integrated Approach to MRI Analysis of Myocardial Perfusion

L. Axel, J.E. McCloud, Q. Yuan. *University of Pennsylvania School of Medicine, Philadelphia, PA*

Introduction: MRI after a contrast agent bolus for myocardial perfusion must overcome several difficulties, including relating signal intensity to agent concentration, input function correction, and extravascular exchange. We here report an integrated approach to solve these problems.

Data Acquisition Methods: Imaging of sheep with LV myocardial infarction was performed on a 1.5–T MRI scanner (GE Medical Systems, Milwaukee, WI), using a segmented k-space fast gradient-echo pulse sequence with an echo-train readout (1). First-pass perfusion images were acquired after the injection of Gd-DTPA-BMA (0.03 mmol/kg). A non-selective 90° saturation pulse was used for T1 weighting. A 4-element phased-array cardiac coil was used. A PD-weighted images was taken (with unchanged receiver gain) before the injection of the contrast agent, using flip angle 3°, longer TR and the same TE, with no saturation pulse.

Perfusion images were analyzed using IDL (RSI, Boulder, CO). The in-plane translation of the heart due to respiratory motion was compensated manually. Signal intensity was measured in ventricular wall regions and the LV cavity blood. The signal intensity from T1-weighted images during first-pass perfusion was divided by the signal intensity from corresponding PD-weighted images, in order to correct for surface coil inhomogeneity, as well as PD and T2. An analytical formula was used to convert this signal intensity ratio time curve into a R1 relaxation time curve. Under the assumption of fast water exchange, contrast agent concentration was then determined by $\Delta R1/\gamma$, where γ is the agent relaxivity. The time-concentration curves were then analyzed to obtain blood flow, etc., using a perfusion/exchange model.

Perfusion Modeling Methods: A. Model Structure: The myocardium can be effectively modeled as a compartment system composed of the intravascular plasma space and extracellular extravascular space (the intracellular space excludes Gd tracer), with another compartment for conductance in the coronary artery: The "true input" to the myocardium is the arterial concentration (Ca), a delayed and blurred version of the LV input. To estimate Ca, we have adopted a lagged normal transfer function model that is scaled by a single parameter (td) (2). The venous drainage (Cv) is determined in part from the convolution of Ca with the capillary transfer function, which is the derivative of the residue function, R, modeled as a Fermi function (3). However, in the first pass with an extravascular agent, there is a net flux of tracer across the capillary wall. A correction term for Cv is determined from the flux and R. For a given set of model parameters, we can predict the tissue concentration from the LV cavity concentrations.

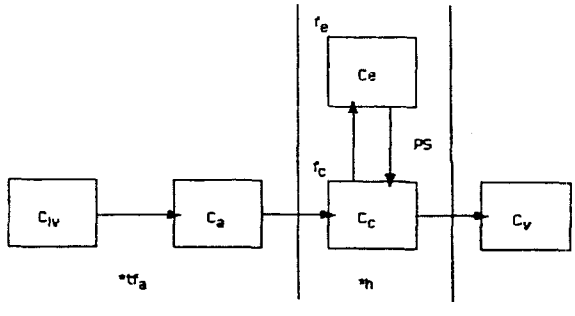

B. Model Fitting: We use an iterative approach to fitting the data to the model. A combination of parameter estimates taken from the raw data and from the literature are used to initialize the model. An initial

value for td (arterial delay) can be estimated from the difference in the contrast appearance times between the LV input and the observed tissue. Once td is found, Ca can be estimated. Assuming that in the rising portion of the tissue concentration curve the tissue approximately integrates the arterial input, the ratio of the observed tissue concentration to integrated arterial plasma concentration can be used to estimate plasma flow, Fp. Tissue fractional plasma volume (fpl) is estimated by first approximating the mean transit time (MTT) of the capillary compartment; fractional capillary plasma volume is obtained from the product of MTT and Fp. Initial values of the remaining parameters are estimated from the literature. Next, iterations are performed to adjust each parameter until the weighted mean square difference between predicted and observed tissue concentrations is minimized.

Result: Representative MRI-derived concentrations are shown below:

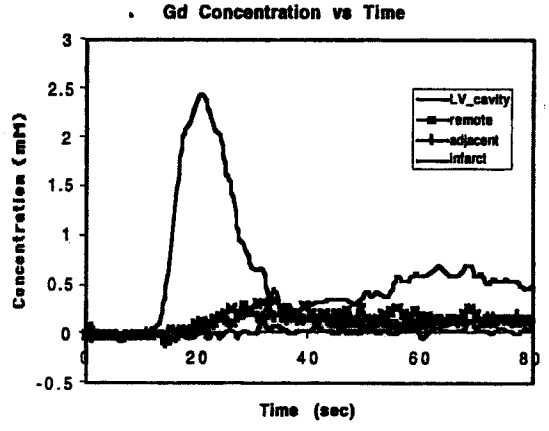

Values obtained from the model fitting agree with those expected from the literature; e.g., normal myocardial flows are on the order of an ml/g/min.

Discussion: This integrated approach to MRI perfusion analysis is promising, but still must be verified with reference methods, such as microspheres.

References

1. Ding S, Wolff SD, Epstein FH. *MRM* 1998; 39:514.
2. Bassingthwaighte *J. Circ Res* 1966; 14: 332.
3. Axel L. *Invest Radiology* 1983; 18: 94–96.

Motion Adapted Gating with Partial Averaging for Phase Contrast Based Quantification of Coronary Flow Reserve in Patients with Aortic Regurgitation

S. Kozerke,[1] J. Schwitter,[2] O.M. Weber,[1] R. Jenny,[2] P. Boesiger[1].
[1]*Inst. of Biom. Eng., Univ. and ETH, Zurich,* [2]*Division of Cardiology, Univ. Hospital Zurich, Switzerland*

Introduction: There has been an ongoing controversy about the optimal timing for aortic valve replacement in patients with aortic regurgitation. In daily clinical practice, decisions are based on semi-quantitative indices as assessed by echocardiography or by invasive angiographic techniques.

However, a considerable number of patients die or develop left-ventricular dysfunction before symptoms become evident. Accordingly there is a lack of appropriate quantitative parameters for prediction of progressing valvular insufficiency. Since experimental studies have shown an impairment of myocardial perfusion reserve with progression in aortic valve disease, the assessment of coronary flow reserve (CFR) might be considered important in these patients.

Objective of this work is the MR based quantification of coronary sinus flow under rest and dipyridamole induced stress condition in patients with mild to severe aortic regurgitation.

The need for sub-millimeter resolution and sufficiently high temporal sampling for the assessment of coronary sinus flow does not allow data acquisition during a single breath-hold. Performing multiple breath-holds is prone to misregistration and requires patient cooperation. Thus, gating strategies for the reduction of artifacts related to respiratory motion have to be incorporated. Time limitations especially under stress condition require gating schemes with high scan efficiency.

Furthermore, due to the distance of the coronary sinus from surface receiver coils a lack of adequate signal-to-noise might hamper reliable measurements.

Methods: For respiratory motion compensation navigator echoes are acquired. Using motion adapted gating (MAG) (1) the phase encoding step is set in real-time according to the measured actual diaphragm shift. In order to maintain the same measuring position under rest and stress condition identical navigator reference positions are used for both scans.

Breathing patterns are subject to temporary changes and long-term drifts, especially under stress condition. To keep a scan efficiency high, slice tracking (2) is used in conjunction with an interactive gating window control. After every breathing cycle the most frequent diaphragm position is determined and possible long-term drifts are displayed. The user can interact by shifting the gating window accordingly to the displayed drift during scanning.

To improve the signal-to-noise ratio (SNR) a phased array coil is used. An additional gain in the SNR is obtained by extending the MAG scheme with profile averaging. A target function defines the minimum number of signal averages depending on the profile number. In case all required profiles are obtained the scan is terminated. However, breathing patterns during stress are subject to temporary changes. Therefore, end-expiration might be no longer the most frequent and stable position in the breathing cycle. In this case profiles others than the required ones can be averaged as well as long as the given target function is not fulfilled. However, the variable SNR level over profiles changes the point spread function (PSF) in phase encoding direction. Due to the additional weighting of k-space introduced by the partial averaging scheme the full-width-at-half-maximum (FWHM) of the PSF becomes wider. Accordingly, for 45% partial averaging the effective width of a single imaging pixel in preparation direction is 1.3 pixel while the SNR gain is of factor 1.2.

Scan parameters for coronary flow measurements are as follows: in-plane resolution: 0.8 × 0.9 mm^2; temporal resolution: 30 ms; velocity encoding: 60 cm/s; T_E 7.8 ms. The central 45% of k-space is to be averaged twice whereas the peripheral k_y-lines are required to be measured once. Gating efficiency was 77% on average during the stress period. Accordingly, scan duration during stress was about 4:05 min (heart rate: 80 beats/min).

The methods were used to quantify CFR in 12 patients with mild to severe aortic regurgitation on a Philips Gyroscan NT 1.5T imager. For CFR calculation, flow measurements were obtained during rest and vasodilatation induced by dipyridamole infusion (0.56 mg/kg for 4 min).

Results: In all patients velocity mapping in the coronary sinus could be performed with the proposed strategies under rest and stress condition. Under rest coronary sinus flow exhibits a biphasic pattern with the major peak during mid-diastole. During stress flow is shifted into the systolic window with only one peak.

Discussion: The proposed strategy to measure coronary sinus flow has proven to be very robust, particularly under stress condition.

References
1. Weiger, M. et al., *MRM* 1997; 38: 322–333.
2. Wang, Y. et al., *Proceedings of ISMRM* 1996; 175.

Ring Tagging for the Assessment of Myocardial Wall Motion

M. Spiegel,[1] R. Luechinger,[1] O.M. Weber,[1] M.B. Scheidegger,[1] J. Schwitter,[2] P. Boesiger.[1] [1]*Inst. of Biomedical Engineering and Medical Informatics, Univ. and ETH, Zurich;* [2]*Division of Cardiology, University Hospital, Zurich, Switzerland*

Introduction: The transmural gradient in myocardial thickening results in overestimation of contractile function by endocardial ejection indices, particularly in hypertrophied ventricles with increased relative wall thickness (1,2). With this in mind, Shimizu (1) proposed a two-shell cylindrical model to calculate midwall circumferential fiber shortening (cFS). This approach confirmed reduced intrinsic contractile function in hypertrophied myocardium (1,2). Further, the extent of fiber shortening is virtually limited by the afterload at end-ejection, i.e. the force acting in the direction of the circumferential fibers. Therefore, the relationship between midwall cFS and circumferential wall stress at end-systole may serve as a load-independent measure of contractility (2). Although conceptually attractive, the two-shell cylindrical model is limited by its geometrical assumptions. Accordingly, a ring tagging approach was developed to directly visualize circumferential fibers during contraction. Conventional myocardial tagging principles as SPAMM (3) or CSPAMM (4), based on the generation of line or grid shaped saturation regions, do not allow accurate determination of the mid-line displacement because of the relatively low resolution of the tag lines. Ring shaped tags have previously been demonstrated to suppress sample ring artifacts from the generation of 2D selective pulses (5). However, these sequences do not offer an easy way to describe arbitrary shapes. The approach selected here fulfils this demand and is direct and simple.

Methods: Ring Tag application: A frequency off-centered RF pulse generates a saturation plane perpendicular to the imaging slice, which is rotated 360 degrees around the center point of the user defined shape. The off-center frequency is thereby varied depending on the position and shape of the desired RingTag contour. Longitudinal magnetization is destroyed in the ring-like structure whereas it is unaffected in the enclosed area and minimally saturated in the surrounding tissue.

RingTag Prescription: The definition of the ring structure is done on a prescan by means of a user friendly planning software on the scanner console. The defined geometrical structure is thereupon automatically forwarded to the acquisition software.

RingTag Imaging: The RingTag preparation is combined with a fast EPI sequence for time efficient imaging. Imaging parameters are FOV = 196 mm, scan matrix 128, slice thickness 8 mm, EPI factor 9, $\alpha = 30°$, TE = 6.2 ms. In-plane image resolution is 1.5 × 1.5 mm and 16–18 heart phases are acquired with a time resolution of 30 ms in a single breath hold of 10 seconds. All measurements were performed on a Philips Gyroscan ACS/NT 1.5T whole body scanner equipped with PowerTrak 6000. Single saturation lines can be applied additional to the ring-like saturation structure which, placed in a star-like manner, improve analysis of circumferential motion components (Fig. 1). The RingTag is easily combined with slice-following (6) by introduction of a slice-selective inversion pulse and a thick readout slice. This guarantees not only measurement of the initially selected image plane over the entire heart cycle despite long axis contraction of the heart, but also prolongs tag line visibility throughout the heart cycle.

Results: The user specified saturation structure was visible in all heart phases of the experiments and easily detectable by the evaluation software based on snakes, taking the prescripted shape as starting point. User specified RingTag positioning was accurate in phantom measurements as well as in volunteers. In the measurements without slice-following, fading of the RingTag was observed as it is known from SPAMM tagging. For non-convex shapes the RingTag saturation planes never affect the enclosed interior area. Therefore, the inner grey value gradient is very steep, enabling an accurate determination of the RingTag position by detection of the inner edge of the ring-like saturation structure. Thus, the precision of the RingTag localization is not directly dependent on the saturation line width, but may be performed with very high, eventually even with sub-pixel accuracy (7).

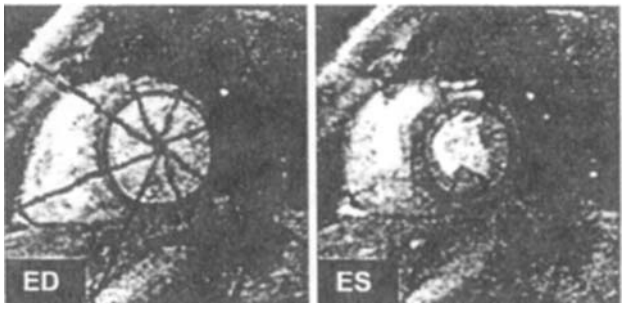

Figure 1. RingTag with star-like saturation lines on a short axis image at end-diastole (left) and end-systole (right).

Discussion: We have demonstrated a new myocardial tagging technique which allows the tracking of user defined ring-like shaped structures that align with mid-myocardial circumferential fiber orientation. In combination with assessment of end-systolic stress, this approach may provide an afterload-corrected measure of LV contractility. Compared to conventional tagging, the detection and evaluation of RingTag images is much easier and therefore can be done very time efficient. The short preparation time of the RingTag sequence (5 to 14ms) allows the combination with conventional line/grid tagging techniques which already was successfully done in phantom experiments allowing for regional assessment of cFS. The combination of RingTag with high speed imaging sequences would give the possibility for the estimation of cFS or ventricular strain properties (8) in real time, even under stress conditions.

References
1. Shimizu G et al. *Circulation*, 1991; 83: 1676.
2. Aurigemma, G.P. et al. *JACC*, 1995; 26: 195.
3. Axel L, Dougherty BS, *Radiology* 1989, 171: 841–845.
4. McKinnon GC et al. *Magn Reson Med*, 1994; 31: 401–413.
5. Hardy CJ et al. *J Magn Reson*, 1992; 99: 623–631.
6. Stuber et al, *Proc ISMRM*, pp. 418–, New York, 1993.
7. Atalar et al. *IEEE Trans Med Imag*, 13,1,152–160, 1994.
8. Wang, Y. et al., *Proceedings of ISMRM* 1996, 175.

Motion Artifact Reduction in Free-Breathing Navigator-Gated 3D Coronary MRA Using Zonal Motion-Adapted Acquisition and Reordering Technique (ZMART)

Michael E. Huber,[1,3] David Hengesbach,[1,3] Matthias Stuber,[1,2] Rene M. Botnar,[1,2] Peter Boesiger,[3] Warren J. Manning[1]. [1]*Beth Israel Deaconess Medical Center & Harvard Medical School, Boston, MA;* [2]*Philips Medical Systems, Best, The Netherlands;* [3]*Institute of Biomedical Engineering and Medical Informatics of the University and ETH, Zurich, Switzerland*

Introduction: Breathing motion during data acquisition may cause severe image artifacts in coronary MR angiograms (MRA). Successful motion compensation strategies have been proposed using MR naviga-

tor techniques combined with sophisticated k-space reordering techniques. However, all these methods are based on a 2D reordering of the acquired profiles in k-space. A further improvement in image quality and a reduction of scanning duration may be expected if true 3D k-space reordering is combined with 3D coronary MRA. Therefore a new Zonal Motion-Adapted Acquisition and Reordering Technique (ZMART) is proposed together with a 3D reordered k-space acquisition scheme for a 3D navigator gaited and corrected segmented k-space gradient echo technique. The method was combined with a prospective adaptive real-time flip angle weighting scheme.

Methods: k-Space Reordering: For conventional motion adapted reordering techniques, a prospective adaptive reordering of the k-profiles as a function of the navigator displacement has been proposed. (1,2) For a 3D approach this reordering strategy needs to be extended for k_y and k_z profiles. Hereby a model priority function is used to describe the importance or weight of each (k_y, k_z)-profile in k-space. The concept of the proposed solution is based on the acquisition of high priority zones in k-space during a very small diaphragmatic displacement, while the less important profiles are subject to weaker displacement conditions. Therefore the gating window and k-space priority function is divided into the same number of sectors (Fig. 1). The navigator displacement value is used to make the prospective decision which profiles of k-space are acquired in the actual shot.

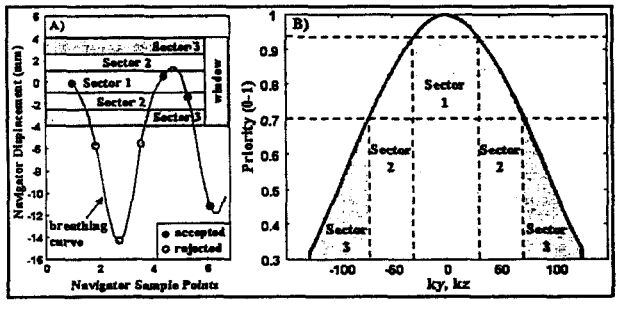

Figure 1. A) Partitioning of the gating window Navigator position dependent k-space filling scheme. B) Gaussian priority function describes importance of k-space into k_y-direction (analogous for k_z-direction.

Flip Angle Weighting: Acquired profiles in k-space are navigator displacement dependent and therefore may result in inhomogeneous distribution of signal intensity between adjacent (k_y, k_z)-profiles. These effects may be minimized using a prospective adaptive flip angle weighting. Based on a priori defined signal distribution in k-space the flip angle series for each shot is calculated prospectively in real-time based on the navigator displacement and a numerical simulation of the Bioch equation for a specific T1 value.

Phantom Study: ZMART was implemented on a commercial. 1.5-T Gyroscan ACS-NT (Philips Medical Systems. Best, NL) scanner with Power-Trak 6000 gradients (23 mT/M, 219μs rise time). A state of the art free-breathing navigator-gated 3D coronary scan (3D TFE with 8 excitations per shot. 260 mm FOV, 4 mm slice thickness, constant flip angle $\alpha = 25°$, TE 2.9ms, TR 10.3ms, 5mm gating window) was compared with the new 3D k-space reordered ZMART methodology using a Gaussian function for the signal weighting in k-space. A periodically moving phantom was used which was loaded with 4 small containers (diameter = 30mm) filled with gelatin and a tube (diameter = 3mm) filled with oil. Image quality was objectively compared (SNR, CNR and edge definition (3).

Results: Experiments with the motion phantom (Fig. 2) together with the values in Table 1 demonstrate the overall improved image quality using ZMART.

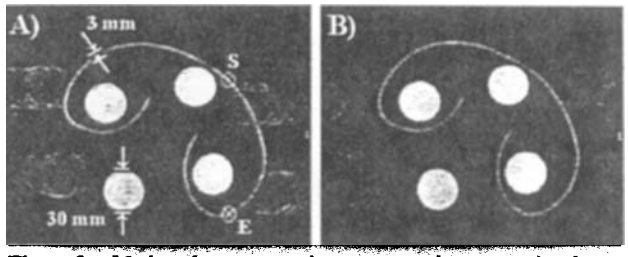

Figure 2. Motion phantom experiments comparing conventional gating (A) with ZMART (B) Vessel edge definition was compared objectively in the segment SE.

Image acquisitions with ZMART and Gaussian flip angle weighting resulted in improved SNR, CNR and values of vessel definition when compared with the conventional navigator gated and corrected 3D acquisition.

Table 1. Image Quality Parameters for Phantom Measurements

	Conventional Gating	ZMART
SNR	15.3	17.7
CNR	11.3	20.6
Sharpness (%)	81.3	82.6

Discussion: The present phantom experiments have shown that the proposed ZMART technique as a combination of 3D k-space reordering and flip angle weighting has the potential to improve image quality in 3D navigator gated and corrected MRI. By acquiring k-space profiles of high information content during small diaphragmatic displacements motion artifacts can be successfully minimized. Since the 3D fill order of k-space is no longer predefined but navigator displacement dependent, a runtime calculation of the applied RF excitation angles is required.

References
1. Weiger M et al. *Magn Reson Med* 1997; 38: 322–33.
2. Jhooti P et al. *Magn Reson Med* 1999; 41(3): 555–562.
3. Botnar RM et al. *Circulation* 1999; 99(24): 3139–3148.

Global and Regional Left Ventricular Dimensions Post Anterior Myocardial Infarction: The Effects of Medical Therapy on Left Ventricular Remodelling

D.J. Beacock,[1] J.P. Ridgway,[1] P.D. Batin,[2] J.I. Wison,[2] U.M. Sivananthan[1]. [1]*Cardiac Magnetic Resonance Unit, The General Infirmary at Leeds;* [2]*Pinderfields General Hospital, Wakefield, West Yorkshire, UK*

Introduction: Left ventricular remodelling describes the complex changes that occur to left ventricular structure and function following damage such as by myocardial infarction (MI). Many studies have demonstrated the prognostic benefits of thrombolysis, beta blockade and ACE inhibition. This study used cardiac MRI to evaluate changes in left ventricular dimensions in a group of patients post anterior myocardial infarction treated with such medical therapies.

Methods: 16 patients were recruited after sustaining an index anterior MI. All patients were cardiovascularly stable with no previous heart or valvular disease. MRI studies were performed at 10 days, 3 months and 6 months post infarction using a Philips ACS NT 1.5T system. Following the localising scans, breath-hold segmented k-space gradient echo imaging was used to obtain a contiguous series of short axis slices parallel to the mitral valve plane (TE 4.6ms, TR 10ms, FOV 340mm).

Slices of 6mm thickness were taken at 10mm gaps to encompass the entire left ventricle. Blood pressure and heart rate were recorded during the scan using a DYNAMAP vital signs monitor.

Images were analysed off line using an independent software analysis package (MASS, University of Leiden, Holland). The first phase after the R wave was taken as end diastole. Epicardial and endocardial contours were manually drawn to describe left ventricular end diastolic volume (LVEDV) and myocardial mass (LVEDM). The end systolic phase was taken as that with the smallest cavity volume. In addition myocardial wall thickness was measured at end diastole and end systole at the base, mid ventricle and apical levels. Measurements were compared to a group of 12 age matched volunteers with no history of cardiovascular disease. Man Whitney U tests were used in comparisons between the infarct and normal groups. Wilcoxon paired tests were used to test differences in the infarct group over time.

Results: At 10 days post infarct, end systolic volume was significantly greater in the infarct group compared to the volunteers (50.3 ± 16.6 vs. 26.4 ± 4.9 ml/m² $p < 0.05$). End diastolic volume and mass were not significantly different (90.3 ± 18.4 vs. 80.8 ± 11.1 ml/m², 63.3 ± 11.1 vs. 68.2 ± 17.5 g/m²). Within the infarct group, there was a trend for all global dimensions to reduce over the study period (LVEDVI 90.3 ± 18.4 vs. 79.8 ± 15.6 ml/m², LVESVI 50.3 ± 16.6 vs. 41.9 ± 16.3, EDLVMI 63.3 ± 11.1 vs. 58.6 ± 11.5 g/m², p = ns all cases). SVI remained stable (42.0 ± 8.7 vs. 41.8 ± 8.7 ml/m²) and EF increased slightly (46.1 ± 9.1 vs. 51.7 ± 8.9%, p = ns).

The figure below shows variations in diastolic and systolic regional wall thickness in the infarct patients during the study (□ 10 days, ▨ 3 months and ■ 6 months post MI). Diastolic wall thickness was reduced only in the anterior infarct regions. Significant increase in thickness was observed in the LV base over time (* denotes $p < 0.05$ compared with 10 day thickness). At 10 days post MI, systolic wall thickness was reduced in basal and apical regions remote to the infarct site. In non-infarct related regions, significant recovery of systolic wall thickness with time was observed at the base and mid ventricle but not at the apex (* $p < 0.05$, † $p < 0.005$ compared with 10 day thickness). No regions demonstrated a systolic thickness greater than in the normal volunteers (result not shown).

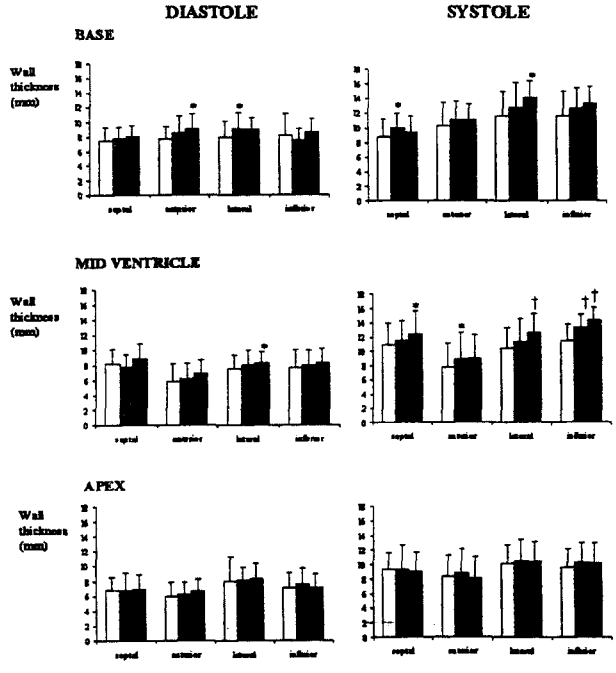

Conclusions: In a study population at high risk of adverse remodelling, the use of optimal medical therapy (thrombolysis, beta blockade and ACEI) was associated with little change in LVEDVI and LVEDMI. End diastolic wall thickness was reduced only at the infarct site. No progressive LV dilatation was observed. Regional end systolic wall thickness appears to be a more sensitive maker of functional recovery than end diastolic.

Left Ventricular Dimensions Measured by Magnetic Resonance Imaging: Reproducibility Between Two Centres

W.H.T. Smith,[1] D.J. Beacock,[1] A.R. Moody,[2] J.R. Hampton,[2] J.P. Ridgway,[1] U.M. Sivananthan[1]. [1]*The General Infirmary at Leeds, UK;* [2]*Queens Medical Centre, Nottingham, UK*

Introduction: Measurement of left ventricular mass and volumes provides fundamental data for the management of patients with hypertension, left ventricular failure and valvular heart disease. Abnormal dimensions can be identified and progress followed with sequential examinations. Magnetic Resonance Imaging (MRI) has been used to measure such variables (1,2) and good agreement between MRI and other techniques (3,4,5) has been described. MRI has been shown to give reproducible measurements (6) but these results are based on measurements from a single centre, using a single MRI system.

This study set out to assess the variation in these measurements made at two independent centres and to confirm the reproducibility of measurements of left ventricular dimensions made by MRI within a single centre. Normal subjects with and those with dilated, poorly functioning ventricles were studied.

Methods: Eleven normal volunteers and eleven patients with a history of controlled congestive heart failure (CHF) were scanned in two independent scanning centres, each using a different MRI system. The scans in Centre 1 were performed on a Philips ACS NT 1.5T system (Philips Medical Systems, Best, Netherlands). Those in Centre 2 were performed on a Siemens Vision 1.5T system (Siemens Medical Systems, Erlangen, Germany). Scans for each subject were obtained within one month of each other. Both centres used the same protocol for image acquisition. Images were analysed by manually drawing contours around the left ventricular epicardial and endocardial borders. Left ventricular end diastolic volume (EDV), end systolic volume (ESV), ejection fraction (EF) and end diastolic mass (EDM), were measured for each study and indexed to body surface area. Each scan was measured twice to determine intra-observer variability (intra-obs.) and by two observers to determine inter-observer variability (inter-obs.). The normal volunteers had two scans in one centre to determine inter-study variability for that centre and all 21 subjects had scans in both centres to determine inter-centre reproducibility. Results are expressed as the coefficient of reproducibility as described by Bland and Altman (7).

Results: The coefficients of reproducibility and mean values for measurements of normal subjects are given in table 1.

Table 1.

		Coefficients of Reproducibility			
	Mean	Intra-obs.	Inter-obs.	Inter-study	Inter-centre
EDV (ml/m²)	81.1	5.3	8.2	10.8	10.1
ESV (ml/m²)	28.2	3.5	5.1	9.0	10.2
EF (%)	65.2	4.8	6.5	7.7	12.2
Mass (g/m²)	68.3	5.5	9.3	8.1	10.8

The coefficients of reproducibility and mean values for measurements of subjects with controlled heart failure are given in table 2.

Table 2.

		Coefficients of Reproducibility		
	Mean	Intra-obs.	Inter-obs.	Inter-centre
EDV (ml/m^2)	126.1	17.0	15.8	22.1
ESV (ml/m^2)	97.0	13.6	14.2	15.5
EF (%)	33.0	4.8	8.1	8.4
Mass (g/m^2)	88.5	9.6	12.4	16.3

Conclusion: This is the first study to assess the reproducibility of measurement of ventricular dimensions using different MRI systems at independent centres. The good reproducibility between studies performed at different centres opens up the prospect of conducting multicentre studies with measurements obtained on different systems being compared.

References

1. Sechtem U, Pfugfelder PW, Gould RG et al. *Radiology* 1987; 163: 697–702.
2. Katz J. Milliken MC, Stray-Gundersen J et al. *Radiology* 1988; 169: 495–498.
3. Utz JA, Herfkens RJ, Heinsimer JA et al. *AJR* 1987; 148: 839–843.
4. Van Rossum AC, Visser FC, Sprenger M et al. *AM J Cardiol* 1988; 62: 628–633.
5. Gaudio C, Tanzilli G. Mazzarotto P et al. *Am J Cardiol* 1991; 67: 411–415.
6. Pattynama PMT, Lamb HJ, van der Velde EA et al. *Radiology* 1993; 187: 261–26.
7. Bland JM and Altman DG. *Lancet* 1986; 8: 307–310

Qualitative Myocardial Perfusion Magnetic Resonance Imaging (MRI): Detection of Angiographic Coronary Artery Disease.

G.R. Cherryman,[1] P.R. Sensky,[2] A. Jivan,[1] C. Reek,[1] N.J. Samanim.[1]
[1]*Glenfield General Hospital NHS Trust, Leicester;* [2]*Depts. of Radiology & Cardiology, University of Leicester, UK*

Background: The need for rapid reporting of cardiac MRI studies in the clinical environment is likely to lead to continued reliance on qualitative interpretation of myocardial perfusion images.

Aim: To establish the value of qualitative reporting of myocardial perfusion images in detecting significant coronary artery stenoses.

Methods: Thirty patients with known angiographically significant coronary artery disease (≥ 50% stenosis in one or more vessels) were imaged with a 1.5 Tesla MRI scanner (Siemens Vision™, Germany). A dynamic inversion recovery snapshot-FLASH sequence (TR = 4.5 ms, TI = 300 ms, TE = 2 ms, FOV 300 mm × 300 mm, slice thickness = 9 mm, 96 × 128 matrix, 25 measures) was used. Basal, midpapillary and apical short axis planes were acquired after a bolus of 0.025 mmol kg^{-1} Gadodiamide (Omniscan, Nycomed, UK) was injected at rest and during adenosine infusion (140 μg kg^{-1} min^{-1} for 6 minutes). A minimum of 15 minutes separated the 2 acquisitions.

An experienced radiologist blinded to clinical and angiographic data reviewed the images. The myocardium was divided into 8 radial regions of interest (ROIs). Images were reviewed for diagnostic acceptability. Stress and rest images were reported together to allow recognition of fixed (similar on rest and stress) and reversible (only apparent on stress) defects. Perfusion in each ROI was classed as being normal (normal enhancement) or abnormal (hypoenhancement). An experienced cardiologist, blinded to MRI perfusion data, analyzed the coronary angiograms. The coronary anatomy was annotated onto a standard Green Lane diagram (Brandt et al, 1977). Stenoses were measured using an automated edge detection system (Quantcor™, Siemens, Erlangen). The most severe stenosis in each vessel was assigned to 1 of 5 categories according to the reduction in cross-sectional area:1) 100%, 2) 90–99%, 3) 75–89%, 4) 50–74% and 5) <50%. Infarction-related coronary vessels were identified from the clinical history, ECG and angiographic findings. The MRI and angiographic data were then collated using the patient's individual coronary anatomy to assign myocardial ROIs to the supplying coronary arterial (CA) territory. For each CA territory perfusion was reported as abnormal if hypoenhancement was detected in one or more MRI ROIs on either the rest and/or the stress scans. Sensitivity, specificity, and posterior probabilities were calculated for the detection of stenoses ≥ 50%. Chi Square was used to calculate the relationship between the level of stenosis and the MRI findings.

Results: All patients completed the protocol. The image quality was sufficiently high to allow detailed qualitative reporting in all patients. In the few ROIs 15/720 (2%) unable to be evaluated this was because of local artefact or because the myocardium was too thin for assessment.

The overall sensitivity for MRI in detecting an angiographically significant stenosis (≥ 50%) was 93% with a specificity of 60%. Following examination a prior probability of 83% was increased to 92% if MRI was positive and reduced to 36% if MRI was negative.

The false positive results on MRI perfusion imaging were considered to be because of incorrect anatomical ROI assignment in 4/6 CA territories. In 3 of these territories hypoenhancement in the septal region extended deeper into the septum than predicted on the angiogram. In the fourth patient with an occluded left anterior descending artery, the anterior area of hypoenhancement extended to involve the apex and apical inferior wall. In the other 2 false positive readings a finding of reversible sub-endocardial hypoenhancement might have been due to occult arterial (micro-vascular) disease. There were 5 CA territories reported as normal on MRI although vessels with significant angiographic stenoses supplied the territory. In 2/5 extensive collateral vessels were seen on the angiogram. In the remaining 3 territories the patients all had extensive triple vessel disease, which may have lead to a reporting error in that mild hypoenhancement appeared normal in comparison to the severe hypoenhancement seen in adjacent ROIs.

Clinical evidence of previous infarction was found in 21/90 (23%) territories. Hypoperfusion was seen in 20/21 (95%) of infarct-related territories. In territories not affected by previous infarction there was a clear relationship between the degree of arterial stenosis and the number of abnormal ROIs (X^2 (4df) = 46.92, $p < 0.001$). In infarct-related territories no relationship between the number of abnormal ROIs and the residual level of occlusion or stenosis could be demonstrated.

Discussion: Qualitative assessment of first pass myocardial perfusion images has a high sensitivity and moderate specificity for the detection of significant angiographic stenoses. The number of abnormal ROIs detected appears to reflect stenosis severity. The difficulties in the interpretation of myocardial perfusion studies in patients with microvascular disease, triple vessel disease and those with well-developed collateral circulation are recognised. The clinical application of qualitative MRI perfusion reporting needs to be evaluated further in prospective diagnostic studies.

Reference

1. Brandt PWT, Partridge JB, Wattie WJ. *Clin Radiol* 1977; 28: 361–365.

Dobutamine/Adenosine Double Stress (DADS) MRI in Patients with Coronary Artery Disease: A One-Stop Assessment of Myocardial Perfusion, Hibernation and Left Ventricular (LV) Function

P.R. Sensky,[1] A. Jivan,[2] N. Hudson,[2] R. Keal,[2] N.J. Samani,[1] G.R. Cherryman.[2] [1]*Departments of Cardiology and Radiology, University of Leicester;* [2]*Glenfield General Hospital NHS Trust, Leicester, UK*

Background: Patients with impaired LV function undergoing surgical revascularization have a relatively high operative risk and require detailed assessment prior to the procedure. Ideally the operator requires an accurate ejection fraction, evidence of reversible perfusion deficits and an estimate of the extent of myocardial hibernation in dysfunctional regions.

Aims: To assess the feasibility of a novel DADS MRI protocol to provide a comprehensive assessment of regional myocardial perfusion, hibernation and function in patients with coronary artery disease (CAD) and LV dysfunction prior to coronary artery revascularization.

Methods: Ten patients, who were awaiting revascularization, were examined with DADS MRI protocol (Figure 1). All patients had angiographic CAD and low ejection fraction (EF). A 1.5 Tesla scanner (Siemens Vision™, Germany) was used for the study. Perfusion was imaged using a dynamic inversion recovery snapshot-FLASH sequence (TR = 4.5 ms, TI = 300 ms, TE = 2 ms, FOV 300 mm × 300 mm, slice thickness = 9 mm, 96 × 128 matrix, 25 measures). Basal, mid-papillary and apical short axis planes were acquired after a bolus of 0.025 mmol kg^{-1} Gadodiamide (Omniscan, Nycomed, UK) was injected at rest and during adenosine infusion (140 μg kg^{-1} min^{-1} for 6 minutes). Systolic function and contractile reserve (CR) were assessed using a breath-hold segmented cine gradient echo sequence (TR = 60 ms, TE = 4.8 ms, 3 SA slices as per perfusion) at rest and at each level of a two -step steady state low dose dobutamine infusion (5 and 10 μg/kg/min).

Each SA slice was divided radially into 8 regions of interest (ROIs). Perfusion images were additionally divided circumferentially into epicardial and subendocardial layers. Two independent observers reported all scans qualitatively. Patient safety, image quality and scanning times were assessed. The site, transmural extent and reversibility of perfusion abnormalities were noted. Global and regional systolic function was evaluated. ROIs with severe systolic dysfunction were examined for the presence of an inotrope-induced CR, indicative of myocardial hibernation.

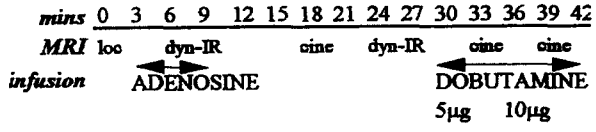

Figure 1. Temporal sequence of DADS MRI protocol. Loc = localiser; dyn-IR = first pass perfusion; cine = function imaging.

Results: All patients completed the protocol with no adverse events. Average scanning time was 38 ± 8 minutes. Rest and stress images were of sufficient quality for perfusion and function assessment in 98.5% and 100% ROIs, respectively. EF ranged from 15–39%. Reversible perfusion defects, mostly limited to the subendocardium, were seen in 26.6% ROIs. Severe systolic dysfunction was observed in 30.4% ROIs. A CR was identified in 32.8% of these ROIs.

Discussion: DADS MRI protocol is feasible, well tolerated and safe, requiring no ionising radiation. The use of two short acting stress agents optimises vasodilatation for perfusion imaging (adenosine) and inotropic stimulus for identification of contractile reserve (dobutamine). Currently the range of information provided by DADS can only be obtained using several different investigative modalities, not all of them easily accessible e.g. positron emission tomography. We have shown that DADS protocol can provide high quality information on the functional significance of CAD, operative risk and likely left ventricular functional recovery following revascularization at a single patient visit. This "one-stop" evaluation of myocardial function and perfusion can be performed on a standard clinical scanner.

Dobutamine Stress MR Imaging of Heart Function Using Real-Time Respiratory Navigator Gating Without Breath-Holding

H.J. Lamb, P. Salverda, H.P. Beyerbacht, P. Kunz, J. Doornbos, A. de Roos. *Leiden University Medical Center & Philips Medical Systems, The Netherlands*

Introduction: Cardiac MRI during dobutamine stress provides an excellent tool for evaluation of myocardial function and viability. Until now, most of these studies are performed with breath-hold (BH) techniques, which are hard to perform for some patients. Recently, real-time respiratory navigator (NAV) gating has shown to be an attractive alternative to BH approaches. NAVs are single-line images, planned perpendicular to the right hemidiaphragm, to measure the diaphragm position in real-time to gate image data acquisition during expiration.

The purpose of the present study was twofold. First, to develop and compare two different strategies for NAV- based respiratory motion correction without BH to image the heart in short-axis view. Second, to apply the most optimal NAV technique to image the human heart during severe pharmacological stress testing and compare the results to a BH approach.

Methods: Eight healthy volunteers were subjected to a series of acquisitions to compare image quality of two different NAV acquisitions. NAVs were acquired preceding (leading, L-NAVs) or preceding and following (L+trailing, LT-NAVs) image data acquisition in each RR interval. NAV results were compared to free breathing (FB) and BH acquisitions. To determine image quality, blinded review was performed by two radiologists and two MR-physicists familiar with cardiac MRI. The score for image quality ranged from 10 (excellent) to 1 (poor), which was based on the conspicuity of endo-and epicardial left ventricular (LV) borders. Ten other healthy volunteers were subjected to a dobutamine stress test as described before (1). Short-axis MR images acquired at rest and during stress were obtained as BH and LT-NAV acquisitions (see Results section). End systolic wall thickening was determined using the MASS software package.

In all subjects, single-slice multi-phase echo-planar MR imaging was performed with a Philips Gyroscan ACS-NT15 at the papillary muscle level of the LV with a 20-cm-diameter circular surface coil. After each α-pulse, seven lines in k-space were acquired, no fat suppression and no signal averaging were applied.

Results: The average score of image quality was 8.5 for the BH acquisition, 6.5 for LT-NAVs, 5.2 for L-NAVs, and 1.2 for the FB acquisition. The difference between BH and LT-NAVs was statistically significant (P = 0.01), as was the difference between LT-NAVs and L-NAVs (P = 0.01).

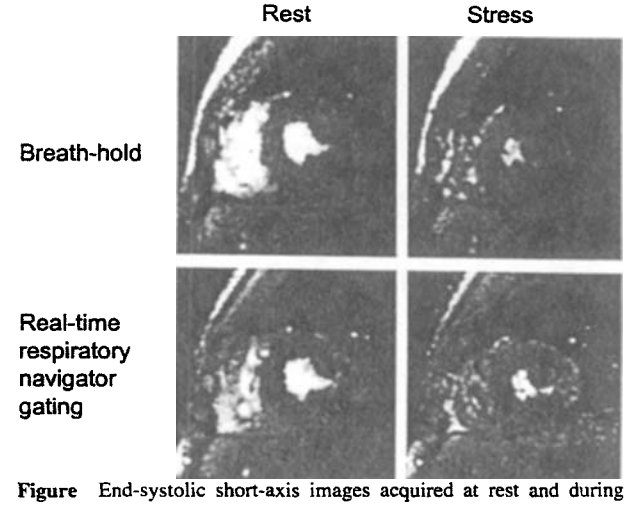

Figure End-systolic short-axis images acquired at rest and during doubtamine stress using multi-shot echo-planar MR imaging and breath-holding or real-time respiratory navigator gating.

Due to stress testing, heart rate increased from 74 ± 11 bpm at rest to 115 ± 17 bpm during dobutamine stress (P < 0.001). An example of BH and NAV acquisitions at rest and during dobutamine stress is given in the Figure. Wall thickening between end diastole and end sys-

tole determined with BH at rest (96 ± 10%) and during stress (149 ± 23%) was similar to values obtained with LT-NAVs at rest (95 ± 8%) and during stress (150 ± 24%). The difference between rest and stress acquisitions was statistically significant for both BH and LT-NAVs ($P < 0.001$).

Conclusions: Real-time respiratory navigator gating can be applied to obtain good quality images of the human heart at rest and during dobutamine stress. Accurate analysis of wall thickening can be performed based on navigator gated MR images. This technique can also be applied as a multi-slice sequence covering the entire LV to study regional wall thickening abnormalities in patients with ischemic heart disease during dobuamine stress testing.

Reference

1. Lamb HJ, Beyerbacht HP, Ouwerkerk R, et al., *Circulation*. 1997; 96: 2969–2977.

Functional and Metabolic Consequences of Aortic Valve Replacement Assessed with MR Imaging and ^{31}P-MR Spectroscopy

H.J. Lamb, H.P. Beyerbacht, A. van der Laarse, J. Doornbos, A. de Roos, E.E. van der Wall. *Leiden University Medical Center, The Netherlands*

Introduction: Patients with aortic valve stenosis (AVS) are subject to an increased pressure load, leading to left ventricular hypertrophy (LVH). LVH is a recognized risk factor for cardiac morbidity and mortality, and is associated with systolic and/or diastolic dysfunction. Previous studies have shown that LVH can also be accompanied by altered myocardial high-energy phosphate (HEP) metabolism (1). It is not known whether these metabolic changes are reversible following AV replacement and if they are related to the functional abnormalities.

Therefore, the purpose of the present study was to determine both LV function and myocardial HEP metabolism and their interrelation, before and after AV replacement.

Methods: Eighteen male patients (average age 62 ± 10 years) with predominant AVS and without significant coronary artery disease at cardiac catheterization were studied with MR imaging and ^{31}P-MR spectroscopy. A subgroup of nine patients was restudied 40 ± 12 weeks after AV replacement. All patients had severe AV disease, the AV pressure gradient was 74 ± 13 mmHg. A group of ten healthy age- matched males (average age 60 ± 4 years) served as controls.

A Philips 1.5-T ACS-NT15 MR system and breath-hold multi-shot echo-planar MR imaging were used to acquire a stack of short-axis slices covering the entire LV. In addition, velocity encoded MR imaging was performed to measure bloodflow across the mitral valve. Technical details concerning image acquisition and analysis were similar as reported previously (2,3).

A Philips 1.5-T Gyroscan S15 MR system and a 10-cm diameter surface coil were used to acquire ^{31}P-MR spectra of the anterior wall of the LV. Volumes were selected using 2d-ISIS + 1D-SI. Acquisition time for a single spectrum was 30 min. Spectra were quantified in the time domain and were corrected for blood contamination and partial saturation. All other technical details were equal as reported previously (4,5,6).

Results: The mean LV mass index decreased from 140 ± 33 g/m^2 to 107 ± 31 g/m^2 ($P < 0.01$) following AV replacement, which was still higher than in controls (69 ± 8 g/m^2, $P < 0.01$). Systolic function was not impaired in patients as compared to controls (data not shown). Diastolic function was impaired in patients as reflected by a decreased Early acceleration peak value indexed to cardiac output (CO) before (0.043 ± 0.008 $s^{-1} \times 10^{-3}$) and after (0.055 ± 0.006 $s^{-1} \times 10^{-3}$, $P < 0.05$) AV replacement, as compared to control values (0.081 ± 0.033 $s^{-1} \times 10^{-3}$, $P < 0.05$).

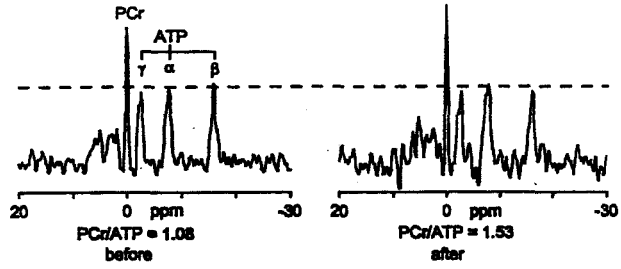

Figure ^{31}P-MR spectra acquired from the LV anterior wall of a patient with severe aortic valve stenosis, obtained before and after aortic valve replacement. Note the increase in myocardial PCr/ATP following valve replacement.

Before AV replacement the myocardial PCr/ATP ratio was 1.24 ± 0.17 in the 18 patients compared to 1.43 ± 0.14 in the controls ($P < 0.01$). Following AV replacement, PCr/ATP normalized from 1.28 ± 0.17 to 1.47 ± 0.14 ($P < 0.05$) in the subgroup of 9 patients. An example of ^{31}P-MR spectra before and after AV replacement is given in the Figure. Before AV replacement a loose but statistically significant correlation was found between myocardial PCr/ATP and the Early deceleration peak/CO ($r = -0.39$, $P < 0.05$). Myocardial PCr/ATP was not correlated to LV mass index.

Conclusions: Severe AVS leads to a decrease in myocardial PCr/ATP which normalizes completely following AV replacement. Before AV replacement, the PCr/ATP ratio is correlated to LV diastolic function. After AV replacement, diastolic function shows a trend towards normalization.

References

1. Neubauer S, Horn M, Pabst T, et al., *J Investig Med* 1997; 45: 453–462.
2. Lamb HJ, Doornbos J, van der Velde EA, et al., *JCAT*. 1996; 20: 942–949.
3. Pluim BM, Lamb HJ, Kayser HWM, et al., *Circulation*. 1998; 97: 666–672.
4. Lamb HJ, Doornbos J, den Hollander JA, et al., *NMR Biomed* 1996; 9: 217–227.
5. Lamb HJ, Beyerbacht HP, Ouwerkerk R, et al., *Circulation*. 1997; 96: 2969–2977.
6. Lamb HJ, Beyerbacht HP, van der Laarse A. et al., *Circulation*. 1999; 99: 2261–2267.

Resection of Left Ventricular Aneurysm: MRI Evaluation of a Forgotten Technique

H.J. Lamb, M.I.M. Versteegh, A. de Roos. *Leiden University Medical Center, The Netherlands*

Introduction: A left ventricular (LV) aneurysm is a late complication of a large myocardial infarction, that is often treated. The main indications for surgery are dyspnea and/or angina pectoris, as well as hardly treatable ventricular arrhythmias. The commonly known techniques are the linear closure and the circular closure. However, hardly known is the 'anatomical repair' (AR)-method as described by Stoney (*1*). This forgotten technique is especially suitable for large anteroseptal aneurysms. We slightly modified this technique; the 'Leiden-AR-method' is further explained in the Figure.

The study of Stoney et al. showed clinical improvement in most patients, but it is not known whether resection of an LV aneurysm leads to improved global LV function. Magnetic resonance imaging (MRI) is a sensitive tool to detect changes in LV function (2,3).

Therefore, the purpose of the present study was to monitor changes in global LV function following LV aneurysm resection with use of MRI.

Methods: Twelve patients (11 male, 1 female, mean age 65 ± 10 years of age) with a large anteroseptal aneurysm were included in the

present study. Cardiac MRI was performed 5 ± 4 days before surgery and 89 ± 13 days after resection of the aneurysm. Most patients also underwent coronary revascularisation.

MRI studies were performed using a standard Philips 1.5T ACS/NT15 MR system. The heart was imaged from apex to base with ten imaging levels in the short-axis orientation, with use of multishot echo-planar gradient-echo MR imaging as described before (2,3).

Epicardial and endocardial borders were outlined manually with a trackball cursor. End-diastolic volume (EDV), end-systolic volume (ESV), stroke volume (SV), and ejection fraction (EF) were calculated. Paired two-tailed t-tests were applied when appropriate. A probability value of $P < 0.05$ was considered statistically significant.

Table 1. Left Ventricular Global Heart Function

Parameter	Pre-surgery	Post-surgery
EDV (ml)	238 ± 63	198 ± 51*
ESV (ml)	156 ± 62	111 ± 43**
SV (ml)	82 ± 14	87 ± 17
EF (%)	37 ± 11	45 ± 10**

EDV indicates end-diastolic volume; ESV, end-systolic volume; SV, stroke volume; EF, ejection fraction. * $P < 0.05$, ** $P < 0.01$ paired t-test with pre-surgery.

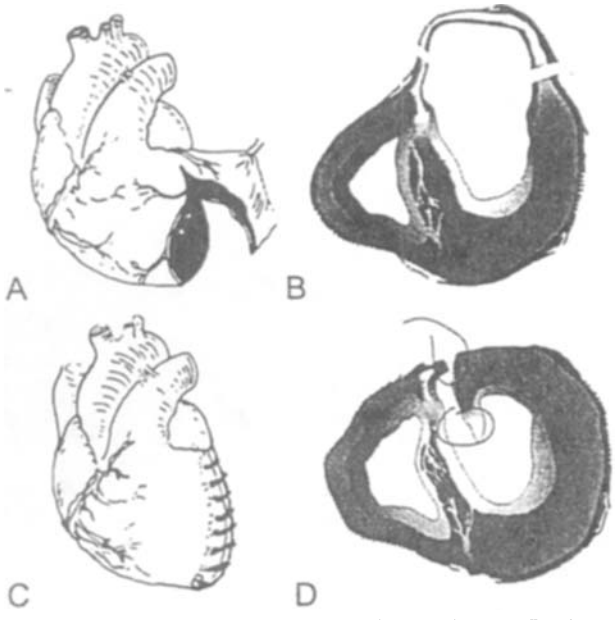

Figure After resection of almost the entire scar tissue (A,B), the lateral edge is sutured at the junction of scar and viable myocardium in the septum with use of a continuous suture (C). A second suture-line is used to bring the free edge of the septal side of the scar to the lateral wall of the LV (C,D). The procedure can easily be combined with a CABG and/or valve surgery.

Results: Table 1 shows global LV function parameters of the patients before and after LV aneurysm resection. Following resection of the LV aneurysm, a decrease was found in EDV from 238 ± 63 ml to 198 ± 51 ml ($P < 0.05$), in ESV from 156 ± 62 ml to 111 ± 43 ml ($P < 0.01$), whereas EF increased from 37 ± 11% to 45 ± 10% ($P < 0.01$). SV remained unchanged compared to values obtained before surgery.

Conclusions: Resection of an LV aneurysm and anatomical remodeling of the LV according to the Leiden-AR-method, leads to a significant improvement in LV function. In addition, it was shown that cardiac MRI is a sensitive tool to study subtle changes in cardiac function.

References

1. Stoney WS, Alford WC Jr, Burrus GR, et al., *Ann Thorac Surg* 1973; 15: 394–404.
2. Lamb HJ, Doornbos J, van der Velde EA, et al., *J Comput Assist Tomogr* 1996; 20:942–949.
3. Lamb HJ, Beyerbacht HP, van der Laarse A. et al., *Circulation*. 1999; 99: 2261–2267.

Blood-Oxygen-Level-Dependend (BOLD) MRI in Healthy Volunteers and Patients with Peripheral Occlusive Arterial Disease (PAOD)

T. Poetsch,[1] T. Niendorf,[2] R. Dietz,[1] M.G. Friedrich.[1] [1]*Franz-Volhard-Klinik, University of Berlin, Germany;* [2]*GE Medical Systems, Leipzig, Germany*

Background: The BOLD effect on the T_2* relaxation of MRI signals has been extensively studied, most of the published data focus on the BOLD effect in the brain (1).

In a recent report LEBON et al. (2) observed the temporal relationship between intensity changes in MRI images and tissue oxygen content, measured by myoglobin proton NMR spectroscopy in the sceletal muscle.

The purpose of this work is to demonstrate the impact of improved perfusion on the oxygenation as visualized by signal intensity changes in T_2* weighted images of skeletal muscle during ischemic stress test imposed on healthy volunteers and PAOD Patients.

Methods: MRI was carried out on an whole body 55 cm free bore 1,5 Tesla MR scanner system (CV/i, GE Medical System, Milwaukee, Wisconsin, USA). T2*-sensitized gradient echo EPI (TE < 50 ms) has been applied in 5 healthy volunteers and 11 Patients with PAOD Fontaine Stage IIb (8 Pat.), III and IV (4 Pat.). The subjects were placed in a supine position with extended legs and a large cuff placed above the knee. The birdcage coil was centered on the largest section of the calf under investigation.

For each Patient 250 images were obtained with a temporal solution of 1,7 s during a protocol consisting of three sections: 60 s resting condition, 240 s leg ischemia (cuff pressure 30–50 mmHg above systemic blood pressure), 120 s postischemic recovery. Offline evaluation included a computer-based calculation of time-signal-intensity curves with resulting parametric images (negative and positive enhancement images).

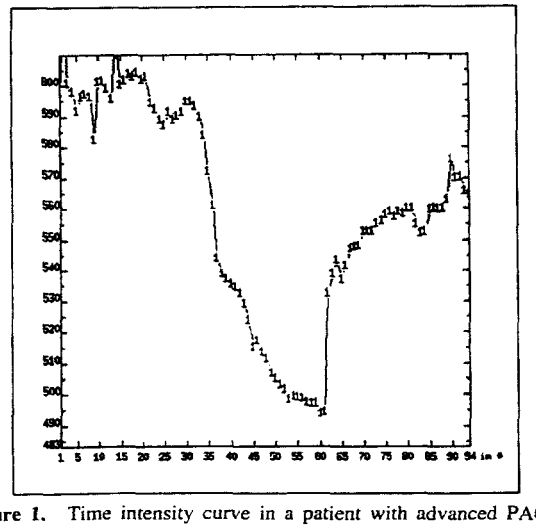

Figure 1. Time intensity curve in a patient with advanced PAOD. There is a delayed recovery of the signal intensity and a lack of overshoot after intermittent ischemia as induced by cuff inflation.

Results: In all cases the image quality was sufficient for analysis.

In all subjects signal intensity decreased immediately after cuff inflation. Upon reperfusion, signal intensity revealed an overshoot in all healthy volunteers but not in Patients with PAOD. In patients with advanced disease, the time of signal recovery to baseline values was significantly longer.

Conclusion: BOLD-MRI using gradient echo EPI detects changes in the skeletal muscle during ischemia. Patients with advanced PAOD may reveal specific patterns of signal intensity curves. Further studies need to address sensitivity and specificity.

References:
1. Haacke EM, Lai S. et al., *Human Brain Mapping* 1997; 5: 341–346
2. Lebon V, Brillault-Salvat, C. et al. *MRM* 40: 551–558

Longterm MRI Follow-up of Patients with Acute Myocarditis

A. Wagner, J. Schulz-Menger, O. Strohm, R. Dietz, and M.G. Friedrich. *Franz-Volhard-Klinik, University of Berlin, Germany*

Background: The longterm course of acute myocarditis is not well understood. Whereas in many (if not most of the) cases it may not even really be noticed by the patient, the disease may be fatal for others.

Methods: We observed the clinical status and the MRI findings from 19 patients during 36 months after acute viral myocarditis. MRI studies were performed on a standard clinical system (Siemens Impact 1.0 T, Siemens AG, Erlangen, Germany). Contrast-enhanced, T1 weighted fast spin echo images were obtained to characterize myocardial tissue enhancement. The myocardial signal increase after Gd-DTPA administration was compared to that of the skeletal muscle (relative enhancement, RE). Left ventricular ejection fraction was measured with breathhold gradient echo cine sequences in contiguous short axis planes (TE 6.1 ms, TR 90 ms, slice thickness 10 mm). The 3 months' data have already been published (1).

Results: From the 19 patients, nobody was lost to follow-up. 1 patient commited suicide due to ther reasons than health.

Of the remaining 18 patients 11 (61%) recovered uneventfully. 2 patients (10.5%) died due to congestive heart failure. Of the remaining 16 patients, 5 patients (31%) were still symptomatic, 3 of them reported a significant impairment of their quality of life. The RE correlated very well with the symptoms as defined by a symptom score.

The RE on day 2 showed a predictive trend for the loss of ejection fraction during 36 months ($p = 0{,}052$).

During month 3 and month 6 there was a relapse of the disease in 3 of the patients in terms of clinical worsening as well as increased RE.

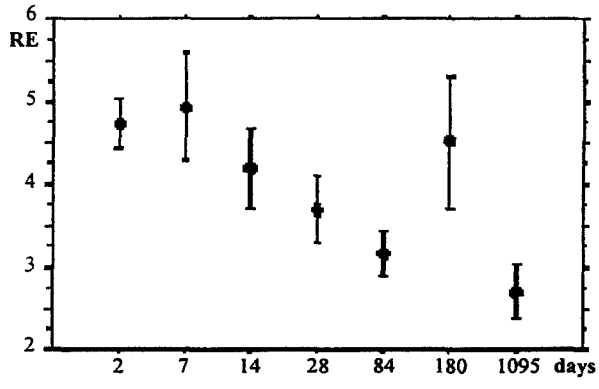

Figure 1. Course of the relative myocardial contrast enhancement (RE) in the 16 surviving patients after acute viral myocarditis. The mean value in normal subjects is 2.5 ± 0.2d (1).

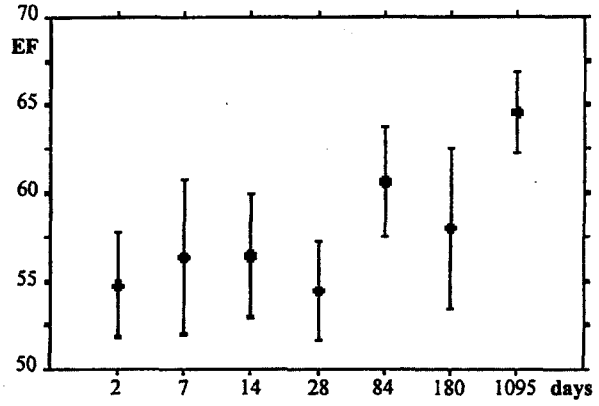

Figure 2. Course of the left ventricular ejection fraction (EF) in the 16 surviving patients after acute viral myocarditis. There is a delayed recovery of LV function correlating to the course of the contrast enhancement as shown in fig. 1.

Conclusion: The full recovery of acute myocaditis seems to last more than 6 months and less than 3 years. The findings in contrast-enhanced MRI correlate with the clinical activity of viral myocarditis and may therefore be suitable in the longterm follow-up of patients.

Reference
1. Friedrich MG, Strohm O, Schulz Menger J. et al. *Circulation* 1998; 97: 1802–9.

Creation of a Stereotactic Cardiac MR Imaging Atlas Template for Intersubject and Intermodality Registration Using Intensity-Based Image Registration

H.I. Litt, L. Axel, A. Blom. *University of Pennsylvania, Philadelphia, PA*

Intersubject and intermodality comparison of imaging studies can be aided by transformation of data into a standard space, i.e., resizing and registering images so that the structures being analyzed have similar size and orientation. This process, called spatial normalization, also allows imaging data from many subjects to be averaged to provide increased statistical power for analysis of anatomic and functional differences in normal and pathologic states.

In neuroimaging, the Talairach atlas (1) provides a standard brain for intersubject comparisons and spatial normalization. An intensity-based algorithm is used to register studies to a modality specific imaging template of the Talairach brain created from averaged datasets of normal subjects (2,3). Intensity-based registration is an automated process that operates directly on pixel intensities; one dataset is transformed into another according to a predefined mathematical model until a cost function based on differences in pixel intensities between the two is minimized. This process allows direct quantitative comparison of anatomic and functional imaging data from different subjects. In contrast, intersubject and cross-modality registration in cardiac magnetic resonance (MR) imaging is often performed by manual or semi-automated methods such as contour tracing, followed by registration of the contours (4,5).

We have applied intensity-based registration to create a cardiac MR atlas template. The atlas is based on data from 21 normal volunteers with no history of cardiac disease (mean age 39 years, range 21 to 79 years, 11 females and 10 males). Short axis cine fast spoiled gradient recalled acquisition in the steady state (GRASS) images were obtained at end-systole and end-diastole (imaging parameters: 1.5 Tesla magnet-

GE Signa, Milwaukee, Wisconsin, 256 * 256 matrix, voxel size 1.0 * 1.0 * 8.0 mm³). Between 9 and 14 images through the heart for each patient were cropped to 128 * 128 pixels and edited to remove all extracardiac structures. The resulting images were initially registered to a single, randomly chosen heart using the *Automated Image Registration* software package (2,6). A twelve parameter affine transformation model (three for each axis and three rotational parameters) was used to register the three dimensional image datasets and the minimized cost function was the standard deviation of the difference image between the transformed input and output. The registered hearts were averaged to produce a preliminary atlas template. The individual studies were then registered to the preliminary template and the re-registered data were averaged to produce the final atlas template.

We will continue to add normal subjects to the atlas, and we intend to create templates for other points in the cardiac cycle and for long-axis or other orientations, which may be useful for other imaging modalities such as echocardiography. The atlas template datasets will be made generally available for other investigators to use and build upon.

The atlas template can be used to normalize subjects in cardiac imaging studies of both normal and pathologic. Spatially normalized data from different subjects can be directly compared to analyze quantitative changes in morphology and function such as age-related or ischemic alterations in chamber volumes or perfusion. In addition, given the anatomic detail of MR imaging, the template can be used for registration and normalization of other imaging modalities, in studies involving one or many modalities (7).

References:

1. Talairach J and Tournoux P. Co-Planar Sterotactic Atlas of the Human Brain. *1998*; Thieme, Stuttgart.
2. Woods RP, Grafton ST, Holmes CJ, Cherry SR, Mazziotta JC. *JCAT* 1998; 22: 141–154.
3. Friston KJ, Ashburner J, Frith CD, et. al. *Hum Brain Map*; 2: 165–189.
4. van der Geest RJ, Buller VG, Jansen E, et. al. *JCAT* 1997; 21(5): 756–65.
5. Gilardi MC, Rizzo G, Savi A, Fazio F. *Quat J Nuc Med* 1996; 40(1): 142–150.
6. Woods RP, Grafton ST, Watson JDG, Sicotte NL, Mazziotta JC. *JCAT* 1998; 22: 155–165.
7. Black KJ, Videen TO, Perlmutter JS. *JCAT* 1996; 20: 855–861.

Left Ventricular Mass Measured by MRI: Effect of Endocardial Trabeculae on the Observed Wall Thickness

J.T. Marcus,[1] J.P.A. Kuijer,[1] M.J.W. Götte,[2] R.M. Heethaar,[1] A.C. Van Rossum.[2] [1]*Dept of Clinical Physics & Informatics,* [2]*Dept of Cardiology, ICaR-VU, Vrije Universiteit, Amsterdam, The Netherlands*

Introduction: An accurate measure of left ventricular (LV) mass is a prerequisite for the assessment of LV hypertrophy due to pressure overload or myocardial diseases. The usual way to quantify the LV mass is by acquiring a stack of parallel short-axis images in cine-mode. These images are used to assess the LV regional and global function as well. In this study we address two effects of LV motion which may have a potentially large influence on the measured LV mass. Due to LV long-axis shortening, there is at least one short-axis slice (the most basal) which shows the LV wall in end-diastole, but not in end-systole (1). Due to LV circumferential shortening, the endocardial trabeculae which are difficult to delineate at end-diastole, appear to join with the solid LV wall during systole. The aim of this study is to quantify the mass contributions provided by the most basal slice, and by the endocardial trabeculae.

Methods Healthy: subjects (n = 24, 11 female), aged 19–30 years, were imaged on a Siemens whole body system at 1.5 T (n = 16), or 1 T (n = 8). Imaging was in breathhold, prospectively ECG triggered, and using segmented k-space (7k, lines per beat) cine imaging. A stack of short-axis image slices was acquired, fully covering the LV (planned at end-diastole) from the very base till the apical point. LV mass was calculated by slice summation using the MASS software package (Leiden University Medical Center, The Netherlands), taking a specific gravity of 1.04 g/cm³. End-diastolic mass, denoted as EDM, was measured without the most basal image slice and papillary muscles (PM). EDM+base is the EDM with most basal slice included. EDM+base+pm includes the PM in addition (2). ESM is the end-systolic mass, always including the PM. ESM was tested vs. EDM+base+pm by paired-samples t-testing.

Results: are resumed in the table below (mean ± std.dev.):

EDM	= 126 ± 28 g
EDM + base	= 143 ± 31 g
EDM + base + pm	= 148 ± 31 g
ESM	= 155 ± 33 g

The contribution of the basal slice to LV mass is 17 ± 4 g (13.5 ± 3%); the PM contribute 5 ± 2 g (3.5 ± 1%). Most striking is the value of ESM, which is larger than the EDM+base+pm ($p = 0.002$), by the amount of 7.5 ± 11 g (5.1 ± 7%).

Discussion: We hypothesize that the endocardial trabeculae are responsible for this 'increased mass'. At *end-diastole* many individual trabeculae are difficult to trace due to their small size, and the trabecular zone is thus largely *excluded* by an observer who traces the endocardial border. Also automated routines often tend to ignore the trabecles due to the poor contrast between trabecular zone and blood pool. The cartoon below, left panel, shows the observed endocardial contour (dashed line) at end-diastole. During *systole* however, the individual trabeculae will join to form a more compact compartment, clearly different from the blood pool. Thus at end-systole (right panel), the observed contour will now *include* the trabeculae, and the apparent 'thickness' is enlarged in part by these joined trabeculae. These included trabeculae probably explain the increased mass at end-systole.

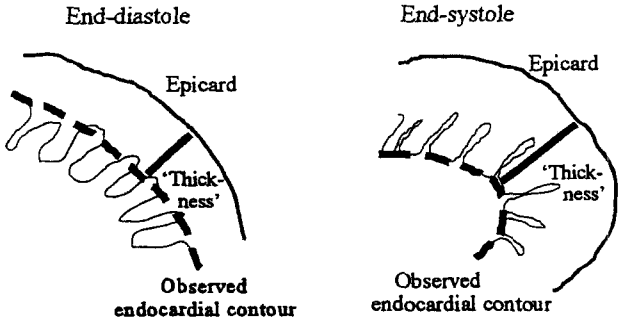

Systolic wall thickening should be re-interpreted in regions with endocardial trabeculae: the observed thickening is partly due to the confluence of endocardial trabeculae during systole.

Conclusion: For a proper comparison of LV mass measures between different MRI sites, it is required that conventions are followed on including the most basal LV slice and the PM to the total LV mass. Also, the consistent difference between the observed end-diastolic and end-systolic mass implies that the cardiac phase of LV mass measurement should be specified.

References:

1. Marcus JT, Götte MJW, DeWaal LK. et al., *JCMR* 1999; 1: 1–6.
2. Lorenz CH, Walker ES, Morgan VL. et al., *JCMR* 1999; 1: 7–21.

Correlation of 3D MR Coronary Angiography with Selective Coronary Angiography: Impact of the Novel Motion Gating Technique

T. Dill, C. Weber, R. Sinkus, P. Steiner, P. Börnert, T. Meinertz, C.W. Hamm. *University Hospital Hamburg and Kerckhoff-Klinik, Bad Nauheim, Phillips Research Laboratories, Division Technical Systems, Hamburg, Germany*

Introduction: Reliable noninvasive assessment of coronary artery stenoses and occlusions with MRI in patients with known or suspected coronary artery disease would be an advantage compared to invasive techniques. So far, inconsistent breathholding is one reason for impaired image quality. The impact of the novel respiratory motion compensation (Motion Adapted Gating, MAG) for visualization of coronary arteries was verified in this study by correlation with selective coronary angiography findings.

Methods: 20 subjects (10 patients/10 healthy volunteers), age 52 +− 20 yrs were investigated. All patients had MRI and selective coronary angiography (SCA) within 2 weeks.

A Phillips Gyroscan ACS-NT (Phillips Medical Systems, Best, Netherlands) operating at 1.5 T, equipped with the PowerTrak 6000 gradient system providing 23 mT/m within 0.2 ms, was used. A newly developed MRI protocol consists of a fat suppressed 3 D TFE (TE/TR: 4 ms/8 ms), ECG-triggered (12 echoes per RR-interval) and respiratory gated T2-sequence.

Respiratory motion was obtained from 3 pencil navigator beams interleaved with one R-R interval. The real time gating algorithm utilizes the concept of k-space weighting in combination with an automatic analysis of the respiratory motion.

The three main coronary arteries (CA) and left main (LM) were evaluated. The results of the patient group were compared to SCA. Qualitative analysis of the images was performed by two blinded investigators.

Results: All 80 CA were adequately visualized in the proximal and middle parts of the vessel. Visibility was graded in four categories: 1 = insufficient, 2 = sufficient, 3 = good, 4 = excellent (see figure).

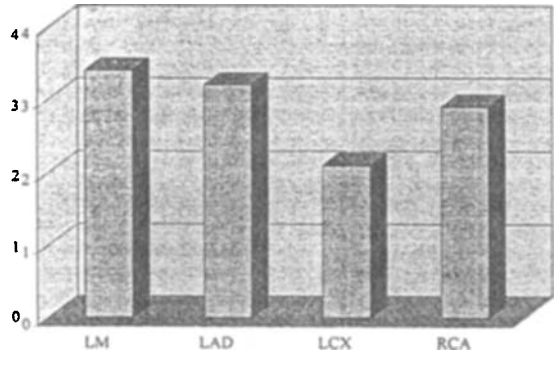

Evaluation of CA stenoses (luminal narrowing > 50%) was best in the LM and in the proximal part of LAD, RCA and Cfx (5/5 stenoses correctly detected) and still of good quality in the middle part (4/5 stenoses correct).

Conclusion: MRI with MAG demonstrates to be a promising new technique for noninvasive imaging of CA due to its ability to compensate changes of the respiratory pattern among free breathing patients.

Good correlation with x-ray angiography findings for the proximal and middle segments of the main CA.

Myocardial Viability Assessment Using Simultaneous T1–T2* Signal Intensity Measurements Can Help Identify Regions of Damage

John Mark,[1] Guangping Dai,[1] Bo Xiang,[1] Jiankang Sun,[1] Jie Shen,[1] William G. Lindsay,[2] Roxanne Deslauriers,[1] Ganghong Tian.[1]
[1]*Institute for Biodiagnostics, National Research Council, Canada;*
[2]*University of Manitoba, Winnipeg, Manitoba, Canada*

Introduction: Recanalization intervention (i.e. angioplasty, bypass graft) is performed on the assumption that viable myocardial cells remain in the region of damage following myocardial infarction. Therefore identification of viability can have significant impact on the prognosis and clinical management of a patient. We attempt to improve the accuracy of myocardial viability assessment by using an interleaved T1 and T2*-weighted pulse sequence and simultaneous measurement of T1 and T2* signal intensity (SI) on the first-pass of bolus injected contrast agent.

Theory: Single measures of T1 or T2* relaxation time or signal intensity may be flawed as indicators of myocardial injury. T1-weighted imaging techniques depend on accumulation of contrast agent in nonviable regions. However, microvascular obstruction may lead to hypoenhanced areas in the infarct zone as a result of reduced blood flow. T2*-weighted images are dependent on contrast distribution. Regional heterogeneity of agent leads to minute magnetic gradients which shorten T2* or decrease signal intensity. In tissue that has lost cell membrane integrity, there will be a rapid redistribution of contrast to the intracellular space, leading to more homogeneity. This may decrease the T2* effect and there may be less T2* shortening in irreversibly damaged areas. However, T2* can also be affected by the concentration of contrast. Regions of reperfused infarct, which accumulate contrast agent, may display a decreased T2* SI. Therefore, T2* SI may only predict membrane damage once effects of contrast agent concentration have been removed. Because T1-weighted images can indirectly assess concentration, a combined T1–T2* measurement may enhance the reliability of contrast-enhanced MRI assessments.

Methods: We simulated myocardial infarction by occlusion of the left anterior descending coronary artery in pigs (n = 8) for 2 h with 1 h reperfusion. Hearts were then isolated and placed in a Helmholtz coil and imaging was performed at 7 Tesla. T1 and T2* SI's were monitored during the first pass of Gd-DTPA using an interleaved T1–T2* imaging sequence. After MR imaging, the hearts were injected with colored microspheres to assess regional blood flow and stained with triphenyl tetrazolium chloride (TTC) to identify the region of infarction.

Results: TTC-staining identified a heterogeneous distribution of damage. In addition to stained and unstained regions (viable and nonviable respectively), we observed an area of lightly stained tissue in the core of the infarct zone (likely due to poor washout of NADH). Correlated to blood flow measures, we identified normal tissue (stained, high regional blood flow), reperfused infarct (no stain, moderate flow), and low-reflow infarct (light stain, marginal flow). Using TTC-stained sections as reference, we observed very distinct patterns in signal intensity time course data related to myocardial damage. The representative plots in Figure 1 show that T2* signal intensity displays differing degrees of recovery at the maximal T1 signal intensity. By comparing this factor at maximal T1 signal (related to maximal contrast agent concentration), the error due to concentration of contrast agent can be corrected. Therefore, the percentage of signal recovery may be related to the severity of tissue damage. We found percentage recovery value were 30.5% in normal, 63% in reperfused infarct and 90% in low-reflow infarct tissues. These gave a $p < 0.0001$ for all comparisons based on percentage recovery (i.e. normal—reperfused infarct, normal—low reflow, . . .) using ANOVA. Lastly, by using fuzzy clustering software to group individual pixels on signal intensity time course data, we were able to obtain an excellent correlation to TTC-stained sections (Figure 2) showing that T1–T2* imaging can identify myocardial injury with high specificity.

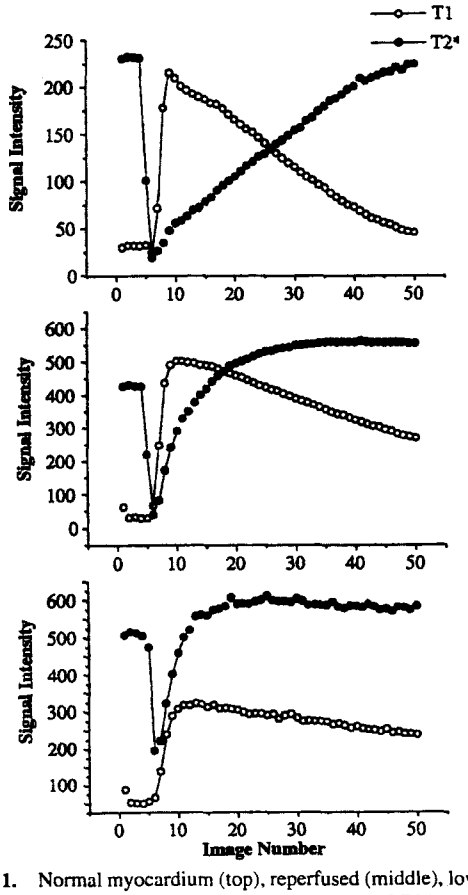

Figure 1. Normal myocardium (top), reperfused (middle), low-reflow infarcted (bottom) clearly show increasing levels of T2* recovery at maximal T1 signal intensity.

Figure 2. Fuzzy clustering of T1–T2* data shows correlation to TTC-staining.

Simultaneous Assessment of Function and Metabolism of the Heterotopically Transplanted Rat Heart for Cardiac Graft Preservation Studies

T. Caus, M. Izquierdo, C. Lan, Y. Le Fur, S. Confort-Gouny, P. Cozzone, M. Bernard. *Centre de Résonance Magnétique Biologique et Médicale (CRMBM), Fac. Med. Marseille, France*

Heterotopic rat heart transplantation model allows physiological reperfusion with blood as well as long term evaluation of heart recovery. However, the heterotopically transplanted heart is not submitted to a workload and the evaluation of function in this model has been usually performed by explanting the heart for evaluation of the contractility in an isolated perfused heart model. We describe here a method to achieve in situ simultaneous assessment of contractility and energetic metabolism using P-31 magnetic resonance spectroscopy.

Inbred male Lewis rats were used as donors and recipients. Hearts (n = 18) were arrested by intra-aortic injection of the CRMBM solution, a specific heart preservation solution (1). Hearts were then stored at 4°C in 100ml of the CRMBM solution during long term ischemia (3 hours). Heterotopic abdominal heart transplantations were performed according to the classical technique of Ono (2). A small latex balloon connected to a pressure catheter was inserted into the left ventricle via the apex through a superficial purse-string. The pressure catheter was exteriorized through a small incision and connected to a Gould recorder for the functional evaluation. P-31 MRS spectra were obtained 1) from the explanted heart at the end of the preservation period in a Bruker-Nicolet WP-200 spectrometer and 2) from the in situ heart 1 hour and 24 hours after transplantation. Animals were then placed in a Bruker-Biospec 47/30 system (4.7 Tesla magnet). P-31 MRS spectra were obtained using a 15 mm diameter ^{31}P surface coil. Acquisitions were triggered with the pressure curve.

Functional and metabolic recovery:

	dp/dtmax (mmHg/sec)	PCr/ATP
1 hour reflow	1331 ± 81	2.29 ± 0.15
24 hour reflow	2081 ± 333*	1.87 ± 0.13*

* $p < 0.05$

The decrease in PCr/ATP ratio after 24 hours of reflow was related to an increase in ATP which may be due to the resynthesis of the precursors of ATP. Thus functional and metabolic recovery are significantly improved after 24 hours of reflow compared to 1 hour.

Although broadely used in ex-vivo perfusion models, ^{31}P MRS has been rarely used to study heart grafts after heterotopic transplantation, except in rejection studies but never with a simultaneous study of contractility. We show here that simultaneous functional and metabolic evaluation of the heterotopically transplanted heart is feasible. Functional and metabolic recovery are significantly improved after 24 hours of reperfusion compared to 1 hour which is the accepted period of reperfusion in the isolated rat heart model. This experimental model should be useful for the evaluation of improved heart preservation solutions from which a significant clinical progress is expected.

References

1. Bernard M, Caus T, Lan C et al. *J Heart Lung Transplant* 1999; 18: 572–581.
2. Ono K, Lindsey ES. *J Thorac Cardiovasc Surg* 1969; 57: 225–229.

Assessment of Oxygenation and Perfusion in Human Myocardium Using T_1, T_2 and T_2*

C.M. Wacker,[1] A.W. Hartlep,[2] M. Bock,[2] G. van Kaick,[2] G. Ertl,[1] L.R. Schad,[2] W.R. Bauer.[1] [1]*Department of Cardiology, University of Wuerzburg;* [2]*German Cancer Research Centre (dkfz), Heidelberg, Germany*

Introduction: The aim of this study is to assess different parameters of myocardial microcirculation without the application of external contrast-agents. Therefore different sequences were developed to get (a) the apparent longitudinal relaxation time T_1 for calculation of myocardial perfusion, (b) the effective transverse relaxation time T_2 to determine myocardial oxygenation, and (c) to get the transverse relaxation time T_2 to differentiate edema and scar.

Materials and Methods: T_1-measurements: The myocardial perfusion p can be calculated from a global ($T_{1,glob}$) and slice-selective ($T_{1,sel}$) prepared T_1-measurement. The relative myocardial fraction of blood and tissue λ is assumed to be 1 (1).

$$p = \lambda\left(\frac{1}{T_{1,blood}}\left(\frac{T_{1,glob}}{T_{1,sel}} - 1\right)\right), [p] = \frac{ml}{\min \cdot g}$$

T_1-measurements were performed using a Saturation-Recovery-Turbo-FLASH-Sequence (2) to assess the apparent T_1 of myocardium after global and slice-selective spin preparation. 9 images are acquired with different saturation time delays (TS) as well as one image without any spin preparation according to an infinite TS. Pixel-by-pixel T_1-calculation results in a T_1-map. All 10 images are acquired during a single breathhold-period of about 15 seconds. ECG-triggering compensates heartbeat-movements. During each cardiac cycle (mid-diastole) one image is acquired. Imaging parameters are: TR/TE/α/FOV/matrix/SL = 2.5 ms/1.1ms/8°/225 × 300mm/80 × 128/10mm.

T_2^*-measurements: The deoxygenation of diamagnetic oxyhemoglobin to paramagnetic deoxyhemoglobin changes local magnetic field inhomogeneities and causes signal lost in T_2^*-images (BOLD-effect). T_2^*-measurements were performed using a gradient-multi-echo sequence (2,3). 10 images were acquired (TE = 6–54ms, ΔTE = 5.4ms) during a breathhold-period of about 15 seconds. During each cardiac cycle, 7 phase encoding lines are acquired with incremented flip angles between 20° and 90° at a repetition time per phase encoding step of 22.5ms. Further imaging parameters are: FOV/matrix/SL = 225 × 300mm/140 × 256/6mm. To suppress the ventricular signal from flowing blood during data acquisition a non-selective 180° hyperbolic secans RF-Pulse inverts the magnetisation. A slice selective re-inversion results in a approximate nulling of the longitudinal magnetisation of the inflaming blood (black blood).

T_2-measurements: T_2-measurements are performed using a multi-spin-echo-sequence. To minimize breath induced motion, navigator-echoes are acquired to detect the diaphragm position. ECG-triggering is to compensate heart beat motion. Due to a myocardial T_1 of about 1 sec, the acquisition time has to be reduced by using a non-selective 90°-pulse immediately after the systolic peak. This preparation allows to use every heart beat. The measurement is performed mid-diastolic 400ms after the systolic peak. A slice-selective 90°-exitation is followed by 8 non-selective composite-180°-pulses to reduce the influence of flowing blood.

Imaging parameters are: TR/TE/α/FOV/matrix/SL/NEX/TA = 600ms/9ms/225 × 300mm/115 × 128/8mm/4/4min. Finally a T_2-map can be calculated. All measurements were performed on a 1.5T whole body scanner (SIEMENS Vision, Germany) using the integrated body coil for RF-excitation and a 4-element phased array coil for signal reception.

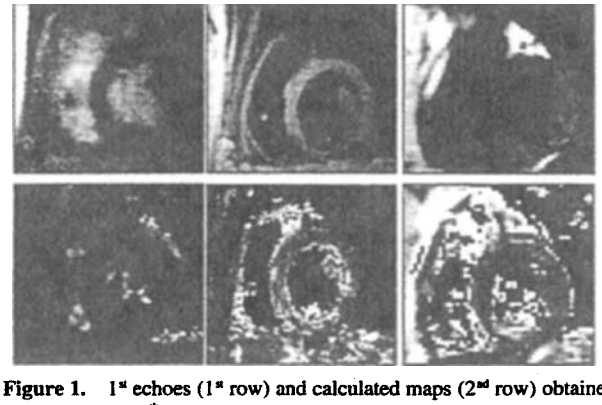

Figure 1. 1st echoes (1st row) and calculated maps (2nd row) obtained from T_1 (left), T_2^* (middle) and T_2-measurements (right).

Table 1. Average values for T_1, T_2, T_2^* and perfusion p:

T_2 [ms]	T_2^* [ms]	$T_{1,glob}$ [ms]	$T_{1,sel}$ [ms]	p [ml/(g × min)]
52 ± 2	35 ± 2	1235 ± 15	1033 ± 15	7 ± 1

Results: Results of measurements performed on a 31-year old volunteer are shown in the figures above. $T_{1,blood}$ was determined in heart chambers of non-selective T_1-maps to 1516 ± 16 ms. The measure time for the whole examination was about 30 min.

Discussion: In this study methods are presented to assess T_1, T_2 and T_2^*. The T_2-measurements were already used in a pilot study of patients with coronary artery disease (4). An analytical approach for the determination of T_2^* is in good agreement with our experimental data (5). The T_1-measurements demonstrate the capability to determine the myocardial perfusion without using external contrast agents. But the accuracy and the spatial solution has to be increased to perform clinical studies. We were able to show the opportunity of human myocardial in-vivo T_2-measurements. T_2-determination (6) might be useful to correct T_2^*-images that suffer from susceptibility-artefacts. The combination of the presented methods might lead to a "one-stop-shop" of myocardial examination including determination of human myocardial perfusion and oxygenation without using external contrast agents.

References

1. Bauer WR. et al., *Magn Reson Med* 1997; 38: 917–923.
2. Li D. et al., *Magn Reson Med* 1996; 36: 16–20.
3. Wacker CM. et al., *Magn Reson Med* 1999; 41: 686–695.
4. Wacker CM. et al., *MAG*MA* 8(1) 1999: 48–54.
5. Bauer WR. et al., *Magn Reson Med* 1999; 41: 51–62.
6. Foltz WD. et al., 7th *ISMRM* 1999; 1273.

Assessment of Myocardial Perfusion and 3D Angiography Under Acute Coronary Stenosis by NMR Imaging in the Isolated Rat Heart

K.-H. Hiller,[1] C. Waller,[2] M. Nahrendorf,[1] S. Voll,[1] G. Ertl,[2] A. Haase,[1] W. R. Bauer.[2] [1]*Physikalisches Institut, Universität Würzburg, Germany;* [2]*Medizinische Universitätsklinik Würzburg, Germany*

Introduction: The aim of this study was to combine a non-contrast-agent NMR method of measuring perfusion and a NMR microscopy method which reflects the state of coronary vessels to investigate the effects of acute stenosis under rest and stress. Both methods were developed by our group (1,2).

The principle of the perfusion measurement is that spins of a selected slice in the short axis view of the heart are inverted and a perfusion sensitive T_1 relaxation of these spins is observed. According to model calculations variations of perfusion P are determined from:

$\Delta(1/T_1) = \Delta P/\lambda$ (λ = tissue/perfusion partition coefficient of water).

Methods: Ten isolated rat hearts were studied (perfusion with Krebs-Henseleit buffer in the Langendorff mode, on-line registration of coronary flow, left ventricular pressure). Measurements of perfusion changes and 3D imaging of the coronary arteries were performed before and 30 min after induction of a defined acute coronary stenosis (200 µm in diameter) (3). Perfusion measurement after induction of stenosis was also performed at rest and at stress during infusion of the vasodilator nitroglycerin (0.5mg/ml/min) to obtain information about the coronary reserve in the ischemic myocardium. NMR-imaging was performed on an 11.75 Tesla magnet (AMX 500, Bruker).

Perfusion measurement: Spins of a slice (short axis view) 4–6 mm below the valvular plane were inverted (slice thickness = 3mm) and T1 maps were gained in this slice by 16 × Snapshot FLASH images

(spatial resolution 140 μm in plane, slice thickness = 1.5 mm, TR = 3.6 ms).

3D Angiography: Coronary vessels were imaged by mid-diastolic triggered flow-weighted 3D gradient echo pulse sequence, with an TE = 1.0ms and TR = 1 heart cycle ~200 ms. $96^2 \times 128$ complex data points were acquired in approximately 30 minutes. Data were zero-filled before Fourier transformation to 128^3 data points (spatial resolution 140 μm). The signal of myocardial tissue was additionally suppressed by a magnetization transfer experiment.

Results: The changes of regional perfusion after acute stenosis determined by T1 measurements showed a significant decrease in the ischemic myocardium below the stenotic coronary vessel (−60.85 ± 8.59% ± SD). In the right ventricular and posterior myocardium of the left ventricle perfusion remained unchanged (1.11 ± 7.52% and −3.09 ± 10.84%). During nitroglycerin stress perfusion increased in the right ventricle and in the posterior myocardium of the left ventricle (30.2 ± 9.3% and 14.81 ± 11.61%) whereas perfusion in the ischemic myocardium showed no response to nitroglycerin infusion (−57.13 ± 3.04%). The relative changes in perfusion were refered to perfusion calculated by the ultrasonic measured coronary flow and heart weight at the starting point. Calculations of global perfusion changes by T_1 and ultrasonic measured coronary flow were in good agreement. The 3D angiogramms visualized the acute induced nonocclusive constriction of the left coronary artery. Also the diminished ramification of coronary vessels below stenosis became evident.

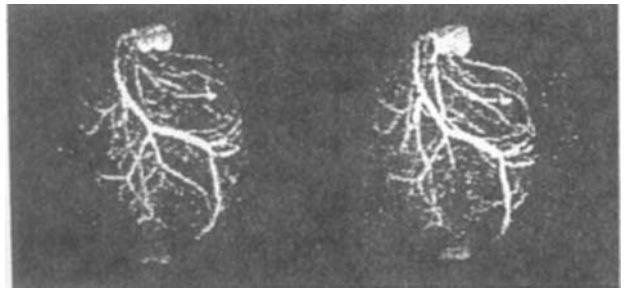

Conclusion: It could be shown that it is possible to obtain accurate values of perfusion changes with the slice selective spin inversion NMR technique. The combination of the two NMR imaging techniques allows the detection of coronary stenosis and study of microcirculatory effects. In comparison to the posterior left myocardium perfusion is highly diminished in the stenotic region at rest. During stress coronary reserve is still reduced in the ischemic region.

References

1. Hiller KH, Bauer WR, Roder F, et al. *MAGMA* 1997; 5(2) Suppl.: 91
2. Roder F, Hiller KH, Henz P, et al. *JMRI* 1997; 7: 316–320.
3. Capasso JM, Jeanty MW, Palackal T, et al. *Am J Physiol* 1989; 257: H1983–H1993.

Non-Contrast Agent Dependent NMR Quantification of Myocardial Perfusion and Mass During Left Ventricular Remodeling

Christiane Waller,[2] Karl-Heinz Hiller,[1] Elke Kahler,[1] Kai Hu,[2] Matthias Nahrendorf,[1] Axel Haase,[1] Wolfgang R. Bauer.[2]
[1]*Physikalisches Institut, Universität Würzburg;* [2]*Medizinische Universitätsklinik, Würzburg, Germany*

Background: Coronary reserve is restricted during left ventricular remodeling in surviving myocardium post myocardial infarction (m.i.). The purpose of the present study was to sequentially quantify perfusion (P) and myocardial mass (M) during cardiac remodeling at rest and during hyperemia.

Methods: Measurements were performed on a Bruker Biospec 7 Tesla spectrometer. Quantitative T_1 maps were acquired using an inversion recovery snapshot FLASH technique. Principle of the method for perfusion measurement is the spin labeling of endogenous water protons within the detection slice. P is determined from a slice selective and a global T_1 experiment according to the following equation:

$$\frac{P}{\lambda} = \frac{T_{1,glob}}{T_{1,blood}} * \left(\frac{1}{T_{1,sel}} - \frac{1}{T_{1,glob}}\right)$$

NMR parameters were: TR 2.25ms, TE 1ms, matrix 64 × 64, FOV 5 × 5cm², slice thickness 3mm. M is determined from a Cine-FLASH sequence out of 1mm imaging slices in a short axis view (NMR parameters: TR 4.3 ms, TE 1.2 ms, matrix 128 × 128. FOV 3–3.5 cm²). Female Wistar rats were anesthetized with sodium pentobarbital. Group 1 (n = 8, m.i. size = 10–35%, mean 26.4%) were measured serially at 8, 12 and 16 weeks after m.i., Animals of group 2 (n = 8) were sham operated and served as control. P was determined (mean ± SEM) at rest and during i.v. infusion of 3mg/(kg * min) of adenosine.

Results: Data of group 1 are obtained from noninfarcted hypertrophied tissue. Data of group 2 represent the whole left ventricle.

	8 Weeks		12 Weeks	
	At Rest	Adenosine	At Rest	Adenosine
P1	45 ± 02*	5.8 ± 0.4#	4.1 ± 0.3 +	4.9 ± 0.2+
M1	521.8 ± 24.2		531.8 ± 32.5	
P2	3.6 ± 0.2	5.2 ± 0.6#	3.9 ± 0.3	5.7 ± 0.3#
M2	516.3 ± 26.3		478.3 ± 27.2	
	16 Weeks			
	At Rest		Adenosine	
P1	3.3 ± 0.2+		3.8 ± 0.2*, +	
M1	622.3 ± 35.4*,+			
P1	3.7 ± 0.2		5.4 ± 0.4 #	
M1	495.1 ± 19.8			

*: group 1 vs. group 2 $p < 0.001$, #: adenosine vs. at rest $p < 0.001$, +: vs. 8 weeks $p < 0.001$

Conclusion: The here presented NMR imaging techniques allow the sequential non invasive in vivo quantification of myocardial perfusion and mass. Perfusion gradually decreases over time in surviving myocardium at rest and during hyperemia. Hypoperfusion is related to hypertrophy and may therefore contribute to the development of heart failure.

Reduced Contracile Reserve and Diastolic Dysfunction in a Transgenic Mouse Model with Heart Specific Overexpression of the β_1-adrenergic Receptor

F. Wiesmann,[1] S. Engelhardt,[2] J. Ruff,[3] C. Ritter,[1] L. Hein,[2] M. Lohse,[2] A. Haase,[3] S. Neubauer[1]. [1]*Medizinische Klinik;* [2]*Institut für Pharmakologie;* [3]*Institut für Experimentelle Physik, Universität Würzburg, Germany*

Motivation: Myocardial contraction and relaxation are energy-dependent processes which are highly regulated by the β-adrenergic receptor system. Purpose of this study was to investigate the consequences of heart specific overexpression (OE) of the β_1-adrenergic receptor on cardiac morphology and function in vivo.

Methods: We studied 12 weeks old male transgenic (TG, 30.0 ± 0.06 g body weight) and wild type mice (WT, 31.4 ± 1.0 g) by high-resolution magnetic resonance imaging (MRI). ECG triggered cine

FLASH MRI was performed on a 7T experimental MR scanner (Bruker BIOSPEC) under inhalative anesthesia with isoflurane. MR imaging parameters were: TE 1.5 ms, TR 4.3 ms, FA 45°, in-plane resolution (120 μm)²; SLT 1 mm, acquisition window per cine frame 8.6 ms. FLASH MRI was performed at rest and during β-adrenergic stimulation with dobutamine (1.5 μg/g BW). Left ventricular (LV) end-diastolic and end-systolic volume (EDV, ESV), stroke volume (SV), ejection fraction (EF), cardiac output (CO), LV mass index (LVMI), LV ejection rate (dV/dt_{max}) and filling rate (dV/dt_{min}) were determined.

Results: TG showed a 25% higher, LVMI compared to WT ($p < 0.01$, Figure 1). There was no significant difference for LV EDV, ESV, SV, EF and CO. At rest, LV ejection and filling rate were similar for TG and WT. However, during inotropic simulation there was no further increase of dV/dt_{max} in the TG, indicating impaired contractile reserve. LV filling rate in the TG significantly decreased during dobutamine ($p < 0.01$), thus indicating diastolic dysfunction under inotropic stress (Figure 2).

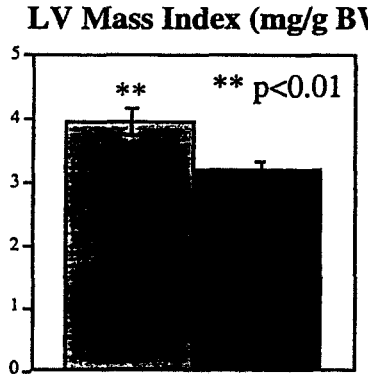

Figure 1

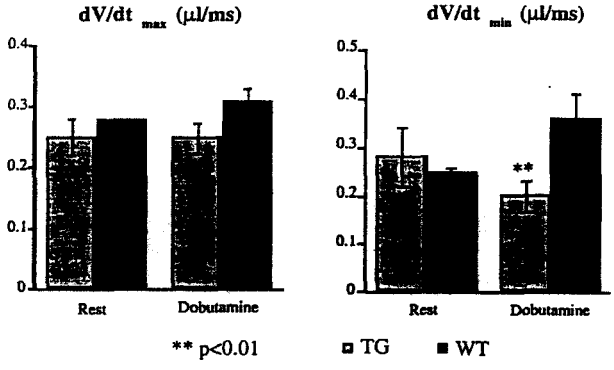

Figure 2

Conclusion: Transgenic mice with OE of the β_1-adrenergic receptor show marked LV hypertrophy, reduced contractile reserve and a significant diastolic dysfunction under β-adrenergic stress already at early age. These findings might be a strong indicator for consecutive development of heart failure in this transgenic mouse model.

The "PCr Overshoot": A Marker for Cardiac Viability

W.T. Evanochko,[1] E. Butterworth,[1] S.D. Buchthal,[1] I. Straeter-Knowlen,[1] J.A. den Hollander,[1] R.B. Jennings,[2] G.H. Pohost.[1]
[1]*University of Alabama at Birmingham, Birmingham, AL;* [2]*Duke University, Durham, NC*

Introduction: Reperfused post-ischemic myocardium has a disordered bioenergetic state. A hallmark is an abnormal elevation of the phosphocreatine (PCr) to ATP ratio thought to be due to altered post-ischemic energy metabolism (1). This phenomenon has been termed the "PCr Overshoot" and occurs even in the presence of subnormal levels of ATP. This readily observable ^{31}P-NMRS phenomenon could prove to be a marker for detecting viable myocardium. To date, there is little information of the full serial duration of this phenomenon in "*in vivo*" large animal models. Therefore this study examined baseline and serial levels in a canine model. This phenomenon might be used to identify clinically salvageable post-ischemic myocardium.

Methods: An open-chest canine model (n = 4) of 12 minutes of ischemia followed by reperfusion (≥6 hrs) was employed. A 2 cm surface coil was sutured to the myocardium and data were acquired using a composite pulse for full excitation transmurally at 4.7T. Spectra were acquired in ≤2.5 minute with an interpulse delay of 6 sec. All spectra were both cardiac and respiratory gated.

Results: Analyses of PCr and ATP (beta) used a line fitting routine (NMR1) and the results were computed in absolute integrals (arb.units). The summed data of PCr for baseline; ischemia; reflow were: 23.5 ± 1.8; 11.6 ± 3.7; 27.2 ± 2.3. The summed data for ATP-b for baseline; ischemia; reflow were: 12.5 ± 0.9; 11.0 ± 1.3; 10.9 ± 0.5 respectively (±S.D). The figure plots the PCr/ATPb ratio for each state. Analysis showed the "PCr overshoot" to be statistically significantly higher than controls during the entire six hour period of reflow ($P < .005$).

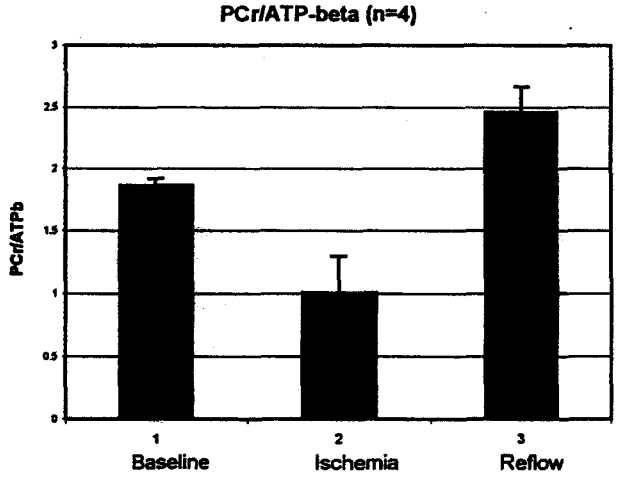

Discussion: The "PCr Overshoot" is present for six hours and clearly is a marker of reversible injury in this model. This phenomenon was apparent for the six hour study interval. Possible explanations for this bioenergetic observation include: the effect of excess P_i on creatine kinase kinetics; depletion of adenine nucleotide substrate; and decreased myocardial work. However, another study has indicated that the overshoot is independent of myocardial work (2). Therefore the "overshoot" can either be due to depletion of the adenine nucleotides or altered creatine kinase kinetics which still needs to be elucidated. Finally, this study examined the "overshoot" reflow period for six hours. Since the phenomenon persists beyond this period, additional studies are necessary to delineate the full extent of the "overshoot". Those studies are currently underway.

References

1. RB Jennings, KA Reimer, C Steenbergen, and CE Murry, Myocardial Ischemia, Dhalla, Innes, Beamish, Eds., Martinus Nijhoff Pub., Boston, 1987, p. 185–198.
2. Kaplan LJ, Bellows CF, Carter S, Blum H, Whitman GJ, Biochimie 1995; 77(4): 245–8

Evaluation of Global Left and Right Ventricular Function During Supine Physical Exercise by Ultra-Fast Magnetic Resonance Imaging

Arno A.W. Roest,[1,2] Patrik Kunz,[2] Hildo J. Lamb,[2] Willem A. Helbing,[2] Ernst E. van der Wall,[1,2] Albert de Roos[1,2]. [1]*Interuniversity Cardiology Institute of The Netherlands, Utrecht;* [2]*Leiden University Medical Center, The Netherlands*

Background: Cardiac response to physical exercise may be impaired in patients with heart disease and can be abnormal in the absence of clear symptoms at rest. Magnetic resonance imaging (MRI) is an excellent tool to evaluate ventricular function, especially of the right ventricle. However, assessment of ventricular response to physical exercise by MRI is difficult due to increased motion artifacts during exercise. Aim of this study was to evaluate left (LV) and right (RV) ventricular response to supine physical exercise with the application of an ultra-fast MRI sequence.

Methods: Ventricular function at rest and during exercise was studied in 15 healthy volunteers using an ultra-fast turbo field echo planar imaging MRI sequence. Individual exercise levels were based on the workload at 60% of the prior measured maximal oxygen uptake. Exercise was performed on a MR compatible ergometer. Ten slices in the short-axis direction covered both left and right ventricle and were obtained using 5 breath-holds. Each breath-hold was performed during an 8-heartbeat suspension of exercise and in this period 2 short-axis slices were acquired.

Results: Ejection fraction (EF) of the LV and the RV increased in all volunteers in response to exercise (LV: +12 ± 5%; RV: +10 ± 4%). Furthermore, increase in stroke volume (SV) from rest to stress of the LV (+15 ± 9ml) and the RV (+14 ± 7 ml) was observed in all subjects. For the LV, increase in EF and SV was the result of a combined decrease in end-systolic volume (ESV) (− 20 ± 11 ml) and end-diastolic volume (EDV) (−6 ± 10ml). Whereas for the RV, increase in EF and SV was the result of a decrease in ESV (−19 ± 10ml).

Conclusion: This study shows that it is feasible to evaluate cardiac response to supine physical exercise in healthy subjects with an ultra-fast MRI sequence. In agreement with literature, SV and EF of both ventricles increased in response to exercise mainly due to a decrease in ESV.

Assessment of Coronary Artery Bypass Graft Flow Reserve Using Magnetic Resonance Imaging and the Doppler Flow Wire

Susan E. Langerak, Johan W. Jukema, Patrik Kunz, Hubert W. Vliegen, Paul Steendijk, Albert de Roos, Ernst E. van der Wall. *Interuniversity Cardiology Institute of the Netherlands and the Depts. of Cardiology and Radiology of the Leiden University Medical Center, Leiden, The Netherlands.*

Background: Coronary flow reserve measurement using the Doppler flow wire is considered an established diagnostic tool in detecting significant coronary artery stenosis. Recent advances in magnetic resonance (MR) flow mapping allow a fast, noninvasive assessment of coronary bypass graft flow during stress with a high temporal resolution. The purpose of our study was to determine the correlation of MR flow mapping with results obtained by the Doppler flow wire.

Methods: Nineteen patients with 24 bypass grafts, who were planned for contrast angiography, underwent breath-hold turbo-field echo-planar-imaging MR flow mapping of the bypass grafts at rest and during intravenous adenosine infusion (140 µg/kg/min). During contrast angiography intracoronary Doppler flow velocity measurements were performed before and after intracoronary adenosine injection (18 µg).

Results: A good correlation was found between MR and intracoronary Doppler flow velocity and flow reserve values (r = 0.78). However, flow velocity was systematically lower by MR in comparison to Doppler flow mapping. A flow velocity reserve of 2.5 ± 0.9 and 2.7 ± 0.9 was found for MR and Doppler flow mapping, respectively.

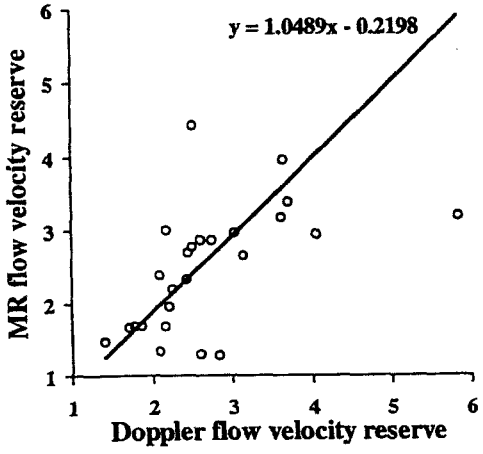

Conclusion: MR flow velocity mapping at rest and during stress allows the assessment of bypass graft function. This offers perspective for the noninvasive detection of coronary bypass graft stenosis and may be used for follow-up of patients after intervention.

Blood-Oxygen-Level-Dependent (BOLD) MRI in Patients with Symptoms of Coronary Artery Disease

M.G. Friedrich,[1] T. Niendorf,[2] J. Schulz-Menger,[1] O. Strohm,[1] and R. Dietz,[1] Franz-Volhard-Klinik.[1] [1]*University of Berlin, Germany;* [2]*GE Medical Systems, Leipzig, Germany*

Background: In patients with symptoms of coronary artery disease (CAD) the verification of myocardial ischemia is important for therapeutical decision-making.

Established perfusion techniques like Thallium scintigraphy and positron emission tomography (PET) suffer from radionuclide activity. Recently, MR perfusion studies were attempted using bolus-application of Gd-DTPA and Adenosine infusion. However, this approach is complicated by a difficult input function of the contrast bolus.

Blood-oxygen-level-dependent (BOLD) MRI visualizes areas of reduced hemoglobin oxygenation (1) and is of proven value for functional brain imaging. (2) BOLD MRI of the myocardium detects signal changes after pharmacological increase of blood supply. (3,4) This study examines whether BOLD MRI is feasible in patients with suspected CAD.

Methods: Experiments were conducted on a 1.5 T cardiovascular scanner (CV/i, GE Medical Systems, Milwaukee, Wisconsin, USA). T_2^*-sensitized gradient echo EPI (TE 17.4 ms) has been applied in 22 patients with a history of stress-induced angina before, during and after continuous infusion of Adenosine over 6 minutes. We compared the results to those of a subsequent (within 24 hours) Thallium study using the same Adenosine protocol. The mean scanner time was 25 minutes including multiplanar visualization of systolic function. Offline evaluation included a computer-based calculation of time-intensity curves

with resulting parametric images (negative and positive enhancement images).

Results: In all but one patients the image quality was sufficient for a signal intensity analysis. Reasons for impaired image quality were a history of implanted intracoronary stents and susceptibility artifacts (lateral myocardium).

As compared to the Thallium results a perfusion deficit was correctly detected in 12/15 patients (sensitivity 80%) and correctly excluded in 5/7 patients (specificity 71%).

Figure 1 and 2 show an example of anterior wall ischemia.

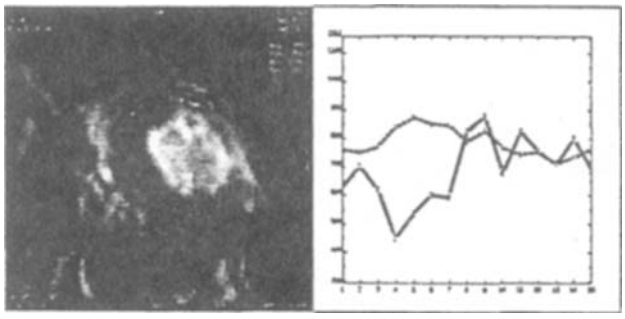

Figure 1. Time intensity curve of the signal change during Adenosine infusion in a patient with a critical stenosis of a diagonal branch. Whereas the signal intensity increases in the septum (dotted line) there is a decrease of signal intensity during Adenosine perfusion in the anterior subendocardium.

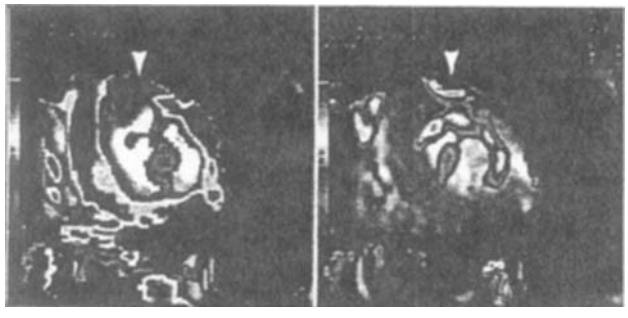

Figure 2. Parametric images of the same study. Left panel (positive enhancement image): In contrast to the residual myocardium there is an anterior circumscribed but transmural lack of signal increase. Right panel (negative enhancement image): In the same area there is a subendocardial signal decrease during Adenosine infusion.

Conclusion: BOLD MRI using gradient echo EPI is suitable for the examination of patients with CAD. It detects areas of reduced perfusion, and parametric image evaluation allows visualization of intramural perfusion gradients. Further studies need to address sensitivity and specificity.

References

1. Ogawa S, Lee TM, Kay AR, et al. *Proc-Natl-Acad-Sci-U-S-A* 1990; 87: 9868–72.
2. Niendorf T. *Magn-Reson-Med* 1999; 41: 1189–98.
3. Li D, Dhawale P, Rubin PJ, Haacke EM, et al. *Magn-Reson-Med* 1996; 36: 16–20.
4. Wacker CM, Bock M, Hartlep AW, et al. *Magn-Reson-Med* 1999; 41: 686–95.

MRI in the Assessment of Subclinical Anthracycline Cardiotoxicity

M.G. Friedrich,[1] R. Waßmuth,[2] A. Wagner,[1] J. Schulz-Menger,[1] O. Strohm,[1] and R. Dietz.[1] [1]*Franz-Volhard-Klinik, University of Berlin, Germany;* [2]*NHLBI, NIH, Bethesda, MA*

Background: Anthracyclines used in antineoplastic therapy may lead to cardiotoxic long term effects in a considerable number of patients. So far no reliable markers to detect early cardiac damage have been found. We tested the ability of magnetic resonance imaging (MRI) to show early changes in myocardial signal and cardiac function after anthracycline therapy.

Methods: In this study 22 patients without preexisting heart disease were investigated before, 3 days after, 28 days after and 180 days after anthracycline therapy using a standard clinical scanner (Siemens Impact 1.0 T, Siemens AG, Erlangen, Germany). Contrast-enhanced, T1 weighted fast spin echo images were obtained to characterize myocardial tissue enhancement. The myocardial signal increase after Gd-DTPA administration was compared to that of the skeletal muscle (relative enhancement). Left ventricular ejection fraction (LVEF) was measured with breathhold gradient echo cine sequences in contiguous short axis planes (TE 6.1 ms, TR 90ms, slice thickness 10mm).

Results: There was no clinical evidence for acute cardiotoxic injury in any of the patients. The relative myocardial signal enhancement increased from 3.83 ± 0.37 to 6.91 ± 1.13 ($p < 0.01$, see fig. 1). LVEF decreased from 67.8 ± 1.4% to 61.9 ± 1.7% after 180 days ($p < 0.05$, see fig. 2). There was a trend towards correlation between the increase of the relative enhancement on day 3 and the LVEF loss at 180 days.

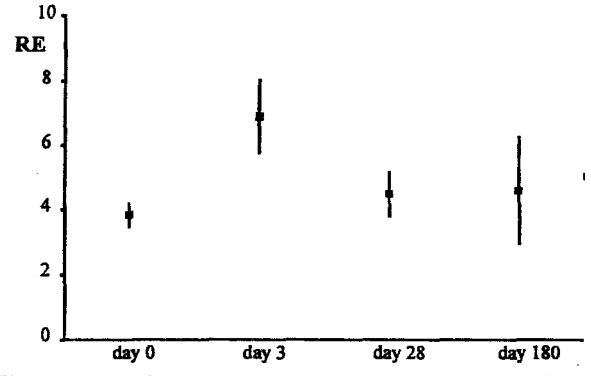

Figure 1. Relative myocardial contrast enhancement (RE) after the onset of anthracycline therapy. There is a significant increase on day 3 with a normalization in most of the patients during the later course.

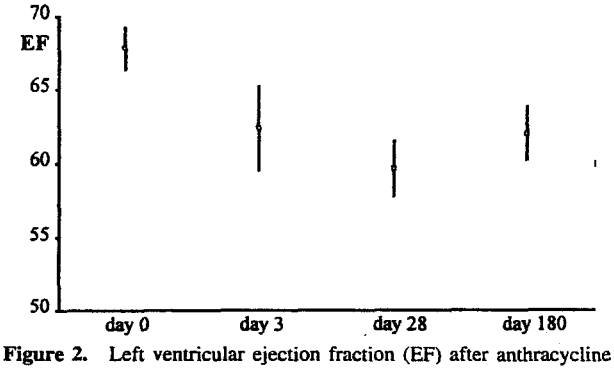

Figure 2. Left ventricular ejection fraction (EF) after anthracycline therapy. There is a small loss early after onset of therapy within the normal range but remained significantly decreased.

Conclusion: MRI detects a subtle loss of left ventricular contractility in asymptomatic patients after anthracycline therapy. Early changes of myocardial contrast accumulation may be a useful early marker of a cardiotoxic myocardial injury.

MRI in Acute Pericarditis: Preliminary Results of a Spanish Collaborative Study

G. Pons-Lladó, F. Carreras, X. Borrás, J. Palmer, J. Llauger, L.J. Jiménez-Borreguero, I. Coma-Canella, J. Pueyo, R. Payá, V. Martínez, J.F. Forteza, J. Palmer-Sancho. *Spanish Collaborative Study Group on MRI in Acute Pericarditis (MRIAP)*

Objective: The value of MRI in the study of pericardial effusion and in constrictive pericarditis has been extensively proven. There is no information however on its usefulness in the assessment of morphological abnormalities in acute pericarditis. The preliminary results of a multicenter study conducted with this aim are presented.

Patients and Methods: A total of 18 patients have been enrolled up to date: 14 males and 4 females, aged 18–73 years (mean: 40 ± 17). All of them had a definite diagnosis of acute pericarditis, idiopathic or viral in origin, based on the presence of at least 2 of 3 clinical findings (suggestive chest pain, pericardial rub and transient diffuse elevation of the ST segment in the EKG).

Two MRI studies were carried out in all patients: one within the first week after the initial symptoms and a second one after 2 months. MRI studies were performed with systems operating at 1.0 T using conventional spin-echo T1 sequences oriented on axial, sagittal and coronal thoracic planes with the following parameters: TR = R − R interval minus 100 msec; TE = 30 msec; slice thickness = 5 mm; interslice = 1.5 mm; field of view = 350 mm; matrix = 192 × 256; number of excitations = 2. A transaxial cine sequence on gradient-echo was also obtained at the ventricular level aimed to detect even small amounts of pericardial effusion.

In those patients in whom a pericardial effusion was absent at the initial examination pericardial thickness was measured by means of a dedicated software. The MRI signal of the pericardium was identified as a thin lineal low intensity signal limitated by two high intensity signals of adipose tissue. In every patient 3 different segments of the pericardial contour were considered for analysis: anterior to the right ventricular wall, adjacent to the right atrial wall, and at the level of the left ventricular free wall. The pericardial thickness was taken at each location as the mean of 3 independent measures. Normal values of pericardial thickness were obtained with the same methodology from a different series of 10 non cardiac patients.

Results: MRI was of adequate quality for the purposes of the study in all 18 patients. Pericardial effusion was present in 4 (22%) patients at the initial study, ranging from mild to large, although in none of them clinical findings of tamponade were detected. These cases were excluded from the analysis of pericardial thickness, although they underwent the second MRI examination.

In the remaining 14 patients, pericardial thickness could be measured in 100% of cases at its anterior aspect, in 86% at the left pericardium and in 79% at the right atrial aspect of it. MRI planes which proved more adequate for the assessment of the different pericardial locations were the axial one for the anterior pericardium, the coronal for the area adjacent to the left ventricle, and the axial and coronal for the right aspect of the pericardium. This allowed the measurement of 37 different pericardial segments at the first study, 41 at the second one, and 25 in normal individuals.

In normal individuals, mean pericardial thickness was 2.1 ± 0.3 (range: 1.6–2.6 mm). Mean thickness in patients during the acute phase of the disease was 2.5 ± 0.6 mm (range: 1.7–4.6 mm) ($p < 0.004$) (see figure).

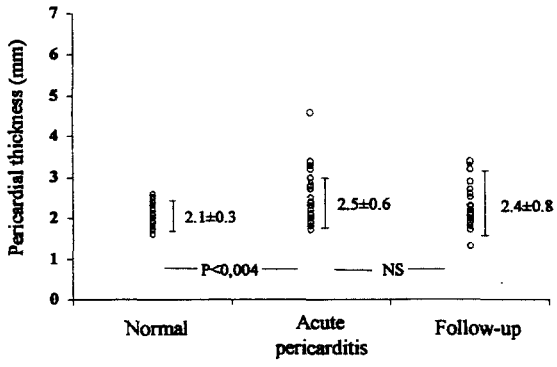

In all patients the pericardial process had clinically receded after the acute phase. At the time of the second examination mean pericardial thickness by MRI was 2.4 ± 0.8 mm (range: 1.3–6.4 mm), a value not different from that in the initial study (see figure). Pericardial effusion was absent in those 4 patients with previous effusion, they exhibiting pericardial thickness (2.5 ± 0.3 mm) not different than that in the rest of patients.

Conclusion: In 22% of patients with idiopathic or viral acute pericarditis MRI detects the presence of pericardial effusion, which is usually absent after 2 months from the acute episode, the pericardial thickness being then comparable to those patients who had no effusion.

In those patients with acute pericarditis but without effusion, a mild but statistically significant increase in pericardial thickness is detected, which persists at 2 months, when signs and symptoms of the disease have disappeared. Overlap of values of pericardial thickness between patients and normal individuals, as well as the intrinsic limitation of MRI resolution at a sub-millimetric level, prevent the use of pericardial thickening as an indicator of the presence of acute pericarditis in individual patients.

Assessment of Coronary Flow Reserve Using Fast Velocity Encoded Cine MRI: Validation Study Using Oxygen-15 Labeled Water and Positron Emission Tomography

H. Sakuma,[1] J.W. Koskenvuo,[2] P. Niemi,[3] N. Kawada,[1] J.O. Toikka,[2] J. Knuuti,[4] H. Laine,[4] M. Saraste,[2] J. Hartiala.[2] [1]*Dept. of Radiology, Mie University, Tsu, Mie, Japan;* [2]*Dept. of Clinical Physiology,* [3]*Dept. of Radiology;* [4]*Turku PET Center, Turku University, Finland*

Introduction: Previous studies using intra-coronary Doppler and positron emission tomography (PET) have demonstrated that measureent of the coronary flow reserve is useful in evaluating functional significance of stenosis in the coronary artery, the outcome of coronary interventions, and altered microcirculation in cardiomyopathies. Fast velocity encoded cine MRI is an emerging application of MRI which can provide flow curves in the human coronary arteries with data acquisition during a single breath-hold time. Previous reports have demonstrated the feasibility of measuring blood flow velocity and vasodilator flow reserve in the human coronary arteries using this technique.

Oxygen-15 labeled water ($H_2{}^{15}O$) has several advantages as a positron emitting tracer for measuring blood flow in comparison with other tracers. Myocardial uptake of N-13-ammmonia and rubidium-82 are dependent on active processes. In contrast, $H_2{}^{15}O$ is freely diffusible and the kinetics are simply related to blood flow. The purpose of this study was to assess whether MR measurements of the coronary flow reserve in the proximal left anterior descending (LAD) artery are comparable to those obtained with PET and $H_2{}^{15}O$ in the corresponding territory.

Materials and Methods: Ten healthy volunteers were evaluated in this study (mean age 39 ± 13 years). Subjects with different age and sport activity were enrolled in this study in order to have a wider range of the coronary flow reserve.

MR images were obtained with a 1.5 Tesla MR imager. Fast velocity encoded cine MR images were acquired on the imaging plane that was perpendicular to the LAD artery using k-space segmentation, section thickness of 5 mm, TR/TE of 16/9 msec, FOV of 24 × 18 cm, and Venc of ± 1 m/s (Figure 1). MR blood flow measurements were obtained before and after intravenous injection of dipyridamole (0.56 mg/kg, over 4 minutes) (Figure 2). Peak flow velocity during the diastolic phase was analyzed with Xphase software (Stephan Maier M.D. Ph.D., Brigham and Womens' Hospital, Boson, MA). The vasodilator flow reserve ratio was calculated as a ratio of hyperemic to the baseline diastolic peak velocities.

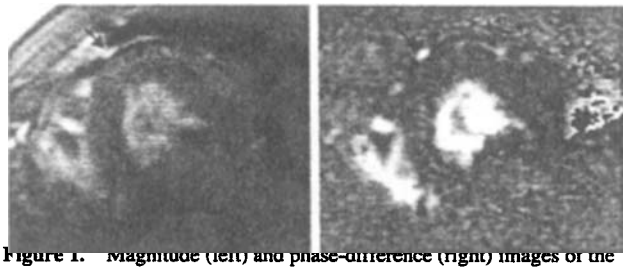

Figure 1. Magnitude (left) and phase-difference (right) images of the left anterior descending artery in volunteers acquired with a fast velocity encoded cine MRI. Arrows: left anterior descending artery.

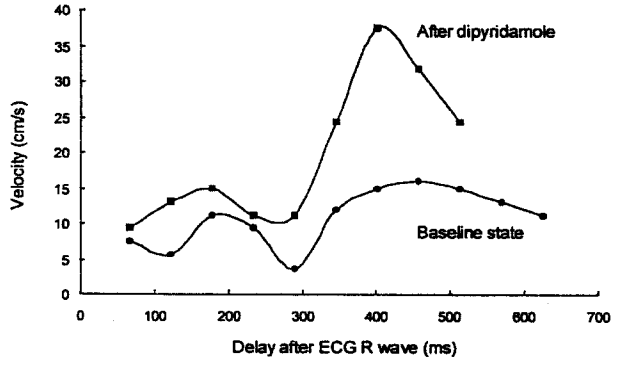

Figure 2. MR blood flow velocity curves in the left anterior descending artery in a volunteer in the baseline state and after dipyridamole administration.

PET data were acquired by using an ECAT 931/08-tomograph. Mean time between MR and PET studies was 8.1 ± 4.3 days (Figure 3). After transmission scan, $C^{15}O$ was inhaled for 2 minutes and three blood samples were taken at 2-minutes intervals. Myocardial blood flow was measured before and 2 minutes after administration of dipyridamole. $H_2{}^{15}O$ was injected and then dynamic PET scanning was started. Regional myocardial blood flow (ml/min/g) and flow reserve in the anterior myocardium was calculated using a single compartment model. The coronary flow reserve was defined as the ratio of baseline-to-hyperemic myocardial blood flow.

Results: Adequate MR and PET images were obtained in the baseline state and after dipyridamole administration in all subjects. No patients experienced chest pain or significant adverse effect with dipyridamole administration. The systolic blood pressure, diastolic blood pressure and heart rate in 10 healthy subjects during PET studies were 130 ± 13 mmHg, 77 ± 11 mmHg, 57 ± 7 beats/min in the basal

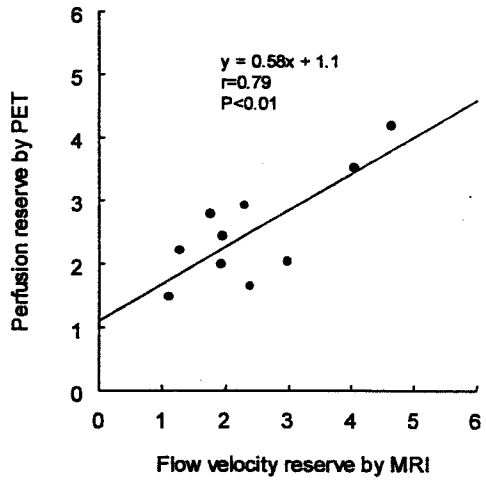

Figure 3. Correlations between the velocity flow reserve in the left anterior descending artery measured by MRI and the perfusion reserve in the anterior myocardium measured by PET.

state, and 125 ± 15 mmHg, 72 ± 10 mmHg, 78 ± 9 beats/min after dipyridamole, respectively. The diastolic peak velocity in the proximal LAD artery measured by MRI was 27.5 ± 10.4 cm/s in the baseline state and 59.8 ± 21.8 cm/s after dypiridamole injection. PET measurement of the coronary blood flow per gram of myocardial mass in the LAD arterial territory was 0.64 ± 0.19 ml/min/g in the baseline state and 1.61 ± 0.66 ml/min/g after dipyridamole. MR measurement of the velocity flow reserve in the proximal LAD artery was 2.44 ± 1.14, which was comparable to the myocardial perfusion reserve measured with PET (2.52 ± 0.84). MR and PET assessments of the coronary flow reserve showed a significant linear correlation ($r = 0.79$, $p < 0.01$).

Conclusion: Breath-hold MR measurement of the flow velocity reserve in the proximal LAD artery correlates well with myocardial perfusion reserve obtained in the anterior myocardium using radio-water PET which is currently recognized as the most accurate approach for measuring regional myocardial perfusion.

Dipyridamole-BOLD MRI Reveals Reduced Oxygen Availability in Hypertension

G.M. Beache, D.A. Herzka, J.L. Boxerman, W.S. Post, A.Z. Faranesh, S.N. Gupta, E.P. Shapiro, J.L. Weiss, M.N. Hill. *Johns Hopkins University, Baltimore, MD*

Introduction: Recent theories on the pathogenesis of coronary artery disease risk factors, such as hypertension, have suggested that endothelial dysfunction may play a significant role in the natural history of atherosclerosis (1). Blood oxygenation level dependent (BOLD) or T2* MRI is based on intrinsic sensitivity to venous oxygen (O_2) saturation, and thus flow. BOLD imaging has been performed in the brain and in epicardial coronary artery disease in the heart. We present data on BOLD imaging of oxygenation changes in response to dipyridamole hyperemia in hypertensive patients.

Methods: Imaging: T2* was estimated using a gated, segmented, spoiled gradient-echo sequence on a Signa 1.5T scanner (GE Medical Systems Milwaukee, WI). Blood pool saturation was applied to reduce flow artifact. Data sets of nine images with equally spaced TEs in the range of 2-26 ms were acquired in a single breathhold. Five RF views, each followed by a nine-echo readout-train, were acquired during a 138 ms diastolic window of each cardiac cycle. Parameters for one echo train were TR/α/RBW = 27.6 ms/30°/± 62.5 kHz, with a matrix of 256 × 120 and FOV 400 × 400 mm (1.56 × 3.33 × 10 mm).

Infusion Protocol: After the acquisition of repeated images to establish a baseline, dipyridamole was administered according to standard practice in stress studies. Post infusion images were acquired approximately every minute for 20 minutes, during the first half-life of dipyridamole kinetics.

Analysis: Each dataset of nine images was combined to generate T2* pixel-by-pixel log fits for each time point. Fits were constrained using a correlation coefficient cut-off (R), of 0.95 (2). Because hypertension is believed to result in a global myocardial abnormality, a single ROI of fixed size and shape in the central myocardium was tracked through time, after performing an automated registration routine. A global signal intensity (SI) time series was generated for each subject and the oxygenation parameter taken as the maximal T2* change due to dipyridamole.

Subjects: Healthy volunteers (N = 6), and hypertensive patients with moderate to severe hypertrophy, documented by echocardiography, and who had no history of coronary artery disease or infarcts (N = 6), were imaged after informed consent.

Results: Mean percent T2* signal change in the healthy controls was 18 ± 8. Mean percent T2* signal change in patients was 6 ± 2.

Discussion: We have obtained preliminary evidence of a reduction of the myocardial T2* response to a maximal dose of the coronary vasodilator dipyridamole in patients with hypertensive hypertrophy. In subjects with intact vasodilator function, dipyridamole hyperemia results in augmentation of flow in excess of physiologic demand, with attendant increase in venous O_2 saturation and signal increase on BOLD MRI. In hypertensive hypertrophy,invasive Doppler flow-wire measurements have documented a blunted flow increase, which corresponds to lesser changes in venous O_2 saturation, and hence reduced signal changes on BOLD MRI. Because these patients were chosen to exclude the possibility of epicardial coronary artery disease, these novel findings, demonstrating reduced oxygen availability, support the presence of microvascular dysfunction in these patients.

References

1. Yang Z, et al. *Coronary Artery Disease* 1991; 2: 338–348.
2. Lebon V, et al. *Magnetic Resonance Imaging* 1998; 16; 7: 721–729.

Is Real-Time Imaging Ready for Quantitative Wall Motion Assessment?

S.J. Flacke, R.M. Setser, S.E. Fischer, C.H. Lorenz. *Center for Cardiovascular Magnetic Resonance, Cardiovascular Division, Barnes-Jewish Hospital, St. Louis, MO*

Introduction: Quantitative wall motion assessment with MRI has previously been shown with conventional ECG-triggered gradient echo cine imaging (1,2). Faster methods of MR image acquisition such as real-time imaging have recently been introduced, and preliminary studies suggest that real-time imaging is well suited for global LV volume and function assessment (3). However, for use in stress testing, real time imaging must have sufficient spatial and temporal resolution to assess regional wall motion. Therefore, as a first step to determine if real-time imaging could be a candidate for wall motion assessment during stress, we sought to compare regional wall thickening by real-time imaging with that derived from conventional cine imaging.

Materials and Methods: Eight subjects with no prior history of cardiovascular disease were imaged on a clinical 1.5T scanner (Gyroscan NT, Philips Medical Systems, Best, NL). Imaging consisted of scout scans to determine the 4-chamber view, followed by acquisition of twelve contiguous slices covering the left ventricle from apex to base. Two sequences were used, conventional ECG-triggered gradient echo and real time imaging. The conventional gradient echo cine sequence parameters were slice thickness 8-9 mm, no gap, TR700-800 ms, TE 5-6 ms, flip angle 35-40 degrees, 15-21 frames per R-R interval, and image resolution 1-2 mm. A segmented EPI sequence (4) was used for real-time imaging with the following parameters: slice thickness 8-9 mm, no gap, TE 3.6 ms, flip angle 30 degrees. EPI factor 11, 0.60 half scan factor, 128 × 70 matrix, 21 frames per slice at 62 ms/frame, and image resolution 2.7 × 4.5 mm. Triggering allowed the first image from each slice to be synchronized to the ECG (trigger delay 33 ms), but subsequent images in the series for each slice were not triggered.

Images were analyzed using the MASS software (Medis, Leiden, Netherlands), to manually define the endocardial and epicardial borders of each image. Care was taken to exclude epicardial fat, and ventricular trabeculae and papillary muscles were excluded. Wall thickness over time was computed using the centerline method for eight circumferential sectors of the myocardium. For each segment the area under the wall-time thickness curve (total area) and the area under the curve between enddiastole and end systole (area to peak) was calculated. Results were compared on a slice by slice and sector by sector basis between the real-time and conventional scanning methods. Differences were assessed using paired sample t-test, with $p < 0.05$ defined as significant.

Results: Figure 1 shows sample images from the conventional and real-time imaging studies. Note the more blurry image appearance of the real time image due to the decreased resolution and partial volume contribution of blood at the endocardial borders and epicardial fat at the outer circumference of the left ventricle. Both methods yielded similar overall average values in this group of young healthy volunteers with values of end diastolic wall thickness in the lower range of normal and an average peak systolic wall thickening of about 100%.

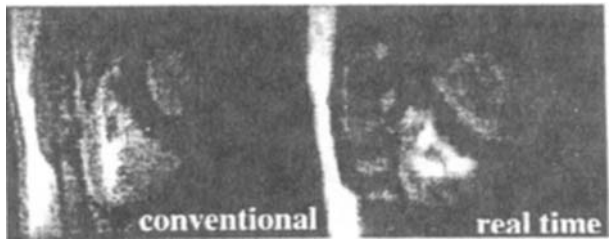

Figure 1. Representative image sample.

However, for single wall thickness measurement in a sector, differences of up to 35% were observed. The percent difference between the two methods for the computed values of each sector is listed in table 1 as mean ± SEM. These differences reached statistical significance for end systolic wall thickness ($p < 0.001$) and the area under the peak of the wall-time-thickness curve ($p < 0.001$).

Table 1. Indices of LV Wall Thickness, Area Under the Wall-Time Thickness Curve (Mean ± SEM) and Mean Percentile Differences Between Conventional and Real Time Imaging Sequences

n = 8	Conventional	Real Time	% Mean Differences
End systolic wall thickness [mm]	12.1 ± 1.95	12.5 ± 1.7	11.5 ± 8
End diastolic wall thickness [mm]	5.91 ± 1.14	5.83 ± 0.88	9.1 ± 7
Total area [mm/ms]	5071 ± 832	5168 ± 866	10.4 ± 9
Area to peak [mm/ms]	2840 ± 502	2673 ± 542	13.6 ± 12

Discussion and Conclusions: We have shown in human volunteers that 10% mean differences of wall thickness measurements are to be

to expected between the real time imaging method presented here and conventional imaging, the latter being considered as the reference method. Through plane motion, poorer resolution and increased partial volume artifacts of the real time images affect the precise detection of endocardial and epicardial borders during contraction and relaxation. The real time sequence used here allows gross evaluation of wall motion. Clinical evaluation will be required to determine if the present method is acceptable for detecting changes in regional wall motion during stress testing, for example. However, if accurate quantitative wall motion assessment is required, spatial resolution will likely need to be increased over that presented here.

References

1. Sechtem U, et al. *Am J Cardiol* 1987; 59: 145–51.
2. Baer FM et al. *JACC* 1998; 31: 1040–47.
3. Setser RM, et al. *Proc ISMRM* 1999
4. Fischer SE, et al. *J Cardiovase Magn Reson J* 1999; 89.

Non-Invasive Evaluation of Endothelial Function Measured as Flow Mediated Changes in Area, Flow and Wall Shear Stress Using MRI

M.S. Hansen, H.G. Flaagoy, S. Oyre, E.M. Pedersen. *Dept. of Cardiothoracic & Vascular Surgery T, MR Research Center and Inst. for Exp. Clin. Research, Aarhus University Hospital, Denmark*

Background: Endothelial dysfunction (reduction of the ability of the endothelium to induce a dilation of a vessel) is an early event in atherogenesis. The methods for evaluation of endothelial function, by estimating flow mediated dilation, are either invasive or based on ultrasound (1,2). The invasive methods are not well suited for repeated studies, and current ultrasound techniques have limited accuracy and measures only the diameter of the vessel to estimate the area dilation. We suggest a new MR-based method, for evaluation of endothelial function, that estimates cross sectional vessel area as well as the hemodynamic parameters flow and wall shear stress (WSS) using the multiple sectored three dimensional paraboloid method (MS3DP) (3). WSS is the proposed stimulus for the flow mediated dilation.

Methods: 7 healthy, non-smoking, young volunteers (age 25 ± 4) were studied by MRI. Phase contrast flow measurements (standard gradient echo sequence, FOV = 51 mm, Matrix = 128, TE = 13 ms, 9 cm circular surface coil) were acquired in the brachial artery. Three baseline measurement were made before a cuff was inflated around the upper arm (300 mmHg for 5 min.). 10 measurement were made at an interval of 128 heartbeats after release of the cuff. The velocity data from peak systole were fitted to a paraboloid using the MS3DP method (24 sectors around the vessel circumference, sector angle 120°, edge layer 0.7 mm) (3), and the cross sectional vessel area was estimated.

Results: The mean baseline cross sectional vessel area was 15.53 mm^2 (diameter = 4.45 mm, area range 9.74 − 22.19 mm^2). This area was significantly (paired t-test, $p < 0.05$) increased throughout the measuring period following the cuff release (Fig. 1). WSS varied around the vessel circumference with an identical pattern before and after cuff release and, was significantly reduced after 256 heartbeats. Flow was not significantly changed. Parabaloid fit statistics showed a mean R^2 = 0.91 (range 0.81 − 0.96) and SD = 0.04 m/s (range 0.03 − 0.08 m/s). The average eliptic component was 6%.

Conclusion: Endothelium dependent vasodilation can be quantified with phase contrast MRI and the MS3DP method. The vessels remained dilated throughout the measuring period in concordance with a previous study (2). The presented method estimates ellipsoid cross sectional vessel area instead of diameter as in the ultrasound evaluation. In addition this study reports the first MRI-based WSS measurements in the brachial artery after flow mediated dilation. It was seen that peak systolic WSS was significantly reduced 256 heartbeats after cuff release whereas volume flow was not significantly changed. Together with the percisting vessel area dilation throughout the measuring period, this indicates a protracted feedback mechanism for the flow mediated response. The MS3DP method is a possible alternative to ultrasound, with potential for measuring not only area changes, but also the hemodynamic aspects of flow mediated endothelial responses, throughout the cardiovascular system.

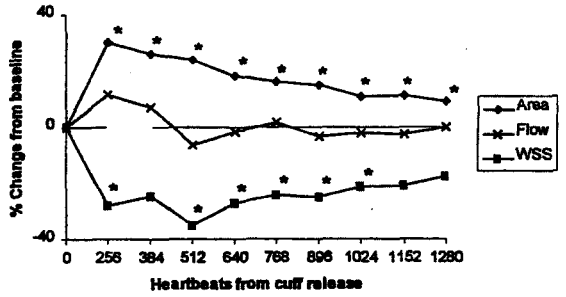

Figure 1. Relative change of area, flow and wall shear stress over time from cuff release. *Significant change from baseline.

References

1. Celermajer DS et al.: *Lancet* 1992; 340: 1111–1115.
2. Corretti, MC et al.: *Am J Physiol* 1995 Apr; 268(4 Pt 2): H1397–404, 3. Oyre S et al.: *Magn. Reson. Med.* 1998; 40: 645–655.

Brachial Artery Reactivity by Cardiovascular Magnetic Resonance

Morten Sorensen,[1] Paul Ong,[2] Carolyn Webb,[2] Christopher Hayward,[2] Peter Gatehouse,[1] Peter Collins,[2] Dudley Pennell.[1] [1]*CMR Unit and* [2]*Cardiology, Royal Brompton Hospital, London, UK*

Background: Measurement of changes in brachial artery diameter by external ultrasound (EXUS) in response to flow mediated dilation (FMD) and nitrate (together brachial artery reactivity-BAR) is widely used to assess vascular function (1). Cardiovascular Magnetic Resonance (CMR) has not been used to measure these changes.

Methods: Brachial artery cross sectional area change in response to reactive hyperaemia, as a measure of endothelial function, (2) was imaged by segmented FLASH (Figure) and measured manually by CMRtools™.

In 8 patients undergoing coronary angiography, BAR was measured by intravascular ultrasound (IVUS) and subsequently compared with CMR and EXUS. Inter-study variability of FMD was assessed by repeated measurements in 10 (CMR) and 9 (EXUS) healthy subjects.

Results: BAR by IVUS correlated with CMR ($r = 0.75$ $p < 0.01$) and EXUS ($r = 0.72$ $p < 0.01$). FMD by CMR area was less in patients ($n = 5$) with coronary artery disease compared to patients ($n = 3$) without disease (4.4% vs. 13.1%, $p = 0.01$), whereas the differences by EXUS diameter were not significant (0.5% vs. 1.9%, $p = 0.29$). FMD by CMR area was significantly larger in magnitude than by EXUS diameter (6.7% vs. 1.1%, $p < 0.03$). The inter-study variability of FMD by CMR was 10% compared with 39% by EXUS. The brachial artery showed significant shape asymmetry (major vs minor diameter: 4.8 mm vs. 4.3 mm. $p < 0.01$).

Conclusion: Vascular function is accurately assessed by CMR, and this has some advantages over EXUS including: improved reproducibility permitting smaller sample sizes to detect significant changes; direct measurement of area and greater magnitude of area change than diameter change, potentially allowing greater sensitivity; and robustness to non-circularity of the brachial vessel allowing avoidance of potential errors that might result during non-uniform dilation. CMR is a promising new technique for non-invasive determination of vascular function.

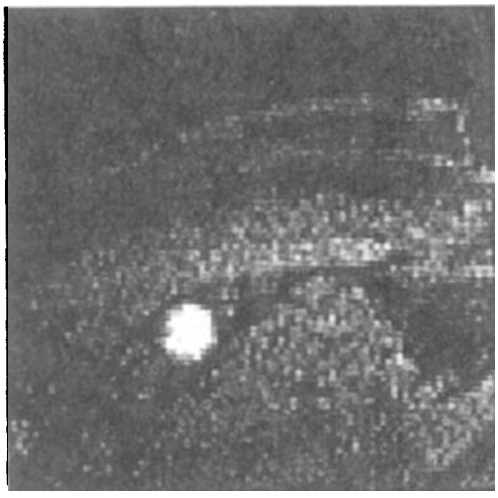

Future improvements of the technique includes semi-automated vessel wall detection and measurement of both flow velocity and area change in response to reactive hyperaemia (3).

References

1. Celermajer DS, Sorensen KE, Gooch VM, et al. *Lancet* 1992; 340 (8828): 1111–1115.
2. Pohl U, Holtz J, Busse R, Bassenge E. *Hypertension* 1986; 8(1): 37–44.
3. Mohiaddin RH, Gatehouse PG, Yang GZ, et al. *Proc 7th ISMRM*, 1999 (abstract).

The Devereux Equation for Calculation of Left Ventricular Mass: Comparison with Simpson's Rule Using Cardiac Magnetic Resonance Imaging

S.G. Myerson, D.J. Pennell. *CMR Unit, Royal Brompton Hospital, London, UK*

Introduction: Left ventricular (LV) hypertrophy is associated with significant excess mortality and morbidity. Studying the prognostic implications of LV mass reduction is hindered by the poor accuracy and reproducibility of LV mass measurement by echocardiography. Part of the problem with echocardiographic LV mass measurement is that measurements are only made of the wall thicknesses and internal diameter at one site and LV mass is calculated using an assumed geometric shape. Small (<1 mm) differences in measurement can have large effects on the calculated mass due to the cubing involved in the equation. We sought to compare the Devereux equation with a standard technique of LV mass measurement using cardiac magnetic resonance (CMR), which has shown to be highly accurate and reproducible.

Method: 219 young male Army recruits had cardiac magnetic resonance scans performed both before and after an identical physical training programme. LV mass was measured by the standard technique of summing myocardial volumes from multiple short axis image slices (employing Simpson's rule), thus measuring the myocardium directly without calculations. Measurements were also made of the septal and posterior wall thicknesses and internal diameter from the basal slice, corresponding to the measurement position for echocardiography at the level of the chordae tendonae. These were used in the Devereux equation to calculate LV mass and the results compared with the standard technique.

Results: Mean (±standard deviation) LV mass measurements pre-training were 182.9 ± 26.7 and 199.3 ± 44.5 g for standard and Devereux methods respectively. Bland-Altman plots showed the 95% limits of agreement between the two techniques pre-training to be ±71.1g (35%) with a mean difference of +16.6g (7.3%). Post-training values were similar with a 95% limit of agreement of ±62.4g (31%) and a mean difference of +15g (6.6%). The standard technique showed a mean increase of 8.6 ± 13.9g ($p < 0.0001$) compared to 10.0 ± 35.9g ($p = 0.0007$) using the Devereux method. The limits of agreement for the change in LV mass were similar: 95% limit ±67.9g. In addition, there was a systematic trend for the Devereux method to overestimate LV mass at higher values and underestimate the lower LV mass values, both pre and post-training and particularly for the change in LV mass

LV mass by the Devereux method correlated reasonably with the standard technique both before and after exercise training ($r = 0.58$, 95% C.I. 0.48–0.66; $p < 0.0001$ and 0.62, 95% C.J. 0.51–0.71; $p < 0.001$ respectively), with poor correlation of the change in LV mass ($r = 0.24$, 95% C.I. 0.08–0.38, $p = 0.04$). The correlation coefficient is however only a measure of the linearity of the relationship between two variables and would thus be expected to be high for two techniques measuring the same variable. It does not indicate anything about the differences between techniques, for which Bland-Altman plots are more appropriate.

Conclusion: Despite the excellent image quality of CMR images, calculations of LV mass using the Devereux equation show large variations from that obtained by direct measurement of the whole ventricle. This is worse for measuring a change in LV mass, in which there is poor correlation and even larger proportional differences with consequent loss of the ability to detect a small change. These results suggest that the assumption of uniform geometric shape in the calculation is incorrect and leads to significant measurement error. The technique can not be recommended for LV mass measurement, either at a single time point or for serial studies.

The Detection of Small Differences in Left Ventricular Growth with CMR: A Randomised Controlled Trial Examining the Angiotensin Converting Enzyme Gene I/D Polymorphism

S.G. Myerson,[1] D.J. Pennell,[1] M. Whittingham,[2] M. Jubb,[2] M.J. World,[2] H.E. Montgomery,[3] S.E. Humphries.[3] [1]*CMR Unit, Royal Brompton Hospital,* [2]*Royal Army Medical College,* [3]*UCL Dept. Cardiovascular Genetics, London, UK*

Background: Left ventricular (LV) hypertrophy is associated with a significant excess cardiovascular mortality and morbidity, although the mechanism underlying the association remains unclear. It has previously been suggested that the deletion (D) rather than the insertion (I) variant of the human angiotensin I-converting enzyme (ACE) gene is associated with higher local myocardial ACE levels, and an increased LV hypertrophic response to exercise. It is thus possible that local tissue ACE expression might account in part for the relationship between LV hypertrophy and cardiovascular risk, and an understanding of the mechanism by which the D allele is related to LV growth response is of importance. Small group differences in left ventricular growth, such as might be expected from a single gene polymorphism, are difficult to detect with confidence and require an accurate and reproducible technique, such as cardiac magnetic resonance (CMR). We sought to confirm the ACE gene I/D polymorphism effect on LV growth and clarify the role of the angiotensin AT_1 receptor, using CMR as the measurement tool.

Method and Results: 141 British Army recruits, homozygous for the ACE gene (79 DD, 62 II), were randomised to receive either losartan (25 mg/day: a sub-hypotensive dose which inhibits tissue AT_1 recep-

tors) or placebo throughout an identical 10-week physical training programme. The study was conducted as a prospective parallel-arm double-blind randomised controlled trial. LV mass was determined by CMR both before and after training. Exercise training was associated with a significant increase in LV mass (8.4g; $p < 0.001$ for the group overall). In the placebo arm, those of DD genotype had a mean increase in LV mass of 12.1g vs. 4.8g for the II genotype ($p = 0.022$). LV growth in the losartan arm was similar: 11.0g vs. 3.7g for DD and II genotypes respectively ($p = 0.034$). The differences between losartan and placebo in either genotype were not significant.

Conclusions: We have confirmed the association of ACE I/D genotype with exercise-induced LV hypertrophy. Losartan in low dose had no effect on LV growth, suggesting that this is mediated via mechanisms other than cardiac angiotensin II AT_1 receptors. The modest changes in LV growth in this study and the small (≈7g) differences between groups were identified with CMR. To detect this difference with echocardiography with 90% power would have required close to 400 subjects in each group compared to 30–40 in this study. This confirms CMR as a powerful tool for examining serial changes in LV mass, as would be required to assess the prognostic implications of LV mass reduction on cardiovascular health.

Reproducibility of Magnetic Resonance Body Composition Analysis and Relevance to Cachexia in Heart Failure

S.G. Myerson, D.J. Pennell. *CMR Unit, Royal Brompton Hospital, London, UK*

Patients with severe cardiac failure who experience profound weight loss ('cardiac cachexia') have a high mortality, independent of other risk factors, and considerable morbidity due to muscle wasting (1,2). The adverse clinical outcomes associated with this condition appear to be due to the loss of lean body mass rather than weight loss itself. While the exact pathogenesis is unclear, immune activation and a catabolic hormonal state play important roles (3). The investigation and attempted treatment of this serious condition are aided by the ability to measure body composition (fat and lean mass) accurately. Abdominal subcutaneous and visceral adipose tissue (AT) are also closely correlated with risk factors for ischaemic heart disease and intra-abdominal fat deposition is a much greater predictor of cardiovascular risk than total obesity.

Thus, the accurate quantification of body composition, including lean body mass and visceral AT is important for determining cardiovascular risk. Magnetic resonance (MR) is an ideal imaging modality, with excellent contrast between adipose and other tissues on spin-echo images and the possibility of regional fat segmentation. Accurate methods have been developed for MR body composition imaging, though the reproducibility of such measurements is of greater importance for studies and clinical situations examining serial changes in body composition and to date, this has not been addressed. This is particularly important for visceral AT, with image degradation from respiratory motion and the diffuse nature of the fat deposition. Lean subjects are especially difficult given the small amount of fat involved.

We developed an automated image processing technique for segmenting AT without a reference phantom, which was also designed to overcome variations in signal intensity across the image due to varying bias field. We examined the reproducibility of abdominal AT quantification using this technique. 10 healthy volunteers (body mass index 19.2 to 29.2 kg/m^2) had repeated MR scans of the abdominal region (diaphragm to perineum) performed on the same day. Adipose tissue quantification was determined and the paired sets from each subject compared (test-retest reliability). The mean values (±S.D.) for total, subcutaneous and visceral AT were 6.65 (±3.28), 5.16 (±2.25) and 1.48 (±1.18) kg respectively. The mean differences (mean %difference) between repeated scans were: total AT: 0.17 kg (2.9%); subcutaneous AT: 0.12 kg (2.7%) and visceral AT: 0.09 kg (8.0%). The repeated values were highly correlated ($r > 0.99$; $p < 0.0001$ for all three measurements), with Bland-Altman plots showing 95% confidence limits for total AT: ±0.40, subcutaneous AT: ±0.26 and visceral AT: ±0.21 kg. These results show excellent reproducibility of the technique, with differences of <0.2 kg for total AT and <0.1 kg for visceral AT between scans. This technique has considerable potential value in studies of the natural history of cardiac cachexia and longitudinal studies of its treatment.

References

1. Anker SD, Ponikowski P, Varney S, et al. Wasting as an independent risk factor for mortality in chronic heart failure. *Lancet* 1997; 349: 1050–1053

2. Anker SD, Coats AJS. Cardiac cachexia: a syndrome with impaired survival and immune and neuroendocrine activation. *Chest* 1999; 115: 836–847

3. Anker SD, Chua TP, Ponikowski P, et al. Hormonal changes and catabolic/anabolic imbalance in chronic heart failure and their importance for cardiac cachexia. *Circulation* 1997; 96: 526–534

Morphological Characterisation of the Right Ventricle in Patients with Left-Bundle-Branch Configured Ventricular Irrhythmia by Magnetic Resonance Imaging

U. Sprengel,[1] N. Oesingmann,[2] C. Müller,[1] A. Rad,[1] T. Dill,[1] A. John,[1] J. Neuzner,[1] H. Pitschner,[1] W. Ricken,[1] Ch. Hamm.
[1]*Kerckhoff-Clinic, Dep. of Cardiology, Bad Nauheim, Germany;*
[2]*Siemens, Erlangen, Germany*

Background: The aim was to characterize the right ventricular myocardium (RVM) in patients with left-bundle-branch (LBB) configured ventricular arrhythmia (VA). These patients underwent 2D-echocardiography and electrophysiological investigation (EPI) to localize the focus of the ventricular arrhythmia. MRI was used to answer whether or not an abnormal fat structure of the right ventricular myocardium correlates with the localization of the arrhythmic substrate.

Method: 227 patients with LBB-configured ventricular arrhythmia underwent MRI (1.5 T Vision, cp-body-array-coil, Siemens). The following sequences were used in corresponding position and orientation:

1. single-slice dark-blood prepared T_1-weighted TSE in breathhold technique (BHT), with and without fat saturation in 4-chamber- and short-axis-view (TR = 0.9 RR, TE = 7 ms, TH = 6 mm). (Fig. 1)
2. single-slice inversion-pulse prepared TSE (TIRM) in breathhold technique (TR = 0.9 RR, TE = 8 ms, TH = 6 mm). The inversion time TI was varied in order to change the T_1-dependent contrast of fat and normal myocardium. (Fig. 2:)
3. Segmented 2D-Flash (CINE) (TR = 80 ms, TE = 4.8 ms, α = 20°, TH = 6 mm) to assess the contractility of the myocardium and aneurysmatic dilations. (Fig. 3)

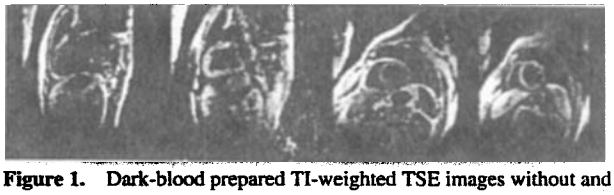

Figure 1. Dark-blood prepared TI-weighted TSE images without and with fat-saturation in 4-chamber- and short-axis-view.

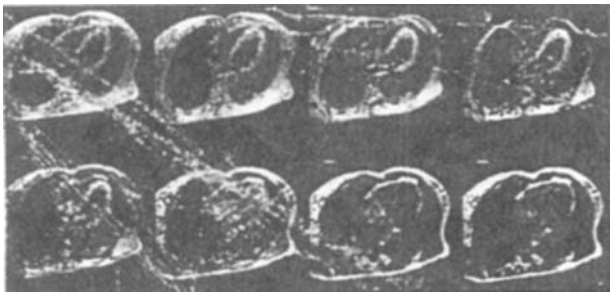

Figure 2. Dark-blood-prepared diastolic IR-TSE images of the heart with different inversion times TI.

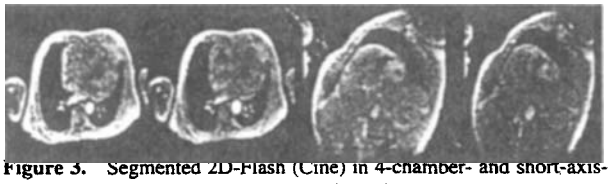

Figure 3. Segmented 2D-Flash (Cine) in 4-chamber- and short-axis-view of the heart in patient with RV-dyplasia.

Results: The origin of LBB-configured ventricular arrhythmia could be detected in the right ventricle by EPI in 87 of 227 patients. 76 of these patients showed neither contractile nor morphological changes of the right ventricle. 2 patients had a chirurgical corrected transposition of the great vessels, 5 showed a dilated right ventricular outflow tract. In 6 patients the criteria of a right ventricular dysplasia were fulfilled. In 2 of these patients with dysplasia of the right ventricle fat tissue could be doubtlessly detected in the right ventricle.

Conclusion: The used combination of sequences allows to detect reliably fatty infiltrations of the myocardium. The frequency of fatty tissue in the right ventricule of patients with LBB configured ventricular arrhythmia as described in literature cannot be observed in our study.

References

1. C. Ricci et. Renata Longo et. al.: *Am J Cardiol* 1992; 70: 1589–1595.
2. Waufermann, T. Wichter, et. al.: *AJR* 1993; 161: 549–555.

How Good Is Qualitative Analysis of 1st Pass Gd-DTPA Multislice Myocardial Perfusion Imaging for Clinical Evaluation?

D.C. Bloomgarden, P. Storey, W. Li, M. Zhang, L. Li, P. Prasad, R. Edelman. *Beth Israel Deaconess Medical Center, Boston, MA*

Introduction: Early experience with 1st pass Gd-DTPA enhanced MR imaging of the myocardium has produced mixed results. Qualitative analysis suffers from variable signal due to surface coil effects and bolus waveform. Quantitative analysis is subject to errors due to low signal-to-noise, motion due to breathing and misgating, and blooming effects from bright blood in the LV cavity. With image post-processing, the human eye may be able to compensate for some of these effects. We report on our experience with qualitative analysis of the 1st pass imaging.

Methods: Cardiac MR was performed on 35 patients undergoing evaluation for experimental myocardial reperfusion studies. All patients had stress (pharmacological) Sestamibi and rest Thalium SPECT imaging and cardiac catheterization within 1 week of the MR examination. The MR examination consisted of multislice (3) saturation recovery fast, TURBO-FLASH imaging. Images were acquired every heartbeat for 40 consecutive beats, while patients held their breath as long as they could. Separate 1st pass MR imaging was performed before and after administration of a pharmacological stress (via IV infusion of 0.142 mg/kg/min dipyridamole over 4 minutes). A minority of patients who experienced typical anginal symptoms required reversal with 125 mg Aminophylline. Image parameters were TR = 2.4ms; TE = 1.1; α = 15°. Qualitative analysis was performed on a subset (n = 5) of patients, by simultaneously viewing the perfusion images from all slices in a "movie" loop display. The myocardium was divided into 12 segments, four regions for each slice. Similar analysis was performed on the SPECT imaging by independent Nuclear Medicine physicians.

Results: Figure 1 show sample images from our MR perfusion studies and stress Sestamibi SPECT images from the same patient. These images demonstrate the same abnormality on the MR and the radionuclide study, however, a larger ischemic region is visualized on the MR images. All evaluated patients had diagnostic quality examinations. No adverse reactions occurred in any of the 24 patients who had dipyridamole in the scanner. Four of 4 perfusion defects identified on Thalium scans were seen on the baseline MR perfusion studies. The number of abnormal segments differed by up to three segments in extent between lesions. More lesions were seen with stress MR than with Sestamibi scanning, although one lesion was missed with MRI.

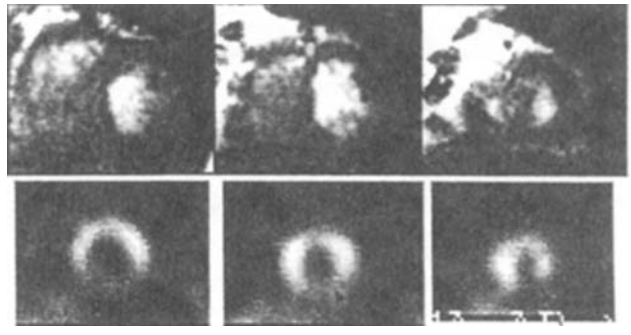

Figure 1. MR perfusion images from TURBO-FLASH, 1st-pass Gd-DTPA sequence and corresponding Sestamibi SPECT from a patient with inferior wall ischemia. The MR images show a larger area of abnormality throughout the entire lateral wall.

Discussion: Careful qualitative analysis of multislice perfusion images at rest and stress does demonstrate areas of myocardial ischemia and infarction. However, there remains important issues regarding optimization of image acquisition strategies and protocols. In particular, can images be acquired with two separate contrast injections (rest and stress) during one study (i.e. within 30 minutes)? Our experience suggests that passive diffusion of Gd-DTPA into infarcted zones may lower sensitivity. Is quantitative analysis superior to the human eye for picking up subtle increases in arrival time and decreases in peak intensity? Cardiac and respiratory motion, as well as "blooming" artifacts may adversely effect computerized analysis, while an experienced observer may be able to compensate for these artifacts. Finally, can new and faster imaging techniques enhance the conspicuity of these lesions. The strengths and limitations of our imaging protocol and analysis will be discussed.

Conclusion: Our limited experience with qualitative analysis of 1st pass perfusion imaging suggests that MR may have a role in the evaluation of patients with advanced or multi-vessel CAD.

References:

1. Wilke N, Jerosch-Herold M. *Card Clin* 1998; 16: 227–246.
2. Penzkofer H. Wintersperger. et al., *Magn Rec Imag:* 1999; 17: 161–170.
3. Lauerma K. Virtanen KS, et al. *Circ.* 1997; 96: 2859–2867.

Carbon Metabolism and Substrate Preference of the Heart as Observed Non-Invasively by In Vivo ^{13}C-Magnetic Resonance Spectroscopy in the Intact Rat

A. Ziegler,[1,2] P.T. Buser,[2] C.E. Zaugg,[2] J. Seelig,[1] B. Künnecke.[3]
[1]*Biocenter,* [2]*University Hospital,* [3]*Hoffman-La Roche; Basel, Switzerland*

Introduction: Various diseases of the heart are associated with a remarkable change in myocardial carbon metabolism and energy substrate preference such as ischemic heart disease, hypertrophy, or diabetes (1). However, the detection of such metabolic alterations and a consequent therapy is limited by the lack of appropriate modalities to assess myocardial carbon metabolism and substrate preference in the intact body. Two available in vivo methods, the invasive technique of arterio-venous difference and the radioactive Positron Emission Tomography, infer metabolism both only indirectly, since intracellular metabolites cannot be evidenced or distinguished from administered substrates. In this context, ^{13}C-Magnetic Resonance Spectroscopy (MRS) has long proven an invaluable tool for assessing carbon metabolism non-invasively in isolated beating hearts and in open-chest models with distinct assessment of substrates and metabolites (2). However, these applications are restricted to surgery, open-chest preparations or tissue biopsies. The present study shows for the first time, that ^{13}C-MRS can assess myocardial carbon metabolism likewise in the intact body.

Materials and Methods: Anesthetised male Sprague-Dawley rats (220 g) were cannulated in the tail vein. Mixtures of different ^{13}C isotopomers of glucose, 3-D-hydroxybutyrate, and acetate in isotonic NaCl solution were infused and the cardiac metabolism was assessed by in vivo ^{13}C-MRS in the intact animal. In vivo ^{13}C-MRS was performed at 7 Tesla on a Bruker Biospec 70/20 spectrometer using a surface coil for signal excitation and reception. Blocks of 300 scans (6 min) were recorded in the pulse-acquire mode using an adiabatic 90° BIR pulse, a spectral width of 250 ppm, and 4k data points. Broadband proton decoupling during the acquisition and NOE were effectuated with a whole body ^{1}H resonator. Signals from superficial tissues were minimised by a saturation slice in the ^{13}C frequency domain which was placed on the chest wall. All acquisitions were respiration- and ECG-gated.

Results: The use of labelled glucose (glc), 3-hydroxybutyrate (βhb), and acetate (ac) as substrates provided specific markers for the glycolysis, ketone body-oxidation, and the direct incorporation of C_2 units into the tricarboxylic acid (TCA) cycle, respectively. Their ^{13}C isotopomer composition was chosen such as to readily label all the primary cardiac metabolites. Indeed, shortly after the start of the infusion, intense resonances of substrates and cardiac metabolites. Indeed, shortly after the start of the infusion, intense resonances of substrates and cardiac metabolites appeared as a result of cellular activity. Glutamate C4 became enriched very rapidly and reached a steady-state level after 30 minutes. Glutamate C3 became also strongly labelled, however at a substantially slower rate. The time difference of the ^{13}C label incorporation into various glutamate isotopomers provided a non-invasive measure of the cardiac TCA cycle activity in situ.

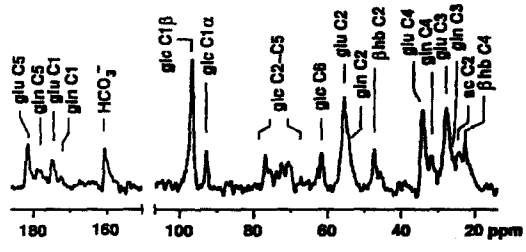

The labelling patterns detected at steady-state allowed the cardiac substrate selection to be evaluated in situ. Figure 1 depicts a representative in vivo ^{13}C-NMR spectrum of the heart (1200 scans, 23 min) acquired after 2 hours of infusion of the three labelled substrates. Strong resonances of the metabolites glutamate (glu), glutamine (gln) and bicarbonate (HCO_3^-) are clearly visible. The same experiment was repeated under identical conditions, however with different combinations of ^{13}C isotopomers in the infusion mixture. The combined data of all labelling experiments suggested that the heart in situ readily metabolised 3-hydroxybutyrate and acetate. In contrast, glucose contributed only negligibly to the cardiac metabolism although it was well extracted from the blood stream and accumulated in the heart.

Conclusion: In the present study, we have demonstrated that ^{13}C-MRS of the rat heart in situ is well feasible at high field strength without the need for surgery. The use of specifically ^{13}C labelled substrates allowed the cardiac TCA cycle activity as well as cardiac substrate preference to be assessed in the intact body. Our data suggest that glucose is not a major substrate of the non-ischemic heart.

References

1. Opie LH, *Cardiovasc Res*, 1992 Aug. 26: 721–33.
2. Künnecke B, C-13 NMR Spectroscopy of Biological Systems, ed. N. Beckmann, Academic Press, 1995.

Clinical Validation of an Automated Boundary Tracking Algorithm on Cardiac Magnetic Resonance Images

L.A. Latson.[1] B. Sturm,[2] K.A. Powell,[3] P.R. Schvartzman,[3] R.D. White.[3] [1]*Case Western Reserve Cleveland,* [2]*The Ohio State University,* [3]*The Cleveland Clinic Foundation, Cleveland, OH*

Background: The goal of this research was to develop an automated algorithm for tracking the borders of the left ventricle (LV) in a cine-MRI gradient-echo temporal data set. The algorithm was validated on four patient populations: healthy volunteers, patients with concentric dilated cardiomyopathy, left ventricular hypertrophy, and left ventricular aneurysm.

Methods: A full tomographic set (~11 slices/case) of short-axis images through systole was obtained for each patient. Initial endocardial and epicardial contours for the end-diastolic (ED) and end-systolic (ES) frames were manually traced on the computer by the most experienced investigator. The ED tracings were used as the starting point for the algorithm. The borders were tracked through each phase of the temporal data set, until the ES frame was reached (~7 phases/slice). Peak gradients along equally spaced chords calculated perpendicular to a centerline determined midway between the endocardial and epicardial borders (1) were used for border detection (Figures 1). A linear regression was used to compare the LV epicardial and endocardial volumes calculated at ES by the algorithm and by the expert tracer.

Results: The results of the algorithm compared favorably with both the endocardial (r^2 = 0.72 – 0.98) and epicardial (r^2 = .96 – .99) volumes of the tracer in the four groups evaluated (Table 1). An example contour is shown in Figure 2.

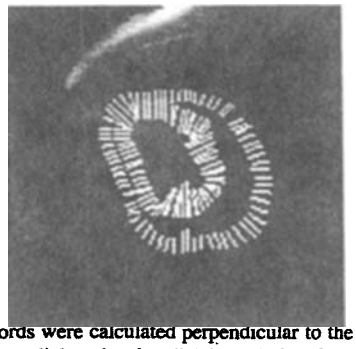

Figure 1. Chords were calculated perpendicular to the centerline between the endocardial and epicardial boundaries. Then the gradient along each chord was calculated. Each chord was divided into two search segments and the point with the highest gradient within each segment was selected as the boundary point.

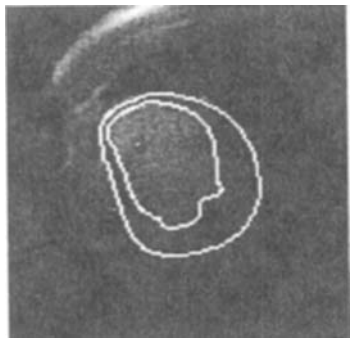

Figure 2. An example of the final contours at end-systole from a patient with left ventricular aneurysm.

Table 1 A Linear Regression was Used to Compare the End-Systolic Endo- and Epicardial Volumes Calculated by the Algorithm to Those of the Experienced Tracer. The r^2 Values are Presented Here

r^2 Values, Volumes by Algorithm vs. Tracer Patient Population	Endo	Epi
Normal	0.87	0.98
Concentric dilated cardiomyopathy	0.98	0.99
Left Ventricular aneurysm	0.75	0.96
Left ventricular hypertrophy	0.72	0.98

Conclusion: We have developed an accurate, robust, and relatively fast semi-automated algorithm for tracking endocardial and epicardial borders in cine-MRI temporal data sets. The resulting calculations are useful in assessing ventricular myocardial mass and function (i.e. ejection fraction). Using this algorithm we were able to successfully track the myocardium in healthy volunteers and in patients with morphologically abnormal hearts.

References

1. Sheehan FH, Bolson EL, et al. *CIRC* 1986; 74: 293–305.
2. Latson LA, Powell KA, et al. In: *Computers in Cardiology* 1998; 741–744.

Selective β-1 Blockade Improves Left Ventricular Energy Status, Systolic and Diastolic Function in the Rats with Postinfarct Heart Failure

E. Omerovic, E. Bollano, M. Basetti, V. Kujacic, Å. Hjalmarson, B. Soussi, F. Waagstein. *Wallenberg and Lundberg Laboratories, Sahlgrenska University Hospital, Göteborg, Sweden*

Background: The results from recent clinical studies support the concept of β-blockade in congestive heart failure (CHF). However, the mechanisms for the beneficial effects of β-blockade in CHF are incompletely understood. The aim of this study was to investigate the effects of selective β_1-blockade on left ventricular (LV) energy status and function in rats during early postinfarct remodeling phase.

Methods: Male Sprague-Dawley rats body weight (BW) 200–250 were used. Myocardial infarction (MI) was induced by ligation of the left coronary artery. Two different groups of rats were studied: rats with MI treated with metoprolol (5mg/kg/h; n = 8) during 4 weeks and rats with MI placebo treated (n = 6). All rats were investigated with ^{31} P MRS and transthoracic echocardiography (ECHO) 3 days (3d) and 4 weeks (4w) after induction of MI. Infarct size was estimated by ECHO and only rats with large MI were selected. Volume-selective ^{31}P MRS was performed on 20 cm bore, 2,35T Bruker Biospec BMT 24/30 magnet using cardiac gated ISIS (Image Selected in Vivo Spectroscopy) method.

Results: The results are summarized in the table. Treatment with metoprolol increased LV PCr/ATP ratio indicating improved myocardial energy reserve. At the same there was improvement in parameters reflecting LV systolic and diastolic function in the rats treated with metoprolol compared to the placebo group.

	PCr/ATP	EF%	DT ms	HR beats/min
Metoprolol	1.2 ± 0.09*	3.4 ± 1.8*	17 ± 03*	−168*
Placebo	0.04 ± 0.056	−9.66 ± 1.8	3 ± 03	−73

The values represent the means ± SEM of the difference before and after the treatment, * = $p < 0{,}05$ v. placebo, PCr/ATP = phosphocreatine/adenosine-3-phosphate ratio, EF = ejection fraction, DT = deceleration time of mitral E-wave, HR = heart rate

Conclusion: Selective β_1-blockade improves myocardial energy status in the rats during early postinfarct period. The benefitial effect on cardiac bioenergetics may be an important mechanism for the improvement in LV systolic and diastolic function.

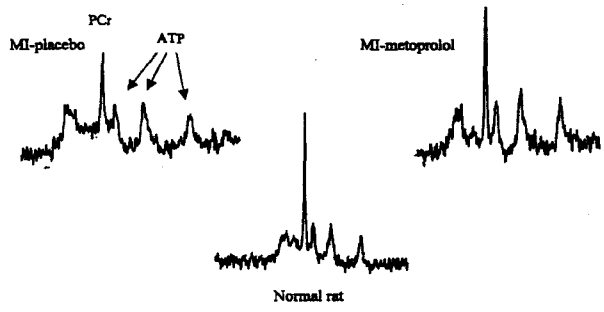

New Protein Binding Gd Chelate with High Vascular Containment for MR Coronary Angiography

Friedrich M. Cavagna,[1] Jie Zheng,[1] Vito Lorusso,[1] Fabio Maggioni,[1] Debiao Li,[2] Paul J. Finn.[2] [1]*Milano Research Center, Bracco S.p.a., Milano, Italy;* [2]*Northwestern University, Dept. of Radiology, Chicago, IL*

Successful contrast enhanced Magnetic Resonance Coronary Angiography (MRCA) will probably hinge on Inversion Recovery 3D Gradient Recalled Echo (IR-3D GRE) sequences and on the availability of intravascular contrast agents.

A key requirement for such agents will be the ability to strongly relax blood while only nulling myocardium at the end of the inversion time (TI). Short repetition times (TR ~ 3 ms) will be mandatory to allow for coverage of the vascular tree with good resolution in a clinically acceptable time.

We present preclinical data and initial experience with MRCA on pigs with a new intravascular contrast agent coded B-22956/1, a low molecular weight gadolinium chelate with unprecedented binding to serum proteins (94% for a 0.5 mM solution in Seronorm®) and vascular containment.

Blood T_1 measured in vivo at 1.5 T in pigs after 0.1 mmol/kg of B-22956/1 was below 100 ms for about 25 min and increased onlyslowly afterwards, while myocardial T_1 was much longer and showed only little change over time [Fig. 1].

Consequently, Multiplanar Reconstructions obtained from Navigator Echo driven MRCA on pigs with IR-3D GRE sequences (TR/TE/TI/α: 3.5 ms/1.8 ms/180 ms/22°), the Right Coronary Artery (RCA) could be clearly delineated up to 1 h after 0.1 mmol/kg of B-22956/1 [Fig. 2].

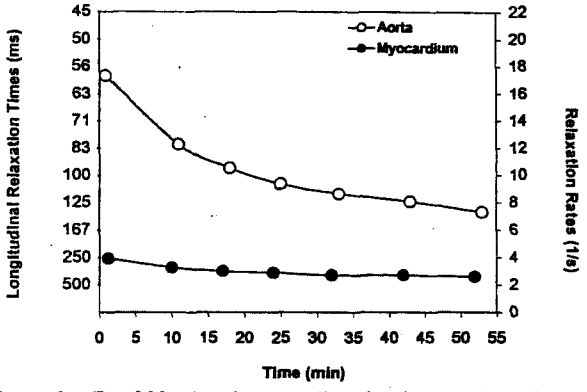

Figure 1. T_1 of blood and myocardium in pigs at 1.5 T after 0.1 mmol/kg of B-22956/1.

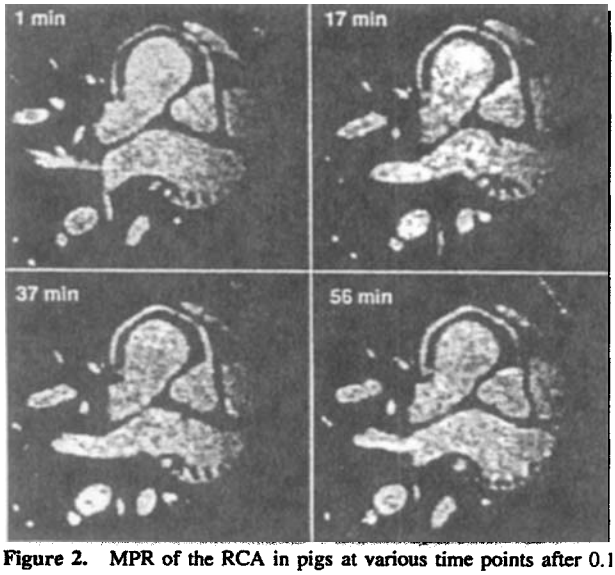

Figure 2. MPR of the RCA in pigs at various time points after 0.1 mmol/kg of B-22956/1.

Functional State of Collateral—Dependent Myocardium Assessed by Quantitative MR Tissue Tagging and Segmental Function Analysis

N.M. Wilke,[1] A. Zenovich,[1] J. Rodenwaldt,[1] Y. Huang,[1] A.M. Mansoor,[1] H. Huang,[1] F. Zhao,[1] M. Jerosch-Herold,[1] M. Urness,[1] L. Axel,[2] [1]*MR Core Laboratory, Department of Radiology;* [2]*University of Minnesota Medical School, Minneapolis, Minnesota;* [3]*University of Pennsylvania, Pittsburgh, PA*

Background: Clinical manifestations of coronary artery disease (angina, infarction) imply a course of gradual development of stenosis in one or more coronary arteries. Noninvasive assessment of the impact of the developing stenosis on the myocardium in terms of its effect on regional myocardial blood flow (MBF) and segmental contractility may provide better understanding of the course of stenosis and may have prognostic implications. It is known that stimulation of native collateral growth occurs when MBF is downregulated (1). However, how the gradual decrease of MBF affects segmental function of the myocardium is not completely understood. In this regard, we hypothesized that functional changes of collateral-dependent myocardium induced by progressive coronary constriction could be assessed with cine MRI and MR tissue tagging.

Methods: After induction of anesthesia (ketamine, 20–30 mg/kg and sodium pentobarbital 20 mg/kg) and a left thoracotomy, a MR-compatible Ameroid conctrictor was placed around the proximal portion of the left circumflex artery (LCx) in 8 pigs to induce gradual stenosis. Five pigs served as sham-operated controls. At 25 ± 5 days post surgical procedure, rest-stress cine MR and MR tagging were performed in the whole-body MR 1.5 T system (Siemens Vision SP). Single slice multiphase short axis images with spatial modulation of magnetization (SPAMM, 2) tissue tagging were obtained using a segmented k-space (TR = 3.2ms, TE = 8ms, flip angle = 10 degrees, FOV = 26cm, pixel dimension = 1.015 mm, SPAMM center-to-center spacing = 4.2mm) to qualitatively assess principal strain λ_1 and λ_2, the direction of the principal strain (β), displacement (δ) and rigid body rotation angle (α). Stress was imposed by administration of Adenosine (IV, 250 μg/kg/min) for the determination of MBF and dobutamine (IV, 5 μg/kg/min) for tagging studies. MBF was measured with three different injections of 3×10^6 microspheres labeled with trace amounts of γ-emitting radionuclides (^{51}Cr, ^{85}Sr, ^{95}Nb or ^{46}Sc) followed by a 10ml flush with 0.9% saline solution. MBF was determined from γ-counts in tissue and in a reference blood specimen from a femoral artery. Contrast fluoroscopic cine angiography with ditriazolate meglumine (75%) was used to assess Ameroid closure and collateral development at 25 ± 3 days post procedure. Cine MR images were analyzed for global function and segmental wall thickening with MASS software (MASS 1.0 University of Leiden, Netherlands) by drawing epi- and endocardial contours followed by automatic dividing of the myocardium into 8 segments throughout the cardiac cycle and chord placement within the segments. SPAMM-tagged images were evaluated using a custom-written analysis package, SPAMMVU (2). Intersection of SPAMM stripes were selected and tracked using a semiautomatic tag detection routine based on a contour model. Triplets of tag intersections were grouped together to form a triangular tiling across the myocardial wall. The deformation of each triangle in end-systole and end-diastole was determined using a 2D strain analysis.

Results:

Myocardial Blood Flow (ml/min/g)

	Rest	Adenosine
LCx	1.2 ± 0.3	1.8 ± 0.5
LAD	1.4 ± 0.3	6.5 ± 0.3
p	NS	<0.0001

Angiographic studies confirmed the closure of the Ameroid constrictors and retrograde collateral filling of the LCx branches distal to the occluder placement at 25 ± 3 days in all animals. MBF at rest in the left anterior descending artery (LAD) bed was not significantly different from MBF in LCx zone. However, with Adenosine-induced hyperemia, MBF in LCx territory was significantly lower than in the LAD segments (see table). Segmental wall thickening showed a trend of decrease in Ameroid pigs. With administration of dobutamine (5 μg/kg/min), the rate-pressure product increased 94.8% on average from the baseline. Compared with sham-operated controls, Ameroid pigs showed a significant increase in displacement (δ) values in the LCx territory at stress (3.4 ± 0.1 vs. 5.6 ± 0.1, $p < 0.05$) but no significant change in λ_2 (rest: 0.8 ± 0.05 vs. 0.8 ± 0.07, stress: 0.85 ± 0.03 vs. 0.75 ± 0.06) was observed. The extent of collateral-dependent myocardium, calculated based on displacement, was 25%. Ejection fraction significantly decreased (10%, $p < 0.05$) at dobutamine loading in the Ameroid pigs versus sham-operated controls. Ameroid-induced collateralization allowed the myocardial segment of the occluded vessel to

restore baseline MBF. However, contraction analysis (the increase of displacement values of the collateralized segment) and a trend towards a decrease in wall thickening in the LCx region versus contractile motion in the remote, non-affected area indicates contractile dysfunction, which may be interpreted as the admixture of stunning and hibernation in the myocardium of the collateralized segment (3).

Conclusion: Quantitative evaluation of regional and global function with MR tissue tagging techniques was used for the first time to demonstrate and facilitate precise assessment of the functional status and extent of collateral-dependent myocardium.

References

1. Lamping KG. *Amer J Physiol.* 1997; 272: H2409–15
2. Axel L. et al. *Radiology* 1989; 172: 349–50
3. Yellon D et al. *New Ischemic Syndromes.* New York, 1997, 234 pp.

Quantification of Dysfunctional Myocardium by Wall Thickening or Strain Analysis: Correlation with Global Ventricular Function and Infarct Size

M.J.W. Götte, J.P.A. Kuijer, P.A.G. Vriend, J.T. Marcus, A.C. van Rossum. *University Hospital VU, Amsterdam, The Netherlands*

Background: The extent and degree of regional contractile dysfunction are both important factors determining long-term prognosis after myocardial infarction (MI) (1). Systolic wall thickening (%WTh) has proven to be an accurate parameter of regional myocardial function (2). However, detection of ventricular wall boundaries is affected by the curvature of the heart wall and the effect of through-plane motion of the heart. Magnetic resonance (MR) tagging in conjunction with strain analysis allows quantitative analysis of regional myocardial function without the need for wall boundary detection (3).

We quantified regional contractile dysfunction in patients with a first MI by using magnetic resonance (MR) imaging in conjunction with wall thickening analysis or strain analysis and correlated this with global ventricular function and enzymatic infarct size.

Methods: Thirteen patients (12 male, age 57 ± 11 years) were studied 103 ± 17 days after a first anterior MI (peak ck-MB 238 ± 119 U/l). Thirteen male volunteers (age 53 ± 7 years) served as controls. Cardiac triggered MR imaging was performed on a 1.5 T imaging system, using a phased-array coil. Cine MR images were processed using the MASS® software package. MR tagged images were analyzed using the SPAMMVU© software package.

A stack of cine MR short-axis images covering the complete left ventricle was used for calculation of ejection fraction (EF). Cine MR short-axis images at basal, mid and apical level were used for measuring %WTh in 12 segments per level. MR tagged images (7 mm grid) obtained at the same 3 levels with corresponding segmental division were used for quantification of intramural function. Strain parameters were the radial stretch (ε_r) and the circumferential shortening (ε_c). Segments with values out of the range of mean value ± 2SD of the control group were defined as abnormal. The number of abnormal segments (maximum 36) representing the extent of regional dysfunction was correlated with EF and peak ck-MB.

Results:

Correlation Between Number of Segments with Abnormal Regional Function and EF

	r	p-value
%WTh	−0.17	*ns*
ε_r	−0.83	<0.001
ε_c	−0.91	<0.001

Correlation Between Number of Segments with Abnormal Regional Function and Peak ck-MB

	r	p-value
%WTh	0.44	*ns*
ε_r	0.66	0.014
ε_c	0.77	0.002

Conclusion: The extent of dysfunction at 3 months after myocardial infarction as quantified by the strain parameters ε_r (radial stretch) and ε_c (circumferential shortening) is better correlated with global dysfunction and enzymatic infarct size, than the extent of dysfunction as quantified by %WTh. The poor correlation of %WTh with global ventricular function is probably caused by compromised epicardial and endocardial wall border tracing in geometrical deformed (remodeled) ventricles.

This study indicates that strain analysis is more accurate than %WTh for the detection of regional contractile dysfunction, which may have implications for the evaluation of ischemic heart disease and assessment of prognosis after infarction.

References

1. Sanz G, Castañer A, Betriu A. et al. *N Eng J Med* 1982; 306: 2065–1070.
2. Holman ER, Vliegen HW, van der Geest RJ. et al. *Magn Res Med* 1995; 34: 161–169.
3. Axel L, Goncalves RC, Bloomgarden D. *Radiology* 1992; 183:745–750.

Improvement of Magnetic Resonance Coronary Angiography Using the New Blood Pool Contrast Agent NC100150 in Patients

W.L.F. Bedaux,[1] M.B.M. Hofman,[1] P.A. Wielopolski,[2] A. Lehning,[3] M. Oudkerk,[2] P.J. de Feyter,[2] C.A. Visser,[1] A.C. van Rossum.[1]
[1]*University Hospital Vrije Universiteit, Amsterdam,* [2]*University Hospital Rotterdam, The Netherlands;* [3]*Nycomed Amersham Imaging, Munich, Germany*

Background: NC100150 (Nycomed Amersham Imaging, Oslo, Norway) is a new blood pool agent for potential use in Magnetic Resonance Coronary Angiography (MRCA). The aim of the study was to assess the improvement of the quality of 3 dimensional (3D) breath-hold (BH) MRCA using this contrast agent in patients.

Methods: Imaging data were acquired from 7 patients referred for diagnostic coronary angiography (CAG) in the evaluation of chest pain. The images were acquired using a 3D BH Volume Coronary Artery Targeted Scan (VCATS) at 1.5 T (Vision, Siemens, Germany) before and after intravenous contrast injection (2.5 mg Fe/kilogram body weight). The postcontrast sequences had adapted flip angle sequencing and used an inversion prepulse to suppress myocardial signal whereas precontrast magnetisation transfer suppression was applied. The length of the coronary arteries and the presence of stenoses visualized within a single slab of 24 mm thickness were evaluated. The signal- and contrast-to-noise ratios to myocardium and fat (SNRs, CNRs) were measured before and after contrast administration.

Results: The visualized lengths of the Left Main (LM), Left Anterior Descending (LAD), Circumflex and Right Coronary Artery (RCA) were respectively 1.2 ± 0.4, 4.1 ± 1.0, 2.4 ± 0.7 and 7.2 ± 1.9 cm. In total 28 segments were evaluated and compared with the data of the CAG. Overall agreement between MRCA and CAG of visually assessed stenosis severity was 82%. The mean SNR post- and precontrast was 12.1 ± 1.7 and 11.9 ± 1.8 respectively; the ratio was 1.0 ± 0.2 ($p = 0.3$). The mean CNR to myocardium post- and precontrast was 9 ± 2 and 4 ± 3 respectively: the ratio was 4 ± 3 ($p = 0.02$). Although sharper vessel delineation and improved myocardial suppression were obtained, CNR to epicardial fat did not change after contrast administration.

Conclusion: NC100150 contrast injection in combination with a BH VCATS allows rapid localization and coverage of the coronary arteries with better vessel delineation and increased myocardial suppression.

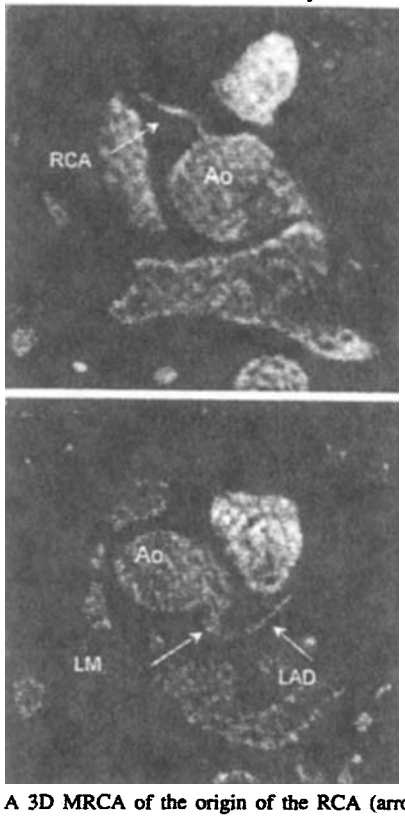

Figure 1. A 3D MRCA of the origin of the RCA (arrow in upper panel) and the LM and LAD (arrow in lower panel) in a transverse view with VCATS.

Optimization of 3D Coronary Artery Imaging Sequence for Intravascular Contrast Agents

Jie Zheng,[1] Friedirch M., Cavagna,[1] Debiao Li,[2] Gerhard Laub,[3] Paul J. Finn.[2] [1]*Bracco, SpA, Milan, Italy;* [2]*Northwestern University;* [3]*Siemens Medical Systems, Chicago, IL*

Introduction: The first-pass contrast-enhanced MR coronary artery imaging by using extravascular agents, such as Gd-DTPA, has shown significantly improved signal-to-noise ratio (SNR) and contrast-to-noise ratio (CNR) over pre-contrast images. However, image resolution and volume coverage still need major improvements. Intravascular contrast agents are necessary to obtain high SNR/CNR and resolution 3D coronary artery image data sets. This work aims at optimizing an inversion-recovery (IR) prepared sequence for 3D contrast enhanced coronary imaging in an pig model.

Materials and Methods: Simulation: A computer simulation was performed to predict the signal intensity of the blood as a function of blood T1. A segmented IR-prepared gradient-echo sequence was used in the simulation with the same parameters (see below). The signal intensity was calculated at the first RF signal since centric reordering scheme was applied in the actual sequence. The flip angles were chosen at either fixed-angle (25°) or variable flip-angles for constant signal intensities. T2* effect was neglected due to low TE.

Animal Study: Six normal domestic pigs were premedicated, anesthesized, and mechanically ventilated though a small animal ventilator. An intravenous line was placed in a ear vein for contrast injection. The MR system is a 1.5-T symphony system (Siemens Medical System, Erlangen, Germany). The imaging sequence for contrast enhancement study is an IR-prepared segmented FLASH sequence with TR/TE = 4.0/1.8 msec and 17 to 21 RF pulses applied within each cardiac cycles, depending on the duration of motionless in the mid-diastole. TI varied according to the RR interval of the pigs. After acquiring precontrast images, a true intravascular agent mixed micelles (Bracco S.p.a, Milan, Italy) was injected to the pigs at five separate times, resulting a cumulative dose of 0.025, 0.05, 0.1, 0.15, and 0.2 mmol./kg. This agent is able to stay in the blood pool for good. A fast T1-measurement was performed after each injection, followed by the 3D scans by using the imaging sequence. The imaging resolution was $0.7(x) \times 0.7(y) \times 1.0(z)$ mm^3. The slab thickness was 70 cm to cover the whole pig heart. A retrospective respiratory gating technique was applied for respiratory motion correction. The imaging time for each 3D scans was approximately 13 min.

Results: The measured blood T1 values after separate contrast injections were 150, 81, 52, 43, and 30 msec. The SNR on the right coronary artery was measured and averaged on the six-pig study. The simulation result agreed well with the experimental result on the SNR of post-contrast images as a function of blood T1 (Figure 1). T1 of 200 msec was found to provide optimal image contrast under a RR interval of 600–700 msec. Using variable flip-angles offered better vessel definition with slightly lower SNR. Figure shows a series right coronary artery images at different blood T1.

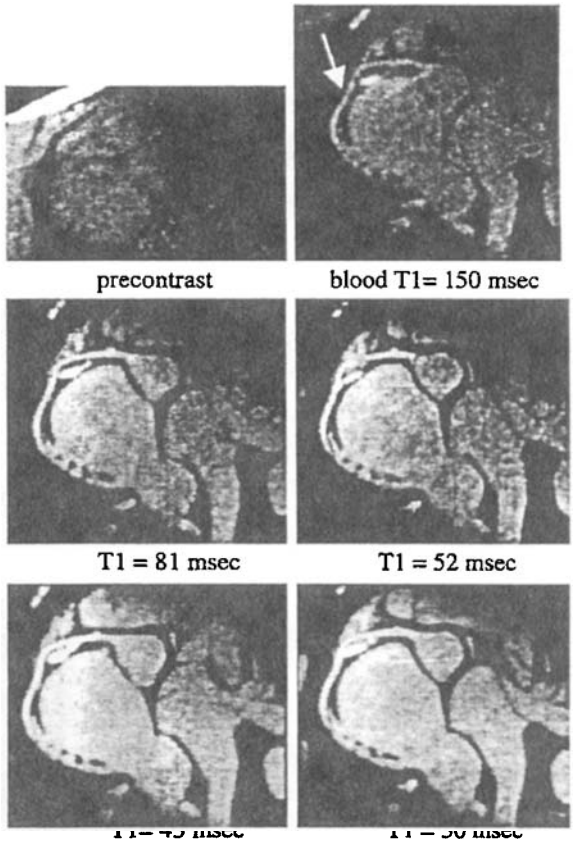

Conclusion: The optimized sequence may provide excellent image contrast and adequate SNR in 3D coronary artery images enhanced by intravascular contrast agents.